Université de Montréal

Design and characterization of thermally-induced shape memory polymers

par Kaojin Wang

Département de chimie

Faculté des arts et des sciences

Thèse présentée à la Faculté des études supérieures et postdoctorales

en vue de l'obtention du grade de philosophiae doctor (Ph.D.) en chimie

Janvier, 2018

Résumé

Les polymères à mémoire de forme (SMP) sont des matériaux intelligents qui peuvent récupérer leur forme permanente à partir d'une forme temporaire lorsqu'ils sont exposés à un stimulus externe. Ils ont attiré beaucoup d'attention en raison de leurs propriétés uniques. Par rapport aux SMPs doubles, les SMPs complexes ayant des mémoires triples, multiples ou bidirectionnelles sont plus attirants en raison de leurs propriétés distinctes. Les SMPs multiples peuvent mémoriser trois formes ou plus, tandis que les SMPs bidirectionnels peuvent basculer entre deux formes distinctes. L'objectif principal de cette thèse est de concevoir des SMPs complexes par des méthodes simples pour des applications particulièrement en biomédecine. Deux systèmes SMP complexes biodégradables à base de bio-composés ou de monomères synthétiques ont été synthétisés.

Pour les SMPs de mémorises multiples, nous avons synthétisé une série de copolymères statistiques avec des groupes pendants d'acide cholique en utilisant une méthode de polymérisation radicalaire simple. Ces copolymères ont une température de transition vitreuse (T_g) réglable, selon le ratio de comonomères, qui montrent à la fois des effets mémoires à double et triple états (PME). Les rapports entre la fixité et la récupération de la mémoire de forme double ou triple peuvent être améliorés par l'incorporation d'un groupe cinnamate dans les copolymères afin de permettre la photo-réticulation du polymère. Les polymères réticulés présentent des rapports de récupération améliorés pour la mémoire de forme double et triple et présentent même des PME quadruples. Le degré de réticulation affecte également les propriétés de mémoire de forme. Les meilleurs comportements de mémoire de forme dans ce genre de polymères ont été obtenus avec une réticulation de 2,2% molaire des monomères.

Les SMP doubles, triples et multiples sont généralement SMP unidirectionnels et leurs transformations de formes sont irréversibles. Les SMP réversibles bidirectionnels (2W-SMP) peuvent basculer automatiquement entre deux formes distinctes lorsqu'elles sont exposées à deux stimuli externes différents. Cependant, la température d'actionnement (T_A) de 2W-SMP est une valeur fixe telle que déterminée par la température de fusion (T_m) du segment actuateur du réseau polymère. Dans cette étude, une série de copolymères statistiques contenant ε-caprolactone (CL) et ω-pentadécalactone (PDL) ont été synthétisés par

polymérisation par ouverture de cycle avec un catalyseur de lipase B de Candida antarctica (CALB). Les segments polymères de ces deux monomères sont co-cristallisables et la T_m des copolymères peut être adapte en ajustant le rapport molaire des comonomères. Après irradiation pour la réticulation de thiol-ène, le réseau de polymères a montré des 2W-PME dans des conditions avec ou sans tension, avec un changement de forme absolu de 13,2%. Des mouvements réversibles comme flexion-extension et enroulement-déroulement ont été observés pour le réseau de polymère. La T_A de 2W-SMP sous conditions sans stress peut être facilement contrôlée en sélectionnant un ou deux prépolymères comme segments du réseau polymère. Le changement de l'élongation absolue des 2W-SMP est augmenté sous les conditions avec ou sans stress, mais le changement d'élongation relative est réduit avec l'augmentation de tension sous condition de stress. L'évolution de la microstructure de 2W-SMPs sous condition sans stress a également été conçu.

Les 2W-SMPs sont souvent actionnés thermiquement, mais le chauffage indirect est souhaitable pour certaines applications. Une série de 2W-SMPs composites actionnés par la lumière a ainsi été préparée par l'incorporation de nanosphères de PDA dans les réseaux polymères contenant le CL et le PDL. Les nanosphères de PDA ont un effet photothermique très prononcé qui peut convertir l'énergie lumineuse en chaleur. La température de l'échantillon augmente selon l'intensité lumineuse et du contenu en nanosphères de PDA. Ces composites polymères présentent d'excellentes 2W-PME sensibles à la lumière sous condition sans stress avec un changement d'angle réversible de 45° lorsque la lumière est allumée puis éteinte. L'échantillon avec un contenu plus élevé en nanosphères de PDA ou sous une intensité lumineuse plus forte cause une ouverture d'angle plus rapide. Un micro-robot qui peut marcher sur une piste en dents de scie lorsque la lumière est allumée et éteinte a également été conçu arec un composite 2W-SMPs.

Mots-clés: Polymères à mémoire de forme, acide cholique, polyester co-cristallisable, polydopamine

Abstract

Shape memory polymers (SMPs) are smart materials that can recover the permanent shape from a temporary shape when exposed to an external stimulus. They have drawn much attention due to their unique properties. In comparison to dual SMPs, complex SMPs with triple, multiple and two-way shape memories are more attractive due to their versatile properties. Triple and multiple SMPs could memorize three and more shapes, while two-way SMPs may automatically switch forth and back between two distinct shapes. The main purpose of this thesis is to design simple complex SMPs for their applications especially in biomedicine. Two biodegradable complex SMP systems based on bio-compounds or synthetic monomers have been synthesized.

For multiple SMPs, we synthesized a series of random copolymers with pendent cholic acid groups by the use of a simple free radical polymerization method. Such copolymers have a glass transition temperature (T_g) range tunable by varying the monomers ratios, allowing the dual and triple shape memory effects (SMEs). The fixity and recovery ratios of dual and triple shape memory may be further improved by the incorporation of cinnamate groups into copolymers to enable a photo-cross-linking of the terpolymer. The cross-linked polymers show much improved recovery ratios for both dual and triple shape memory and even exhibit quadruple SMEs. The degree of cross-linking also affects the shape memory properties. The best shape memory behaviors were obtained with a 2.2 mol% cross-linking of the total monomers in the terpolymer.

Dual, triple and multiple SMPs are usually one-way SMPs, and their shape transformations are irreversible. Two-way reversible SMPs (2W-SMPs) may switch between two different shapes automatically when they are exposed to two reverse external stimuli. However, the actuation temperature (T_A) of 2W-SMP is at a fixed value as it is determined by the melting temperature (T_m) of the actuator segment of the polymer network. In this study, a series of random copolymers containing ε-caprolactone (CL) and ω-pentadecalactone (PDL) were synthesized through ring opening polymerization catalyzed by *Candida antarctica* lipase B (CALB). The polymers segments made of these co-monomers are co-crystallizable and the T_ms of the copolymers may be changed by adjusting the molar ratio of the co-monomers.

Upon light irradiation which induces thiol-ene cross-linking, the polymer network showed 2W-SMEs under both stress-free and stress conditions with the absolute shape change up to 13.2%. Bending-unbending and coiling-uncoiling reversible shape motions were observed for the polymer network. The T_A of the 2W-SMP under stress-free conditions may be tuned by simply selecting one or two different prepolymers as segments in the polymer network. The absolute strain change of 2W-SMPs increased under both stress-free and stress conditions, but the relative strain change reduced with increasing tensile stress under stress conditions. The evolution of the microstructure of 2W-SMPs under stress-free conditions was also elaborated.

The 2W-SMPs are often actuated thermally, but indirect heating is desirable for certain applications because of its convenience. Thus, a series of light-actuated 2W-SMP composites were prepared via the incorporation of tiny amounts of polydopamine (PDA) nanospheres into polymer networks made of CL and PDL. PDA nanospheres have a strong photothermal effect which may convert energy of light into heat. The temperature change of the sample is larger with higher light intensity and higher content of PDA nanospheres. Such polymer composites exhibited excellent light-responsive 2W-SMEs under stress-free conditions with a reversible angle change of 45° when the light was turned on and off. The sample with a higher content of PDA nanospheres or under a stronger light led to a faster angle opening. A micro-robot is also designed and made of the 2W-SMP composite, which may walk on a home-made track with right triangle sawteeth when the light is turned on and off.

Keywords: Shape memory polymers, cholic acid, co-crystallizable polyesters, polydopamine

Table of Contents

List of Figures

List of Tables

List of Schemes

List of acronyms, abbreviations and symbols

1W-SME	One-way shape memory effect
1W-SMP	One-way shape memory polymer
2W-SME	Two-way shape memory effect
2W-SMP	Two-way shape memory polymer
AIBN	2,2'-azobis(2-methylpropionitrile)
ATR	Attenuated total reflection
AuNPs	Gold nanoparticles
AuNRs	Gold nanorods
CA	Cholic acid
CALB	*Candida antarctica* lipase B
CB	Carbon black
CIE	Cooling induced elongation
CL	ε-caprolactone
CNT	Carbon nanotube
CP	Copolymer
DA	Dopamine
DC	Degree of cross-linking
DCC	Dicyclohexylcarbodiimide
DCM	Dichloromethane
DMA	Dynamic mechanical analysis
DMF	*N*,*N*-dimethylformamide
DMPA	4-(dimethylamino)pyridine
DMSO	Dimethyl sulfoxide
DSC	Differential scanning calorimeters
ED-ROMPs	Entropy-driven ring opening metathesis polymerization
ESO	Epoxidized soybean oil
EVA	Poly(ethylene-*co*-vinyl acetate)

FTIR	Fourier-transform infrared spectroscopy
GO	Graphene oxide
HAM	*N*-methylol acrylamide
HEMA	2-hydroxyethyl methacrylate
HIFU	High intensity focused ultrasound
HOBA	Hexadecyloxybenzoic acid
IR	Infrard
LCE	Liquid crystalline elastomer
MCA	Cholic acid-based methacrylate monomer
MCE	Cinnamic acid-based methacrylate monomer
MEA	2-methoxyethyl acrylate
MIC	Melting induced contraction
M_n	Number average molecular weight
MPEG	Poly[(ethylene glycol) methyl ether methacrylate]
M_w	Weight average molecular weight
MWCNT	Multi-walled carbon nanotube
NIR	Near infrared
NR	Natural rubber
P(3HB-*co*-3HV)	Poly(3-hydroxybutyrate-*co*-3-hydroxyvalerate)
P(MMA-BA)	Poly(methyl methacrylate-*co*-butyl acrylate)
PCL	Poly(ε-caprolactone)
PDA	Polydopamine
PDI	Polydispersity index
PDL	ω-pentadecalactone
PDLA	Poly(D-lactide)
PDLLA	Poly(D,L-lactide)
PDO	*p*-dioxanone
PE	Polyethylene
PEG	Poly(ethylene glycol)

PHAs	Polyhydroxyalkanoates
PLA	Poly(lactic acid)
PLLA	Poly(L-lactide)
PMMA	Poly(methyl methacrylate)
POSS	Polyhedral oligosilsesquioxane
PP	Polypropylene
PPC	Poly(propylene carbonate)
PPDL	Poly(ω-pentadecalactone)
PPDO	Poly(*p*-dioxanone)
PTMEG	Poly(tetramethylene ether) glycol
R_f	Fixity ratio
R_r	Recovery ratio
SAXS	Small angle X-ray scattering
SEC	Size exclusion chromatography
SME	Shape memory effect
SMP	Shape memory polymer
SPOSS	Star-shaped polyhedral oligomeric silsesquioxane
SWCNT	Single-walled carbon nanotube
T_A	Actuation temperature
T_{cl}	Clearing temperature
T_d	Deformation temperature
TEA	Triethylamine
TEM	Transmission electron microscopy
T_c	Crystallization temperature
T_f	Flowing temperature
T_g	Glass transition temperature
TGA	Thermogravimetric analyses
THF	Tetrahydrofuran
T_m	The melting temperature

TP	Terpolymer
TPU	Thermoplastic polyurethans
TspPOSS	Trisilanolphenyl polyhedral oligomeric silsequioxane
T_{trans}	Transition temperature
UPy	Ureidoyrimidine
UV	Ultraviolet
UV-Vis	Ultraviolet-visible
VGCF	Vapor grown carbon fibers
WAXD	Wide angle X-ray diffraction
ΔH_c	Crystalline enthalpy
ΔH_m	Melting enthalpy

To: my family members and Prof. Julian Zhu

Acknowledgements

First and foremost, I would like to express my sincere thanks to my supervisor Prof. Julian Zhu for providing me an opportunity to study in his group, for his guidance through my study and research, for his constant encouragement and unending enthusiasm to explore new fields. His advice, patience, encouragement and profound knowledge on both my research and career have been priceless.

I would like to thank all my committee members, Prof. C. Géraldine Bazuin and Prof. Michel Lafleur for their critical comments and helpful suggestions, for taking their precious time to review my plan and progress. I also want to thank Prof. Christian Pellerin for his guidance in the first year of my studies.

I am grateful to the China Scholarship Council for a scholarship. I also thank the financial support from Natural Sciences and Engineering Research Council of Canada (NSERC), Fonds de recherche du Québec-nature et technologies (FRQNT), and University of Montreal.

I also would like to express my appreciation to my colleagues in the research laboratory for their help during my study. A special thanks to Dr. Yong-guang Jia, a postdoc in the Zhu group, who trained me on chemical synthesis and paper writing, and to Drs. Satu Strandman, Hu Zhang, Meng Zhang, Wang Liao, Hongjun Yang, Xin Wang, Mohammadtaghi Savoji, Murugan Veerapandian, Eric Habib, and Messrs. Hu, Zhu, I-Huang Tasi, Nicolas Levaray, Puzhen Li, Zhiyuan Ma, and Alexander Cunningham.

I am also very thankful to Mr. Sylvain Essiembre for his help of DSC, TGA, DMA training, Mr. Pierre Menard-Tremblay for FTIR training, Madame Francine Belanger for the help during the SAXS measurements, Mr. Maris Thierry for the help during WAXD measurements, Mr. S. Kelly Sears for TEM measurements.

I would like to thank my family. Words cannot express how grateful I am to my parents and my elder brother. At the end, I would like express huge appreciation to my wife Jin

Zhao whose patience and encouragements supported me spiritually throughout my Ph.D. study, and to my lovely daughter Monique whose birth filled my life with joy.

Chapter 1

Introduction

1.1 Shape memory polymers

Smart materials may be made of polymers that are capable of manifesting property changes in response to changes in the external environment. Shape memory polymers (SMPs) are one of such materials that can be fixed to a temporary shape and recover its permanent shape upon application of an external stimulus, such as temperature in change,[1] light,[2] electricity,[3] magnetism,[4] microwave,[5,6] ultrasound,[7-9] solvent,[10-12] pH,[13-16] metal ion,[17] etc. Such polymers have attracted much attention from researchers in past decades owing to their potential applications in biomedicine,[18] aerospace,[19] robotic industry,[20] sensors,[21] actuators,[22] etc. Figure 1.1 shows the annual number of citations of "shape memory polymers" in the Web of Science database from 1995 to 2017. The exponential increase of citation numbers illustrates the growing interest in the mechanism and applications. Dual SMPs are the basic form of SMPs that could memorize two shapes, one temporary and one permanent shape, in a shape memory cycle. Most of the polymers may endow a certain dual shape memory effect (SME) because they have at least one reversible thermal transition.[23] Therefore, it is easy to design a dual SMP. However, dual SMPs could not meet more complex requirements in certain applications, promoting the development of complex SMPs, such as multiple and two-way reversible SMPs. Three or more shapes can be memorized for triple and multiple SMPs.[24] In comparison to dual SMPs, complex SMPs are more interesting and versatile. One-way SMPs have one permanent shape and one or more temporary shapes, depending on the number of transition states that they may accommodate, corresponding to dual, triple, and multiple SMPs. The temporary shapes recover directly, or through intermediate temporary shape(s), the permanent shape, when the material is subject to an external stimulus (usually heat). Two-way reversible SMPs (2W-SMPs) may change back and forth between two distinct shapes automatically when activated by two different stimuli. This subject will be addressed in more details in Chapter 2.

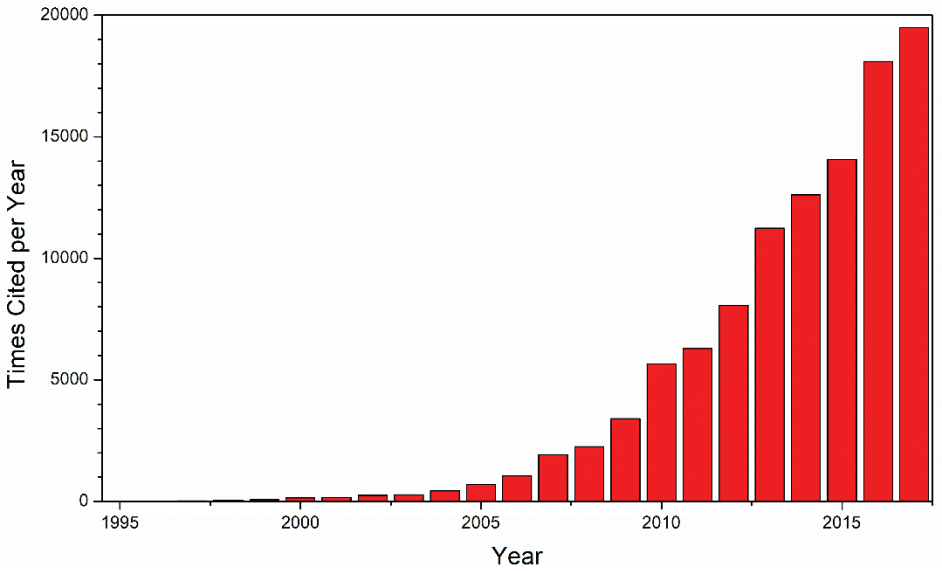

Figure 1.1 Histogram showing the number of citations per year based on a search from the Web of Science using a keyword "shape memory polymers" (Jan. 2018)

1.2 One-way multiple SMPs

Dual SMPs can recover the permanent shape from a temporary shape upon exposure to an external stimulus, which require a thermal transition temperature (T_{trans}). They are relatively simple and easy to design and make. Triple and multiple SMPs, however, require two or more distinct T_{trans}s or a broad T_{trans} that can incorporate multiple steps of transitions, thereby allowing the memorization of three or more shapes (one permanent shape plus two or more temporary shapes). They are useful and sometimes required for certain applications. The first triple SMP system based on semi-crystalline polymer networks with two distinct T_ms was reported by Lendlein and coworkers in 2006.[26] In the following years, all triple SMPs were focused on polymers with two separate thermal transition temperatures (T_{trans}).[27,28] In 2010, a commercial glassy polymer with one broad glass transition temperature (T_g) was found to show multiple shape memory effect (SMEs).[29] Triple and multiple SMPs may be used in more complex conditions since they feature three or more temporary shapes. Triple SMEs have been achieved by utilizing two reversible thermal transitions or one single broad thermal transition. Multiple SMEs could be realized in a similar fashion by introducing additional discrete transition(s) or broadening the single transition used for triple SMPs. Triple and multiple shape memory properties strongly

depend on the cross-linking density (including physical and chemical cross-linking). It is also known that a higher cross-linking density would allow the sample to recover more fully its original shape but with a lower performance in keeping its temporarily-fixed shape.[30] There is a need to design simpler and better-performing polymers that are easy to prepare.

1.3 Two-way reversible SMPs

Two-way SMPs (2W-SMPs) can change between two or more distinct "permanent" shapes when they are triggered by two or more different external stimuli. They are more difficult to achieve and have become the most desired shape memory materials due to their unique properties. Mather and coworkers developed 2W-SMPs, and found that pre-stretched polycyclooctene with chemical cross-linking structure featured contraction upon heating and elongation on cooling under a constant tensile stress.[31] Most of the 2W-SMEs reported so far are activated by direct or indirect heating, where the heating can be sourced from light, magnetism, electricity, microwave, or ultrasound. One exception are polydomain azobenzene-based liquid crystal elastomers (LCEs), where the bending and unbending shape changes could be realized by switching between two irradiation light wavelengths of 366 and 540 nm due to *trans-cis* isomerization of the azobenzene.[32] Two types of thermally induced 2W-SMEs have been reported: under stress and stress-free conditions. Just as the name implies, for 2W-SME under stress, the sample only shows reversible shape changes when a permanently applied external load is imposed on it, limiting complex shape transformations. Hence, 2W-SMPs under stress-free conditions are more desirable for many applications.

1.4 Objectives and the scope of this thesis

Polymers containing two or more distinct thermal transitions or a single broad thermal transition may endow multiple SMEs. However, the synthesis of these SMPs is usually complicated, and/or a transition metal catalyst is used during the synthesis. The actuation temperature (T_A) of SMPs is usually at a fixed temperature or can only be tuned in a small range. All these drawbacks limit the practical applications of multiple SMPs. 2W-SMPs can be realized on liquid crystalline elastomers (LCEs) and semi-crystalline polymer networks.

Semi-crystalline polymer networks are easier to design and synthesize. The T_A of 2W-SMP is determined and limited by the T_m of the polymers. It is also of interest to develop 2W-SMPs that can be actuated by other stimuli than heat.

The main objective of this thesis is to design SMPs that may have multiple SMEs with simpler and greener synthetic methods and two-way reversible SMEs preferably in the presence of nontoxic catalysts, especially the SMPs that can be triggered by other stimuli than direct heating. To this end, we developed two different SMP systems based on bio-compounds and/or biodegradable prepolymers and investigated their shape memory behavior and the evolution of the microstructure in shape memory cycles. The multiple SMPs based on a series of random copolymers bearing cholic acid and oligo(ethylene glycol) are synthesized through the use of a simple free radical polymerization method. In order to further improve the recovery ratios, cinnamate group is incorporated into a random copolymer to synthesize a terpolymer that can be photo-cross-linked. The cross-linked terpolymer shows much improved dual, triple and quadruple SMEs. The 2W-SMPs are prepared by photo-cross-linking homopolymers and random copolymers which are synthesized easily with various molar ratios of co-crystallizable comonomers, lactones with different hydrocarbon chain lengths, by the use of ring opening polymerization method in presence of an enzyme, Candida antartica lipase B (CALB). The T_A of 2W-SMPs under stress-free conditions can be tuned by selecting two different prepolymers. Into this 2W-SMP system we introduced polydopamine (PDA) nanospheres with good photothermal effects and used light to actuate the 2W-SME. A micro-robot was also designed and made and shown to be capable of locomotion when the light was turned on and off repeatedly.

This thesis consists of six chapters, including this general introduction (Chapter 1), review paper (Chapter 2), research papers (Chapters 3 to 5) and a general conclusion (Chapter 6). All the presented work was done by the author of this thesis under the supervision of Professor Julian Zhu. Dr. Yong-Guang Jia was a postdoctoral fellow in our group, he helped with the correction of the papers and sometimes involved in the discussions, solving synthetic problems and helping with the experimental design. Therefore, he is the co-author of the review paper and two of the research papers.

Chapter 2 reviews the progress of thermally-induced triple and multiple, and two-way SMPs through direct and indirect heating methods. We summarized the literature work to present the concepts, the programming procedures, the molecular mechanism, classification, and design strategies of complex SMPs. In addition, some examples of the applications of these types of SMPs were also described. This review has been submitted for publication. (Wang, K.; Jia, Y. -G.; Zhu, X. X. Multiple and two-way reversible shape memory polymers: Design strategies and applications, *Prog. Mater. Sci.*).

Chapter 3 describes a series of random copolymers or terpolymers made of biological compounds (cholic acid, cinnamic acid and oligo(ethylene glycol)). Their broad T_gs accommodated dual and triple SMEs. The chemical cross-linked structure could enhance shape memory behavior. Moreover, the cross-linked terpolymer manifested good quadruple SMEs. This paper has been published in *ACS Biomaterials Science & Engineering*. (Wang, K.; Jia, Y. -G.; Zhu, X. X. Biocompound-based multiple shape memory polymers reinforced by photo-cross-linking. *ACS Biomater. Sci. Eng.* **2015,** 1, 855-863.)

Chapter 4 describes the synthesis of a series of homopolymers and random copolymers by the use of various molar ratios of cocrystallizable monomeric units (CL and PDL). The melting temperatures (T_ms) of these prepolymers are tunable. After photo-cross-linking upon thiol-ene reaction, the polymer network manifested 2W-SME under stress and stress-free conditions. The tunable actuation temperatures (T_As) of 2W-SMP under stress-free condition could be tuned by selecting one or two prepolymers as their two segments. This paper has been published in *Macromolecules*. (Wang, K.; Jia, Y. -G.; Zhu, X. X. Two-way reversible shape memory polymers made by cross-linked co-crystallizable random copolymers with tunable actuation temperatures. *Macromolecules* **2017,** 50, 8570-8579.)

Chapter 5 presents the preparation of photo-responsive 2W-SMP composites via the incorporation of PDA nanospheres into the 2W-SMP system designed in Chapter 4 making use of the photothermal effect of PDA. 2W-SMEs under stress-free conditions were observed when the light was switched on and off. In addition, we designed a robot which is capable of locomotion on a track with right triangle sawteeth based on a 2W-SMP composite. This paper has been submitted for publication. (Wang, K.; Zhu, X. X. Two-way

reversible shape memory polymers containing polydopamine nanospheres: Light actuation and robotic locomotion. *J. Mater. Chem. B*)

Chapter 6 is a general conclusion summarizing the work carried out with future perspectives for this work.

1.5 References

1. Gautrot, J. E.; Zhu, X. X. Shape memory polymers based on naturally-occurring bile acids. *Macromolecules* **2009,** 42, 7324-7331.

2. Lendlein, A.; Jiang, H. Y.; Junger, O.; Langer, R. Light-induced shape-memory polymers. *Nature* **2005,** 434, 879-882.

3. Liu, X.; Li, H.; Zeng, Q.; Zhang, Y.; Kang, H.; Duan, H.; Guo, Y.; Liu, H. Electro-active shape memory composites enhanced by flexible carbon nanotube/graphene aerogels. *J. Mater. Chem. A* **2015,** 3, 11641-11649.

4. Razzaq, M. Y.; Behl, M.; Nöchel, U.; Lendlein, A. Magnetically controlled shape-memory effects of hybrid nanocomposites from oligo(ω-pentadecalactone) and covalently integrated magnetite nanoparticles. *Polymer* **2014,** 55, 5953-5960.

5. Du, H.; Liu, X.; Yu, Y.; Xu, Y.; Wang, Y.; Liang, Z. Microwave-induced poly(ionic liquid)/poly(vinyl alcohol) shape memory composites. *Macromol. Chem. Phys.* **2016,** 217, 2626-2634.

6. Du, H.; Yu, Y.; Jiang, G.; Zhang, J.; Bao, J. Microwave-induced shape-memory effect of chemically crosslinked moist poly(vinyl alcohol) networks. *Macromol. Chem. Phys.* **2011,** 212, 1460-1468.

7. Bhargava, A.; Peng, K.; Stieg, J.; Mirzaeifar, R.; Shahab, S. Focused ultrasound actuation of shape memory polymers; acoustic-thermoelastic modeling and testing. *RSC Adv.* **2017,** 7, 45452-45469.

8. Lu, X.; Fei, G.; Xia, H.; Zhao, Y. Ultrasound healable shape memory dynamic polymers. *J. Mater. Chem. A* **2014,** 2, 16051-16060.

9. Li, G.; Yan, Q.; Xia, H.; Zhao, Y. Therapeutic-ultrasound-triggered shape memory of a melamine-enhanced poly(vinyl alcohol) physical hydrogel. *ACS Appl. Mater. Interfaces* **2015,** 7, 12067-12073.

10. Gu, X.; Mather, P. T. Water-triggered shape memory of multiblock thermoplastic polyurethanes (TPUs). *RSC Adv.* **2013,** 3, 15783-15971.

11. Du, H.; Zhang, J. Solvent induced shape recovery of shape memory polymer based on chemically cross-linked poly(vinyl alcohol). *Soft Matter* **2010,** 6, 3370-3376.

12. Quitmann, D.; Gushterov, N.; Sadowski, G.; Katzenberg, F.; Tiller, J. C. Solvent-sensitive reversible stress-response of shape memory natural rubber. *ACS Appl. Mater. Interfaces* **2013,** 5, 3504-3507.

13. Meng, H.; Zheng, J.; Wen, X.; Cai, Z.; Zhang, J.; Chen, T. pH- and sugar-induced shape memory hydrogel based on reversible phenylboronic acid-diol ester bonds. *Macromol. Rapid Commun.* **2015,** 36, 533-537.

14. Xiao, Y. Y.; Gong, X. L.; Kang, Y.; Jiang, Z. C.; Zhang, S.; Li, B. J. Light-, pH- and thermal-responsive hydrogels with the triple-shape memory effect. *Chem. Commun.* **2016,** 52, 10609-10612.

15. Li, Y.; Chen, H.; Liu, D.; Wang, W.; Liu, Y.; Zhou, S. pH-responsive shape memory poly(ethylene glycol)-poly(ε-caprolactone)-based polyurethane/cellulose nanocrystals nanocomposite. *ACS Appl. Mater. Interfaces* **2015,** 7, 12988-12999.

16. Han, X. J.; Dong, Z. Q.; Fan, M. M.; Liu, Y.; li, J. H.; Wang, Y. F.; Yuan, Q. J.; Li, B. J.; Zhang, S. pH-induced shape-memory polymers. *Macromol. Rapid Commun.* **2012,** 33, 1055-1060.

17. Le, X.; Lu, W.; Xiao, H.; Wang, L.; Ma, C.; Zhang, J.; Huang, Y.; Chen, T. Fe^{3+}-, pH-, thermoresponsive supramolecular hydrogel with multishape memory effect. *ACS Appl. Mater. Interfaces* **2017,** 9, 9038-9044.

18. Wang, K.; Strandman, S.; Zhu, X. X. A mini review: Shape memory polymers for biomedical applications. *Front. Chem. Sci. Eng.* **2017,** 11, 143-153.

19. Liu, Y.; Du, H.; Liu, L.; Leng, J. Shape memory polymers and their composites in aerospace applications: a review. *Smart Mater. Struct.* **2014,** 23, 023001.

20. Peng, Q.; Wei, H.; Qin, Y.; Lin, Z.; Zhao, X.; Xu, F.; Leng, J.; He, X.; Cao, A.; Li, Y. Shape-memory polymer nanocomposites with a 3D conductive network for bidirectional actuation and locomotion application. *Nanoscale* **2016,** 8, 18042-18049.

21. Li, X.; Serpe, M. J. Understanding the shape memory behavior of self-bending materials and their sse as sensors. *Adv. Funct. Mater.* **2016,** 26, 3282-3290.

22. Behl, M.; Kratz, K.; Noechel, U.; Sauter, T.; Lendlein, A. Temperature-memory polymer actuators. *Proc. Natl. Acad. Sci. U. S. A.* **2013,** 110, 12555-12559.

23. Xie, T. Recent advances in polymer shape memory. *Polymer* **2011,** 52, 4985-5000.

24. Zhao, Q.; Qi, H. J.; Xie, T. Recent progress in shape memory polymer: New behavior, enabling materials, and mechanistic understanding. *Prog. Polym. Sci.* **2015,** 49-50, 79-120.

25. Kaojin Wang, Y.-G. J., X.X. Zhu. Two-way reversible shape memory polymers made of cross-linked cocrystallizable random copolymers with tunable actuation temperatures. *Macromolecules* **2017**, 50, 8570-8579.

26. Bellin, I.; Kelch, S.; Langer, R.; Lendlein, A. Polymeric triple-shape materials. *Proc. Natl. Acad. Sci. U.S.A.* **2006,** 103, 18043-18047.

27. Behl, M.; Bellin, I.; Kelch, S.; Wagermaier, W.; Lendlein, A. One-step process for creating triple-shape capability of AB polymer networks. *Adv. Funct. Mater.* **2009,** 19, 102-108.

28. Bellin, I.; Kelch, S.; Lendlein, A. Dual-shape properties of triple-shape polymer networks with crystallizable network segments and grafted side chains. *J. Mater. Chem.* **2007,** 17, 2885-2891.

29. Xie, T. Tunable polymer multi-shape memory effect. *Nature* **2010,** 464, 267-270.

30. Wang, K.; Jia, Y.-G.; Zhu, X. X. Biocompound-based multiple shape memory polymers reinforced by photo-cross-linking. *ACS Biomater. Sci. Eng.* **2015,** 1, 855-863.

31. Chung, Taekwoong.; Romo-Uribe, Angel.; Mather, Patrick T. Two-way reversible shape memory in a semicrystalline network. *Macromolecules* **2008,** 41, 184-192.

32. Yu, Y. L.; Nakano, M.; Ikeda, T. Directed bending of a polymer film by light-miniaturizing a simple photomechanical system could expand its range of applications. *Nature* **2003,** 425, 145-145.

Chapter 2

Multiple and two-way reversible shape memory polymers: Design strategies and applications*

Abstract

Shape memory polymers (SMPs) are capable of changing their shapes in a pre-defined manner under a stimulus, and have gained considerable interest in the past decades. Although a number of stimulus-responsive SMPs have been developed, thermally-induced SMPs are still the most common. This review presents the concepts, the programming procedures, the molecular mechanism, classification, design strategies and the recent progress of thermally-induced SMPs, including dual, triple, multiple SMPs and two-way reversible SMPs (2W-SMPs) activated by direct and indirect heating methods. Examples of applications of these types of SMPs are also presented and discussed.

2.1 Introduction

Shape memory materials, including shape memory ceramics, shape memory alloys and shape memory polymers (SMPs), are regarded as smart materials with the capability of recovering its permanent shape from a temporary shape under an external stimulus, such as heat, light, pressure, electrical field, magnetic field, pH or solvent.[1-4] SMPs are among the most important due to their good shape change (up to 1000% recoverable deformation),[5] low density, tailorable properties (e.g., thermal transition temperature (T_{trans}), rigidity, biodegradability, etc.), programmability and controllability of recovery behavior, and low

*Wang, K.; Jia, Y.-G.; Zhu, X.X. Submitted to *Progress in Materials Science* for publication as a review.

cost. The term SMP was first used in 1984 by CDF Chimie Company (France).[6] However, interest was limited due to the lack of applications in the early days of SMPs. Lendlein et al. reported that SMPs may be used as self-tightening sutures for minimum invasive surgery in 2002, raising much interest for SMPs in biomedical applications.[7]

Various actuation stimuli of SMPs may be applied as mentioned above. Thermally-induced SMPs, the most common stimulus, may be directly triggered by heating with a hot gas or water. Indirect heating methods have been also developed due to the inconvenience of directly activating the SMPs in certain applications. For example, SMPs incorporated with functional fillers may be triggered by light, electricity, magnetism, microwave or ultrasound,[8,9] but they are still intrinsically triggered by heat, since different forms of energy may be converted into heat through the functional fillers. For the intrinsically light-induced SMPs, reversible photo-responsive molecular switches are incorporated into the polymer, and shape fixity and recovery may be realized with various light wavelengths.[10-12] Water or other solvents may be used as a trigger in which solvent molecules are dispersed into the polymer and serve as plasticizers leading to a reduction in T_{trans} and consequently resulting in shape recovery.[13-19]

Most thermally-induced SMPs have a permanent shape provided by cross-linked phases, including chemical and physical cross-linking, such as crystalline domains[20,21] or strong supramolecular interactions.[22] Their temporary shapes are fixed by frozen molecular chains during vitrification, crystallization or anisotropization below a certain T_{trans}, such as the glass transition temperature (T_g), the crystallization temperature (T_c) and the clearing temperature (T_{cl}, a thermal transition temperature of liquid crystal polymers). According to the number of shape transitions, thermally-induced SMP may be categorized into dual, triple and multiple SMPs. Most SMPs are able to recover its permanent shape from a temporary shape under an external stimulus, but cannot reverse to its temporary shape. Such SMPs are called one-way SMPs (1W-SMPs). Other SMPs may reversibly vary between two distinct shapes under two different external stimuli, and are known as two-way reversible SMPs (2W-SMPs). Here, two different external stimuli may be of the same type (such as heating and cooling, or different wavelengths of light) or different types (such as light and cooling, or electric current and cooling, etc.).

SMPs have drawn a great deal of attention from researchers in different fields. As a result, numerous review papers have appeared in the literature with different emphases of the subject. These include papers covering the general concepts of SMPs[23-30] or specific aspects, such as SMP composites and nanocomposites,[6,31-35] shape memory hydrogels,[36] triple SMPs,[37] reversible SMPs,[38] SMPs bearing reversible binding groups,[39] shape memory epoxy resins,[40] stimuli-responsive SMPs,[35,41-43] electro-active SMPs,[32] SMPs with multiple transitions,[44] and textile,[45] biomedical,[46-49] and aerospace[50] applications of SMPs. Some review papers on self-healing polymers also mentioned SMPs.[51-53] To the best of our knowledge, there are no reviews in the literature that systematically treated the subject of multiple and two-way shape memory effects (SMEs) through both direct and indirect heating. Therefore, a comprehensive review on multiple and two-way SMPs is still needed.

In this review, we start by defining the terms and strategies of material design by discussing dual SMEs, but our emphasis will be placed on multiple SMEs and particularly 2W-SMEs as well as SMEs actuated by indirect heating, for which we will define the terms and concepts later in the text. We focus this paper on the thermally-induced SMPs, including direct and indirect heating-activated SMPs. We summarize the concept, the programming procedure, the molecular mechanisms, the design strategies as well as recent development in thermally-induced SMPs activated by direct and indirect heating method.

2.2 Dual SMPs

2.2.1 Programming and mechanism

Dual SMPs are the conventional and basic form of SMPs containing only one shape transition from a temporary shape to a permanent shape in response to a stimulus. In this paper, dual SMPs are addressed briefly for a better understanding of complex SMPs (multiple and 2W-SMPs), since several reviews have focused on them. Their programming procedures and molecular mechanisms may be generally summarized in Figure 2.1.[4, 27-30,40] The SMP is first heated to a deformation temperature ($T_d > T_{trans}$) and held isothermally for a certain time length to reach heat conduction equilibrium, since the sample exhibits rubbery elasticity at this temperature and the chain mobility is significantly activated. The polymer chain

conformations are changed under an external loading, resulting in macroscopic shape change (deformed shape) and stored elastic energy. The sample is then cooled to a fixation temperature ($T_f < T_{trans}$) and held isothermally to freeze the movement of the polymer chains. The elastic energy is kinetically trapped, and a temporary shape is fixed after unloading the external force. When the SMP is reheated above T_{trans} without stress, the chain mobility is reactivated, the corresponding stored elastic energy is released, and the SMP recovers its permanent shape.

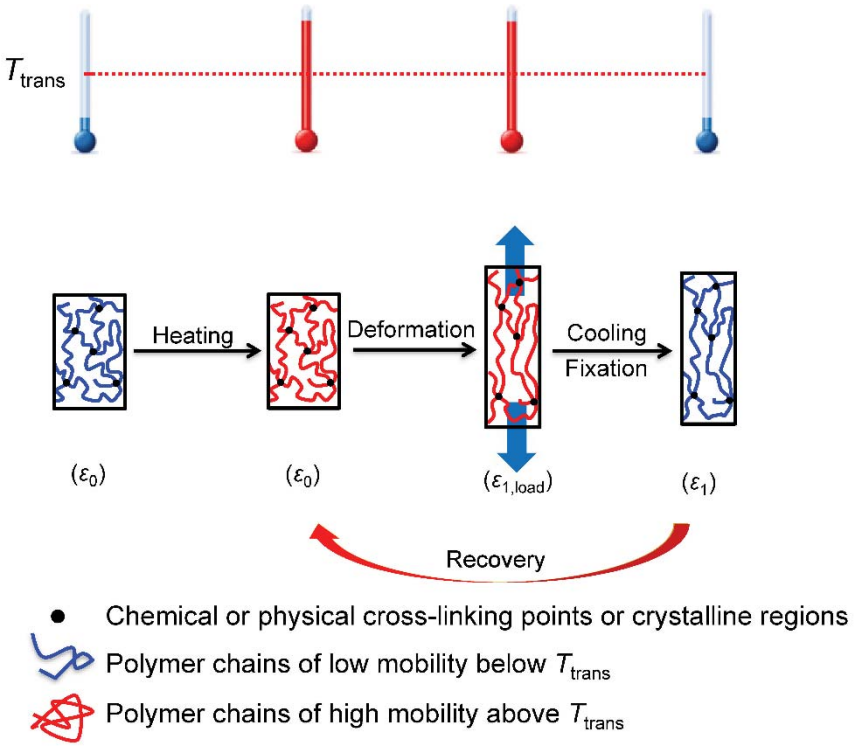

Figure 2.1 Schematic illustration and the molecular mechanism of a dual SME.

Two parameters can be used to describe the dual SMEs. The first one is the shape fixity ratio (R_f), which quantifies the ability of the sample to maintain an imposed mechanical deformation after the load is removed. The other is the shape recovery ratio (R_r), quantifying the ability of the sample to recover its permanent shape:[52]

$$R_f = \frac{\varepsilon(N)}{\varepsilon_{load}(N)} \times 100\% \qquad (2.1)$$

$$R_r = \frac{\varepsilon(N) - \varepsilon_{rec}(N)}{\varepsilon(N) - \varepsilon_{rec}(N-1)} \times 100\% \quad (2.2)$$

where ε_{load} is the maximum strain before removing the external force, ε denotes the strain after cooling and unloading, ε_{rec} indicates the strain after the recovery step, and N represents the number of cycles in the shape memory experiment.[53]

For a dual SMP, the temporary shape fixation and permanent shape recovery are determined by a reversible T_{trans}, where the chain mobility is trapped (shape fixation) and liberated (shape recovery) when changing the temperature below and above T_{trans}, respectively. Many polymers may manifest a certain dual SME when they have at least one reversible thermal transition (T_g for a glassy polymer, melting transition (T_m) for a semi-crystalline polymer, or T_{cl} for a liquid crystalline polymer). Irreversible slippage may occur between the polymer chains under an external force at a temperature higher than the T_{trans} of the sample, leading to reduced entropy, thereby reducing the entropy-related elastic energy, the driving force for the shape recovery. As a result, the recovery ratio becomes lower.[55] Such irreversible slippage between polymer chains may be prevented by chemical and/or physical cross-linking. The entropy-related elastic energy is increased and stored by prohibiting the slippage, resulting in a high recovery ratio. Thus, based on the nature of the reversible thermal transition and the cross-linking, conventional dual SMPs can be divided into two classes: (1) chemically cross-linked polymers with one T_g or T_m or T_{cl}, and (2) physically cross-linked polymers with one T_g or T_m or T_{cl}. In this review, dynamic covalent bonds, such as transesterification,[60,61] Diels-Alder bonds,[62] disulfide bonds,[63] etc. are considered as chemical cross-linking, while dynamic bonds, such as hydrogen bonding,[56] ionic interactions,[57] π-π stacking interactions,[58] and metal-ligand co-ordination interactions,[59] are categorized as physical cross-linking.

2.2.2 Chemically cross-linked polymers

The simplest SMPs are chemically cross-linked polymers with a sharp T_g. This class of materials generally has excellent shape recovery ratios due to the absence of molecular slippage between polymer chains. However, they are difficult to reprocess once their shape is set, because the original shape is covalently fixed. The temporary shape of glassy SMPs is fixed by vitrification below the T_g, while the permanent shape is recovered by heating the

temperature above the T_g. For example, chemically cross-linked polyimides with the high T_g of around 320 °C as the T_{trans} exhibit a very good dual SME (Figure 2.2), and their R_f and R_r reached as high as 99.2% and 98.9%, respectively.[64]

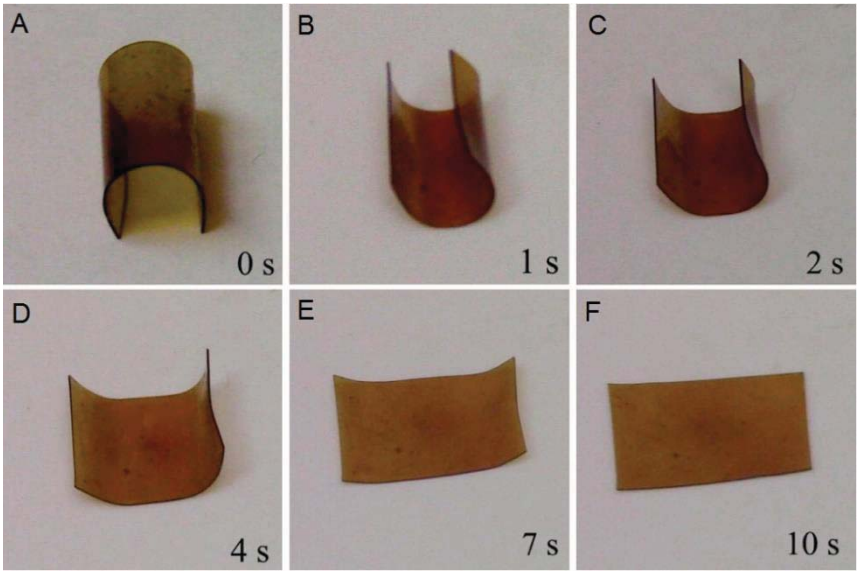

Figure 2.2 Shape recovery process of a thermoset polyimide. Reprinted with permission from Ref. 64. Copyright (2015) American Chemical Society.

For the chemically cross-linked semi-crystalline SMPs having a T_m as the critical temperature, the temporary shape is fixed by crystallization below T_c instead of vitrification, while the permanent shape is recovered by melting the crystalline phase above T_m. Similar to the former class, the permanent shapes are set by the chemically cross-linked network and may not be reshaped after processing. For example, cross-linked poly(ethylene glycol)-poly(ε-caprolactone) (PEG-PCL) copolymers can change from temporary linear shapes to permanent spiral shapes with T_ms close to body temperature.[65] Xie's group utilized dynamic covalent bonds for cross-linking poly(urea-urethane), which exhibited self-healing, reprocessability, and dual shape memory behaviors (Figure 2.3).[61]

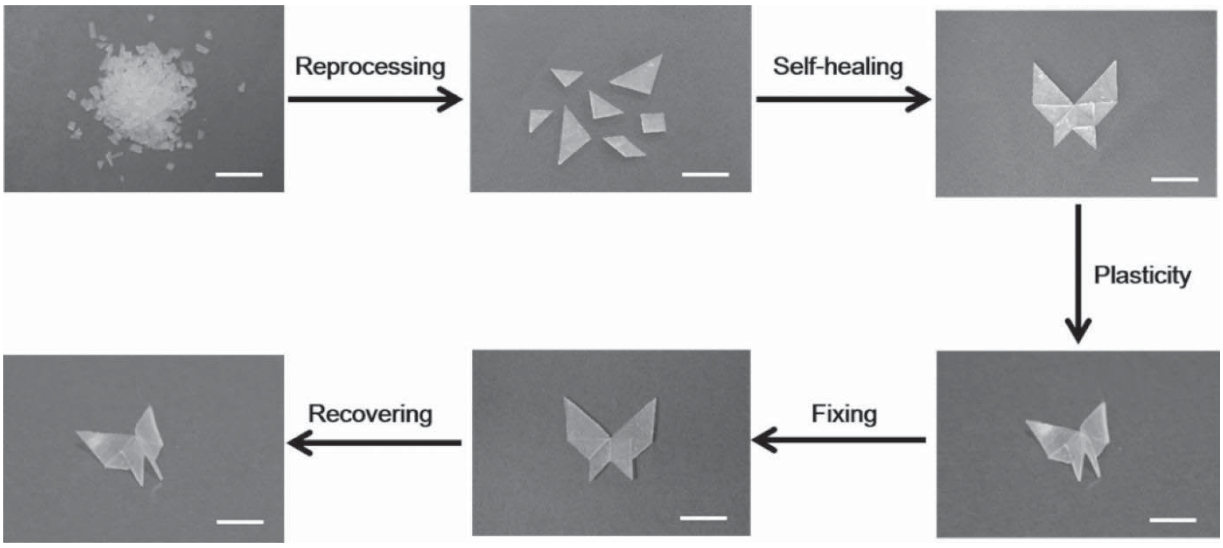

Figure 2.3 Dynamic covalent bonds cross-linked poly(urea-urethane) showing reprocessing, self-healing, plasticity, and a dual SME. Reprinted with permission from Ref. 61. Copyright (2017) American Chemical Society.

T_{cl} can also be used as a transition temperature for chemically cross-linked liquid crystalline SMPs. The temporary shape is fixed upon cooling below T_{cl} (isotropic-anisotropic transition temperature), whereas the recovery shape returns upon heating above T_{cl}. For example, a main-chain smectic liquid crystalline elastomer (LCE) was prepared from a main-chain polydibenzoate with methacrylate end groups followed by thermal cross-linking, which displayed a remarkable dual SME (both R_f and $R_r > 98\%$) actuated by a T_{cl} of 98 °C (Figure 2.4).[66]

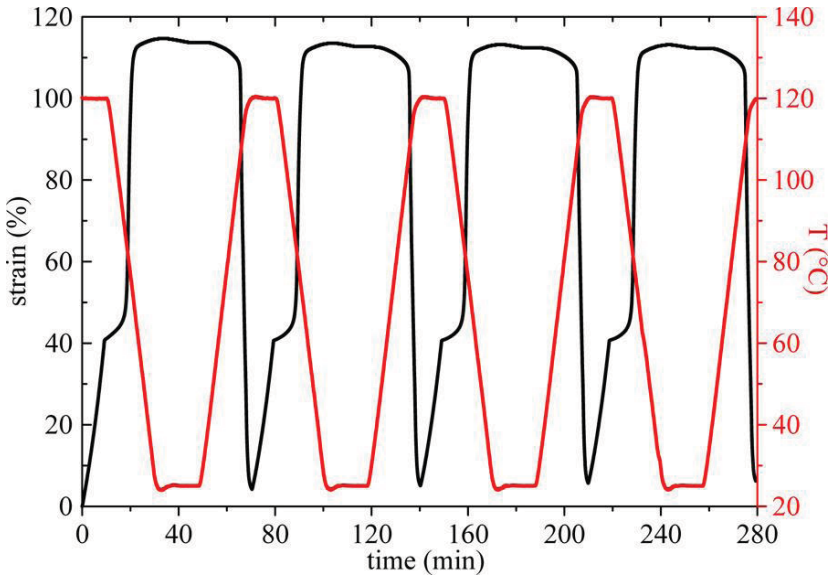

Figure 2.4 Consecutive dynamic mechanical analysis (DMA) curves of the dual SME of the polydibenzoate-based LCE. Reprinted with permission from Ref. 66. Copyright (2016) American Chemical Society.

2.2.3 Physically cross-linked polymers

The commonly known physically cross-linked glassy polymers consist of a physical cross-linking phase (high temperature transition phase) and a thermal transition phase (low temperature transition phase). Thus, when the sample is deformed above its T_{trans}, the physical cross-linking structure sets the permanent shape. Herein, dynamic bonds, such as extensive chain entanglements, hydrogen bonding, ionic interactions, metal-ligand coordination, and π–π stacking, may serve for physical cross-linking. They can be processed and reshaped when the temperature surpasses the flowing temperature of the sample. Inomata et al. reported that a dual shape memory behavior was drastically enhanced by grafting PEG onto a poly(methyl methacrylate) (PMMA) backbone in comparison to PMMA homopolymer.[67] A sustainable copolymer with a T_g at 1 °C poly(glucarodilactone undecenoate-*co*-isosorbide undecenoate) P(GDLU-*co*-IU) derived from glucose and castor oil displayed very good dual SMEs induced by physical cross-linking when the temperature was above its T_g (Figure 2.5).[68]

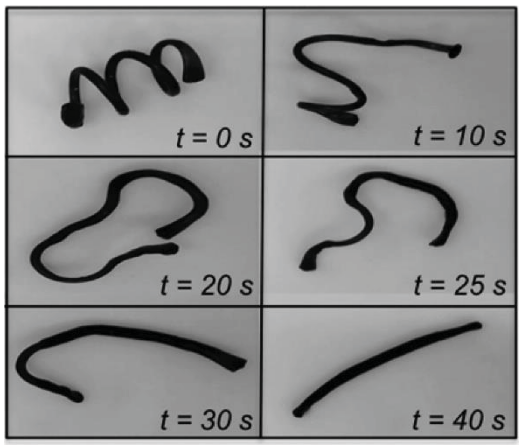

Figure 2.5 Recovery process of a dual SME in P(GDLU-co-IU) at 35 °C. Reprinted from Ref. 68 with permission. Copyright (2015) American Chemical Society.

For physically cross-linked semi-crystalline polymers, the thermal transition temperature (melting temperature T_m) is a relatively sharp transition in most cases. Like as chemically cross-linked semi-crystalline SMPs, the crystallization can fix the temporary shape below T_c, and melting of the crystalline phase above T_m allows the permanent shape recovered. One recent example of this kind of polymer is a family of high molecular weight PCL-PEG thermoplastic polyurethanes, which can recover their permanent shape from a highly-deformed shape (> 800%) (Figure 2.6). A temporary three-dimensional network formed by entanglements acted as physical cross-linking above T_m, thus preventing flow.[69]

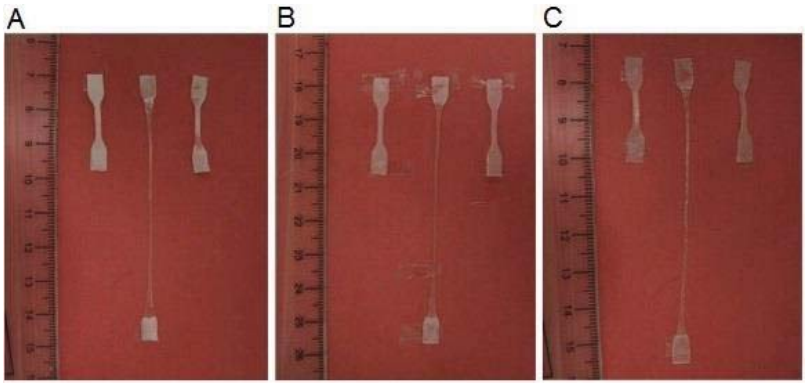

Figure 2.6 Dual SME of PCL–PEG polyurethanes: (A) PCL_{100}, (B) PCL_{50}–PEG_{50}, and (C) PEG_{100}. Reprinted from Ref. 69 with permission. Copyright 2012 from Elsevier Ltd.

Physically cross-linked liquid crystalline SMPs is similar to chemically cross-linked dual SMPs and can also be triggered by heating above T_{cl}. One representative example is a main-

chain thermotropic liquid crystalline polyester synthesized by polycondensation from mesogenic dial (4,4'-bis(6-hydroxyhexyloxy)biphenyl and 2-phenylsuccinic acid) (Figure 2.7A). This polyester exhibited a very good dual SME with a value of > 99% for both R_f and R_r (Figure 2.7B). The phenyl rings in the side groups form strong π–π interactions, preventing macroscopic sample flow when the temperature surpasses its T_{cl}.[70]

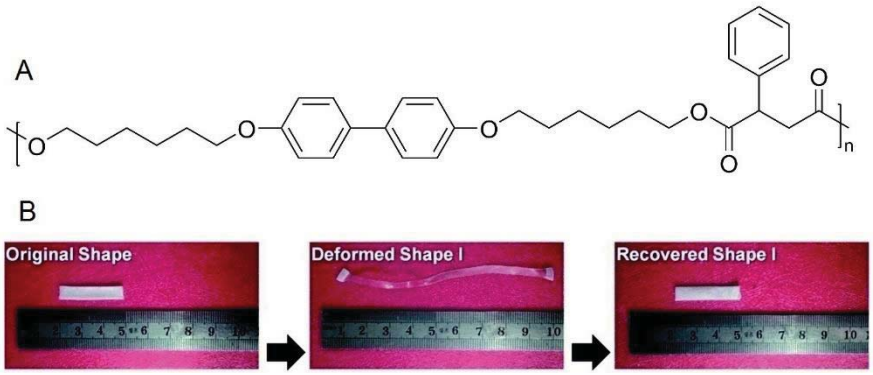

Figure 2.7 (A) Chemical structure of main-chain liquid crystalline polyester and (B) its shape recovery process. Adapted from Ref. 70 with permission. Copyright (2014) Royal Society of Chemistry.

2.3 Triple and multiple SMPs

2.3.1 Programming and mechanism

Triple SMPs are able to memorize three shapes (two temporary shapes and one permanent shape). This concept can also be extended to multiple SMPs, remembering more than two temporary shapes. Unlike the dual SME depending on only one thermal transition for one temporary shape, the triple and multiple SME is based on one broad or at least two separated thermal transitions, which may be a T_g, a T_m or a T_{cl}.

As shown in Figure 2.8, the programming procedures and molecular mechanism of the triple SME for polymers with two distinct T_{trans}s ($T_{trans1} < T_{trans2}$) are illustrated. When the permanent shape (ε_0) is first heated above both T_{trans}s, the mobility of all polymer chains is activated. The sample is deformed by applying an external stress, thus all elastic energies are stored. The deformed shape is then cooled between T_{trans1} and T_{trans2}, the polymer chains of the phase with high T_{trans} are frozen and the corresponding elastic energy is stored in the frozen

phase. After removing the external force, the unfrozen polymer chains will shrink to release the corresponding elastic energy at the temperature between T_{trans1} and T_{trans2}. Only the elastic energy of the phase with high T_{trans} is truly stored in the first temporary shape (ε_1).[71] This temporary shape is further deformed by imposing a second external force, and then cooled below T_{trans1}, where all polymer chains are frozen and the elastic energy is stored in the frozen sample. After releasing the external stress and keeping the same temperature, the second temporary shape is fixed (ε_2). For the recovery process, the sample is heated between T_{trans1} and T_{trans2}, the chain mobility of the phase with low T_{trans} is reactivated, and the corresponding stored elastic energy is released. The sample recovers its first temporary shape ($\varepsilon_{1,rec}$). Finally, the remaining elastic energy is also released above T_{trans2}, and the sample shrinks to its permanent shape ($\varepsilon_{0,rec}$). For quadruple SME, one more deformation, fixation and recovery procedure is performed. The molecular mechanism is similar to that of the triple SME.

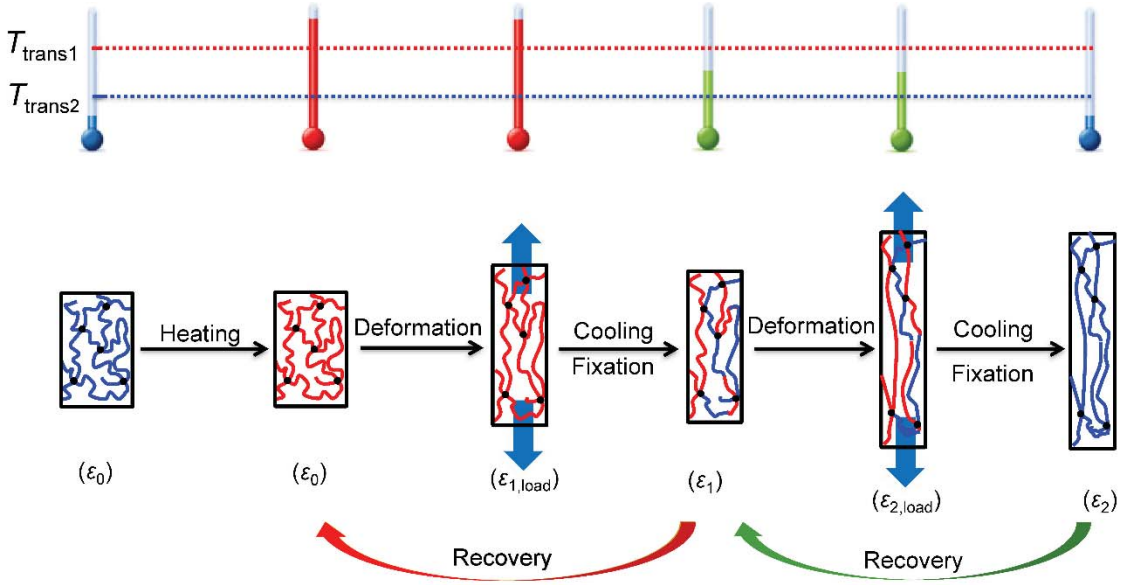

Figure 2.8 Schematic illustration and the molecular mechanism of a conventional triple shape memory cycle.

For triple and multiple SMPs, eqs (2.1) and (2.2) are expanded to eqs (2.3) and (2.4) for calculating R_f and R_r.[54]

$$R_f(X \rightarrow Y) = \frac{\varepsilon_Y - \varepsilon_X}{\varepsilon_{Y,load} - \varepsilon_X} \times 100\% \qquad (2.3)$$

$$R_r(\mathrm{Y} \rightarrow \mathrm{X}) = \frac{\varepsilon_Y - \varepsilon_{X,rec}}{\varepsilon_Y - \varepsilon_X} \times 100\% \quad (2.4)$$

where X and Y indicate two different shapes, $\varepsilon_{Y,load}$ is the maximum strain before removing the external force, ε_Y and ε_X represent fixed strains after cooling and unloading, and $\varepsilon_{X,rec}$ denotes the strain after recovery step.

2.3.2 Design strategies

In general, two strategies may be used to design a triple and multiple SME. The first one is to incorporate a broad thermal transition range into the polymer,[72,73] while the second one is to introduce two or more discrete thermal transitions into the polymer.[74] In general, any transitions in a polymer occur gradually within a temperature range, where a part of the transition phase is still hard while the rest is soft.[71] A broad thermal transition range can be regarded as an infinite number of transitions.[54] Therefore, the mechanisms of triple and multiple SMPs with a broad thermal transition are similar to those of triple and multiple SMPs with two or more distinct thermal transitions.

2.3.2.1 Triple and multiple SMPs with a broad transition

The first strategy to design triple or multiple SMPs is easy to realize since many polymers have been demonstrated to show broad thermal transitions. For example, Xie's group first exploited the multiple SME with a broad T_g based on a commercial polymer (Nafion, Figure 2.9).[54] They recently designed polyurethanes cross-linked through dynamic covalent bonds (transcarbamoylation) with one broad T_g, showing a good triple SME and permanent shape reconfigurability.[75] Miscible polymer blends could also meet the requirement of the first approach. Samuel et al. designed multiple SMPs using miscible poly(L-lactic acid) (PLLA)/PMMA blends with broad T_gs.[76] Multiple SMPs with a broad T_g can also be extended to random copolymers. Norbornene-based copolymers bearing cholic acid pendant groups exhibit good thermally-induced dual, triple, and quadruple SMEs.[77] Methacrylate-based copolymers with cholic acid and oligo(ethylene glycol) pendant groups showed both dual and triple SMEs. Cinnamic acid-based methacrylate monomer was incorporated into the copolymers followed by photo-cross-linking, and the resulting terpolymer shows improved

dual and triple SMEs and even very good quadruple SME.[55] Similarly, a compositional gradient copolymer may also exhibit excellent multiple SMEs.[78] Zhou and coworkers reported one type of star-shaped polyurethane with a wide T_m range, resulting in an excellent triple SME.[79]

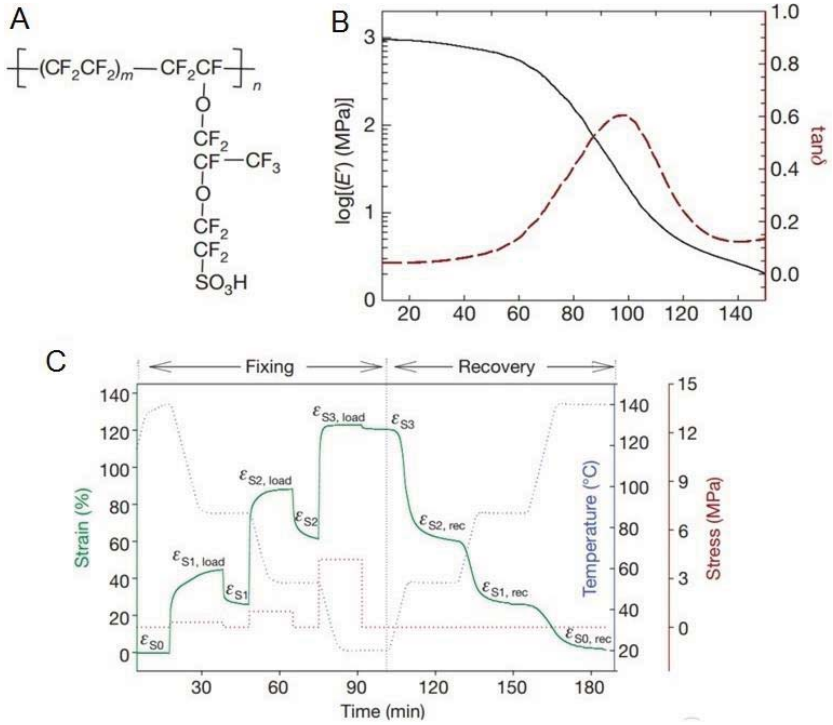

Figure 2.9 (A) Molecular structure of Nafion; (B) dynamic mechanical analysis curve; and (C) quantitative thermal mechanical cycle of a quadruple SME. Reproduced from Ref. 54 with permission. Copyright 2010 from Nature Publishing Group.

2.3.2.2 Triple SMPs with two transitions

The second strategy for designing triple SMPs may have a combination of two different thermal transitions, such as (1) two melting transitions, (2) one glass transition and one melting transition, (3) two glass transitions, and (4) one glass transition and one liquid crystalline transition.

Behl and Lendlein first reported a triple SMP with two semi-crystalline phases in a CLEG network obtained by introducing PEG segments as side chains with one end dangling into a PCL network (Figure 2.10).[80] Wang and coworkers synthesized poly(ε-caprolactone)/poly(p-dioxanone) (PCL/PPDO) interpenetrating polymer networks with two well-separated melting

peaks, endowing the polymer with an excellent triple SME.[81] Two semi-crystalline polymer blends were also reported to show triple SME. Cuevas and coworkers blended two semi-crystalline polymers (polycyclooctene and polyethylene, PE), followed by covalent cross-linking with the cross-linker, dicumyl peroxide, endowing a triple SME with excellent recovery ratios up to 95－100%.[82] In a similar way, Zhao et al. fabricated chemically cross-linked PE/polypropylene (PP) blends, showing the triple SME due to the two melting transitions.[83] Doping a liquid crystal mesogen into a semi-crystalline SMP may also be used to fabricate this type of triple SMP. Chen and coworkers incorporated hexadecyloxybenzoic acid (HOBA) into poly(1,6-hexamethylene adipate)-based shape memory polyurethane (SMPU) with a T_m transition for preparing a liquid-crystalline triple SMPU. This composite exhibited a triple SME owing to the T_m of the SMPU, the T_m of HOBA, and a self-healing property due to the melting of HOBA under a heating-cooling cycle.[84]

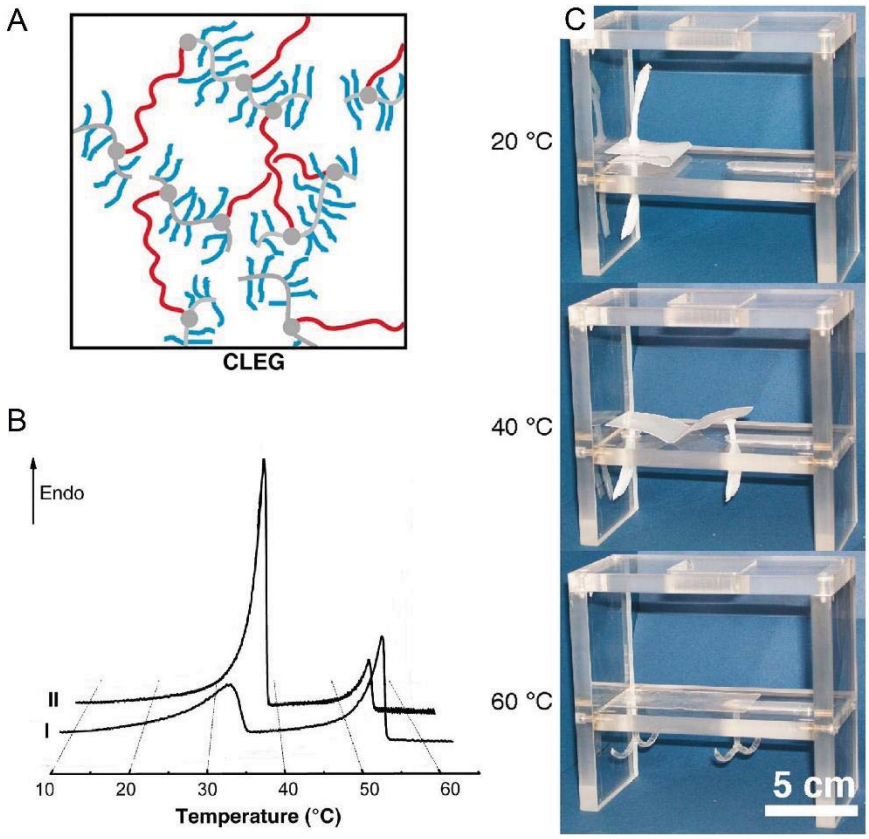

Figure 2.10 (A) Architecture of CLEG polymer network (red: PCL segments; blue: PEG side chains; gray: cross-links); (B) DSC curves: I, CL(60)EG; II, CL(30)EG; (C) series of photographs illustrating the triple shape effect of CL(50)EG (heating to 40 °C and 60 °C).

Reproduced from Ref. 80 with modification. Copyright (2006) National Academy of Sciences, U.S.A.

For triple SMPs containing a soft segment T_m of and a hard segment T_g, Lendlein and coworkers reported that MACL consisting of poly(cyclohexyl methacrylate) chains cross-linked by PCL segments with one glass transition and one melting transition shows a thermally-induced triple SME.[80] Zhou and coworkers synthesized a PCL-based polyurethane bearing cinnamate groups. This polymer has one T_m and one T_g and shows a triple shape memory after the cinnamon pendants are photo-cross linked (Figure 2.11).[85] Wang's group fabricated PDLLA-Poly(tetramethylene ether) glycol (PTMEG) networks via the photo-cross linking of anthracene groups, in which the T_m of the PTMEG segment and the T_g of the PDLLA segment were utilized as T_{trans} to endow the polymer network with a triple SME.[86]

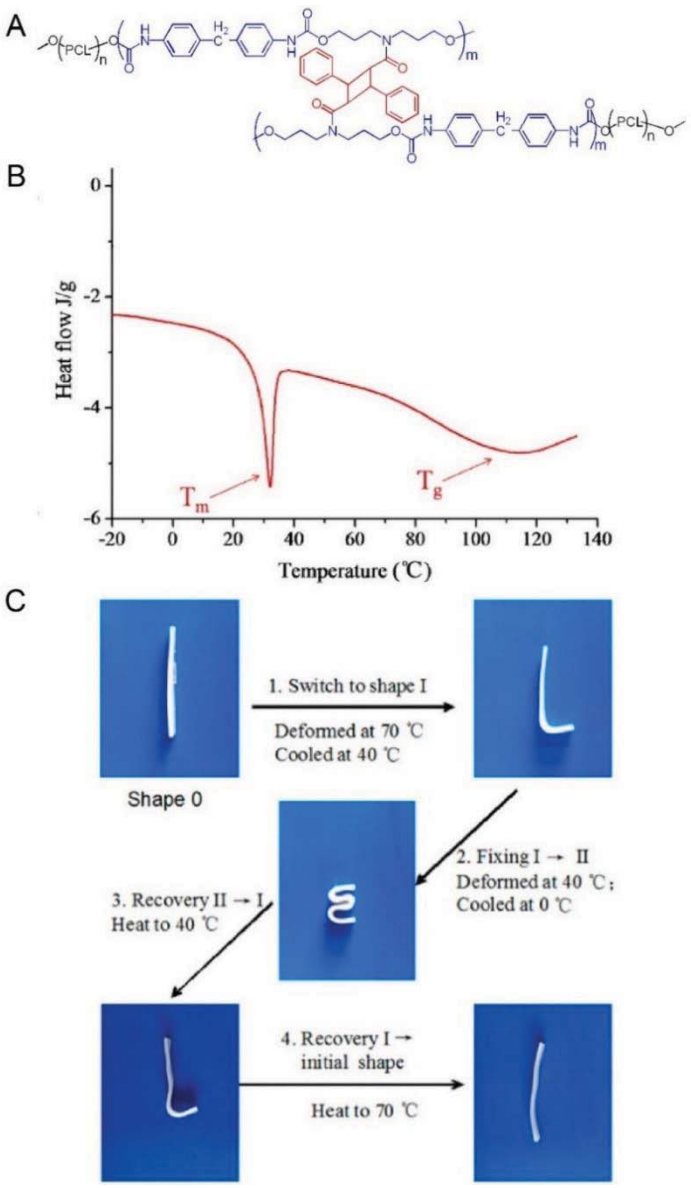

Figure 2.11 (A) Molecular structure, (B) DSC curves, and (C) shape fixing and recovery of triple shape memory polyurethanes. Reprinted from Ref. 85 with modification. Copyright (2013) American Chemical Society.

Reports on triple SMPs based on two T_gs are scarce. One example is a material with two interpenetrating polymer networks formed by sequential, selective thiol-Michael addition reactions, exhibiting a triple SME due to the two separate T_gs (10 and 60 °C) (Figure 2.12).[87] The other example concerns bilayer polymers consisting of two epoxy dual SMPs of well-separated T_gs, displaying a triple SME.[88]

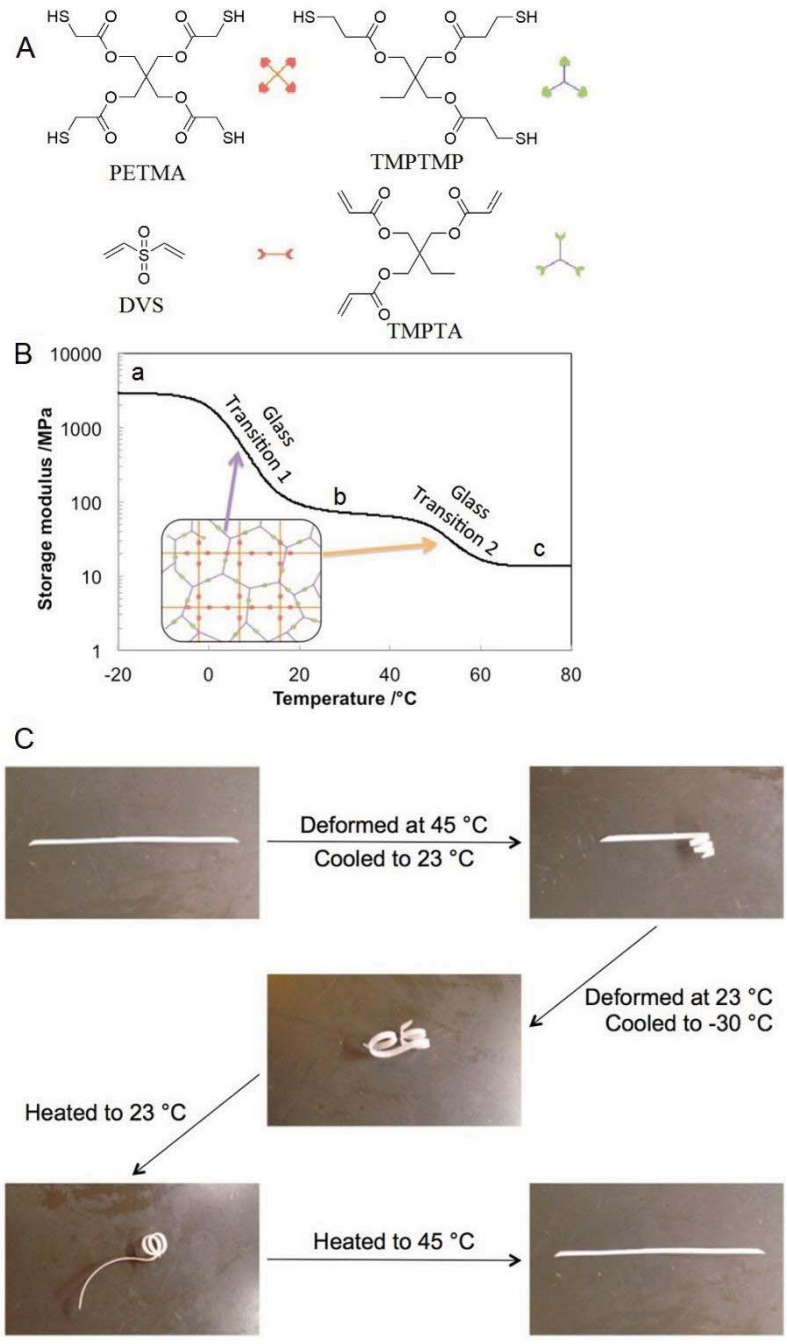

Figure 2.12 (A) Chemical structures of the monomers for the preparation of SMPs, (B) the storage modulus and (C) triple SME of the polymer networks. Reproduced from Ref.87 with modification. Copyright (2014) American Chemical Society.

Triple SMPs can also be based on one T_g and one liquid crystal T_{cl}.[89-94] Ahn and coworkers synthesized side-chain liquid crystalline random terpolymer networks by the use of three

monomers, serving as liquid crystal unit, cross-linker and plasticizer, via ring-opening metathesis polymerization. The polymer network showed the discrete T_g and T_{cl}, endowing triple SME.[89-91] More recently, Wen et al. fabricated a series of side-chain liquid crystalline SMPU networks containing 4'-hydroxy-4-biphenylcarbonitrile mesogenic unit (Figure 2.13A). The distinct thermal transitions (T_g and T_{cl}) of the SMPU served as T_{trans} for triggering a triple SME (Figures 2.13B and C).[92] This type of triple SMP can also be designed by simply doping mesogenic molecules into a glassy SMP to achieve an additional phase transition. One example is a supramolecular side-chain liquid crystalline polymer, which was prepared by tethering two azobenzene mesogens to poly(4-vinyl pyridine) through H-bonding. The supramolecular complex exhibited a thermally induced triple SME governed by a T_g and a T_{cl}.[93] Similarly, Chen and colleagues prepared a series of liquid crystalline SMPU complexes by mixing a liquid crystal mesogen, 4-hexadecyloxybenzoic acid (HOBA), with various SMPUs. The HOBA was tethered to the SMPU via strong H-bonding between the SMPU and the HOBA. These complexes displayed a triple SME due to the two distinct thermal transitions.[94,95]

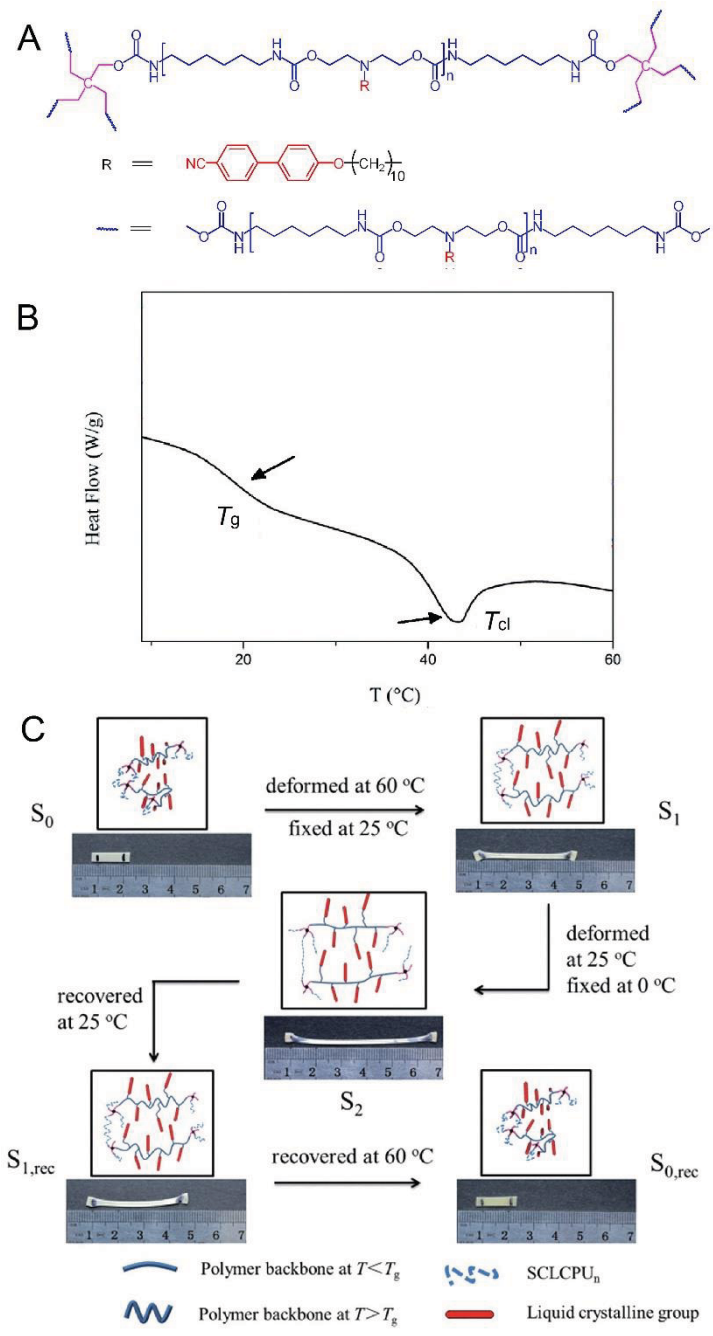

Figure 2.13 (A) Molecular structure, (B) DSC heating curves, and (C) visual triple SME of liquid crystalline SMPU. Reproduced from Ref. 92 with modification. Copyright (2015) Royal Society of Chemistry.

2.3.2.3 Multiple SMPs with three or more transition temperatures

Multiple SMPs with three or more thermal transitions were reported rarely due to the limitation of complex multiphase incorporation in one polymeric material. Kolesov et al. designed cross-linked binary and ternary polymer blends with two or three crystalline phases, which show triple and quadruple SMEs, respectively.[96] More recently, Wang's group synthesized a series of linear multiblock copolymers containing PCL segments and liquid crystal segments in the main chain (Figure 2.14A). The multiblock copolymers possessed two well-separated T_gs (25 and 44 °C), one for each phase-separated segment, one T_{cl} (66 ºC) for the liquid crystal segment, and one T_m (156 ºC) for the PCL segment (Figure 2.14B). As shown in Figure 2.14C, the two distinct T_gs and one T_{cl} were used as T_{trans}s to trigger quadruple SME.[97] The incorporation of a broad thermal transition and a separated thermal transition into a polymer network could also be used to design multiple SMPs. A typical example is that Li et al. fabricated a quintuple SMP using PMMA/PEG semi-interpenetrating polymer networks with a broad T_g range (45 – 125 ºC) and an additional T_m (~30 ºC) from the PEG crystallites.[98]

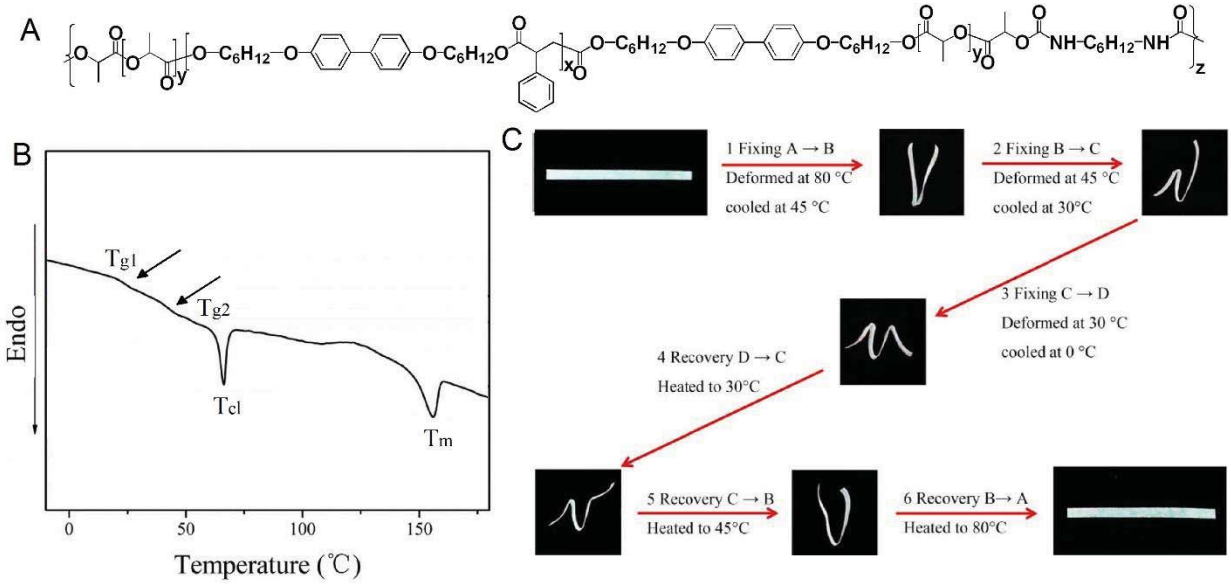

Figure 2.14 (A) Chemical structure, (B) DSC heating curves, and (C) visual quadruple SME of a PCL-based multiblock copolymer. Reproduced from Ref. 97 with modification. Copyright (2016) American Chemical Society.

Moreover, some polymers are composed of three or more distinctly different parts in the material, in which each part is designed to have a different T_{trans}. For example, Zhuo et al. synthesized a series of random copolymers with different molar ratios of 2-methoxyethyl acrylate (MEA) and N-methylol acrylamide (HAM) (Figure 2.15A). The T_gs of the resultant copolymers with 30, 50, and 70 mol% HAM were 7.5, 33.1, and 55.2 °C, respectively (Figure 2.15B). A sample combined the above three copolymer regions using a multiple-step polymerization method, and it exhibited a quadruple SME due to the different T_gs of each region (Figure 2.15C).[99]

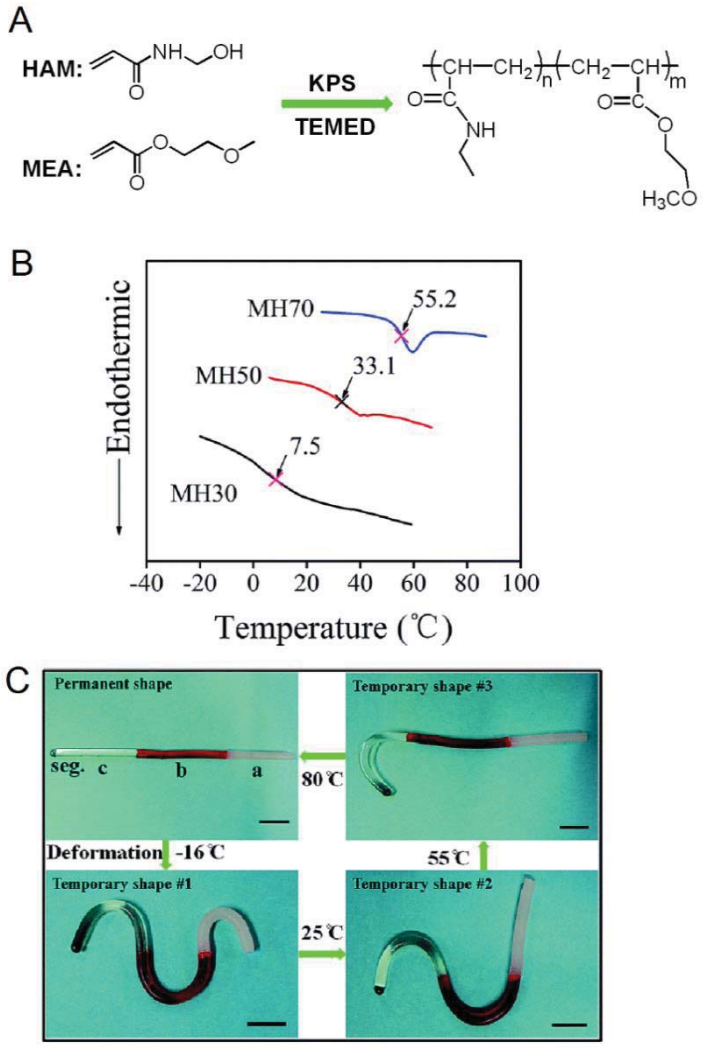

Figure 2.15 (A) Synthetic route; (B) DSC profiles; and (C) quadruple SME of the three region sample consisting of 30, 50, and 70 mol% HAM. Reproduced from Ref. 99 with modification. Copyright (2016) Royal Society of Chemistry.

2.3.3 Types of cross-linking

Like for the dual SME, a higher cross-linking density leads to a higher recovery ratio. Triple and multiple SMPs can also be classified according to the nature of the cross-linking, either chemical or physical cross-linking, or a combination of both.

Chemically cross-linked polymers. The chemically cross-linked polymer blends in Ref. 82 and 83 discussed above possess two separated T_ms, endowing good triple SMEs. Similarly, Wang et al. prepared chemically cross-linked polycyclooctene−multiwalled carbon nanotube (MWCNT)/PE nanocomposites, endowing electrically and thermally actuated triple SMEs.[100] Photo-cross-linking polymer networks were also designed to show triple SMEs.[55,85,86] Chemically cross-linked PPDO-PEG networks were synthesized by coupling an OH-terminated PPDO prepolymer having three arms and PEG-diol with 1,6-hexamethylene diisocyanate. They exhibited excellent dual and triple SMEs because of the two separated T_ms of the phase-sepatated PPDO and PEG segments.[101]

Physically cross-linked polymers. A polyurethane network made of PCL diol, 4,4-diphenylmethane diisocyanate, propionic acid and pentaerythritol was shown to form strong hydrogen bonds between the COOH of propionic acid in the polymer and pyridine ring of the mesogenic units (cholesteryl isonicotinate), endowing a triple shape memory effect.[102] Partially zinc-neutralized poly(ethylene-*co*-methacrylic acid), a semi-crystalline ionomer with a broad T_m arising from ionic interactions of the metal salt groups in the ionomer, exhibits dual, triple, and quadruple SMEs.[103] Zwitterionic polyurethanes display not only dual, but also triple and quadruple SMEs owing to the strong hydrogen bonding and electrostatic forces.[104,105]

Combination of chemically and physically cross-linked polymers. The combination of covalent cross-linking and hydrogen bonding were also used to design triple SMPs. For example, PCL/PPDO interpenetrating polymer networks comprised of self-complementary hydrogen bonding and covalent cross-linking show very good triple SMEs.[81] Ware et al. synthesized a triple SMP from the copolymerization of alkyl acrylates, bisphenol A ethoxylate diacrylate and 2-ureido-4-pyrimidine (UPy)-functionalized acrylate. The combination of a chemical cross-linked (meth)acrylate network and a hydrogen-bonded network yielded triple SMPs based on their glass transition and the dissociation of the hydrogen bonds. Here, the

disruption of the hydrogen bonds can also be considered as a thermal transition, because the polymer chains have so differet chain mobilities when the sample is cooled below or heated above the dissociation temperature of hydrogen bonds. Thereby, the T_g and this dissociation temperature worked as two separated thermal transitions, while the chemical cross-linking was used for fixing a permanent shape.[106]

2.4 Two-way reversible SMPs (2W-SMPs)

All the SMPs mentioned above are one-way SMP with one-directional shape recovery to finally reach its permanent shape. 2W-SMP can vary between two or more distinct "permanent" shapes under two different external stimuli.[45,107] Two-way reversible shape memory effects (2W-SMEs) can be classified into two categories: 2W-SME under stress and stress-free conditions. An external force is loaded in both cases after the temperature is raised above the T_ms or T_{cl}s of all segments of the sample, which is then deformed and cooled below the T_cs ot T_{cl}s of all segments. For the stress condition, this force is maintained (Figure 2.16A); for the stress-free condition, the external force is removed at this point (Figure 2.16B), overcoming the limitations of the external stress. Thereby, the 2W-SME under the stress-free condition can be more versatile in its applications. Both 2W-SMEs are based mainly on crystallization-induced elongation (CIE) upon cooling and melting-induced contraction (MIC) upon heating, expect the case of 2W-SME under stress-free conditions based on laminated polymer structure.

2.4.1 2W-SME under stress conditions

2.4.1.1 Programming and mechanism

2W-SMPs were found to be a LCE or a semi-crystalline polymer network. The programming procedures and mechanism of the 2W-SME under stress condition is summarized in Figure 2.16A. The sample is first heated above its T_m, all crystals are melted, resulting in the reactivation of all polymer chains. The sample is then deformed to a high temperature strain (ε_H) under a constant stress, resulting in a reduced entropy of polymer chains, which in turn yields a contraction force. Finally, a stress balance is achieved between the stretching stress and the contraction force. If the sample is cooled below its T_c, the

contraction force decreases because of the reduced chain mobility, thereby, resulting in an elongation of the material occurs due to the crystallization of polymer chains along the stretching direction, leading to a low temperature strain (ε_L). The polymer chains in the crystalline phase are frozen, and their entropy is trapped, and the related elastic energies are stored. When the sample is heated above its T_m, the crystalline phase is melted, releasing the entropy-related elastic energy and producing another contraction force. At this moment, the contraction force is greater than the stretching force due to the further reduced entropy. The sample contracts until these two forces reach a balance, leading to a high temperature strain (ε_H). This phenomenon is called MIC. When the sample is cooled below its T_c again, the contraction force decreases. The polymer chains crystallize along the stretching direction, resulting a further elongation (ε_L). Thus, in the crystalline polymer system, 2W-SME is based on the CIE upon cooling and MIC upon heating under a non-zero tensile stress condition.[108] An elongation similar to CIE of the crystallizable polymers may also occur due to the anisotropization of a LCE below its T_{cl}. Likewise, a contraction similar to MIC will occur when LCE is heated above its T_{cl}.[109] The sample undergoes a reversible elongation-contraction transition upon cooling or heating the sample below T_c or T_{cl} and above T_m or T_{cl}.

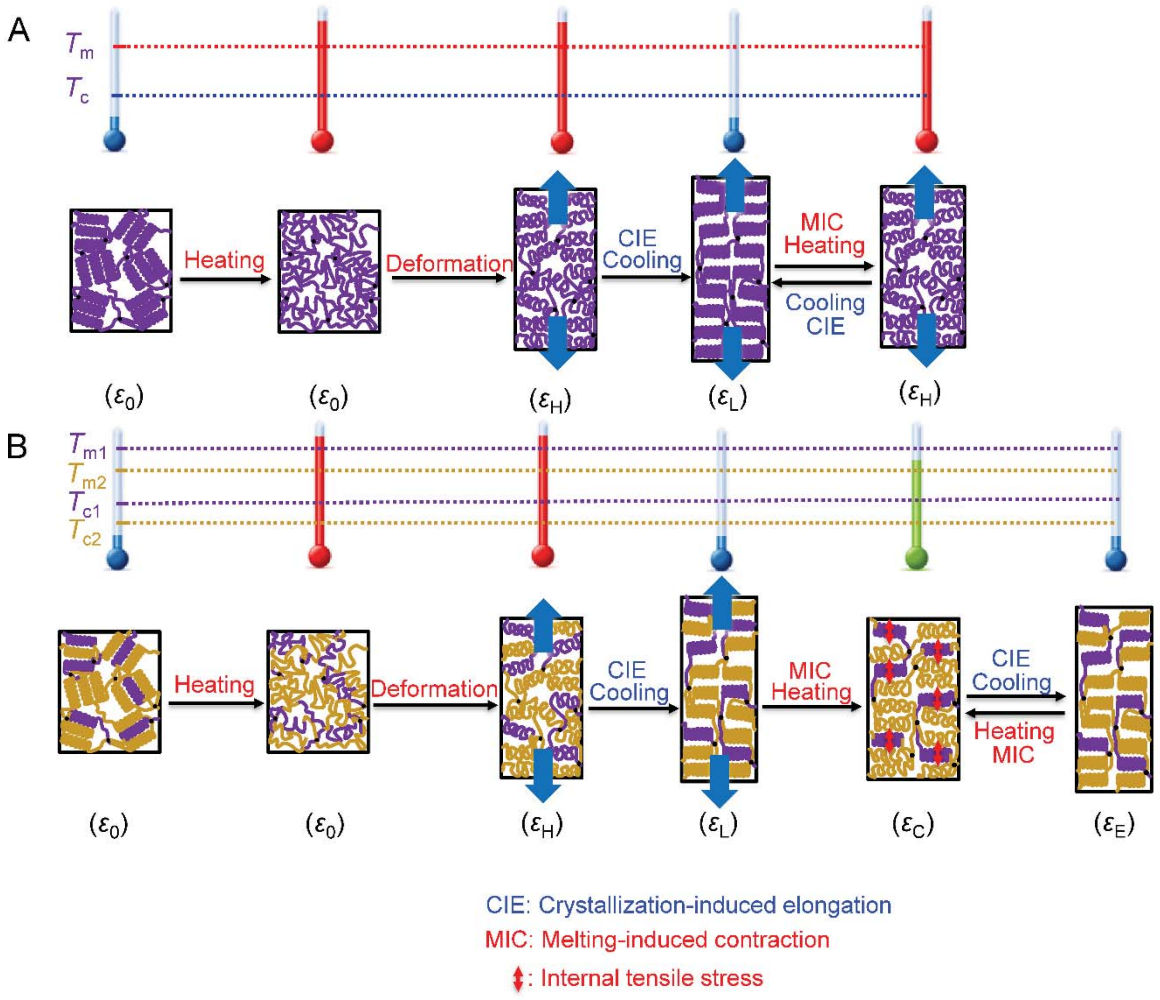

Figure 2.16 Schematic illustration and the molecular mechanism of two-way reversible SME under (A) stress and (B) stress-free conditions.

For the quantification of 2W-SME under stress condition, two parameters, the absolute strain change (ε'_s) and the relative strain change (ε''_s), are utilized to calculate the characteristics of 2W-SME. They are defined as[110]

$$\varepsilon'_s = \varepsilon_L - \varepsilon_H \tag{2.5}$$

$$\varepsilon''_s = \frac{\varepsilon'_s}{\varepsilon_L} \times 100\% \tag{2.6}$$

where ε_H is the strain at high temperature (deformation temperature) before cooling and ε_L is the maximum strain after CIE.

2.4.1.2 Liquid crystalline elastomers (LCEs)

LCEs have been long known to show 2W-SME under stress conditions. Ratna and coworkers designed two nematic side chain LCEs in 2001 and observed reversible strain elongation and contraction under a stress of 210 kPa.[111] Mather's group fabricated a liquid crystalline network by cross-linking a thermotropic unsaturated polyester, which possessed a T_g of 80 °C and a T_{cl} of 156 °C, endowing the polymer network with 2W-SME under stress condition and one-way triple SME.[112-116] They also synthesized a series of main-chain smectic-C LCEs with various cross-link densities through the control of prepolymer molecular weight, showing 2W-SME under stress condition. The reversible strain increased with increasing external load and cross-linking densities, reaching up to 30%.[113] More recently, Mather and co-workers fabricated a liquid crystalline hydrogel from a liquid crystalline diene and PEG-based dithiol. The LCE was demonstrated to show thermo- and water-induced dual SMEs and 2W-SME under stress condition.[114] Wang et al. synthesized monodomain polysiloxane-based LCE films through two-stage photo-cross-linking method, displaying 2W-SME under stress condition (Figure 2.17).[115] Lama and colleagues prepared a series of smectic epoxy-based elastomers incorporating various amounts of MWCNTs. The polymer nanocomposites possess a T_g and a T_{cl}, endowing the polymers with both one -way triple SME and 2W-SME under stress condition. The actuation temperatures (T_As) and the stress threshold required to trigger 2W-SME could be controlled by choosing the content of CNTs.[116]

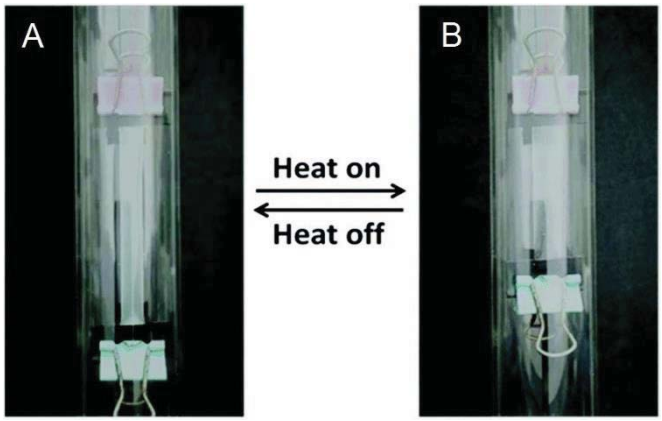

Figure 2.17 Digital photos showing 2W-SME under stress condition of a polysiloxane-based LCE film (A) at room temperature and (B) heated above its T_{cl}. Reprinted from Ref. 115 with permission. Copyright 2017 Royal Society of Chemistry.

2.4.1.3 Semi-crystalline polymer networks

However, the synthesis of LCEs is not trivial and represents a notable drawback for their widespread application. Mather's group extended the 2W-SME to cross-linked semi-crystalline polymer networks, where chemically cross-linked polycyclooctene exhibit 2W-SME with various constant external stresses, and the reversible strain change may be tuned by changing the external stress (Figure 2.18).[117]

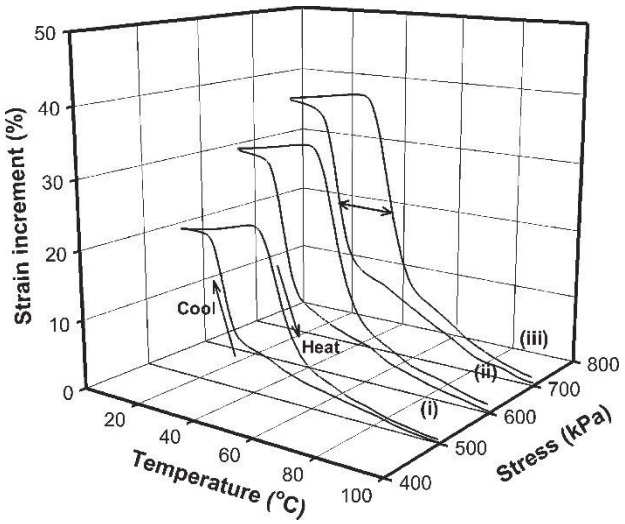

Figure 2.18 Strain increment of 2W-SME under stress condition for cross-linked polycyclooctene with different external stresses: (i) 500, (ii) 600, and (iii) 700 kPa. Reprinted with permission from Ref. 117. Copyright (2008) American Chemical Society.

Subsequently, 2W-SMPs under stress condition were also reported by other groups in semi-crystalline polymer networks. Xie et al. reported that semi-crystalline poly(ethylene-*co*-vinyl acetate) networks with various cross-linking densities show 2W-SME, and the absolute strain change increases linearly with the external stress and decreases with cross-linking density under the same stress.[110] In addition, a set of semi-crystalline PCL systems, such as the PCL/polyhedral oligosilsesquioxane (POSS) chemical/physical double networks,[118] shape memory polyurethanes,[119] cross-linked PCL-*co*-PEG foams,[120] and chemically cross-linked PCL,[121-124] have been shown to display 2W-SMEs under a suitable constant stress. Bai and colleagues extended 2W-SME to a tough (high Young's modulus) PCL polymer network.[125] Similarly, Kolesov and coworkers also studied 2W-SME of cross-linked polyethylenes with different degrees of branching and/or linear PE. The crystalline structure and morphology were also investigated during two-way shape memory cycles. They found that the specific crystalline texture of the samples comprise lamellae, whose folded chains are tilted to the basal surface of lamellae.[126] Lendlein's group extended the concept of 2W-SME to two-way reversible triple SME, which switched between three distinct "permanent" shapes under four different external stimuli. In this system, a polyurethane network of PCL and poly(*ω*-pentadecalactone) (PPDL) segments was prepared. This semi-crystalline network has two distinct T_ms ($T_{m,PCL} \approx 34$ °C, $T_{m,PPDL} \approx 64$ °C) and varies reversibly among three shapes with a constant external loading,[127] but the requirement of an external force limits their potential applications.

2.4.2 2W-SME under stress-free condition

For this kind of 2W-SME, the sample can switch between two distinct shapes upon two different external stimuli without external stress, overcoming the problem of requiring constant tension (Figure 2.16B). It has been pursued in the SMP community for many years. Based on the preparation method and the nature of cross-linking, 2W-SMPs may be subdivided into four categories: (1) laminated polymer composites, (2) chemically cross-linked semi-crystalline polymer networks with one broad T_m or two T_ms, (3) semi-crystalline polymer networks prepared via a two-stage cross-linking method, and (4) thermoplastic semi-crystalline polymers with one broad T_m or two T_ms. The programming procedures and molecular mechanisms of each category are not the same; thus they are discussed separately.

2.4.2.1 Laminated polymers

Firstly, some laminated structures with double SMP layers may exhibit this type of 2W-SME.[128-130] Imai and Sakurai used two SMP layers with two different T_gs ($T_{g1} < T_{g2}$), which are glued together with adhesive. The memory shape relating to T_{g1} was first formed upon heating above T_{g1}. After heating to T_{g2}, the memory shape relating to T_{g2} cancelled the memory shape of T_{g1} since the memory shape of T_{g2} was set to be the reverse shape of the memory shape of T_{g1}. Then the sample was returned to its original shape which was maintained after cooling below T_{g1}. When the sample was heated above T_{g1}, the memory shape of T_{g1} was formed again.[128] Kang et al. prepared 2W-SMPs by combining a poly(styrene-butadiene-styrene) (SBS) elastomer containing curing agents with a SMPU. As shown in Figure 2.19, the SMPU/SBS core/shell composite prepared was first deformed at a temperature higher than T_{trans} of SMPU. The composite was then cooled down under constant strain conditions, and the temporary shape was fixed. After that, the SBS shell was cured using UV light for removing the force history of the shell. After unloading, the composite contracted due to the relaxation of the SMPU upon heating. At the same time, a compressive force was exerted on the cured shell, producing a tensile force. For the subsequent cooling, the composite extended because the tensile force resulted in CIE.[129] The reversible strain change is usually very small (< 10%) in laminated structures.

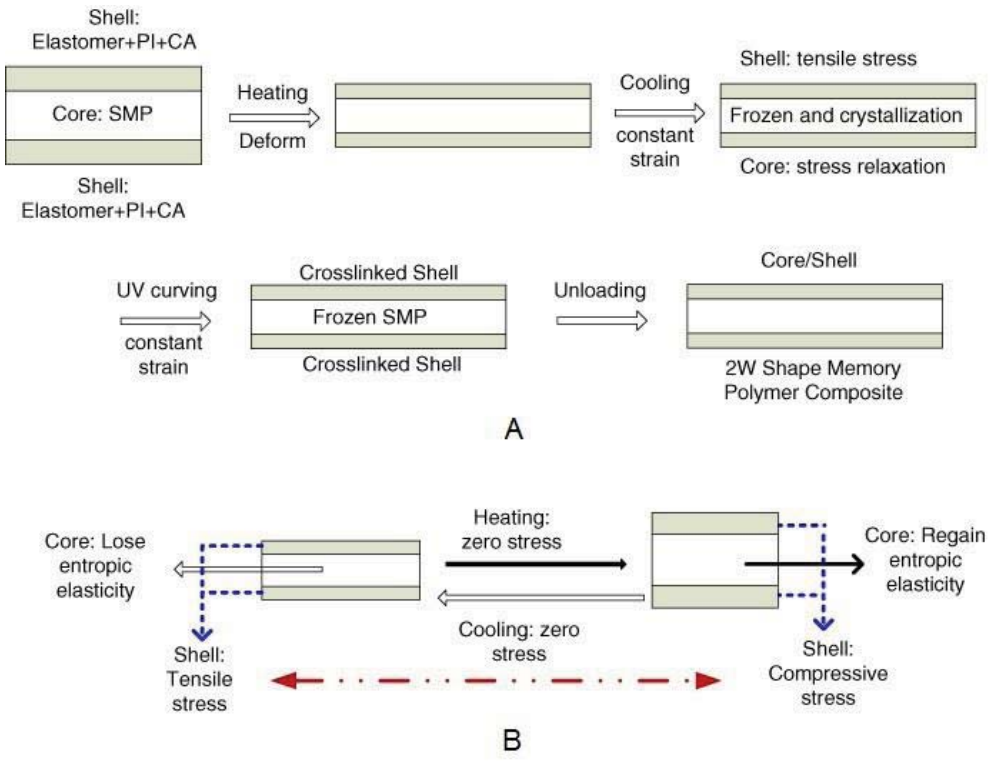

Figure 2.19 (A) Preparation process of 2W-SMP composite and (B) the mechanism of 2W-SME. Reprinted with permission from Ref. 129. Copyright 2012 IOPscience.

2.4.2.2 Chemically cross-linked semi-crystalline polymers

The second type of 2W-SME under stress-free condition is realized on semi-crystalline polymer networks with one broad T_m or two T_ms. The programming procedures and the molecualr mechanism of this type of 2W-SME are the same as those of 2W-SME under stress condition before the second heating step. As shown in Figure 2.16B, after CIE, the deformation stress is unloaded, and then the sample is heated to a T_A between the two distinct T_ms or in the T_m range. One part of the crystalline phase is melted and the other part is unchanged in the polymer network. The entropy of the polymer chains relating to the lower T_m tends to increase (i.e., the polymer chains tend to relax), yileding an contraction force. The sample contracts, and the contraction force decreases. Simultaneously, the remaining crystalline phase is compressed, producing an increasing internal tensile force. The sample, finally, contracts to an intermediate shape (ε_C) until these two forces are equal. When the

specimen is cooled below its T_c, the chain mobility decreases. The polymer chains crystallize along the stretching direction, resulting in an further elongation (ε_E).

To be consistent with 2W-SME under stress condition, the same two parameters, the absolute strain change (ε') and the relative strain change (ε'') are used to quantify the characteristics of this type of 2W-SME under stress-free condition. Thus, eqs (2.5) and (2.6) are extended to

$$\varepsilon' = \varepsilon_E - \varepsilon_C \tag{2.7}$$

$$\varepsilon'' = \frac{\varepsilon'}{\varepsilon_L} \times 100\% \tag{2.8}$$

where ε_E is the strain after CIE without stress, ε_C is the strain after unloading and heating to T_A, ε_L is the maximum strain after CIE.

Lendlein's group found that the same polymer network as in Ref. 127 exhibited 2W-SME under stress-free condition. The key element is the separation of the "shifting-geometry determining function" (which determines the shape shifting geometry, controlld by the PPDL crystalline phase with its higher T_m) from the "actuator function" (which expands during cooling and collapses during heating, controlled by the PCL crystalline phase with its lower T_m) on the level of phase morphology. The actuator domains extend during cooling and contract during heating in the direction determined by the shifting-geometry determining domains.[131] Sheiko's group reported that a cross-linked semi-crystalline elastomer, poly(octylene adipate) (POA), with one crystalline phase exhibits 2W-SME. When the sample is heated to the midpoint of the melting range, the melted part of the crystalline phase works as the actuator domains and the still-crystallized part plays the role of the shifting-geometry determining domain.[132] Subsequently, they found that two-way shape memory properties (the degree of reversibility and shape recovery rate) increased with increasing cross-linking density.[133] Zhou and coworkers designed a cross-linked polymer network containing well-defined six-arm PEG-PCL, exhibiting 2W-SME under stress-free condition with the cyclic heating and cooling between 43 and 0 °C (Figure 2.20).[134] Chen et al. found that commerical poly(ethylene-*co*-vinyl acetate) (EVA) semi-crystalline elastomers exhibited 2W-SME under both stress and stress-free conditions.[135] A $\varepsilon_{c,s}$ value of 6.7% was obtained with a cross-linking

density of 212 mol/cm^3, while no 2W-SME under stress-free condition was observed with a cross-linking density of 126 mol/cm^3.[136] Our group recently synthesized tunable T_ms of random copolymers with various molar ratios of cocrystallizable monomeric units (CL and PDL). The polymer network was made by cross-linking two random copolymers which exhibited excellent 2W-SME under both stress and stress-free conditions (Figure 2.20). The T_A of 2W-SMEs under stress-free condition may be tuned in a broad range by selecting a mixture of prepolymers followed by photo-cross-linking.[137] Its memory shapes can be erased upon heating to a temperature above both T_ms and reprogrammed to other shapes.

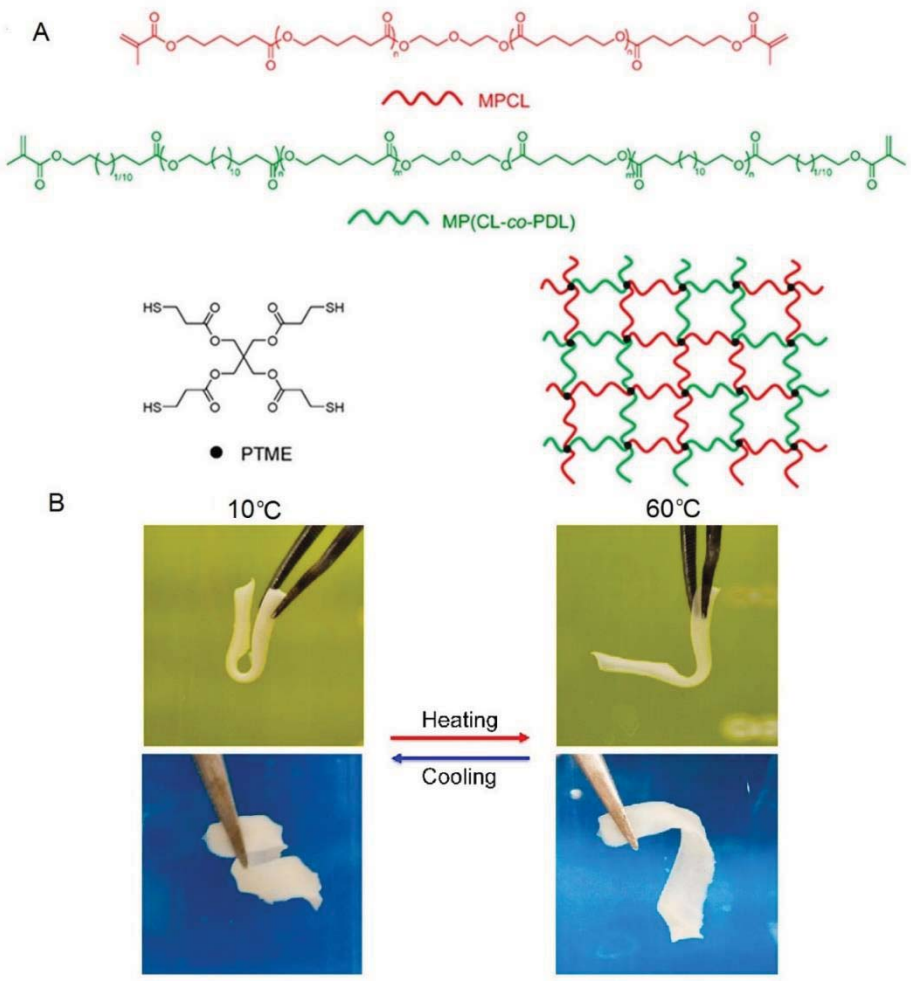

Figure 2.20 (A) Chemical structure, and (B) 2W-SME under stress-free condition of the polymer network made by cross-linking a mixture of homopolymer PCL and random copolymer P(CL-*co*-PDL)$_{1:2}$ (2:1 weight ratio). Adapted with permission from Ref. 137. Copyright (2017) American Chemical society.

2.4.2.3 Polymer networks prepared via the two-stage cross-linking method

A two-stage cross-linking strategy was also used to fabricate a 2W-SMP. As shown in Figure 2.21, the mixture of epoxy terminated PTMEG, 2-hydroxyethyl acrylate terminated PCL and cross-linkers was irradiated for pre-curing. After evaporation, the gel-like film was stretched and then heated for the second cross-linking. In this case, an interpenetrating network was obtained with a crystalline phase (responsible for the reversible shape shrinkage at high temperature) and an elastomeric component (providing the stretching force for shape extension during the cooling process). As shown in Figure 2.21, the original polymer was heated above the T_m of PCL (B_1), leading to a shrunken shape (B_2). When the polymer was cooled to room temperature, the sample recovered its original shape (B_3). One of the key factors in this work is to pre-program in the synthesis process, so that the sample cannot be reprogrammed to other shapes.[107] Meng et al. fabricated 2W-SMPs by stretching a melted pre-cross-linked PCL network followed by UV irradiation for further cross-linking. When the load was removed above T_m, the polymer network balanced to an intermediate shape, which was between the original and load-bearing shape. When cooled, internal stress induced crystallization, leading to elongation of the sample. Upon heating, the sample returned to its equilibrium shape due to the relaxation of melting molecular chains.[138] Similarly, Fan et al. designed a 2W-SMP by two-step cross-linking of SBS/PCL based PU blend, in which the separated SBS phase provided the internal expansion stress.[139] This method may also be extended to LCEs and their composites. Yang's group synthesized a polysiloxane-based side-chain LCE containing azobenzene incorporated with 1 wt% single-walled CNTs (SWCNTs) through two-step cross-linking process, presenting 2W-SME under stress-free condition.[140] As mentioned above, the polysiloxane-based LCE films were also prepared via the two stage curing method, exhibiting 2W-SME under stress-free condition.[115] For this type of 2W-SMP, its memory shapes are fixed and cannot be erased upon heating.

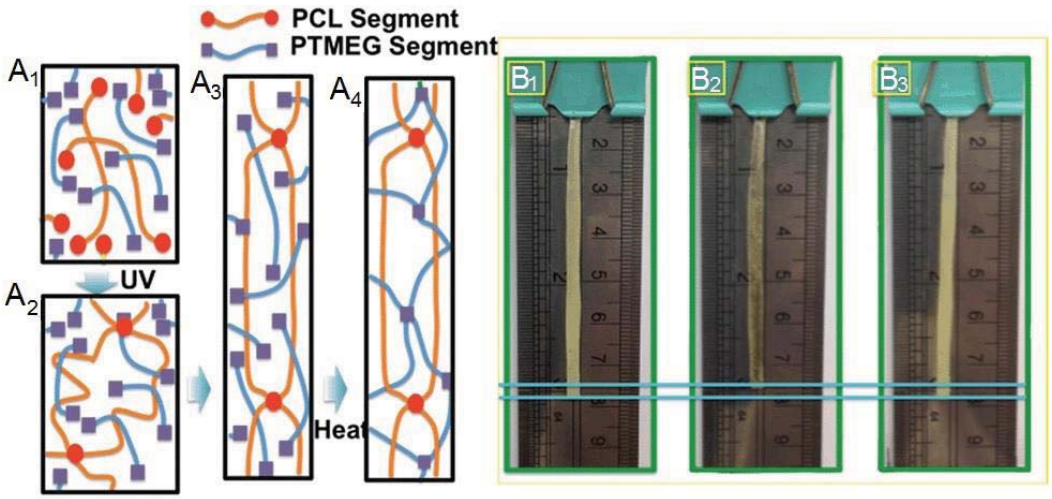

Figure 2.21 ($A_{1–4}$) Design of polymer networks through a two-stage cross-linking process, and ($B_{1–3}$) the resulting 2W-SME under stress-free condition. Reprinted with permission from Ref. 107. Copyright (2014) The Royal Society of Chemistry.

2.4.2.4 Thermoplastic polymers

Chemically cross-linked polymer network has been considered to be a necessary condition because it may prevent flowing of the sample above its T_m. However, some thermoplastic polymers were reported to show 2W-SME under stress-free condition. For example, a conventional semi-crystalline ionomer, poly(ethylene-*co*-methacrylic acid) with a T_g of 53.1 °C and a broad T_m ranging from 56 to 100 °C exhibited a 2W-SME when both the deformation and the actuation temperatures were set in its T_m range.[140] Maiti's group synthesized PCL- and PTMEG-based thermoplastic polyurethanes (TPUs) with a hard segment (PCL) content of 30%, exhibiting 2W-SME under stress-free condition. In this case, the sample was deformed above the T_m of the soft segment and below the T_m of the hard segment. The soft segment (PTMEG) worked as actuator domains, while the hard segment (PCL) played a role of skeleton.[142] More recently, Gao et al. synthesized ethylene/1-octene diblock olefin copolymer, possessing a very broad T_m range from around -40 to 95 °C. The deformation and actuation temperatures were also set in the T_m range, resulting in 2W-SME under stress-free condition (Figure 2.22). In this work, the partial crystal domains with higher T_m served as skeleton.[143] Obviously, thermoplastic polymers may be reprocessed, thus

avoiding the synthesis of a new polymer. However, the reversible shape change of this kind of 2W-SMPs is not as good as chemically cross-linked networks.

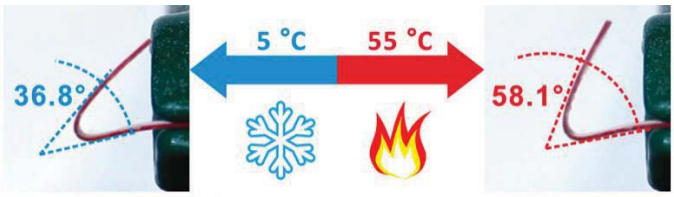

Figure 2.22 Photographs showing the reversible angle change under stress-free condition of the diblock olefin copolymer. Reprinted from Ref. 143. Copyright (2017) American Chemical society.

In summary, these four types of 2W-SMPs under stress-free conditions contain three phases. The first one is either chemically cross-linked or within a transition with the highest T_{trans}, preventing macroscopic flow of the sample and holding the permanent shape. The second one is the shifting-geometry determining phase, which may be a semi-crystalline or an elastic amorphous phase. It supplies a stretching tensile force when compressed due to the contraction of sample. The last one is the actuation phase, which is generally semi-crystalline or liquid crystalline. The melting and crystallization of this phase upon heating above T_m or cooling below T_c result in the shrinkage and elongation of the macroscopic shape, respectively.

2.5 Other stimuli responsive SMPs

2.5.1 Programming and mechanism

Stimuli responsive SMPs (other than those based on direct heating) include intrinsically stimuli-actuated SMPs (without temperature change) and indirect heating responsive SMPs (with temperature change). The former may be actuated by light, solvents, pH, metal ions, CO_2, etc. Reversible photo-responsive molecular switches were incorporated into the polymers for designing intrinsically light-induced SMPs, and their shape fixity and recovery could be realized with different wavelengths of light.[9-11] Water or organic solvents could trigger an SME due to the role they play as plasticizers in the polymer matrix, resulting in a reduction of T_{trans}, and leading to shape recovery.[12-18] For other stimuli responsiveness, such as pH, metal

ions, and CO_2, reversible molecular switches are also incorporated into the polymers which can cross-link and then decross-link with a different stimulus, resulting in shape fixity and recovery.[144-148] Unlike SMPs triggered by direct heating, indirect heating-responsive SMPs can recover its permanent shape triggered by stimuli, such as light, electricity, magnetism, microwave and ultrasound, as summarized in Table 2.1. When functional materials are incorporated into thermally-induced SMPs, the heat produced by the stimuli can induce the shape recovery. Thus, the molecular mechanisms are the same as that of direct heating-induced SMPs (Figure 2.1). Their programming procedures are similar with that of direct heating-induced SMPs, except the procedures of shape recovery. As shown in Figure 2.1, the temporary shape (ε_1) may recover its permanent shape ($\varepsilon_{0,rec}$) when the sample is indirectly heated above its T_{trans} by the stimulus. The indirect heating method has many advantages, as compared with direct external heating, such as convenient, local and uniform heating, and remote control.

Table 2.1 SMPs incorporated with various functional fillers and the various stimuli were reported by literatures.

Fillers	External Stimuli			
	Light	Electrical currents	Magnetic field	Microwave
AuNPs	[149-153]			
AuNRs	[154,155]			
CNTs	[156-158]	[100,169-179]		[208,209]
Graphene	[159-163]	[169,80-184]	[192]	
CB	[164]	[168,185-189]		
Iron oxide			[192-207]	[208]
Others	[165](ink); [166](titanium nitride nanoparticles); [167,168](ligands)	[190,191](carbon nanofiber)		[210](water); [211](SiC); [212](poly(ionic liquid))

2.5.2 Photo-induced SMPs

The photo-induced SMPs discussed here are based on a photothermal effect; i.e., they absorb light, heating the exposed part of the polymer to above its T_{trans}, thereby activating its shape recovery locally. To date, several photothermal fillers have been used, such as gold

nanoparticles (AuNPs) or nanorods (AuNRs), carbon nanotubes (CNTs), graphene, carbon black (CB), ink, organic dyes, ligands, etc. These fillers are capable of absorbing certain wavelengths of light and converting luminous energy into heat efficiently. Organic dyes and ligands may be grafted to the polymer structure, while the other fillers must be dispersed well in the polymer, resulting in polymer composites.

AuNPs have been widely used in SMPs due to their good photothermal effect. Zhao's group reported on hydroxyl-terminated PCL oligomers tethered onto gold nanoparticles via ligand exchange, and then mixed with branched PCL oligomers and cross-linked with hexamethylene diisocyanate. The prepared film recovered its initial unrolled shape when it was irradiated with a 532 nm laser for 25 s. Moreover, through laser light exposure of designated areas of the sample, the corresponding shape recoveries were realized sequentially.[150] They also reported a unique photothermal effect based on cross-linked poly(ethylene oxide) with 0.5 wt% of AuNPs. A temperature gradient in the polymer was formed by controlling light absorption of AuNPs. The pre-strain polymer film showed complex shape transformations and executed delicate mechanical work on light-controlled anisotropic polymer chain relaxation and strain energy release.[152] More recently, small amounts of AuNPs were incorporated into semi-crystalline EVA, and 2W-SME under stress-free condition was observed upon turning 532 nm light on and off (Figure 2.23).[153] AuNRs also possess a very good photothermal effect, and light polarization can be used to control shape recovery of SMP/AuNR composites. AuNRs incorporated in poly(vinyl alcohol) (PVA) were aligned by stretching the composite film, resulting in a light absorbance at 785 nm depending on the polarization direction. Moreover, shape recovery only occurs when light polarization is parallel to the AuNRs.[154]

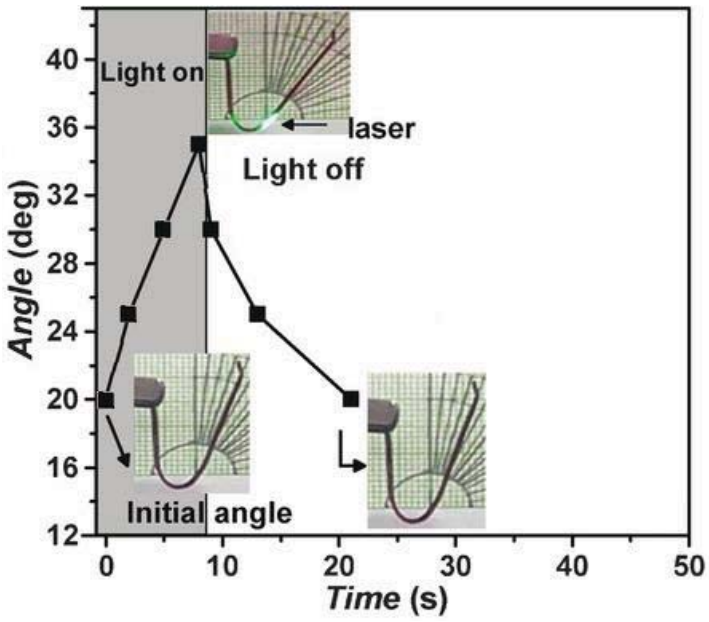

Figure 2.23 Angle change of semi-crystalline EVA (0.1 wt% AuNPs) when the laser (532 nm, 1.13 W/cm^2) was turned on and off. Adapted from Ref. 153 with modification. Copyright 2017 Wiley VCH.

CNTs possess strong absorptions in the visible and near infrared (NIR) regions, which may be incorporated into SMPs for triggering thermal induced SME. Kohlmeyer and co-workers prepared Nafion nanocomposites with a small amount of SWCNT (0.5 wt%), exhibiting both macroscale and microscale multiple SME. Nafion is able to memorize multiple temporary shapes due to its broad thermal transition.[54] The temporary shapes were programmed at different temperatures, which were realized by adjusting the intensity of 808 nm IR (Figure 2.24).[156] The photothermal effect of CNTs was also applied to LCEs to show 2W-SME under both stress and stress-free conditions. Li and coworkers synthesized nematic LCEs embedded with SWCNTs, displaying 2W-SME under stress conditions triggered by white light.[158] Polysiloxane-based LCE composites in Ref. 140 also realized NIR induced 2W-SME under stress-free conditions.

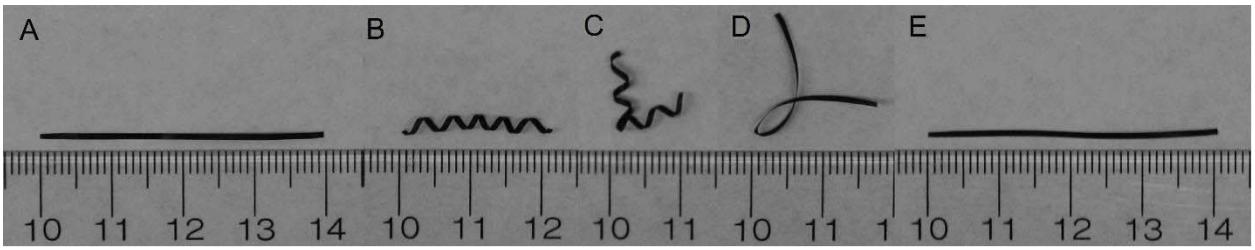

Figure 2.24 Photographs showing photo-controlled multiple SME of a Nafion composite with 0.5 wt% SWCNT: (A) Original shape. (B) A coil formed through 808 nm IR laser (6 mW/mm^2, T = 70 − 75 °C), and followed by cooling. (C) The second temporary shape programmed by localized bending under irradiation of 808 nm IR laser (25 mW/mm^2, T = 140 − 150 °C) and then cooling. (D) Uncoiling recovered at 75 °C in oven while the bending remained. (E) Bending removed for recovering the original shape via 808 nm IR laser (T = 140 − 150 °C). Reprinted with permission from Ref. 156. Copyright (2012) American Chemical Society.

Similar to CNT, graphene can also be embedded into SMPs for photothermal induced SME. Liang et al. developed a TPU nanocomposite loaded with 1 wt% sulfonated graphene. The stretched film contracts fast when it exposed to IR light (> 600 nm).[161] Zhou et al. fabricated a PCL-based PU nanocomposite film with a certain amount of graphene oxide (GO) and 4'-ethyoxy-4-(11-hydroxyundecyloxy)-azobenzene, endowing the nanocomposite with a photo-responsive triple SME due to the combination of the photomechanical feature of azobenzene compounds and the photothermal effect of GO.[162] Yang et al. synthesized LCE/graphene nanocomposites using the *in situ* UV photopolymerization via two-stage cross-linking coupled with a hot-stretching process, yielding fast NIR-responsive 2W-SME under stress conditions.[163]

CB and ink were also investigated as photothermal fillers by some researchers. Leng et al. investigated IR-induced SME of a styrene-based SMP and its nanocomposite loaded with CB. It was found that both the pure SMP and the SMP/CB nanocomposite could be activated by IR light in vacuum, while the shape recovery speed of the nanocomposite is faster than that of the pure SMP due to the stronger IR absorption of 400 - 4000 cm^{-1}.[164] Liu and coworkers patterned black ink on either side of a pre-strained polystyrene sheet using a laserjet printer. The inked areas of the polymer sheet were heated locally above its T_g by the absorption of

light. As a result, the planar sheet folded into a three-dimensional object due to the relaxation and shrinkage of the inked areas.[165]

2.5.3 Electro-responsive SMPs

As is well known, polymers are typically electrical insulators. A certain electrical conductivity can be achieved if enough electrical conductive fillers are incorporated. If electrical current passes through conductive SMPs, resistive joule heating may be generated to heat SMPs above their T_{trans} for electrical triggering of shape recovery. Conductive fillers used to achieve an electro-active SME include CNTs, CB, graphene, carbon nanoparticles, carbon nanofibers, and metal nanoparticles.

SMP/CNTs composites are among the most investigated electro-responsive SMPs.[170-179] Goo et al. first reported electro-active SMP loaded with CNTs treated with acid for improving electrical conductivity and mechanical properties. The composites exhibited electro-active shape recovery with an energy conversion efficiency of 10.4%.[174] Recently, Fu and coworkers first prepared poly(propylene carbonate) (PPC)/PLA polymer blends, and then incorporated MWCNTs for realizing electro-active SME. The composite with 3 wt% CNTs showed the highest shape recovery rate and reached an equilibrium R_r of 97% within 30 s at 30 V (Figure 2.25).[178]

Graphene may also be used as electrical conductive filler due to its excellent thermal and electrical conductive properties. Tang et al. incorporated a vapor-grown carbon nanofiber (VGCF)-graphene hybrid filler into a bio-based polyester for preparing polyester/VGCF/graphene composites. The electrical conductivity and mechanical properties of the composites were enhanced due to the synergistic effects of VGCF and graphene. The ternary composites revealed excellent electro- and IR-triggered SME with higher shape recovery ratio, stronger recovery stress and faster shape response at a voltage of 30 V, compared with polyester/VGCF composites.[182] Rana and coworkers incorporated functionalized graphene sheets as cross-linkers in the PCL-based prepolymer. The resulting composite showed a recovery ratio of 97%, a fixity ratio of 95%, and recovered its permanent shape in 10 s at 50 V.[183] More recently, Wang et al. fabricated epoxy-based SMP composites

by coating reduced GO paper onto the surface of SMP sheet, exhibiting a recoverability of approximately 100% taking only 5 s at 6 V.[184]

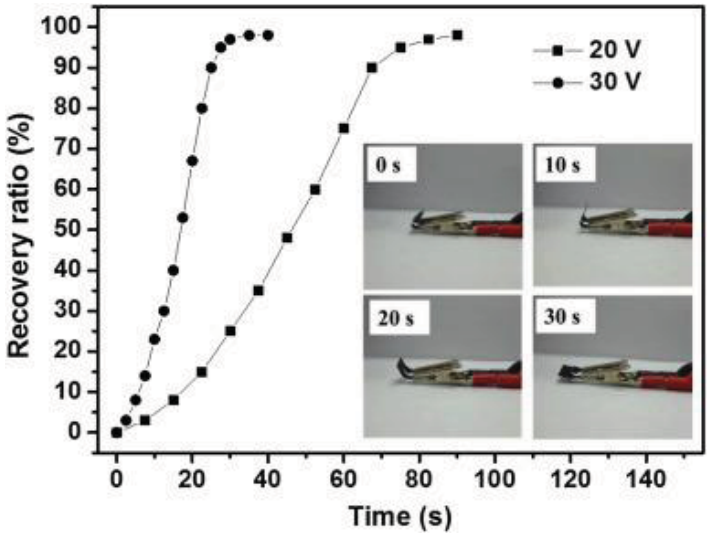

Figure 2.25 Plot of shape recovery ratio *vs* time for PPC/PLA/CNT (70/30/3 by weight) composite under two constant voltages (20 V, 30 V). Inset pictures show the electro-active shape memory behavior of the composite at 30 V. Reprinted with permission from Ref. 178. Copyright 2016 from Elsevier Ltd.

Qi and coworkers introduced CB nanoparticles to PLA/TPU blend (70/30 by weight), which changed the morphology from "sea-island" to a co-continuous structure with an increase in CB content due to the self-networking capability of CB and strong affinities between CB and TPU, which resulted in a superior shape memory property. The composite with 8 wt% CB exhibited good electro-active shape memory behavior, which could recover its original shape in 80 s under 30 V (Figure 2.26).[188] Moreover, a SMPU/CB composite with a laminated structure was reported to exhibit an electro-active 2W-SME under stress-free conditions. The SMPU/CB composite layer was stretched to 50% strain at a temperature above its T_m and cooled to room temperature for fixation. Afterwards, the composite layer was glued with a substrate layer, giving obtained 2W-SMP laminates, which bent with passing electric current and unbent upon cooling without electric current.[189]

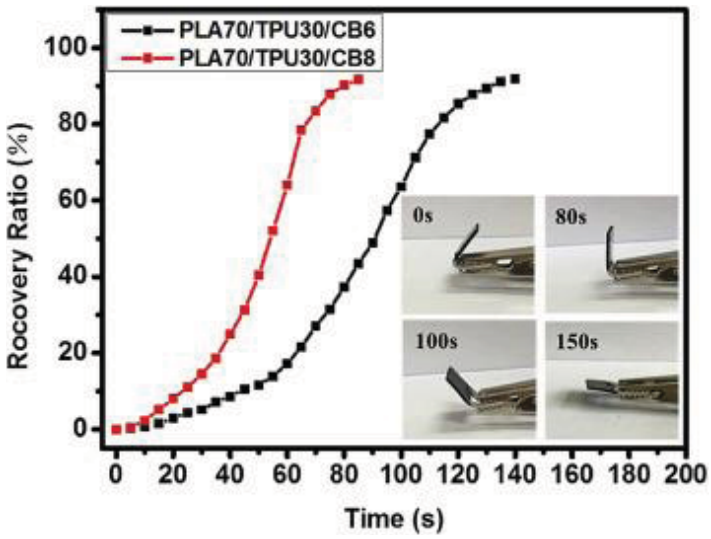

Figure 2.26 Plot of shape recovery ratio *vs* time for PLA/TPU/CB (70/30/6 and 70/30/8 by weight) composites under the voltage of 30 V. Inset pictures displaying the electro-active shape recovery behavior of PLA/TPU/CB (70/30/6) composite. Reprinted with permission from Ref. 188. Copyright 2017 from Elsevier Ltd.

Other electrical conductive fillers were also used to enhance the electrical conductivity of SMPs. Lu et al. dispersed carbon nanofibers in distilled water with the aid of surfactants, which then self-assembled to form multi-layered nanopaper, used to make SMP nanocomposites by a resin transfer molding process with a PU-based SMP resin. The electrically actuated shape recovery of SMP nanocomposites with four-layered nanopaper was completed in 80 s at 30 V.[191] In their later research, reduced GO was self-assembled and grafted onto carbon fibers to improve the interfacial bonding with the SMP matrix. A layer of synthesized Ag nanoparticles was deposited onto GO for bridging the gap between GO and the carbon fibers and improving the electrical conductivity of the SMP composites. The shape recovery took 36 s when a constant voltage of 8.6 V was applied.[180]

2.5.4 Magnetic-responsive SMPs

Magnetic-actuated SMPs may be obtained by incorporating magnetic nanoparticles into SMPs. The transfer from electromagnetic energy to heat energy results in the shape recovery under an alternating magnetic field. The fillers of iron oxide particles, such as Fe_3O_4, have been usually used to realize magnetic-active SME.[192-207] Yang et al. prepared SMP

nanocomposites from Fe_3O_4 particles modified with oleic acid and polynorbornene-based copolymer via solution casting method. The average diameter of modified Fe_3O_4 nanoparticles was around 50-70 nm and the nanocomposites recovered its permanent shape in 186 s when deposited in an alternating magnetic field.[202] Puig et al. fabricated superparamagnetic nanocomposites by dispersion of oleic acid-stabilized magnetite Fe_3O_4 nanoparticles in an epoxy system. The composite with 8 wt% of Fe_3O_4 particles recovered its original shape after exposing to the alternating magnetic field for 60 s (Figure 2.27).[203] Magnetically controlled 2W-SMP nanocomposites were first obtained by Lendlein et al via cross-linking a mixture of three-arm PDL oligomers and PDL oligomers-grafted magnetic nanoparticles with 1, 6-hexane diisocyanate. Herein, magnetic nanoparticles were synthesized by co-precipitating iron salts ($FeCl_3 \cdot 6H_2O$ and $FeCl_2 \cdot 4H_2O$) in alkaline solutions.[204,205].

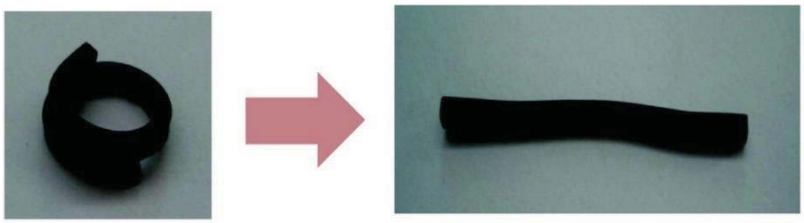

Figure 2.27 Photographs of a shape recovery process of the polymer nanocomposite with 8 wt % of oleic acid-stabilized Fe_3O_4 nanoparticles before (coil) and after (bar) exposure to the alternating magnetic field for 60 s. Reprinted with permission from Ref. 203. Copyright (2012) American Chemical Society.

2.5.5 Microwave-responsive SMPs

Microwaves are a portion of electromagnetic spectrum with wavelengths ranging from 1 mm to 1 m and can be transmitted, reflected or absorbed depending on materials. Food and water can be heated in ceramic container by absorbing microwave. Therefore, some dielectric fillers were embedded into SMPs to enhance the absorption of microwave, such as CNTs, Fe_3O_4, water molecules, silicon carbide (SiC), and even poly(ionic liquid). The molecules of these fillers move along the rapidly oscillating electric field direction due to the dipole moment. Thus, friction is generated between molecules, resulting in heat.

Besides superb thermal and electrical conductivity, CNTs also have high microwave absorbing ability. Leng's group embedded different CNTs (1, 3, 5wt%) into a styrene-based shape memory resin for preparing nanocomposites and found that the absorption ratio increased with the increase of CNTs and microwave frequency. 99.84% of microwave energy could be absorbed by SMP composite with 5 wt% CNTs at a frequency of 40 GHz. As shown in Figure 2.28, the composites with 1, 3 and 5 wt% CNTs could recover their permanent shape within 30 s with R_rs of 72.5, 94 and 99.5%, respectively.[209] Water is the most common and economic filler, which could be absorbed by some hydrophilic polymers, such as PVA. Du et al. synthesized chemical cross-linked PVA, which was then immersed into pure water to absorb water molecules. They found that the samples with a higher water content recovered their original shapes faster at a certain level of microwave power output. Dry samples did not show the shape recovery even when microwave irradiated for a long time.[210]

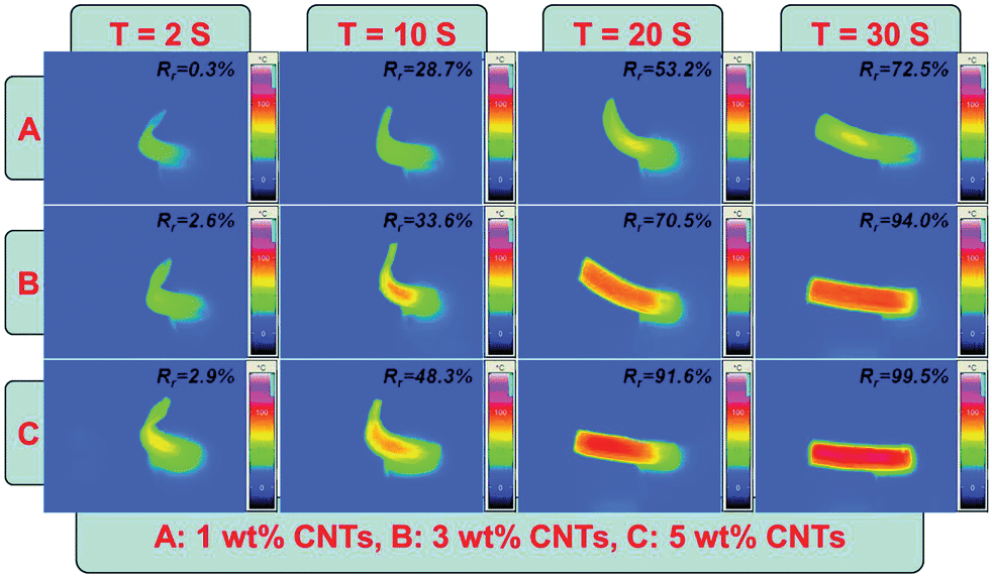

Figure 2.28 Digital photographs of the shape recovery process of the SMP composites with 1, 3, 5 wt% CNTs under microwave radiation (2.45 GHz). Reprinted with permission from Ref. 209. Copyright (2014) The Royal Society of Chemistry.

SiC can be used as a microwave absorber for heating SMPs, because it has good thermal and chemical stability, strong microwave absorption property and low thermal expansion coefficient. In the PVA/SiC composites fabricated by Du et al., the greater SiC content and applied microwave power led to higher recovery rates.[211] In another work, they synthesized

poly(ionic liquid) (Figure 2.29), which was then introduced into PVA solution as a microwave absorber due to the anion-cation pairs, generating strong microwave absorption ability to form poly(ionic liquid)/PVA polymer networks. The PVA composite with 30 wt% poly(ionic liquid) recovered its original shape within 20 s under 400 W irradiation.[212]

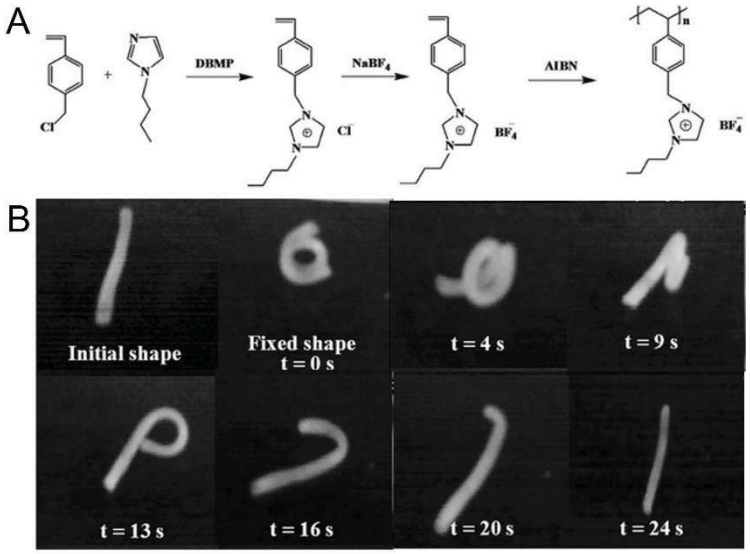

Figure 2.29 (A) The structure of poly(ionic liquid); (B) microwave-induced shape recovery behavior of poly(ionic liquid)/PVA polymer networks. Reproduced from Ref. 212 with modification. Copyright 2016 Wiley VCH.

2.5.6 Ultrasound-responsive SMPs

Ultrasound has frequencies above 20 kHz that exceed the audible limit of humans hearing. High intensity focused ultrasound (HIFU) can concentrate ultrasound beams on a spot, which may cause a local rise in temperature. This may induce selective tissue necrosis without damage to surrounding or overlying tissues. Thus, HIFU has been studied as a noninvasive treatment to replace conventional therapies for many decades. HIFU was used to trigger SMP directly due to its thermal effect.[213-215]

Zhao's group utilized HIFU to induce the shape recovery of poly(methyl methacrylate-*co*-butyl acrylate) (P(MMA-BA)). Multiple intermediate shapes were achieved by turning on or off the HIFU exposure, which synchronously controlled the release of loaded drugs. The rate of shape recovery and drug release could be tuned by adjusting the HIFU exposure intensity

and duration.[216] Subsequently, they found that the shape recovery rate and ratio first increased and then decreased with an increase of the sample thickness. In addition, low MMA/BA ratio and cross-link density led to faster temperature rise and thus quicker shape recovery rate and higher R_r.[217] More recently, Zhao and coworkers found dynamically cross-linked PCL-based PU exhibited shape memory-assisted self-healing effect due to the Diels–Alder reaction (Figure 2.30). Herein, the polymer sample was cut and bent to obtain a crack, and subjected to HIFU treatment. The crack immediately closed due to heating induced the shape recovery and started to heal after the crack closure due to the Diels–Alder bonds scission, flow, and crack closure.[218] Furthermore, a shape memory PVA physical hydrogel could be triggered by therapeutic ultrasound owing to the melting crystallized domains of PVA.[219]

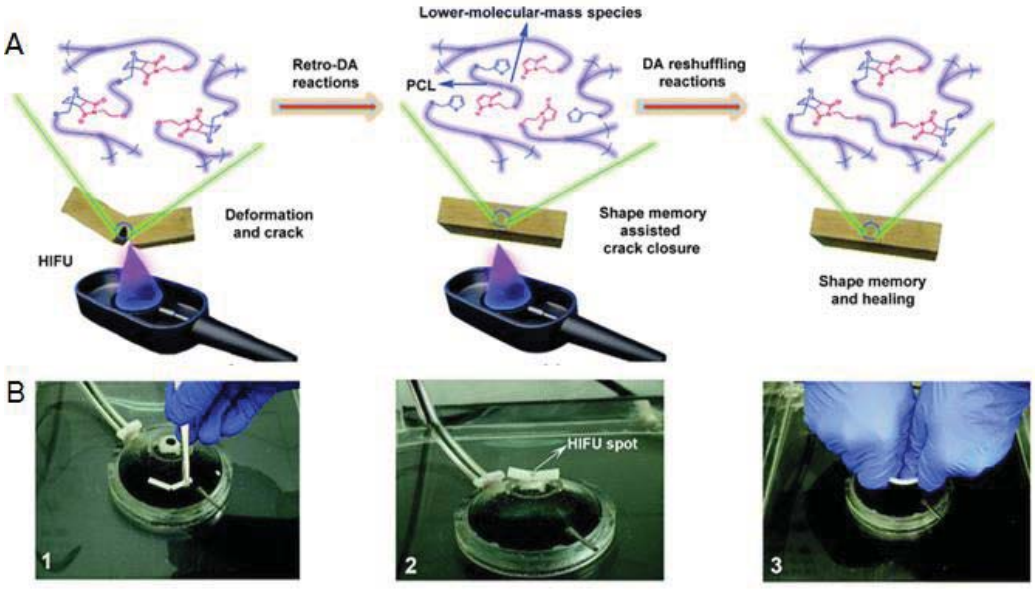

Figure 2.30 (A) Schematic illustration and (B) digital photographs of HIFU-triggered shape memory assisted self-healing of PCL-based PU containing Diels–Alder bonds. Reproduced from Ref. 218 with modification. Copyright (2014) Royal Society of Chemistry.

2.6 Applications of SMPs

SMPs have drawn great interest in many fields due to their unique properties, such as for biomedical applications, and in the aerospace, automotive and robot industries. Their applications are exemplified by dual SMPs, triple and multiple SMPs, and 2W-SMPs.

2.6.1 Applications of dual SMPs

Dual SMPs may be used in biomedicine as well as in aerospace applications. Typical biomedical applications include drug delivery carriers,[65,220-222] self-expansion stents,[223] endovascular clot removal,[224] self-tightening sutures,[7,225] deployable surgical devices,[226] artificial bandages and lenses,[227] artificial vascular grafts,[228,229] micro-vascular actuators,[230] tissue engineering,[231-233] and in orthopedic applications.[234] The actuation temperatures of SMPs should be close to or slightly higher than body temperature. The most viable way is the utilization of indirect heating method, such as NIR laser, magnetic field or HIFU. These stimuli could heat the SMP at a precise position inside the body. As described previously, Wang and colleagues prepared a dual-drug-eluting stent with a T_m close to body temperature, and then mitomycin C was first conjugated with and then curcumin was coated to this stent. A continuous release of mitomycin C over 70 days and curcumin over 14 days was achieved.[65] In PCL/trisilanolphenyl polyhedral oligomeric silsequioxane (TspPOSS) shape memory nanocomposite films, ~25% of loaded theophylline was released from films with 10 wt% TspPOSS after 2 days.[221]

Dual SMPs can also be used as self-expansion stents and endovascular clot removal devices. Li and coworkers designed and synthesized block copolymer (PCL-P(3HB-3HV)) containing hyperbranched three-arm PCL as the switching segment and microbial polyester poly[(*R*)-3-hydroxybutyrate-*co*-(*R*)-3-hydroxyvalerate] (P(3HB-3HV)) as the crystallizable hard segment. PCL-P(3HB-3HV) block copolymers were also shown to be as safe materials with good biocompatibility. The stent made from the PCL-P(3HB-3HV) film shows nearly complete self-expansion at 37 °C within only 25 s (Figure 2.31).[235] Dual SMPs were used to develop an intravascular laser-activated therapeutic device, which could be deployed by laser heating for mechanically removing the blood clot and restoring blood flow to the brain.[224] Dual SMP made of PCL/PPDO multiblock copolymers may be used as sutures, which self-tighten upon heating slightly above body temperature.[7,225]

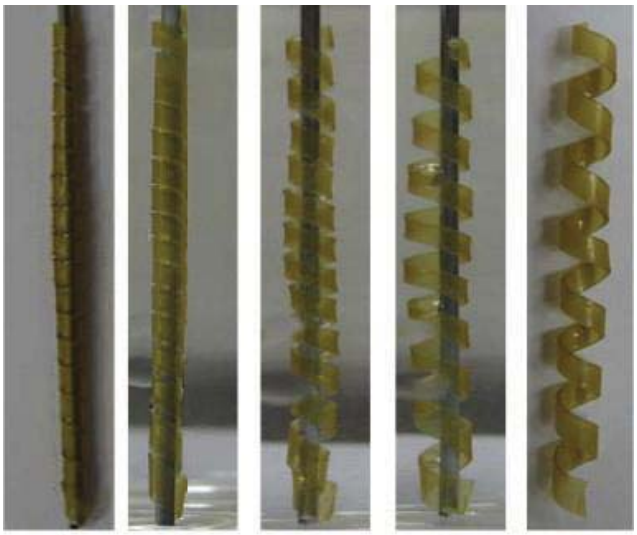

Figure 2.31 Photographs exhibiting the self-expansion of the stent made from PCL-P(3HB-3HV) with original outer diameter of 3.45 mm. Reprinted from Ref. 235. Copyright 2010 Wiley VCH.

Dual SMPs have great interest for self-deployable structures in aerospace applications, e.g., in solar arrays, solar sails, sunshields, hinges, or radar antennas.[50,236] As an example, Leng's group reported that fabrics made of thermoset styrene-based SMP composites reinforced by carbon fiber could be used as a deployable hinge. The solar array prototype deployed from 90° to ~0° in 80 s when the SMP composite hinge was heated by applying a voltage of 20 V.[237]

Besides biomedical and aerospace applications, dual SMPs can also be used as actuators,[238,239] sensors,[240-243] tuning of surface micropatterns,[244,245] reshapeable products,[246] self-peeling dry adhesives,[247-250] smart textiles,[251-254] and optical devices.[255-257]

2.6.2 Applications of triple and multiple SMPs

Triple and multiple SMPs with two or more temporary shapes may meet complex requirements of some applications in smart biomedical devices. Lendlein reported cross-linked polymer networks (CLEG) composed of PCL and PEG, which can be implanted into the human body as a removable stent with a compressed shape A. This stent may be extended to shape B at a desired position, and finally contracted to shape C at 60 °C for easy removed (Figure 2.32).[80] Lendlein and colleagues fabricated triple SMPs with a one-step programming process, increasing the attractiveness of their applications in medical fields, such as fixation

devices for assembling technology or tube repair systems allowing a re-uptake of the temporary tube replacement.[258] Zwitterionic polymers with multiple SME may also have some potential applications, such as sequential warnings, auto feed, controlled drug release and sequential collection of electronic waste.[104]

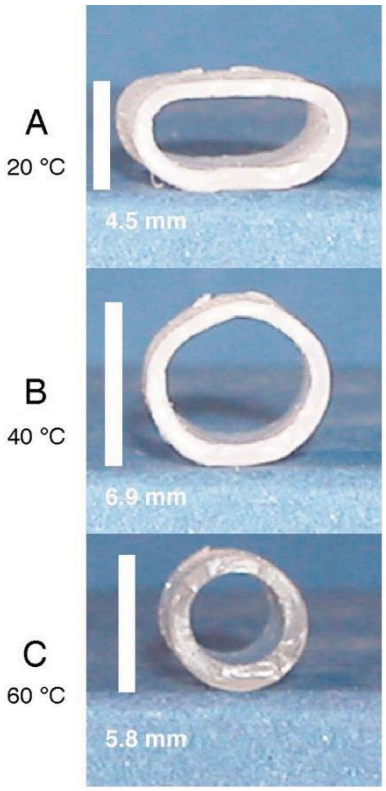

Figure 2.32 Photographs showing the recovery process of triple SME; shapes B and C were recovered by heating to 40 and 60 °C, respectively, beginning from shape A. Reprinted with permission from Ref. 80. Copyright (2006) National Academy of Sciences, U.S.A.

Triple and multiple SMPs may also meet requirements in aerospace applications. For example, as discussed early in Section 2.3.2.3, Zhuo et al. fabricated a three-layer device of copolymer films with 30 mol% (outer layer), 50 mol% (mid-layer), and 70 mol% (in-layer) HAM. Such a device self-deployed at 25, 55 and 80 °C sequentially (Figure 2.33). Thus, the controlled recovery process of the self-deployable device made it an ideal candidate for aerospace applications.[99] Moreover, electrospun membranes prepared from Nafion enable complex deformations, possessing wide potential applications, such as smart textiles, artificial intelligence robots, and in biomedical engineering.[259,260]

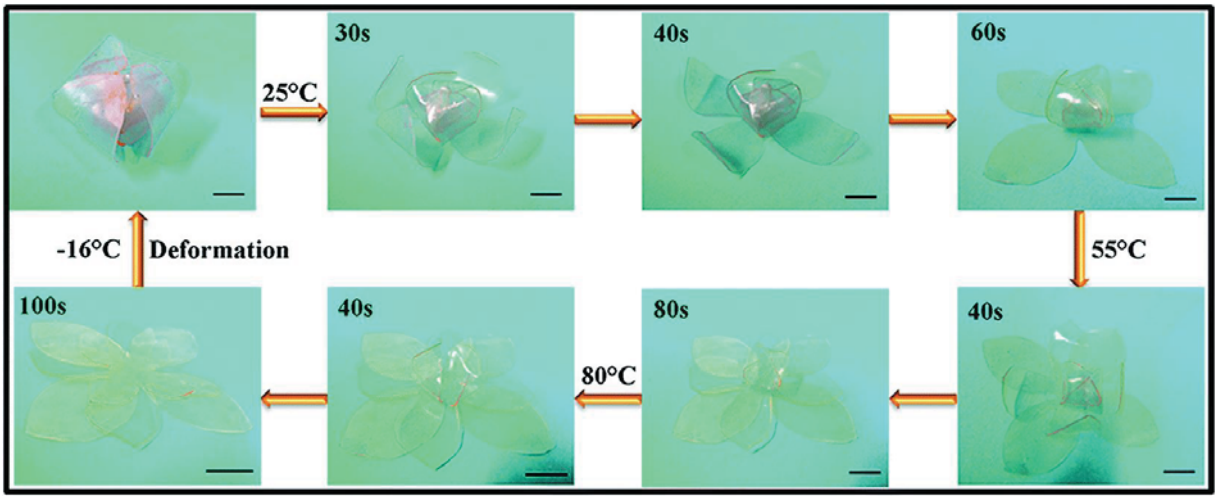

Figure 2.33 Self-deployable device consisting of three layers with distinct T_{trans}s. Reprinted from Ref. 99 with permission. Copyright 2016 Royal Society of Chemistry.

2.6.3 Applications of 2W-SMPs

The intrinsic irreversibility of 1W-SMPs may be a limitation since full reversibility requires the use of 2W-SMPs in applications, such as actuators, textiles, footwear and artificial muscles.[45,111,261] Artificial muscles that are able to convert contraction and elongation into weight lifting motions have been developed.[262-266] 2W-SMPs may be employed as fibers of spacer fabrics with thermally-responsive thicknesses, or as an artificial tendon.[107] Micrometer-sized particles were fabricated using 2W-SMP of PEG-PCL polymer network[134] with potential use as a reversibly convertible drug delivery carrier. 2W-SMPs may also be used to control the surface features from macroscopic to micro/nanoscales. Sheiko and coworkers studied the first usage of reversible shape memory for the actuation of two-way transitions between microscopically patterned substrates (Figure 2.34).[267] They also utilized two-way reversible shape memory for replicating and controlling the shape of sub-*μm* features used in optical applications.[268]

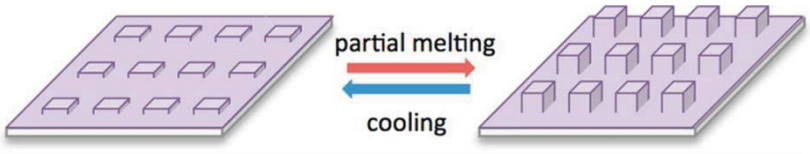

Figure 2.34 The application of 2W-SMP for switching micropatterned surface. Reprinted from Ref. 267 with permission. Copyright (2014) American Chemical Society.

The conversion from stimuli into mechanical energy in 2W-SMPs may realize walking or swimming. Under the cyclic external stimuli, the samples are capable of self-locomotion as micro-robotics. Peng et al. fabricated an electro-responsive 2W-SMP composite with a laminated structure from an epoxy-based polymer and CNT sponge. 2W-SME was realized by alternately applying two different voltages to top and bottom layer respectively. A higher voltage (8 V) was applied for stimulating the layer and dominating the shape change, whereas a lower voltage (2 V) was used for softening and accommodating the deformation produced by the other layer (Figure 2.35A). This 2W-SMP composite was further designed into an inchworm-type robot as shown in Figures 2.35B and C. This robot moved forward about 8 mm in 10 minutes by alternating voltages of 2 and 8 V with a cycling time of 120 seconds (Figure 2.35D).[269]

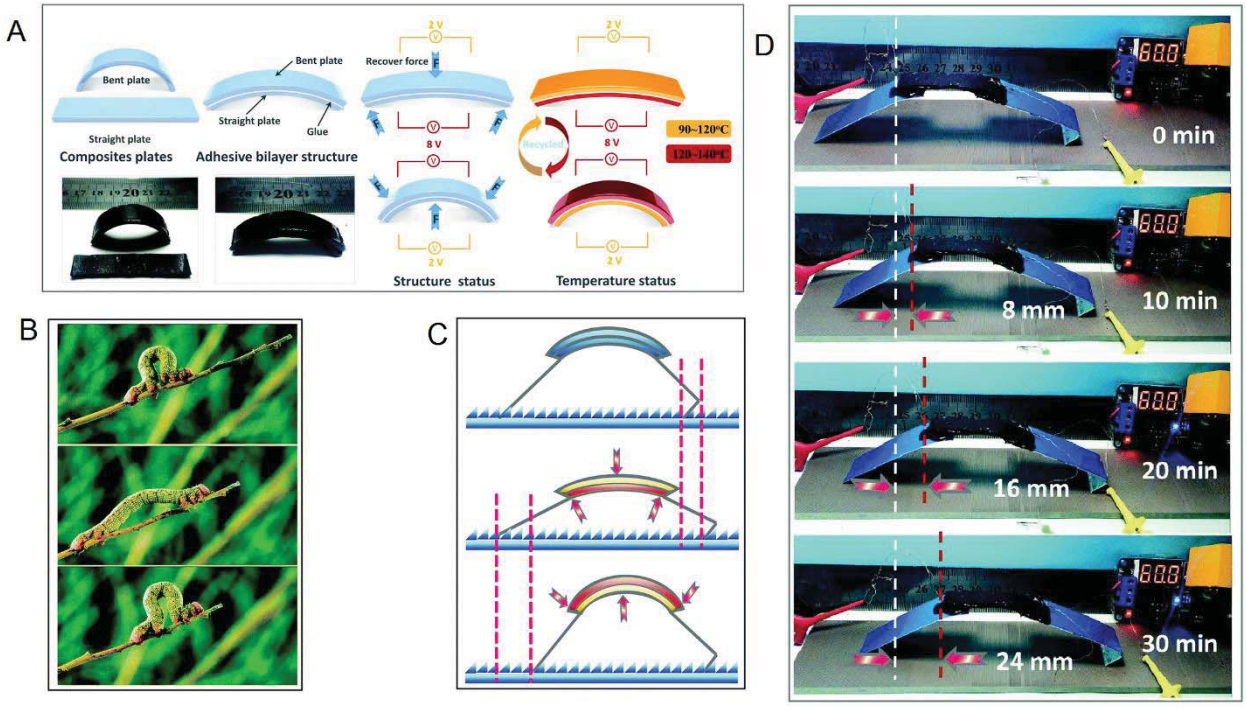

Figure 2.35 (A) Fabrication of the laminated 2W-SMP composite by combining two layers with curved and straight initial shapes, and illustration of the mechanism under alternating electrical stimulation. 2W-SMP composite was designed to an inchworm-type robot. (B) Photographs showing inchworm locomotion. (C) The principles of designed inchworm-type robot locomotion; (D) the locomotion of inchworm-type robot, moving 24 mm in 30 minutes. Adapted from Ref. 269 with permission. Copyright (2016) Royal Society of Chemistry.

2.7 Conclusions and outlook

The preceding review of the concept, programming procedures, molecular mechanisms, design strategies and applications of thermal induced dual, triple, multiple, and 2W-SMPs triggered by direct and indirect heating lead to the concluding points below:

(1) *Effect of cross-linking*: Most polymers may exhibit a certain dual SME due to their at least one reversible thermal transition, which usually need to be enhanced by a cross-linked structure. Physically cross-linked SMPs have better processability and recyclability, while conventional chemical cross-linking offers better mechanical properties, recoverability and reproducibility because of their inherent lower slippage between molecular chains. The recently developed SMPs cross-linked through dynamic covalent bonds possess both advantages of physically and conventional chemically cross-linked SMPs.

(2) *Types of transition temperature*: In the design triple and multiple SMPs, one may opt to use a broad thermal transition or two or more thermal transitions. The strategy of a broad transition is more practical in the preparation of multiple SMPs due to the ease of synthesis. Besides conventional thermal transitions (T_g, T_m and T_{cl}), dissociation of hydrogen bonds could also be used as one of the separated thermal transitions in the design of such SMPs.

(3) *Stress and stress-free conditions*: 2W-SMPs under stress conditions contain two phases: the actuation phase and the chemically cross-linked phase. 2W-SMPs under stress-free conditions have been demonstrated for cross-linked semi-crystalline polymers and also for thermoplastic semi-crystalline polymers. Besides shifting-geometry determining and actuation phases in 2W-SMPs under stress-free condition, another essential phase is one that is chemically cross-linked or that has a broad transition where the highest T_{trans} prevents the macroscopic flow of the sample and holds the permanent shape.

(4) *Indirect heating*: Dual SMPs and complex SMPs (triple, multiple, and 2W-SMPs) can also be activated by indirect heating, extending their applications as, for example, deployable hinges in aerospace application, and remote-control medical instruments. SMPs triggered by other stimuli can exhibit novel properties not realizable by direct

heating methods, such as gradient shape recovery, spatially controlled shape recovery, complex shape transformations, etc.

SMPs have drawn an increasing interest from researchers to design and prepare novel SMPs for various applications. The work presented in this paper point to the following potential directions in the future:

(1) SMPs cross-linked by dynamic covalent bonds, especially for 2W-SMPs, are more advantageous due to their reprocessibility, good mechanical properties and good recoverability. The usefulness of 2W-SMPs makes it a promising direction of future research. New approaches to design 2W-SME under stress-free conditions will also be in high demand for this type of materials.

(2) SMPs with precisely tunable transition temperatures are highly desired for a variety of applications. For example, biomedical applications require a switching temperature near body temperature, while SMPs used in aerospace required high transition temperatures. SMPs having multi-functionality (two or more types of SMEs integrated in one SMP, biodegradability or biocompatibility) are also attractive.

(3) The speed of shape change and response time are key factors for actuators. More effort must be made on the design of SMPs with fast response and shape change that can be tuned after device manufacturing process.

(4) Due to the limitations of direct heating in some special fields, such as human body, indirect heating may provide a useful alternative. Complex SMPs with triple, multiple SMEs and 2W-SMEs may meet the demanding needs in the future. Therefore, multiple stimuli-responsive complex SMPs, especially 2W-SMPs, are becoming more attractive materials.

2.8 Acknowledgments

Financial support from NSERC of Canada, FQRNT of Quebec, and the Canada Research Chair program is gratefully acknowledged. K. Wang is grateful to the China Scholarship Council for a scholarship. The authors are members GRSTB funded by FRSQ.

2.9 References

1. Gautrot, J. E.; Zhu, X. X. Shape memory polymers based on naturally-occurring bile acids. *Macromolecules* **2009,** 42, 7324-7331.

2. Wei, Z. G.; Sandstrom, R.; Miyazaki, S. Shape-memory materials and hybrid composites for smart systems - Part I Shape-memory materials. *J. Mater. Sci.* **1998,** 33, 3743-3762.

3. El Feninat, F.; Laroche, G.; Fiset, M.; Mantovani, D. Shape memory materials for biomedical applications. *Adv. Eng. Mater.* **2002,** 4, 91-104.

4. Hornbogen, E. Comparison of shape memory metals and polymers. *Adv. Eng. Mater.* **2006,** 8, 101-106.

5. Zhang, L.; Jiang, Y.; Xiong, Z.; Liu, X.; Na, H.; Zhang, R.; Zhu, J. Highly recoverable rosin-based shape memory polyurethanes. *J. Mater. Chem. A* **2013,** 1, 3263.

6. Ratna, D.; Karger-Kocsis, J. Recent advances in shape memory polymers and composites: a review. *J. Mater. Sci.* **2007,** 43, 254-269.

7. Lendlein, A.; Langer, R. Biodegradable, elastic shape-memory polymers for potential biomedical applications. *Science* **2002,** 296, 1673-6.

8. Li, G.; Fei, G. X.; Liu, B.; Xia, H. S.; Zhao, Y. Shape recovery characteristics for shape memory polymers subjected to high intensity focused ultrasound. *RSC Adv.* **2014,** 4, 32701-32709.

9. Li, W.; Liu, Y.; Leng, J. Shape memory polymer nanocomposite with multi-stimuli response and two-way reversible shape memory behavior. *RSC Adv.* **2014,** 4, 61847-61854.

10. Wu, L.; Jin, C.; Sun, X. Synthesis, properties, and light-induced shape memory effect of multiblock polyesterurethanes containing biodegradable segments and pendant cinnamamide groups. *Biomacromolecules* **2011,** 12, 235-41.

11. Lendlein, A.; Jiang, H. Y.; Junger, O.; Langer, R. Light-induced shape-memory polymers. *Nature* **2005,** 434, 879-882.

12. Lee, K. M.; Koerner, H.; Vaia, R. A.; Bunning, T. J.; White, T. J. Light-activated shape memory of glassy, azobenzene liquid crystalline polymer networks. *Soft Matter* **2011,** 7, 4318-4324.

13. Gu, X.; Mather, P. T. Water-triggered shape memory of multiblock thermoplastic polyurethanes (TPUs). *RSC Adv.* **2013,** 3, 15783-15971.

14. Wu, T.; Frydrych, M.; O'Kelly, K.; Chen, B. Poly(glycerol sebacate urethane)-cellulose nanocomposites with water-active shape-memory effects. *Biomacromolecules* **2014,** 15, 2663-2671.

15. Wang, L.; Yang, X. F.; Chen, H. M.; Yang, G.; Gong, T.; Li, W. B.; Zhou, S. B. Multi-stimuli sensitive shape memory poly(vinyl alcohol)-graft-polyurethane. *Polym. Chem.* **2013,** 4, 4461-4468.

16. Quitmann, D.; Gushterov, N.; Sadowski, G.; Katzenberg, F.; Tiller, J. C. Solvent-sensitive reversible stress-response of shape memory natural rubber. *ACS Appl. Mater. Interfaces* **2013,** 5, 3504-7.

17. Liu, Y.; Li, Y.; Yang, G.; Zheng, X.; Zhou, S. Multi-stimuli responsive shape-memory polymer nanocomposite network cross-linked by cellulose nanocrystals. *ACS Appl. Mater. Interfaces* **2015**, 7, 4118-4126.

18. Ramdas, M. R.; Kumar, K. S. S.; Nair, C. P. R. Heat and solvent responsive polytriazole: shape recovery properties in different solvents. *RSC Adv.* **2016,** 6, 53602-53613.

19. Fang, Z.; Kuang, Y.; Zhou, P.; Ming, S.; Zhu, P.; Liu, Y.; Ning, H.; Chen, G. Programmable shape recovery process of water-responsive shape-memory poly(vinyl alcohol) by wettability contrast strategy. *ACS Appl. Mater. Interfaces* **2017,** 9, 5495-5502.

20. Wang, M. T.; Luo, X. L.; Zhang, X. Y.; Ma, D. Z. Shape memory properties in poly(ethylene oxide)-poly(ethylene terephthalate) copolymers. *Polym. Adv. Technol.* **1997,** 8, 136-139.

21. Luo, X. L.; Zhang, X. Y.; Wang, M. T.; Ma, D. H.; Xu, M.; Li, F. K. Thermally stimulated shape-memory behavior of ethylene oxide ethylene terephthalate segmented copolymer. *J. Appl. Polym. Sci.* **1997,** 64, 2433-2440.

22. Li, J.; Viveros, J. A.; Wrue, M. H.; Anthamatten, M. Shape-memory effects in polymer networks containing reversibly associating side-groups. *Adv. Mater.* **2007,** 19, 2851-2855.

23. Behl, M.; Zotzmann, J.; Lendlein, A. Shape-memory polymers and shape-changing polymers. *Adv. Polym. Sci.* **2009,** 226, 1-40.

24. Lendlein, A.; Kelch, S. Shape-memory polymers. *Angew. Chem. Int. Ed.* **2002,** 41, 2034-2057.

25. Liu, C.; Qin, H.; Mather, P. T. Review of progress in shape-memory polymers. *J. Mater. Chem.* **2007,** 17, 1543-1558.

26. Xie, T. Recent advances in polymer shape memory. *Polymer* **2011,** 52, 4985-5000.
27. Hu, J.; Zhu, Y.; Huang, H.; Lu, J. Recent advances in shape–memory polymers: Structure, mechanism, functionality, modeling and applications. *Prog. Polym. Sci.* **2012,** 37, 1720-1763.
28. Berg, G. J.; McBride, M. K.; Wang, C.; Bowman, C. N. New directions in the chemistry of shape memory polymers. *Polymer* **2014,** 55, 5849-5872.
29. Hager, M. D.; Bode, S.; Weber, C.; Schubert, U. S. Shape memory polymers: Past, present and future developments. *Prog. Polym. Sci.* **2015,** 49-50, 3-33.
30. Zhao, Q.; Qi, H. J.; Xie, T. Recent progress in shape memory polymer: New behavior, enabling materials, and mechanistic understanding. *Prog. Polym. Sci.* **2015,** 49-50, 79-120.
31. Wang, W.; Liu, Y.; Leng, J. Recent developments in shape memory polymer nanocomposites: Actuation methods and mechanisms. *Coordin. Chem. Rev.* **2016,** 320-321, 38-52.
32. Liu, Y.; Lv, H.; Lan, X.; Leng, J.; Du, S. Review of electro-active shape-memory polymer composite. *Compos. Sci. Technol.* **2009,** 69, 2064-2068.
33. Leng, J.; Lan, X.; Liu, Y.; Du, S. Shape-memory polymers and their composites: Stimulus methods and applications. *Prog. Mater. Sci.* **2011,** 56, 1077-1135.
34. Huang, W. M.; Yang, B.; Zhao, Y.; Ding, Z. Thermo-moisture responsive polyurethane shape-memory polymer and composites: a review. *J. Mater. Chem.* **2010,** 20, 3367-3381.
35. Meng, H.; Li, G. A review of stimuli-responsive shape memory polymer composites. *Polymer* **2013,** 54, 2199-2221.
36. Lu, W.; Le, X.; Zhang, J.; Huang, Y.; Chen, T. Supramolecular shape memory hydrogels: a new bridge between stimuli-responsive polymers and supramolecular chemistry. *Chem. Soc. Rev.* **2017,** 46, 1284-1294.
37. Behl, M.; Lendlein, A. Triple-shape polymers. *J. Mater. Chem.* **2010,** 20, 3335-3345.
38. Zhou, J.; Sheiko, S. S. Reversible shape-shifting in polymeric materials. *J. Polym. Sci., Part B: Polym. Phys.* **2016,** 54, 1365-1380.
39. Lewis, C. L.; Dell, E. M. A review of shape memory polymers bearing reversible binding groups. *J. Polym. Sci., Part B: Polym. Phys.* **2016,** 54, 1340-1364.
40. Santhosh Kumar, K. S.; Biju, R.; Reghunadhan Nair, C. P. Progress in shape memory epoxy resins. *React. Funct. Polym.* **2013,** 73, 421-430.

41. Meng, H.; Mohamadian, H.; Stubblefield, M.; Jerro, D.; Ibekwe, S.; Pang, S. S.; Li, G. Q. Various shape memory effects of stimuli-responsive shape memory polymers. *Smart Mater. Struct.* **2013,** 22, 093001.

42. Sun, L.; Huang, W. M.; Ding, Z.; Zhao, Y.; Wang, C. C.; Purnawali, H.; Tang, C. Stimulus-responsive shape memory materials: A review. *Mater. Des.* **2012,** 33, 577-640.

43. Habault, D.; Zhang, H.; Zhao, Y. Light-triggered self-healing and shape-memory polymers. *Chem. Soc. Rev.* **2013,** 42, 7244-7256.

44. Zhao, Q.; Behl, M.; Lendlein, A. Shape-memory polymers with multiple transitions: complex actively moving polymers. *Soft Matter* **2013,** 9, 1744-1755.

45. Hu, J. L.; Chen, S. J. A review of actively moving polymers in textile applications. *J. Mater. Chem.* **2010,** 20, 3346-3355.

46. Small, W. t.; Singhal, P.; Wilson, T. S.; Maitland, D. J. Biomedical applications of thermally activated shape memory polymers. *J. Mater. Chem.* **2010,** 20, 3356-3366.

47. Serrano, M. C.; Ameer, G. A. Recent insights into the biomedical applications of shape-memory polymers. *Macromol. Biosci.* **2012,** 12, 1156-1171.

48. Chan, B. Q.; Low, Z. W.; Heng, S. J.; Chan, S. Y.; Owh, C.; Loh, X. J. Recent advances in shape memory soft materials for biomedical applications. *ACS Appl. Mater. Interfaces* **2016,** 8 ., 10070-10087.

49. Wang, K.; Strandman, S.; Zhu, X. X. A mini review: Shape memory polymers for biomedical applications. *Front. Chem..Sci. Eng.* **2017,** 11, 143-153.

50. Liu, Y.; Du, H.; Liu, L.; Leng, J. Shape memory polymers and their composites in aerospace applications: a review. *Smart Mater. Struct.* **2014,** 23, 023001.

51. Liu, Y.; Genzer, J.; Dickey, M. D. “2D or not 2D”: Shape-programming polymer sheets. *Prog. Polym. Sci.* **2016,** 52, 79-106.

52. Yang, Y.; Ding, X.; Urban, M. W. Chemical and physical aspects of self-healing materials. *Prog. Polym. Sci.* **2015,** 49-50, 34-59.

53. Zhang, P.; Li, G. Advances in healing-on-demand polymers and polymer composites. *Prog. Polym. Sci.* **2016,** 57, 32-63.

54. Xie, T. Tunable polymer multi-shape memory effect. *Nature* **2010,** 464, 267-70.

55. Wang, K.; Jia, Y.-G.; Zhu, X. X. Biocompound-based multiple shape memory polymers reinforced by photo-cross-linking. *ACS Biomater. Sci. Eng.* **2015,** 1, 855-863.

56. Chen, H.; Li, Y.; Tao, G.; Wang, L.; Zhou, S. Thermo- and water-induced shape memory poly(vinyl alcohol) supramolecular networks crosslinked by self-complementary quadruple hydrogen bonding. *Polym. Chem.* **2016,** 7, 6637-6644.

57. Yasin, A.; Li, H.; Lu, Z.; Rehman, S. u.; Siddiq, M.; Yang, H. A shape memory hydrogel induced by the interactions between metal ions and phosphate. *Soft Matter* **2014,** 10, 972-977.

58. Wang, Q.; Bai, Y.; Chen, Y.; Ju, J.; Zheng, F.; Wang, T. High performance shape memory polyimides based on π–π interactions. *J. Mater. Chem. A* **2015,** 3, 352-359.

59. Wang, L.; Di, S.; Wang, W.; Zhou, S. Self-healing and shape memory capabilities of copper-coordination polymer network. *RSC Adv.* **2015,** 5, 28896-28900.

60. Zhao, Q.; Zou, W.; Luo, Y.; Xie, T. Shape memory polymer network with thermally distinct elasticity and plasticity. *Sci. Adv.* **2016,** 2, e1501297.

61. Fang, Z.; Zheng, N.; Zhao, Q.; Xie, T. Healable, reconfigurable, reprocessable thermoset shape memory polymer with highly tunable topological rearrangement kinetics. *ACS Appl. Mater. Interfaces* **2017,** 9, 22077-22082.

62. Zhang, G.; Zhao, Q.; Yang, L.; Zou, W.; Xi, X.; Xie, T. Exploring dynamic equilibrium of diels–alder reaction for solid state plasticity in remoldable shape memory polymer network. *ACS Macro Lett.* **2016,** 5, 805-808.

63. Michal, B. T.; Jaye, C. A.; Spencer, E. J.; Rowan, S. J. Inherently photohealable and thermal shape-memory polydisulfide networks. *ACS Macro Lett.* **2013,** 2, 694-699.

64. Xiao, X. L.; Kong, D. Y.; Qiu, X. Y.; Zhang, W. B.; Zhang, F. H.; Liu, L. W.; Liu, Y. J.; Zhang, S.; Hu, Y.; Leng, J. S. Shape-memory polymers with adjustable high glass transition temperatures. *Macromolecules* **2015,** 48, 3582-3589.

65. Yang, C. S.; Wu, H. C.; Sun, J. S.; Hsiao, H. M.; Wang, T. W. Thermo-induced shape-memory PEG-PCL copolymer as a dual-drug-eluting biodegradable stent. *ACS Appl. Mater. Interfaces* **2013,** 5, 10985-10994.

66. Martínez-Gómez, A.; Fernández-Blázquez, J. P.; Bello, A.; Pérez, E. Preparation and properties of a main-chain smectic liquid-crystalline elastomer with shape-memory ability. *Macromolecules* **2016,** 49, 5306-5314.

67. Inomata, K.; Nakagawa, K.; Fukuda, C.; Nakada, Y.; Sugimoto, H.; Nakanishi, E. Shape memory behavior of poly(methyl methacrylate)-graft-poly(ethylene glycol) copolymers. *Polymer* **2010,** 51, 793-798.

68. Shearouse, W. C.; Lillie, L. M.; Reineke, T. M.; Tolman, W. B. Sustainable polyesters derived from glucose and castor oil: building block structure impacts properties. *ACS Macro Lett.* **2015,** 4, 284-288.

69. Gu, X.; Mather, P. T. Entanglement-based shape memory polyurethanes: Synthesis and characterization. *Polymer* **2012,** 53, 5924-5934.

70. Yang, R.; Chen, L.; Ruan, C.; Zhong, H.-Y.; Wang, Y.-Z. Chain folding in main-chain liquid crystalline polyesters: from π–π stacking toward shape memory. *J. Mater. Chem. C* **2014,** 2, 6155-6164.

71. Sun, L.; Huang, W. M. Mechanisms of the multi-shape memory effect and temperature memory effect in shape memory polymers. *Soft Matter* **2010,** 6, 4403-4406.

72. Bai, Y.; Jiang, C.; Wang, Q.; Wang, T. Multi-shape-memory property study of novel poly(ε-caprolactone)/ethyl cellulose polymer networks. *Macromol. Chem. Phys.* **2013,** 214, 2465-2472.

73. Kolesov, I. S. Multiple shape-memory behavior and thermal-mechanical properties of peroxide cross-linked blends of linear and short-chain branched polyethylenes. *Express Polym. Lett.* **2008,** 2, 461-473.

74. Zotzmann, J.; Behl, M.; Feng, Y.; Lendlein, A. Copolymer networks based on poly(ω-pentadecalactone) and poly(ε-caprolactone) segments as a versatile triple-shape polymer system. *Adv. Funct. Mater.* **2010,** 20, 3583-3594.

75. Zheng, N.; Hou, J.; Xu, Y.; Fang, Z.; Zou, W.; Zhao, Q.; Xie, T. Catalyst-free thermoset polyurethane with permanent shape reconfigurability and highly tunable triple-shape memory performance. *ACS Macro Lett.* **2017,** 6, 326-330.

76. Samuel, C.; Barrau, S.; Lefebvre, J.-M.; Raquez, J.-M.; Dubois, P. Designing multiple-shape memory Polymers with miscible polymer blends: evidence and origins of a triple-shape memory effect for miscible PLLA/PMMA blends. *Macromolecules* **2014,** 47, 6791-6803.

77. Shao, Y.; Lavigueur, C.; Zhu, X. X. Multishape memory effect of norbornene-based copolymers with cholic acid pendant groups. *Macromolecules* **2012,** 45, 1924-1930.

78. Luo, Y.; Guo, Y.; Gao, X.; Li, B. G.; Xie, T. A general approach towards thermoplastic multishape-memory polymers via sequence structure design. *Adv. Mater.* **2013,** 25, 743-748.

79. Yang, X.; Wang, L.; Wang, W.; Chen, H.; Yang, G.; Zhou, S. Triple shape memory effect of star-shaped polyurethane. *ACS Appl. Mater. Interfaces* **2014,** 6, 6545-6554.

80. Bellin, I.; Kelch, S.; Langer, R.; Lendlein, A. Polymeric triple-shape materials. *Proc. Natl. Acad. Sci. U.S.A.* **2006,** 103, 18043-18047.

81. Xiao, L. P.; Wei, M.; Zhan, M. Q.; Zhang, J. J.; Xie, H.; Deng, X. Y.; Yang, K. K.; Wang, Y. Z. Novel triple-shape PCU/PPDO interpenetrating polymer networks constructed by self-complementary quadruple hydrogen bonding and covalent bonding. *Polym. Chem.* **2014,** 5, 2231-2241.

82. Cuevas, J. M.; Rubio, R.; German, L.; Laza, J. M.; Vilas, J. L.; Rodriguez, M.; Leon, L. M. Triple-shape memory effect of covalently crosslinked polyalkenamer based semicrystalline polymer blends. *Soft Matter* **2012,** 8, 4928-4935.

83. Zhao, J.; Chen, M.; Wang, X.; Zhao, X.; Wang, Z.; Dang, Z. M.; Ma, L.; Hu, G. H.; Chen, F. Triple shape memory effects of cross-linked polyethylene/polypropylene blends with cocontinuous architecture. *ACS Appl. Mater. Interfaces* **2013,** 5, 5550-5556.

84. Chen, S.; Yuan, H.; Zhuo, H.; Chen, S.; Yang, H.; Ge, Z.; Liu, J. Development of liquid-crystalline shape-memory polyurethane composites based on polyurethane with semi-crystalline reversible phase and hexadecyloxybenzoic acid for self-healing applications. *J. Mater. Chem. C* **2014,** 2, 4203-4212.

85. Wang, L.; Yang, X.; Chen, H.; Gong, T.; Li, W.; Yang, G.; Zhou, S. Design of triple-shape memory polyurethane with photo-cross-linking of cinnamon groups. *ACS Appl. Mater. Interfaces* **2013,** 5, 10520-10528.

86. Xie, H.; Cheng, C.-Y.; Du, L.; Fan, C.-J.; Deng, X.-Y.; Yang, K.-K.; Wang, Y.-Z. A facile strategy to construct PDLLA-PTMEG network with triple-shape effect via photo-cross-linking of anthracene groups. *Macromolecules* **2016,** 49, 3845-3855.

87. Chatani, S.; Wang, C.; Podgórski, M.; Bowman, C. N. Triple shape memory materials incorporating two distinct polymer networks formed by selective thiol–michael addition reactions. *Macromolecules* **2014,** 47, 4949-4954.

88. Xie, T.; Xiao, X.; Cheng, Y. T. Revealing triple-shape memory effect by polymer bilayers. *Macromol. Rapid Commun.* **2009,** 30, 1823-1827.

89. Ahn, S.-k.; Deshmukh, P.; Kasi, R. M. Shape memory behavior of side-chain liquid crystalline polymer networks triggered by dual transition temperatures. *Macromolecules* **2010,** 43, 7330-7340.

90. Ahn, S.-k.; Kasi, R. M. Exploiting microphase-separated morphologies of side-chain liquid crystalline polymer networks for triple shape memory properties. *Adv. Funct. Mater.* **2011,** 21, 4543-4549.

91. Ahn, S. K.; Deshmukh, P.; Gopinadhan, M.; Osuji, C. O.; Kasi, R. M. Side-chain liquid crystalline polymer networks: exploiting nanoscale smectic polymorphism to design shape-memory polymers. *ACS Nano* **2011,** 5, 3085-95.

92. Wen, Z.; Zhang, T.; Hui, Y.; Wang, W.; Yang, K.; Zhou, Q.; Wang, Y. Elaborate fabrication of well-defined side-chain liquid crystalline polyurethane networks with triple-shape memory capacity. *J. Mater. Chem. A* **2015,** 3, 13435-13444.

93. Fu, S.; Zhang, H.; Zhao, Y. Optically and thermally activated shape memory supramolecular liquid crystalline polymers. *J. Mater. Chem. C* **2016,** 4, 4946-4953.

94. Chen, S.; Yuan, H.; Chen, S.; Yang, H.; Ge, Z.; Zhuo, H.; Liu, J. Development of supramolecular liquid-crystalline polyurethane complexes exhibiting triple-shape functionality using a one-step programming process. *J. Mater. Chem. A* **2014,** 2, 10169-10181.

95. Chen, S.; Yuan, H.; Ge, Z.; Chen, S.; Zhuo, H.; Liu, J. Insights into liquid-crystalline shape-memory polyurethane composites based on an amorphous reversible phase and hexadecyloxybenzoic acid. *J. Mater. Chem. C* **2014,** 2, 1041-1049.

96. Kolesov, I. Shape-memory behavior of cross-linked semi-crystalline polymers and their blends. *Express Polym. Lett.* **2015,** 9, 255-276.

97. Li, M.-q.; Song, F.; Chen, L.; Wang, X.-l.; Wang, Y.-z. Flexible material based on poly(lactic acid) and liquid crystal with multishape memory effects. *ACS Sustain. Chem. Eng.* **2016,** 4, 3820-3829.

98. Li, J.; Liu, T.; Xia, S.; Pan, Y.; Zheng, Z.; Ding, X.; Peng, Y. A versatile approach to achieve quintuple-shape memory effect by semi-interpenetrating polymer networks containing broadened glass transition and crystalline segments. *J. Mater. Chem.* **2011,** 21, 12213-12217.

99. Zhuo, S.; Zhang, G.; Feng, X.; Jiang, H.; Shi, J.; Liu, H.; Li, H. Multiple shape memory polymers for self-deployable device. *RSC Adv.* **2016,** 6, 50581-50586.

100. Wang, Z.; Zhao, J.; Chen, M.; Yang, M.; Tang, L.; Dang, Z. M.; Chen, F.; Huang, M.; Dong, X. Dually actuated triple shape memory polymers of cross-linked polycyclooctene-carbon nanotube/polyethylene nanocomposites. *ACS Appl. Mater. Interfaces* **2014,** 6, 20051-20059.

101. Niu, Y.; Zhang, P.; Zhang, J.; Xiao, L.; Yang, K.; Wang, Y. Poly(*p*-dioxanone)–poly(ethylene glycol) network: synthesis, characterization, and its shape memory effect. *Polym. Chem.* **2012,** 3, 2508-2516.

102. Chen, H. M.; Liu, Y.; Gong, T.; Wang, L.; Zhao, K. Q.; Zhou, S. B. Use of intermolecular hydrogen bonding to synthesize triple-shape memory supermolecular composites. *RSC Adv.* **2013,** 3, 7048-7056.

103. Dolog, R.; Weiss, R. A. Shape memory behavior of a polyethylene-based carboxylate ionomer. *Macromolecules* **2013,** 46, 7845-7852.

104. Chen, S.; Mo, F.; Stadler, F. J.; Chen, S.; Ge, Z.; Zhuo, H. Development of zwitterionic copolymers with multi-shape memory effects and moisture-sensitive shape memory effects. *J. Mater. Chem. B* **2015,** 3, 6645-6655.

105. Chen, S.; Mo, F.; Yang, Y.; Stadler, F. J.; Chen, S.; Yang, H.; Ge, Z. Development of zwitterionic polyurethanes with multi-shape memory effects and self-healing properties. *J. Mater. Chem. A* **2015,** 3, 2924-2933.

106. Ware, T.; Hearon, K.; Lonnecker, A.; Wooley, K. L.; Maitland, D. J.; Voit, W. Triple-shape memory polymers based on self-complementary hydrogen bonding. *Macromolecules* **2012,** 45, 1062-1069.

107. Wu, Y.; Hu, J.; Han, J.; Zhu, Y.; Huang, H.; Li, J.; Tang, B. Two-way shape memory polymer with "switch–spring" composition by interpenetrating polymer network. *J. Mater. Chem. A* **2014,** 2, 18816-18822.

108. Ma, L.; Zhao, J.; Wang, X.; Chen, M.; Liang, Y.; Wang, Z.; Yu, Z.; Hedden, R. C. Effects of carbon black nanoparticles on two-way reversible shape memory in crosslinked polyethylene. *Polymer* **2015,** 56, 490-497.

109. Rousseau, I. A.; Mather, P. T. Shape memory effect exhibited by smectic-C liquid crystalline elastomers. *J. Am. Chem. Soc.* **2003,** 125, 15300-15301.

110. Li, J.; Rodgers, W. R.; Xie, T. Semi-crystalline two-way shape memory elastomer. *Polymer* **2011,** 52, 5320-5325.

111. Thomsen, D. L.; Keller, P.; Naciri, J.; Pink, R.; Jeon, H.; Shenoy, D.; Ratna, B. R. Liquid crystal elastomers with mechanical properties of a muscle. *Macromolecules* **2001,** 34, 5868-5875.

112. Qin, H.; Mather, P. T. Combined one-way and two-way shape memory in a glass-forming nematic network. *Macromolecules* **2009,** 42, 273-280.

113. Burke, K. A.; Rousseau, I. A.; Mather, P. T. Reversible actuation in main-chain liquid crystalline elastomers with varying crosslink densities. *Polymer* **2014,** 55, 5897-5907.

114. Torbati, A. H.; Mather, P. T. A hydrogel-forming liquid crystalline elastomer exhibiting soft shape memory. *J. Polym. Sci., Part B: Polym. Phys.* **2016,** 54, 38-52.

115. Wang, L.; Liu, W.; Guo, L.-X.; Lin, B.-P.; Zhang, X.-Q.; Sun, Y.; Yang, H. A room-temperature two-stage thiol–ene photoaddition approach towards monodomain liquid crystalline elastomers. *Polym. Chem.* **2017**, 8, 1364-1370.

116. Lama, G. C.; Cerruti, P.; Lavorgna, M.; Carfagna, C.; Ambrogi, V.; Gentile, G. Controlled actuation of a carbon nanotube/epoxy shape-memory liquid crystalline elastomer. *J Phys. Chem. C* **2016,** 120, 24417-24426.

117. Chung, T.; Rorno-Uribe, A.; Mather, P. T. Two-way reversible shape memory in a semicrystalline network. *Macromolecules* **2008,** 41, 184-192.

118. Lee, K. M.; Knight, P. T.; Chung, T.; Mather, P. T. Polycaprolactone-POSS chemical/physical double networks. *Macromolecules* **2008,** 41, 4730-4738.

119. Hong, S. J.; Yu, W. R.; Youk, J. H. Two-way shape memory behavior of shape memory polyurethanes with a bias load. *Smart Mater. Struct.* **2010,** 19, 035022.

120. Baker, R. M.; Henderson, J. H.; Mather, P. T. Shape memory poly(ε-caprolactone)-*co*-poly(ethylene glycol) foams with body temperature triggering and two-way actuation. *J. Mater. Chem. B* **2013,** 1, 4916-4920.

121. Huang, M.; Dong, X.; Wang, L.; Zhao, J.; Liu, G.; Wang, D. Two-way shape memory property and its structural origin of cross-linked poly(ε-caprolactone). *RSC Adv.* **2014,** 4, 55483-55494.

122. Pandini, S.; Baldi, F.; Paderni, K.; Messori, M.; Toselli, M.; Pilati, F.; Gianoncelli, A.; Brisotto, M.; Bontempi, E.; Riccò, T. One-way and two-way shape memory behaviour of semi-crystalline networks based on sol–gel cross-linked poly(ε-caprolactone). *Polymer* **2013,** 54, 4253-4265.

123. Pandini, S.; Passera, S.; Messori, M.; Paderni, K.; Toselli, M.; Gianoncelli, A.; Bontempi, E.; Riccò, T. Two-way reversible shape memory behaviour of crosslinked poly(ε-caprolactone). *Polymer* **2012,** 53, 1915-1924.

124. Raquez, J. M.; Vanderstappen, S.; Meyer, F.; Verge, P.; Alexandre, M.; Thomassin, J. M.; Jerome, C.; Dubois, P. Design of cross-linked semicrystalline poly(ε-caprolactone)-based networks with one-way and two-way shape-memory properties through Diels-Alder reactions. *Chemistry* **2011,** 17, 10135-10143.

125. Bai, Y. K.; Zhang, X. R.; Wang, Q. H.; Wang, T. M. A tough shape memory polymer with triple-shape memory and two-way shape memory properties. *J. Mater. Chem. A* **2014,** 2, 4771-4778.

126. Kolesov, I.; Dolynchuk, O.; Jehnichen, D.; Reuter, U.; Stamm, M.; Radusch, H. J. Changes of crystal structure and morphology during two-way shape-memory cycles in cross-linked linear and short-chain branched polyethylenes. *Macromolecules* **2015,** 48, 4438-4450.

127. Zotzmann, J.; Behl, M.; Hofmann, D.; Lendlein, A. Reversible triple-shape effect of polymer networks containing polypentadecalactone- and poly(ε-caprolactone)-segments. *Adv. Mater.* **2010,** 22, 3424-3429.

128. Imai, S.; Sakurai, K. An actuator of two-way behavior by using two kinds of shape memory polymers with different T_gs. *Precis. Eng.* **2013,** 37, 572-579.

129. Kang, T.-H.; Lee, J.-M.; Yu, W.-R.; Youk, J. H.; Ryu, H. W. Two-way actuation behavior of shape memory polymer/elastomer core/shell composites. *Smart Mater. Struct.* **2012,** 21, 035028.

130. Taya, M.; Liang, Y.; Namli, O. C.; Tamagawa, H.; Howie, T. Design of two-way reversible bending actuator based on a shape memory alloy/shape memory polymer composite. *Smart Mater. Struct.* **2013,** 22, 105003.

131.Behl, M.; Kratz, K.; Zotzmann, J.; Nochel, U.; Lendlein, A. Reversible bidirectional shape-memory polymers. *Adv. Mater.* **2013,** 25, 4466-4469.

132. Zhou, J.; Turner, S. A.; Brosnan, S. M.; Li, Q.; Carrillo, J.-M. Y.; Nykypanchuk, D.; Gang, O.; Ashby, V. S.; Dobrynin, A. V.; Sheiko, S. S. Shapeshifting: Reversible shape memory in semicrystalline elastomers. *Macromolecules* **2014,** 47, 1768-1776.

133. Li, Q.; Zhou, J.; Vatankhah-Varnoosfaderani, M.; Nykypanchuk, D.; Gang, O.; Sheiko, S. S. Advancing reversible shape memory by tuning the polymer network architecture. *Macromolecules* **2016,** 49, 1383-1391.

134. Gong, T.; Zhao, K.; Wang, W.; Chen, H.; Wang, L.; Zhou, S. Thermally activated reversible shape switch of polymer particles. *J. Mater. Chem. B* **2014,** 2, 6855-6866.

135. Qian, C.; Dong, Y.; Zhu, Y.; Fu, Y. Two-way shape memory behavior of semi-crystalline elastomer under stress-free condition. *Smart Mater. Struct.* **2016,** 25, 085023.

136. Dolynchuk, O.; Kolesov, I.; Jehnichen, D.; Reuter, U.; Radusch, H.-J.; Sommer, J.-U. Reversible shape-memory effect in cross-linked linear poly(ε-caprolactone) under stress and stress-free conditions. *Macromolecules* **2017,** 50, 3841-3854.

137. Wang, K.; Jia, Y.-G.; Zhu, X. X. Two-way reversible shape memory polymers made of cross-linked cocrystallizable random copolymers with tunable actuation temperatures. *Macromolecules* **2017,** 50, 8570-8579.

138. Meng, Y.; Jiang, J.; Anthamatten, M. Shape actuation via internal stress-induced crystallization of dual-cure networks. *ACS Macro Lett.* **2015,** 4, 115-118.

139. Fan, L. F.; Rong, M. Z.; Zhang, M. Q.; Chen, X. D. A facile approach toward scalable fabrication of reversible shape-memory polymers with bonded elastomer microphases as internal stress provider. *Macromol. Rapid Commun.* **2017**, 38, 1700124.

140. Wang, M.; Sayed, S. M.; Guo, L. X.; Lin, B. P.; Zhang, X. Q.; Sun, Y.; Yang, H. Multi-stimuli responsive carbon nanotube incorporated polysiloxane azobenzene liquid crystalline elastomer composites.. *Macromolecules* **2016,** 49, 663-671.

141. Lu, L.; Li, G. One-way multishape-memory effect and tunable two-way shape memory effect of ionomer poly(ethylene-co-methacrylic acid). *ACS Appl. Mater. Interfaces* **2016,** 8, 14812-14823.

142. Biswas, A.; Aswal, V. K.; Sastry, P. U.; Rana, D.; Maiti, P. Reversible bidirectional shape memory effect in polyurethanes through molecular flipping. *Macromolecules* **2016,** 49, 4889-4897.

143. Gao, Y.; Liu, W.; Zhu, S. Polyolefin thermoplastics for multiple shape and reversible shape memory. *ACS Appl. Mater. Interfaces* **2017,** 9, 4882-4889.

144. Le, X.; Lu, W.; Xiao, H.; Wang, L.; Ma, C.; Zhang, J.; Huang, Y.; Chen, T. Fe_3^+-, pH-, thermoresponsive supramolecular hydrogel with multishape memory effect. *ACS Appl. Mater. Interfaces* **2017,** 9, 9038-9044.

145. Xu, B.; Zhang, Y.; Liu, W. Hydrogen-bonding toughened hydrogels and emerging CO_2-responsive shape memory effect. *Macromol. Rapid Commun.* **2015,** 36, 1585-1591.

146. Han, Y.; Bai, T.; Liu, Y.; Zhai, X.; Liu, W. Zinc ion uniquely induced triple shape memory effect of dipole-dipole reinforced ultra-high strength hydrogels. *Macromol. Rapid Commun.* **2012,** 33, 225-231.

147. Meng, H.; Zheng, J.; Wen, X.; Cai, Z.; Zhang, J.; Chen, T. pH- and sugar-induced shape memory hydrogel based on reversible phenylboronic acid-diol ester bonds. *Macromol. Rapid Commun.* **2015,** 36, 533-537.

148. Le, X.; Lu, W.; Zheng, J.; Tong, D.; Zhao, N.; Ma, C.; Xiao, H.; Zhang, J.; Huang, Y.; Chen, T. Stretchable supramolecular hydrogels with triple shape memory effect. *Chem. Sci.* **2016,** 7, 6715-6720.

149. Abbott, D. B.; Maity, S.; Burkey, M. T.; Gorga, R. E.; Bochinski, J. R.; Clarke, L. I. Blending with non-responsive polymers to incorporate nanoparticles into shape-memory materials and enable photothermal heating: The effects of heterogeneous temperature distribution. *Macromol. Chem. Phys.* **2014,** 215, 2345-2356.

150. Zhang, H.; Xia, H.; Zhao, Y. Optically triggered and spatially controllable shape-memory polymer–gold nanoparticle composite materials. *J. Mater. Chem.* **2012,** 22, 845-849.

151. Zhang, H.; Zhao, Y. Polymers with dual light-triggered functions of shape memory and healing using gold nanoparticles. *ACS Appl. Mater. Interfaces* **2013,** 5, 13069-13075.

152. Zhang, H.; Xia, H.; Zhao, Y. Light-controlled complex deformation and motion of shape-memory polymers using a temperature gradient. *ACS Macro Lett.* **2014,** 3, 940-943.

153. Ge, F.; Lu, X.; Xiang, J.; Tong, X.; Zhao, Y. An optical actuator based on gold-nanoparticle-containing temperature-memory semicrystalline polymers. *Angew. Chem. Int. Ed.* **2017,** 56, 6126-6130.

154. Zhang, H.; Zhang, J.; Tong, X.; Ma, D.; Zhao, Y. Light polarization-controlled shape-memory polymer/gold nanorod composite. *Macromol. Rapid Commun.* **2013,** 34, 1575-1579.

155. Zheng, Y.; Li, J.; Lee, E.; Yang, S. Light-induced shape recovery of deformed shape memory polymer micropillar arrays with gold nanorods. *RSC Adv.* **2015,** 5, 30495-30499.

156. Kohlmeyer, R. R.; Lor, M.; Chen, J. Remote, local, and chemical programming of healable multishape memory polymer nanocomposites. *Nano Lett.* **2012,** 12, 2757-2762.

157. Lu, H.; Yao, Y.; Huang, W. M.; Leng, J.; Hui, D. Significantly improving infrared light-induced shape recovery behavior of shape memory polymeric nanocomposite via a synergistic effect of carbon nanotube and boron nitride. *Compos. Part B: Eng.* **2014,** 62, 256-261.

158. Li, C.; Liu, Y.; Lo, C.-w.; Jiang, H. Reversible white-light actuation of carbon nanotube incorporated liquid crystalline elastomer nanocomposites. *Soft Matter* **2011,** 7, 7511-7516.

159. Yu, L.; Yu, H. Light-powered tumbler movement of graphene oxide/polymer nanocomposites. *ACS Appl. Mater. Interfaces* **2015,** 7, 3834-3839.

160. Park, J. H.; Kim, B. K. Infrared light actuated shape memory effects in crystalline polyurethane/graphene chemical hybrids. *Smart Mater. Struct.* **2014,** 23, 025038.

161. Liang, J.; Xu, Y.; Huang, Y.; Zhang, L.; Wang, Y.; Ma, Y.; Li, F.; Guo, T.; Chen, Y. Infrared-triggered actuators from graphene-based nanocomposites. *J. Phys. Chem. C* **2009,** 113, 9921-9927.

162. Zhou, L.; Liu, Q.; Lv, X.; Gao, L.; Fang, S.; Yu, H. Photoinduced triple shape memory polyurethane enabled by doping with azobenzene and GO. *J. Mater. Chem. C* **2016,** 4, 9993-9997.

163. Yang, Y.; Zhan, W.; Peng, R.; He, C.; Pang, X.; Shi, D.; Jiang, T.; Lin, Z. Graphene-enabled superior and tunable photomechanical actuation in liquid crystalline elastomer nanocomposites. *Adv. Mater.* **2015,** 27, 6376-6381.

164. Leng, J. S.; Wu, X. L.; Liu, Y. J. Infrared light-active shape memory polymer filled with nanocarbon particles. *J. Appl. Polym. Sci.* **2009,** 114, 2455-2460.

165. Liu, Y.; Boyles, J. K.; Genzer, J.; Dickey, M. D. Self-folding of polymer sheets using local light absorption. *Soft Matter* **2012,** 8, 1764-1769.

166. Ishii, S.; Uto, K.; Niiyama, E.; Ebara, M.; Nagao, T. Hybridizing poly(ε-caprolactone) and plasmonic titanium nitride nanoparticles for broadband photoresponsive shape memory films. *ACS Appl. Mater. Interfaces* **2016**, 2016, 8, 5634–5640.

167. Wu, Y.; Hu, J.; Zhang, C.; Han, J.; Wang, Y.; Kumar, B. A facile approach to fabricate a UV/heat dual-responsive triple shape memory polymer. *J. Mater. Chem. A* **2015,** 3, 97-100.

168. Kumpfer, J. R.; Rowan, S. J. Thermo-, photo-, and chemo-responsive shape-memory properties from photo-cross-linked metallo-supramolecular polymers. *J. Am. Chem. Soc.* **2011,** 133, 12866-12874.

169. Wei, K.; Zhu, G. M.; Tang, Y. S.; Li, X. M.; Liu, T. T. The effects of carbon nanotubes on electroactive shape-memory behaviors of hydro-epoxy/carbon black composite. *Smart Mater. Struct.* **2012,** 21, 085016.

170. Liu, X.; Li, H.; Zeng, Q.; Zhang, Y.; Kang, H.; Duan, H.; Guo, Y.; Liu, H. Electro-active shape memory composites enhanced by flexible carbon nanotube/graphene aerogels. *J. Mater. Chem. A* **2015,** 3, 11641-11649.

171. Xiao, Y.; Zhou, S.; Wang, L.; Gong, T. Electro-active shape memory properties of poly(ε-caprolactone)/functionalized multiwalled carbon nanotube nanocomposite. *ACS Appl. Mater. Interfaces* **2010,** 2, 3506-3514.

172. Zhou, J.; Li, H.; Liu, W.; Dugnani, R.; Tian, R.; Xue, W.; Chen, Y.; Guo, Y.; Duan, H.; Liu, H. A facile method to fabricate polyurethane based graphene foams/epoxy/carbon nanotubes composite for electro-active shape memory application. *Compos. Part A: Appl. Sci. Manuf.* **2016,** 91, 292-300.

173. Shao, L.-n.; Dai, J.; Zhang, Z.-x.; Yang, J.-h.; Zhang, N.; Huang, T.; Wang, Y. Thermal and electroactive shape memory behaviors of poly(L-lactide)/thermoplastic polyurethane blend induced by carbon nanotubes. *RSC Adv.* **2015,** 5, 101455-101465.

174. Cho, J. W.; Kim, J. W.; Jung, Y. C.; Goo, N. S. Electroactive shape-memory polyurethane composites incorporating carbon nanotubes. *Macromol. Rapid Commun.* **2005,** 26, 412-416.

175. Raja, M.; Ryu, S. H.; Shanmugharaj, A. M. Influence of surface modified multiwalled carbon nanotubes on the mechanical and electroactive shape memory properties of polyurethane (PU)/poly(vinylidene diflouride) (PVDF) composites. *Colloids Surf, A* **2014,** 450, 59-66.

176. Raja, M.; Ryu, S. H.; Shanmugharaj, A. M. Thermal, mechanical and electroactive shape memory properties of polyurethane (PU)/poly (lactic acid) (PLA)/CNT nanocomposites. *Eur. Polym. J.* **2013,** 49, 3492-3500.

177. Du, F.-P.; Ye, E.-Z.; Yang, W.; Shen, T.-H.; Tang, C.-Y.; Xie, X.-L.; Zhou, X.-P.; Law, W.-C. Electroactive shape memory polymer based on optimized multi-walled carbon nanotubes/polyvinyl alcohol nanocomposites. *Compos. Part B: Eng.* **2015,** 68, 170-175.

178. Qi, X.; Dong, P.; Liu, Z.; Liu, T.; Fu, Q. Selective localization of multi-walled carbon nanotubes in bi-component biodegradable polyester blend for rapid electroactive shape memory performance. *Compos. Sci. Technol.* **2016,** 125, 38-46.

179. Mahapatra, S. S.; Yadav, S. K.; Yoo, H. J.; Ramasamy, M. S.; Cho, J. W. Tailored and strong electro-responsive shape memory actuation in carbon nanotube-reinforced hyperbranched polyurethane composites. *Sens. Actuators, B* **2014,** 193, 384-390.
180. Lu, H. B.; Liang, F.; Gou, J. H.; Leng, J. S.; Du, S. Y. Synergistic effect of Ag nanoparticle-decorated graphene oxide and carbon fiber on electrical actuation of polymeric shape memory nanocomposites. *Smart Mater. Struct.* **2014,** 23, 085034.

181. Sen, I.; Seki, Y.; Sarikanat, M.; Cetin, L.; Gurses, B. O.; Ozdemir, O.; Yilmaz, O. C.; Sever, K.; Akar, E.; Mermer, O. Electroactive behavior of graphene nanoplatelets loaded cellulose composite actuators. *Compos. Part B: Eng.* **2015,** 69, 369-377.
182. Tang, Z.; Kang, H.; Wei, Q.; Guo, B.; Zhang, L.; Jia, D. Incorporation of graphene into polyester/carbon nanofibers composites for better multi-stimuli responsive shape memory performances. *Carbon* **2013,** 64, 487-498.
183. Rana, S.; Cho, J. W.; Tan, L. P. Graphene-crosslinked polyurethane block copolymer nanocomposites with enhanced mechanical, electrical, and shape memory properties. *RSC Adv.* **2013,** 3, 13796-13803.
184. Wang, W.; Liu, D.; Liu, Y.; Leng, J.; Bhattacharyya, D. Electrical actuation properties of reduced graphene oxide paper/epoxy-based shape memory composites. *Compos. Sci. Technol.* **2015,** 106, 20-24.
185. Wang, K.; Zhu, G.-m.; Yan, X.-g.; Ren, F.; Cui, X.-p. Electroactive shape memory cyanate/polybutadiene epoxy composites filled with carbon black. *Chin. J. Polym. Sci.* **2016,** 34, 466-474.
186. Wang, Y.; Zhu, G.; Cui, X.; Liu, T.; Liu, Z.; Wang, K. Electroactive shape memory effect of radiation cross-linked SBS/LLDPE composites filled with carbon black. *Colloid Polym. Sci.* **2014,** 292, 2311-2317.
187. Wei, K.; Zhu, G.; Tang, Y.; Li, X. Electroactive shape-memory effects of hydro-epoxy/carbon black composites. *Polym. J.* **2012,** 45, 671-675.
188. Qi, X.; Xiu, H.; Wei, Y.; Zhou, Y.; Guo, Y.; Huang, R.; Bai, H.; Fu, Q. Enhanced shape memory property of polylactide/thermoplastic poly(ether)urethane composites via carbon black self-networking induced co-continuous structure. *Compos. Sci. Technol.* **2017,** 139, 8-16.

189. Chen, S.; Yang, S.; Li, Z.; Xu, S.; Yuan, H.; Chen, S.; Ge, Z. Electroactive two-way shape memory polymer laminates. *Polym. Compos.* **2015,** 36, 439-444.

190. Lu, H.; Yao, Y.; Zhu, S.; Yang, Y.; Lin, L. Fabrication of free-standing octagon-shaped carbon nanofibre assembly for electrical actuation of shape memory polymer nanocomposites. *Pigm Resin Technol.* **2015,** 44, 157-164.

191. Lu, H.; Liang, F.; Yao, Y.; Gou, J.; Hui, D. Self-assembled multi-layered carbon nanofiber nanopaper for significantly improving electrical actuation of shape memory polymer nanocomposite. *Compos. Part B: Eng.* **2014,** 59, 191-195.

192. Lee, S. H.; Jung, J. H.; Oh, I. K. 3D networked graphene-ferromagnetic hybrids for fast shape memory polymers with enhanced mechanical stiffness and thermal conductivity. *Small* **2014,** 10, 3880-3886.

193. Bai, S.; Zou, H.; Dietsch, H.; Simon, Y. C.; Weder, C. Functional iron oxide nanoparticles as reversible crosslinks for magnetically addressable shape-memory polymers. *Macromol. Chem. Phys.* **2014,** 215, 398-404.

194. Cai, Y.; Jiang, J.-S.; Liu, Z.-W.; Zeng, Y.; Zhang, W.-G. Magnetically-sensitive shape memory polyurethane composites crosslinked with multi-walled carbon nanotubes. *Compos. Part A: Appl. Sci. .Manuf.* **2013,** 53, 16-23.

195. Wang, Y.; Ye, J.; Tian, W. Shape memory polymer composites of poly(styrene-b-butadiene-b-styrene) copolymer/liner low density polyethylene/Fe_3O_4 nanoparticles for remote activation. *Appl. Sci.* **2016,** 6, 333.

196. Liu, Y.; Xu, K.; Chang, Q.; Darabi, M. A.; Lin, B.; Zhong, W.; Xing, M. Highly flexible and resilient elastin hybrid cryogels with shape memory, injectability, conductivity, and magnetic responsive properties. *Adv. Mater.* **2016,** 28, 7758-7767.

197. Razzaq, M. Y.; Behl, M.; Lendlein, A. Magnetic memory effect of nanocomposites. *Adv. Funct. Mater.* **2012,** 22, 184-191.

198. Cai, Y.; Jiang, J.-S.; Zheng, B.; Xie, M.-R. Synthesis and properties of magnetic sensitive shape memory Fe_3O_4/poly(ε-caprolactone)-polyurethane nanocomposites. *J. Appl. Polym. Sci.* **2013,** 127, 49-56.

199. Schmidt, A. M. Electromagnetic activation of shape memory polymer networks containing magnetic nanoparticles. *Macromol. Rapid Commun.* **2006,** 27, 1168-1172.

200. Xia, S.; Li, X.; Wang, Y.; Pan, Y.; Zheng, Z.; Ding, X.; Peng, Y. A remote-activated shape memory polymer network employing vinyl-capped Fe_3O_4 nanoparticles as netpoints for durable performance. *Smart Mater. Struct.* **2014,** 23, 085005.

201. Zhang, X.; Lu, X.; Wang, Z.; Wang, J.; Sun, Z. Biodegradable shape memory nanocomposites with thermal and magnetic field responsiveness. *J. Biomater. Sci. Polym. Ed.* **2013,** 24, 1057-1070.

202. Yang, D.; Huang, W.; He, X.; Xie, M. Electromagnetic activation of a shape memory copolymer matrix incorporating ferromagnetic nanoparticles. *Polym. Int.* **2012,** 61, 38-42.

203. Puig, J.; Hoppe, C. E.; Fasce, L. A.; Pérez, C. J.; Piñeiro-Redondo, Y.; Bañobre-López, M.; López-Quintela, M. A.; Rivas, J.; Williams, R. J. J. Superparamagnetic nanocomposites based on the dispersion of oleic acid-stabilized magnetite nanoparticles in a diglycidylether of bisphenol A-based epoxy matrix: Magnetic hyperthermia and shape memory. *J. Phys. Chem. C* **2012,** 116, 13421-13428.

204. Razzaq, M. Y.; Behl, M.; Nöchel, U.; Lendlein, A. Magnetically controlled shape-memory effects of hybrid nanocomposites from oligo(ω-pentadecalactone) and covalently integrated magnetite nanoparticles. *Polymer* **2014,** 55, 5953-5960.

205. Razzaq, M. Y.; Behl, M.; Kratz, K.; Lendlein, A. Multifunctional hybrid nanocomposites with magnetically controlled reversible shape-memory effect. *Adv. Mater.* **2013,** 25, 5730-5733.

206. Gu, S.-Y.; Jin, S.-P.; Gao, X.-F.; Mu, J. Polylactide-based polyurethane shape memory nanocomposites (Fe_3O_4/PLAUs) with fast magnetic responsiveness. *Smart Mater. Struct.* **2016,** 25, 055036.

207. Mohr, R.; Kratz, K.; Weigel, T.; Lucka-Gabor, M.; Moneke, M.; Lendlein, A. Initiation of shape-memory effect by inductive heating of magnetic nanoparticles in thermoplastic polymers. *Proc. Natl. Acad. Sci. U. S. A.* **2006,** 103, 3540-3545.

208. Kalita, H.; Karak, N. Hyperbranched polyurethane/Fe_3O_4 nanoparticles decorated multiwalled carbon nanotube thermosetting nanocomposites as microwave actuated shape memory materials. *J. Mater. Res.* **2013,** 28, 2132-2141.

209. Yu, K.; Liu, Y.; Leng, J. Shape memory polymer/CNT composites and their microwave induced shape memory behaviors. *RSC Adv.* **2014,** 4, 2961-2968.

210. Du, H.; Yu, Y.; Jiang, G.; Zhang, J.; Bao, J. Microwave-induced shape-memory effect of chemically crosslinked moist poly(vinyl alcohol) networks. *Macromol. Chem. Phys.* **2011,** 212, 1460-1468.

211. Du, H.; Song, Z.; Wang, J.; Liang, Z.; Shen, Y.; You, F. Microwave-induced shape-memory effect of silicon carbide/poly(vinyl alcohol) composite. *Sens. Actuators, A* **2015,** 228, 1-8.

212. Du, H.; Liu, X.; Yu, Y.; Xu, Y.; Wang, Y.; Liang, Z. Microwave-induced poly(ionic liquid)/poly(vinyl alcohol) shape memory composites. *Macromol. Chem. Phys.* **2016,** 217, 2626-2634.

213. Bao, M.; Zhou, Q.; Dong, W.; Lou, X.; Zhang, Y. Ultrasound-modulated shape memory and payload release effects in a biodegradable cylindrical rod made of chitosan-functionalized PLGA microspheres. *Biomacromolecules* **2013,** 14, 1971-1979.

214. Han, J.; Fei, G.; Li, G.; Xia, H. High intensity focused ultrasound triggered shape memory and drug release from biodegradable polyurethane. *Macromol. Chem. Phys.* **2013,** 214, 1195-1203.

215. Bhargava, A.; Peng, K.; Stieg, J.; Mirzaeifar, R.; Shahab, S. Focused ultrasound actuation of shape memory polymers; acoustic-thermoelastic modeling and testing. *RSC Adv.* **2017,** 7, 45452-45469.

216. Li, G.; Fei, G.; Xia, H.; Han, J.; Zhao, Y. Spatial and temporal control of shape memory polymers and simultaneous drug release using high intensity focused ultrasound. *J. Mater. Chem.* **2012,** 22, 7692-7696.

217. Li, G.; Fei, G.; Liu, B.; Xia, H.; Zhao, Y. Shape recovery characteristics for shape memory polymers subjected to high intensity focused ultrasound. *RSC Adv.* **2014,** 4, 32701-32709.

218. Lu, X.; Fei, G.; Xia, H.; Zhao, Y. Ultrasound healable shape memory dynamic polymers. *J. Mater. Chem. A* **2014,** 2, 16051-16060.

219. Li, G.; Yan, Q.; Xia, H.; Zhao, Y. Therapeutic-ultrasound-triggered shape memory of a melamine-enhanced poly(vinyl alcohol) physical hydrogel. *ACS Appl. Mater. Interfaces* **2015,** 7, 12067-12073.

220. Serrano, M. C.; Carbajal, L.; Ameer, G. A. Novel biodegradable shape-memory elastomers with drug-releasing capabilities. *Advanced materials* **2011,** 23, 2211-2215.

221. Kashif, M.; Yun, B.-m.; Lee, K.-S.; Chang, Y.-W. Biodegradable shape-memory poly(ε-caprolactone)/polyhedral oligomeric silsequioxane nanocomposites: sustained drug release and hydrolytic degradation. *Mater. Lett.* **2016,** 166, 125-128.

222. Chen, H.; Li, Y.; Liu, Y.; Gong, T.; Wang, L.; Zhou, S. Highly pH-sensitive polyurethane exhibiting shape memory and drug release. *Polym. Chem.* **2014,** 5, 5168-5174.

223. Chen, M. C.; Tsai, H. W.; Chang, Y.; Lai, W. Y.; Mi, F. L.; Liu, C. T.; Wong, H. S.; Sung, H. W. Rapidly self-expandable polymeric stents with a shape-memory property. *Biomacromolecules* **2007,** 8, 2774-2780.

224. Small Iv, W.; Wilson, T. S.; Benett, W. J.; Loge, J. M.; Maitland, D. J. Laser-activated shape memory polymer intravascular thrombectomy device. *Opt. Express* **2005,** 13, 8204-8213.

225. Jing, X.; Mi, H. Y.; Huang, H. X.; Turng, L. S. Shape memory thermoplastic polyurethane (TPU)/poly(epsilon-caprolactone) (PCL) blends as self-knotting sutures. *J. Mech. Behav. Biomed.* **2016,** 64, 94-103.

226. Buckley, P. R.; McKinley, G. H.; Wilson, T. S.; Small, W.; Benett, W. J.; Bearinger, J. P.; McElfresh, M. W.; Maitland, D. J. Inductively heated shape memory polymer for the magnetic actuation of medical devices. *IEEE Trans. Biomed. Eng.* **2006,** 53, 2075-2083.

227. Hasnat Kabir, M.; Hazama, T.; Watanabe, Y.; Gong, J.; Murase, K.; Sunada, T.; Furukawa, H. Smart hydrogel with shape memory for biomedical applications. *J Taiwan Iist Chem E* **2014,** 45, 3134-3138.

228. Gong, T.; Zhao, K.; Liu, X.; Lu, L.; Liu, D.; Zhou, S. A dynamically tunable, bioinspired micropatterned surface regulates vascular endothelial and smooth muscle cells growth at vascularization. *Small* **2016,** 12, 5769-5778.

229. Liu, D.; Xiang, T.; Gong, T.; Tian, T.; Liu, X.; Zhou, S. Bioinspired 3D multilayered shape memory scaffold with a hierarchically changeable micropatterned surface for efficient vascularization. *ACS Appl. Mater. Interfaces* **2017,** 9, 19725-19735.

230. Lantada, A. D.; Romero, A. D.; Tanarro, E. C. Micro-vascular shape-memory polymer actuators with complex geometries obtained by laser stereolithography. *Smart Mater. Struct.* **2016,** 25, 065018.

231. Grunlan, M. A. Z., Dawei; Schoener, Cody A.; Saunders, William B. Shape memory polymer scaffolds for tissue defects. *US patent* **2017,** 20170021060.

232. Liu, X.; Zhao, K.; Gong, T.; Song, J.; Bao, C.; Luo, E.; Weng, J.; Zhou, S. Delivery of growth factors using a smart porous nanocomposite scaffold to repair a mandibular bone defect. *Biomacromolecules* **2014,** 15, 1019-1030.

233. Gong, T.; Li, W.; Chen, H.; Wang, L.; Shao, S.; Zhou, S. Remotely actuated shape memory effect of electrospun composite nanofibers. *Acta Biomater.* **2012,** 8, 1248-1259.

234. Antony, G. J.; Jarali, C. S.; Aruna, S. T.; Raja, S. Tailored poly(ethylene) glycol dimethacrylate based shape memory polymer for orthopedic applications. *J. Mech. Behav. Biomed. Mater.* **2017,** 65, 857-865.

235. Xue, L.; Dai, S.; Li, Z. Biodegradable shape-memory block co-polymers for fast self-expandable stents. *Biomaterials* **2010,** 31, 8132-8140.

236. RM, S. Self-deploying trusses containing shape-memory polymers. *NASA Tech. Briefs* **2008**, May, 20-21.

237. Lan, X.; Liu, Y. J.; Lv, H. B.; Wang, X. H.; Leng, J. S.; Du, S. Y. Fiber reinforced shape-memory polymer composite and its application in a deployable hinge. *Smart Mater. Struct.* **2009,** 18, 024002.

238. Song, J. J.; Chang, H. H.; Naguib, H. E. Biocompatible shape memory polymer actuators with high force capabilities. *Eur. Polym. J.* **2015,** 67, 186-198.

239. Fang, L.; Fang, T.; Liu, X.; Chen, S.; Lu, C.; Xu, Z. Near-infrared light triggered soft actuators in aqueous media prepared from shape-memory polymer composites. *Macromol. Mater. Eng.* **2016,** 301, 1111-1120.

240. Luo, H. S.; Li, Z. W.; Yi, G. B.; Wang, Y. J.; Zu, X. H.; Wang, H.; Huang, H. L.; Liang, Z. F. Temperature sensing of conductive shape memory polymer composites. *Mater. Lett.* **2015,** 140, 71-74.

241. Gong, X. B.; Liu, L. W.; Liu, Y. J.; Leng, J. S. An electrical-heating and self-sensing shape memory polymer composite incorporated with carbon fiber felt. *Smart Mater. Struct.* **2016,** 25, 035036.

242. Li, X.; Serpe, M. J. U Understanding the shape memory behavior of self-bending materials and their use as sensors. *Adv. Funct. Mater.* **2016,** 26, 3282-3290.

243. Luo, H.; Ma, Y.; Li, W.; Yi, G.; Cheng, X.; Ji, W.; Zu, X.; Yuan, S.; Li, J. Shape memory-enhanced water sensing of conductive polymer composites. *Mater. Lett.* **2015,** 161, 189-192.

244. Fang, L.; Chen, S.; Fang, T.; Fang, J.; Lu, C.; Xu, Z. Shape-memory polymer composites selectively triggered by near-infrared light of two certain wavelengths and their applications at macro-/microscale. *Compos. Sci. Technol.* **2017,** 138, 106-116.

245. Li, W.; Gong, T.; Chen, H.; Wang, L.; Li, J.; Zhou, S. Tuning surface micropattern features using a shape memory functional polymer. *RSC Adv.* **2013,** 3, 9865-9874.

246. Yang, W.; Lu, H.; Huang, W.; Qi, H.; Wu, X.; Sun, K. Advanced shape memory technology to reshape product design, manufacturing and recycling. *Polymers* **2014,** 6, 2287-2308.

247. Xie, T.; Xiao, X. Self-peeling reversible dry adhesive system. *Chem. Mater.* **2008,** 20, 2866-2868.

248. Eisenhaure, J.; Kim, S. An internally heated shape memory polymer dry adhesive. *Polymers* **2014,** 6, 2274-2286.

249. Eisenhaure, J. D.; Xie, T.; Varghese, S.; Kim, S. Microstructured shape memory polymer surfaces with reversible dry adhesion. *ACS Appl. Mater. Interfaces* **2013,** 5, 7714-7717.

250. Boesel, L. F.; Greiner, C.; Arzt, E.; del Campo, A. Gecko-inspired surfaces: a path to strong and reversible dry adhesives. *Adv. Mater.* **2010,** 22, 2125-2237.

251. Hu, J. L.; Lu, J. Shape memory polymers in textiles. *Adv. Sci. Technol.* **2012,** 80, 30-38.

252. Castano, L. M.; Flatau, A. B. Smart fabric sensors and e-textile technologies: a review. *Smart Mater. Struct.* **2014,** 23, 053001.

253. Hu, J. L.; Meng, H. P.; Li, G. Q.; Ibekwe, S. I. A review of stimuli-responsive polymers for smart textile applications. *Smart Mater. Struct.* **2012,** 21, 053001.

254. Hu, J.; Chen, S. A review of actively moving polymers in textile applications. *J. Mater. Chem.* **2010,** 20, 3346-3355.

255. Xu, H.; Yu, C.; Wang, S.; Malyarchuk, V.; Xie, T.; Rogers, J. A. Deformable, programmable, and shape-memorizing micro-optics. *Adv. Funct. Mater.* **2013,** 23, 3299-3306.

256. Fang, Y.; Ni, Y.; Choi, B.; Leo, S. Y.; Gao, J.; Ge, B.; Taylor, C.; Basile, V.; Jiang, P. Chromogenic photonic crystals enabled by novel vapor-responsive shape-memory polymers. *Adv. Mater.* **2015,** 27, 3696-3704.

257. Schauer, S.; Meier, T.; Reinhard, M.; Rohrig, M.; Schneider, M.; Heilig, M.; Kolew, A.; Worgull, M.; Holscher, H. Tunable diffractive optical elements based on shape-memory polymers fabricated via hot embossing. *ACS Appl. Mater. Interfaces* **2016,** 8, 9423-9430.

258. Behl, M.; Bellin, I.; Kelch, S.; Wagermaier, W.; Lendlein, A. One-step process for creating triple-shape capability of AB polymer networks. *Adv. Funct. Mater.* **2009,** 19, 102-108.

259. Zhang, F.; Zhang, Z.; Liu, Y.; Lu, H.; Leng, J. The quintuple-shape memory effect in electrospun nanofiber membranes. *Smart Mater. Struct.* **2013,** 22, 085020.

260. Zhang, F. H.; Zhang, Z. C.; Luo, C. J.; Lin, I. T.; Liu, Y.; Leng, J.; Smoukov, S. K. Remote, fast actuation of programmable multiple shape memory composites by magnetic fields. *J. Mater. Chem. C* **2015,** 3, 11290-11293.

261. Ge, F.; Zhao, Y. A new function for thermal phase transition-based polymer actuators: autonomous motion on a surface of constant temperature. *Chem. Sci.* **2017,** 8, 6307-6312.

262. Ariano, P.; Accardo, D.; Lombardi, M.; Bocchini, S.; Draghi, L.; De Nardo, L.; Fino, P. Polymeric materials as artificial muscles: an overview. *J. Appl. Biomater. Funct. Mater.* **2015,** 13, 1-9.

263. Islam, M. R.; Li, X.; Smyth, K.; Serpe, M. J. Polymer-based muscle expansion and contraction. *Angew. Chem. Int. Ed.* **2013,** 52, 10330-10333.

264. Li, X.; Serpe, M. J. Understanding and controlling the self-folding behavior of poly (N-isopropylacrylamide) microgel-based devices. *Adv. Funct. Mater.* **2014,** 24, 4119-4126.

265. Yang, Q.; Fan, J.; Li, G. Artificial muscles made of chiral two-way shape memory polymer fibers. *Appl. Phys. Lett.* **2016,** 109, 183701.

266. Fan, J.; Li, G. High performance and tunable artificial muscle based on two-way shape memory polymer. *RSC Adv.* **2017,** 7, 1127-1136.

267. Turner, S. A.; Zhou, J.; Sheiko, S. S.; Ashby, V. S. Switchable micropatterned surface topographies mediated by reversible shape memory. *ACS Appl. Mater. Interfaces* **2014,** 6, 8017-6021.

268. Tippets, C. A.; Li, Q.; Fu, Y.; Donev, E. U.; Zhou, J.; Turner, S. A.; Jackson, A. M.; Ashby, V. S.; Sheiko, S. S.; Lopez, R. Dynamic optical gratings accessed by reversible shape memory. *ACS Appl. Mater. Interfaces* **2015,** 7, 14288-14293.

269. Peng, Q.; Wei, H.; Qin, Y.; Lin, Z.; Zhao, X.; Xu, F.; Leng, J.; He, X.; Cao, A.; Li, Y. Shape-memory polymer nanocomposites with a 3D conductive network for bidirectional actuation and locomotion application. *Nanoscale* **2016,** 8, 18042-18049.

Chapter 3

Biocompound-based multiple shape memory polymers reinforced by photo-cross-linking*

Abstract

For the design of shape memory polymers with potential biomedical applications, we synthesized methacrylate-based monomers bearing biological compounds such as cholic acid and cinnamic acid in addition to oligo(ethylene glycol) as pendant groups and opted to use a simple radical polymerization method for the preparation of the copolymers. The glass transition temperatures of these polymers are broad and tunable and can thus accommodate dual and triple shape memory behaviors. The fixity ratios of dual and triple shape memory are all above 91%. The recovery ratio of dual shape memory is 89.5%, while the two recovery ratios of triple shape memory are 53.2 and 81.5%, respectively. To further improve the shape memory properties, a cinnamic acid-based methacrylate monomer was incorporated into the copolymers to enable photo-cross-linking of the terpolymer. After irradiation, the fixity ratios remain high, while the recovery ratios of dual and triple shape memories are much improved. The terpolymers after light irradiation even show the quadruple shape memory property. Different irradiation times were tested to optimize the shape memory effects. The recovery ratio of dual shape memory of such terpolymers can reach as high as 98.6%, while the recovery ratios of triple and quadruple shape memories are improved to the range of 75.3 to 99.1%.

---

*Wang, K.; Jia, Y. -G.; Zhu, X. X. *ACS Biomater. Sci. Eng.* **2015,** 1, 855-863.

3.1 Introduction

Shape memory polymers are regarded as smart materials that can return to their permanent shape from a temporary shape upon exposure to an external stimulus, such as temperature change,[1-3] light[4,5] or solvent.[6] They have drawn much research attention due to their potential applications in biomedicine,[7-10] smart textiles,[11] actuators,[12] and self-peeling reversible dry adhesive.[13] Thermo-induced shape memory effect is more common, and most of these polymers have a permanent shape provided by cross-linked phases, and a temporary shape fixed by frozen molecular chains during vitrification or crystallization by cooling below a transition temperature (T_{trans}). The cross-linked phases include chemical and physical cross-linking, such as crystalline domains[14-16] or strong supramolecular interactions.[17] The transition temperatures include glass transition temperature and melting point. Recently, multiple shape memory polymers have attracted much attention.[1,2,18,19] A multiple shape memory polymer may remember two or more temporary shapes and can meet more stringent requirements for various specific and complicated applications. Generally, two strategies may be used to design a multiple shape memory polymer. The first is to incorporate two or more discrete thermal transitions into the polymer,[14,20] while the second is to introduce a broad transition temperature range to the polymer.[1,2,19] Currently known triple shape memory effects of the former system were tuned only by varying the ratio among the reversible phases or changing the reversible phase transition temperatures.[21-23] The multiple shape memory effects of the latter system can be easily tailored on demand by selecting suitable temperatures as T_{trans} in the transition range, thus avoiding the synthesis of a new polymer and providing a larger degree of design freedom for the practical uses,[24] such as in biomedical applications.

Cholic acid is a naturally-occurring compound in the human body and animals and may serve as an ideal building block for the synthesis of biomaterials due to its multiple functional groups and biocompatibility.[25] The incorporation of cholic acid groups should provide rigidity to the polymer imparted by its steroidal skeleton. Poly(ethylene glycol) (PEG), regarded as a biocompatible polymer, is often used to adjust the glass transition temperature of the polymer as the flexible part.[2,24] Physical or chemical cross-linking usually provides the shape memory effect.[26-29] Long branched or grafted side chains attached to the main chain can significantly enhance the entanglements of the polymer.[30,31] PEG may also form hydrogen bonds with

cholic acid, which may strengthen the physical cross-linking. The incorporation of both cholic acid and PEG may endow the polymers with attractive properties as shape memory materials. It is thus attractive to design shape memory polymer consisting of cholic acid and PEG. Our group has developed a series of multiple shape memory polymers based on norbornene derivatives of cholic acid and PEG via ring-opening metathesis polymerization.[2] However, Ru contamination, complex operation and expensive catalyst are the shortcomings of ring-opening metathesis polymerization, which may in turn limit their biomedical applications. Therefore, we attempt to use a simple polymerization method for the preparation of biocompatible polymers with shape memory effects. Conventional free radical polymerization method can meet the design of biomaterials.

To this end, we designed and synthesized a series of methacrylate-based polymers bearing cholic acid and oligo(ethylene glycol) pendants. The adjustable broad T_{trans} ranges may be achieved by varying the ratio of monomers through a simple radical polymerization method. A small fraction of cinnamate groups (a nontoxic molecule from cinnamon or some other plants was widely used in biomedical applications[32,33]) was then introduced into the copolymer and used to enhance the shape memory effects by photo-cross-linking. Reinforcement of the materials by cross-linking through photo-irradiation of the polymers after thermoplastic processing helps to overcome the poor processability of thermoset polymers.

3.2 Experimental Section

3.2.1 Materials

Cholic acid (CA, ≥ 98%), 2-hydroxyethyl methacrylate (HEMA, 97%), cinnamoyl chloride (98%), dicyclohexylcarbodiimide (DCC, 99%), 4-(dimethylamino)pyridine (DMAP, ≥ 99%) and triethylamine (≥ 99.5%) were purchased from Sigma-Aldrich. Poly[(ethylene glycol) methyl ether methacrylate] (MPEG) (average M_n = 300 g/mol) was purchased from Sigma-Aldrich and purified prior to polymerization by passing through the neutral alumina column to remove the inhibitors. 2,2′-Azobisisobutyronitrile (AIBN, Sigma, 98%) was recrystallized twice from methanol. $CDCl_3$ (99.8% D) and DMSO-d_6 (99.9% D) were purchased from

Sigma-Aldrich. Dichloromethane (DCM), tetrahydrofuran (THF) and *N,N*-dimethylformamide (DMF) were dried using a solvent purification system from Glass Contour.

3.2.2 Synthesis of monomer

The cholic acid-based methacrylate monomer (MCA) was prepared by reacting HEMA with CA in the presence of DCC and DMAP (Scheme 3.S1A) according to published procedures.[34]

To synthesize the cinnamic acid-based methacrylate monomer (MCE), 1 mL triethylamine was added to 10 mL DCM solution of HEMA (0.882 mL, 7.05 mmol) in a round bottom flask equipped with a magnetic stir bar and placed in an ice-water bath. Cinnamoyl chloride (1 g, 5.9 mmol) in 10 mL DCM was added dropwise to the mixture under stirring. After 1 h, the ice-water bath was removed, and stirring was continued overnight. The reaction mixture was washed with 0.1 M HCl (50 mL × 2), saturated $NaHCO_3$ (50 mL × 2) and brine solution (50 mL × 2). After drying the organic layer over Na_2SO_4 and removing the solvent by rotary evaporation, the crude product was purified by column chromatography on silica gel (dichloromethane : hexane = 1 : 2). Yield: 56.7%.

3.2.3 Polymerization

A representative synthetic procedure of the random copolymer is described here. MCA (0.58 g, 1.11 mmol), MPEG (0.51 g, 1.70 mmol), AIBN (0.75 mg, 4.57 μmol; from 0.75 mL 1 mg/mL solution of AIBN in DMF) and 3 mL DMF were placed in a 25 mL round-bottom flask with a magnetic stir bar. The mixture was purged with N_2 for 20 min and placed into a preheated oil bath at 70 °C for 24 h. The system was then quenched in an ice-water bath and exposed to air. The reaction mixture was poured into distilled water to dissolve DMF and to precipitate the polymer. The precipitate was redissolved in THF and precipitated again from ethyl ether, and this process was repeated twice. The polymer was dried under vacuum at 30 °C for 24 h. The feed molar ratios of monomers were varied to obtain copolymers of various compositions. The copolymers P(MCA-MPEG) are denoted as CP with numbers in the subscript to indicate the feed ratios of comonomers. For example, $CP_{2:3}$ indicates a copolymer with MCA and MPEG molar ratio of 2:3, as indicated in Table 3.1. Then a

terpolymer (TP) was synthesized with same composition as $CP_{2:3}$ and, in addition, a third comonomer MCE was added to the mixture of all three comonomers with a ratio of 9.1 mol%. The same synthetic procedure was used.

3.2.4 Polymer characterization

Size exclusion chromatography (SEC) was carried out on a Breeze system from Waters equipped with a 717 plus auto-sampler, a 1525 Binary HPLC pump, a 2410 refractive index detector and two consecutive Waters columns (Phenomenex, 5 µm, 300 mm × 7.8 mm; Styragel HR4, 5 µm, 300 mm × 7.8 mm). DMF containing 0.05 mol/L LiBr was filtered through 0.2 µm nylon Millipore filters. The flow rate of the eluent (DMF) was 1 mL/min. SEC was calibrated using poly(methyl methacrylate) standards (2500-296 000 g/mol). ^{1}H NMR spectra in $CDCl_3$ or DMSO-d_6 were recorded on a Bruker AV400 spectrometer operating at 400 MHz for protons. Fourier transform infrared spectroscopy (FTIR) was used to evaluate the degree of photo-cross-linking of the cinnamate groups after irradiation using the attenuated total reflection (ATR) method on a FTIR spectrometer (NICOLET 6700). All spectra were recorded by averaging 32 scans at a 4-cm^{-1} resolution.

Thermogravimetric analyses (TGA) were performed on a Hi-Res TGA 2950 (TA Instruments) under a flow of nitrogen. T_{dec} was defined as the onset of the decomposition temperature. Differential scanning calorimetry (DSC) measurements were carried out on a DSC 2910 (TA Instruments) at a heating rate of 10 °C/min. For $CP_{1:3}$, $CP_{1:4}$ and PMPEG, the DSC measurements were carried out on a DSC 823^e (Mettler Toledo) with the same procedure as other polymers. The temperature and heat flow were calibrated with indium. T_g was defined as the midpoint of change in the slope on the second heating cycle, and the T_g range was determined by the onset and offset of the changes in heat capacity of the samples.

Polymer films for shape memory tests were prepared by evaporating a concentrated THF solution (100 mg/mL) of the desired polymer in a Teflon mold (2 cm × 2 cm) at ambient temperature and pressure for 48 h and then under reduced pressure for 24 h. Smaller rectangular samples (3.5 mm × 2.0 cm) were cut from these films and used for shape memory tests (the dimensions of the films were measured with an electronic digital caliper with a precision of 0.01 mm). For shape memory tests of photo-cross-linked TP, the rectangular

samples were irradiated by a 100-W light with a 365-nm wavelength for various time periods as shown in Scheme 3.1B. The irradiation distance was kept at 1 cm. The terpolymers were denoted to indicate the irradiation time in minutes (Table 3.2).

Dynamic mechanical analysis (DMA) was performed on a DMA 2980 (TA Instruments). For shape memory experiments, the controlled force mode was used. At least three consecutive cycles were performed for each sample. Since the programming temperature and time may have influences on the shape memory behavior, for example, increasing the holding time at deformation temperature improves the shape fixity,[35] the same procedure was used for all dual shape memory experiments. The specimen was first equilibrated at a deformation temperature ($T_d = T_{g,offset} + 15$ °C) for 5 minutes to reach heat conduction equilibrium before being deformed, because the sample can exhibit rubbery elasticity at this temperature, and then cooled to a fixation temperature ($T_f = T_{g,onset} - 15$ °C) and held isothermally for 10 minutes before unloading to freeze the movement of the polymer chains. The temporary shape was fixed for another 10 minutes after unloading the external force. It was then heated to a recovery temperature above the T_g ($T_r = T_{g,offset} + 15$ °C) to recover its permanent shape.

Two parameters are used to describe shape memory properties of the materials. One is the shape fixity ratio (R_f), which quantifies the ability of the material to fix the mechanical deformation shape (temporary shape). The other one is the shape recovery ratio (R_r), which quantifies the ability of the material to recover its permanent shape. They are defined below for the dual and multiple shape-memory experiments (eqs 3.1 - 3.4). The results listed in this paper are average values obtained from three consecutive experiments (values shown in Tables 3.S2-S4 in the supporting information) performed on each sample. For the dual shape memory experiments, they are respectively defined in the following expressions:[1]

$$R_f = \frac{\varepsilon(N)}{\varepsilon_{load}(N)} \times 100\% \tag{3.1}$$

$$R_r = \frac{\varepsilon(N) - \varepsilon_{rec}(N)}{\varepsilon(N) - \varepsilon_{rec}(N\text{-}1)} \times 100\% \tag{3.2}$$

where ε_{load} is the maximum strain before unloading the external stress, ε is the strain after cooling and unloading, ε_{rec} is the strain after the recovery step, and N is the cycle number of the shape memory experiments.

For all triple shape memory experiments, the sample was kept at $T_{g,offset}$ + 15 °C for 5 min and then stretched at a ramp force of 0.1 N/min. The sample was then cooled to $T_{g,offset}$ – 10 °C while keeping the external stress for 10 min. The external force was then removed, and the temperature was kept at $T_{g,offset}$ – 10 °C for 20 min to fix the first temporary shape. The sample was further deformed at $T_{g,offset}$ – 10 °C, and then the DMA chamber was cooled to $T_{g,onset}$ – 15 °C and kept isothermal for 10 min. After releasing the external stress and keeping isothermal for 10 min, the second temporary shape was fixed. The DMA chamber was heated to $T_{g,offset}$ – 10 °C and kept isothermal for 60 min to recover the first temporary shape. Finally, the sample was heated to $T_{g,offset}$ + 15 °C and kept isothermal for 60 min to recover its permanent shape. For quadruple shape memory experiments, their fixation temperatures were $T_{g,offset}$ − 5, $T_{g,offset}$ − 15 and $T_{g,onset}$ − 15 °C, respectively. The fixation time is 30 min. The procedure is the same as that used for the triple shape memory experiments.

For multiple shape memory effects, eqs (3.1) and (3.2) are extended to eqs (3.3) and (3.4) to calculate R_f and R_r.[1]

$$R_f(X \rightarrow Y) = \frac{\varepsilon_y - \varepsilon_x}{\varepsilon_{y,load} - \varepsilon_x} \times 100\% \tag{3.3}$$

$$R_r(Y \rightarrow X) = \frac{\varepsilon_y - \varepsilon_{x,rec}}{\varepsilon_y - \varepsilon_x} \times 100\% \tag{3.4}$$

where X and Y represent two different shapes, $\varepsilon_{y,load}$ denotes the maximum strain before unloading the external stress, ε_y and ε_x are fixed strains after cooling and unloading, and $\varepsilon_{x,rec}$ is the strain after the recovery step.

3.3 Results and discussion

3.3.1 Characterization of CPs

The molecular structure of MCA was confirmed by ^{1}H NMR spectrum (Figure 3.S1B). The copolymers (Scheme 3.1A) were obtained with different molar ratios of MCA and MPEG through free radical polymerization. The ^{1}H NMR spectrum of PMCA (Figure 3.S1D) was recorded in the DMSO-d_6 as it is insoluble in $CDCl_3$. The disappearance of vinyl peaks at around 5.50 and 6.10 ppm suggests the polymers were synthesized successfully. The monomer molar ratios in this series of CPs were obtained from the integration ratio of intensities of -OCH_3 protons at 3.38 ppm (3H, f-***H***) from MPEG units to the methyl protons at 0.69 ppm (3H, 18'-***H***) from MCA units. The molecular characteristics and properties of the polymers are summarized in Table 3.1. For all CPs, the molar ratio of the comonomers is almost the same as that in the feed, indicating MCA and MPEG have similar reactivity ratio. The molecular weights and PDI of the polymers are characteristic of the radical polymerization method used.

Scheme 3.1 Structure of (A) CP and (B) TP, and preparation of photo cross-linked TP.

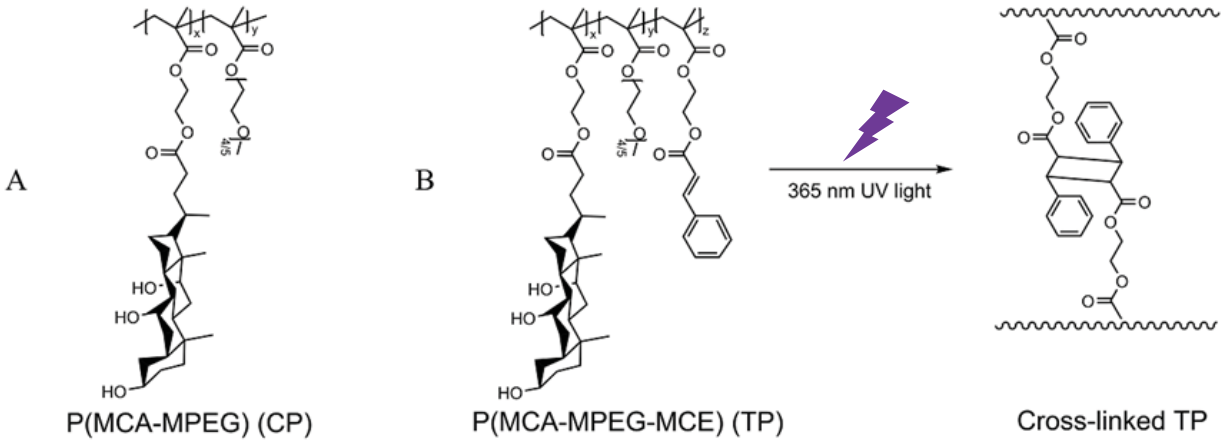

The TGA results (Figure 3.S2A) show that PMCA has no decomposition below 300 °C. The thermal stability of the CPs decreases with lower MCA content in the CP. Figure 3.1A shows that all of the polymers display a single T_g between the T_gs of the two corresponding homopolymers, indicating they are random copolymers. No melting peaks were visible in the DSC curves of the polymers, suggesting that they are amorphous. When the amount of MCA units in these CPs increases from 0 to 100%, the T_g rises from –61 to 162 °C (Table 3.1).

Figure 3.S3 shows the relation between T_g and MCA content in this series of CP. The experimental $T_{g,expt}$ values match well with the theoretical $T_{g,theo}$ values calculated from the Fox equation.[36] Therefore, the T_g can be easily tuned by varying the comonomer ratio. In addition, the broad glass transition ranges may also be attributed to the relatively broad molecular weight distribution and microphase-separated nanodomains.[37] The local T_g is determined by their local compositions in the nanodomains. The PMCA-rich nanodomains may have higher local T_g than the PMPEG-rich nanodomains.

Table 3.1 Molecular characteristics and properties of polymers with various molar ratios of monomers.

Polymer[a]	Feed[b]	Polymer[c]	M_n[d] (kg/mol)	PDI[d]	$T_{g,onset}$[e] (ºC)	T_g[f] (ºC)	$T_{g,offset}$[e] (ºC)
	MCA : MPEG						
PMCA	1.00 : 0	1.00 : 0	181	1.90	149	162	166
$CP_{1:1}$	1.00 : 1.00	1.00 : 0.99	231	1.69	42	60	71
$CP_{2:3}$	1.00 : 1.50	1.00 : 1.51	107	2.05	13	33	45
$CP_{1:2}$	1.00 : 2.00	1.00 : 2.10	124	2.06	5	16	31
$CP_{1:3}$	1.00 : 3.00	1.00 : 3.07	85	2.05	–48	–16	16
$CP_{1:4}$	1.00 : 4.00	1.00 : 3.96	67	1.75	–58	–28	0
PMPEG	0 : 1.00	0 : 1.00	131	1.87	–72	–61	–50
	MCA : MPEG : MCE						
TP	1.00 : 1.50 : 0.25	1.00 : 1.60 : 0.24	114	1.94	15	33	44

[a]Polymerization conditions: [monomer]:[AIBN] = 600:1, [monomer] = 0.6 mol/L in DMF, 24 h. The numbers in the subscript denote monomers molar ratios in the feed. [b]Molar ratio of monomers in the feed. [c]Molar ratio of monomers in the polymers calculated from the ratio of ^{1}H NMR peak integrations. [d]Measured by SEC. Reaction time in all cases was 24 h. [e]Measured by DSC. Defined by the onset and offset of the changes in the heat capacity, respectively. [f]Defined as the midpoint in the change of heat capacity.

3.3.2 Shape memory properties of CPs

The dual shape memory property of $CP_{2:3}$ was studied as a representative example of the copolymers in this series, as its T_g is close to body temperature (37 °C). As shown in Table 3.1, $CP_{2:3}$ has a broad T_g ranging from 13 to 45 °C. The shape memory effects could be tuned by the selection of operation temperatures in the T_g range (T_f, T_d and T_r).[1,24,26] In this work, we

chose $T_{g,onset}$ – 15 °C as T_f, and $T_{g,offset}$ + 15 °C as T_d and T_r for dual shape memory experiments. These samples were removed of any residual stress/strain from the processing step before stretching. As shown in the Figure 3.1B, the sample was first elongated at 60 °C (T_d), and it was then cooled to –2 °C (T_f) and the external force was unloaded to fix the temporary shape (R_f = 99.3%). When the sample was heated to 60 °C (T_r) again, it gradually recovered its permanent shape, and an average recovery ratio (R_r) of 89.5% was obtained (Table 3.2). The dual shape memory experiments of $CP_{1:2}$ yielded similar R_f = 99.7% and R_r = 76.4% (Figure 3.S5A). Irreversible slippage between the polymer chains may occur to a certain extent during the deformation at a high temperature, which should lead to a smaller reduction in entropy. The entropy-related elastic energy, which is the driving force for the shape recovery, is thus smaller. As a consequence, the recovery ratio becomes lower.[26] Previously, very good dual shape memory properties were obtained for norbornene-based CPs with similar pendent groups.[2] This may be attributed to a physically cross-linked structure as a result of entanglements of high molecular weight polymer chains.[29] The molecular weight of norbornene-based CP is around 4 times higher than that of methacrylate-based CP, so the chain entanglements should be more extensive than for the samples used in this work.

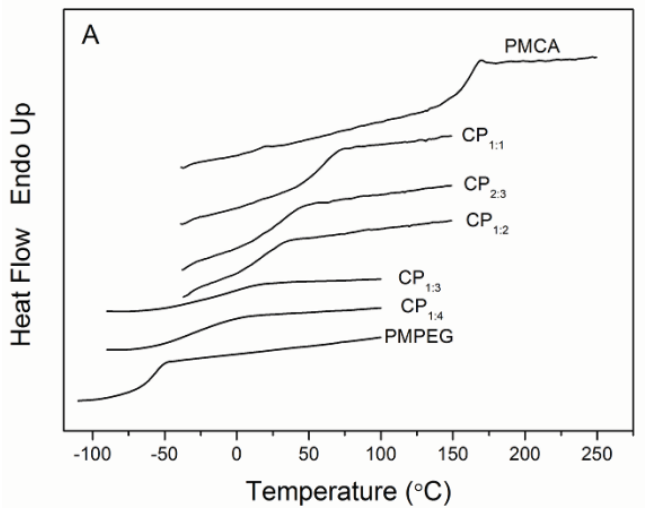

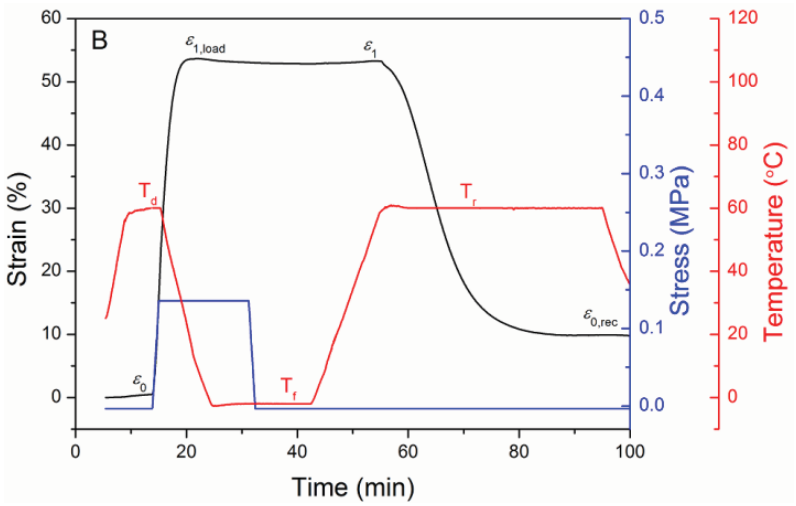

Figure 3.1 (A) DSC traces of CPs with various ratios of MCA to MPEG. (B) A typical dual shape memory effects of $CP_{2:3}$ at $T_d = T_r = T_{g,offset} + 15 = 60$ °C and at $T_f = T_{g,onset} - 15 = -2$ °C. Average values (original values listed in Table 3.S2): $R_f = 99.3\%$, $R_r = 89.5\%$.

Table 3.2 The degree of cross-linking (DC) determined by IR, fixity ratios (R_f), and recovery ratios (R_r) of dual shape memory effects of $CP_{2:3}$ and TPs with various irradiation time.

Sample	Irradiation time (min)	DC[a] (%)	Molar fraction of cross-linked MCE[b] (mol%)	Dual shape memory (%)	
				R_f	R_r
$CP_{2:3}$	0	0	0	99.3 ± 0.1	89.5 ± 5.3
TP	0	0	0	99.3 ± 0.1	83.5 ± 1.3
TP(15)	15	10.0	0.8	99.5 ± 0.0	94.8 ± 0.9
TP(30)	30	16.6	1.4	99.6 ± 0.1	96.0 ± 0.5
TP(60)	60	25.8	2.2	99.6 ± 0.1	98.6 ± 0.5
TP(120)	120	38.1	3.2	99.5 ± 0.1	99.4 ± 0.2

[a]Measured by ATR-FTIR. [b]Indicates the molar percentage of cross-linked cinnamate group in all comonomers present in the terpolymer ([Cross-linked MCE]/{[MCA]+[MPEG]+[MCE]}).

In general, triple and multiple shape memory effects can be achieved by utilizing two or more reversible thermal transitions (T_{trans}).[14,23,38] In recent years, some polymers with broad transition temperatures have been reported to show multiple shape memory effects, and multi-gradient temperatures were chosen as T_{trans} in the glass transition range.[1,2,24,39] In this work, polymers with a broad T_g range are likely to display multiple shape memory properties. Thus, triple shape memory effects of $CP_{2:3}$ were also investigated, and the average recovery ratios

$R_r(2\rightarrow1)$ and $R_r(1\rightarrow0)$ are 53.2 and 81.5%, respectively (Table 3.3 and Figure 3.S6A). Similar results of triple shape memory of $CP_{1:2}$ were also observed, and their recovery ratios are 44.4 and 65.3%, respectively (Figure 3.S5B). These values may be improved by cross-linking in the polymer network.

3.3.3 Characterization of TPs

To enable cross-linking, cinnamic acid may be used to make a terpolymer. The double bond of cinnamic acid can be cross-linked and decross-linked with UV light of different wavelengths.[4,5,40] Therefore, cinnamate group was incorporated into the CP. Such a TP was photo-cross-linked with a 365 nm UV light to enhance the recovery ratio of dual and multiple shape memory effects.

The TP was obtained by polymerization of MCA, MPEG and MCE with a molar ratio of 4:6:1 in the feed (Scheme 3.1B). The composition of TP was determined by NMR analysis from the integration ratio of -C***H***$_3$ protons at 0.69 ppm (MCA units) to the -OC***H***$_3$ protons at 3.38 ppm (MPEG units) and to the -C(O)C***H***=CH-Ph proton at 6.56 ppm (MCE fragment) (Figure 3.S1F). The average molecular weight (M_n) and PDI of TP are almost the same as those of $CP_{2:3}$ (Table 3.1).

The thermal stability of the TPs with different irradiation time periods, measured by TGA (Figure 3.S2B), shows a small decrease with a longer irradiation time, probably caused by a partial decomposition of the TP with a longer irradiation. Figure 3.2A shows the DSC curves of TP at different irradiation time periods and of $CP_{2:3}$. The results are summarized in Table 3.S1. Before irradiation, the T_g is the same as that of $CP_{2:3}$ and increases slightly with longer irradiation time due to relatively low chemical cross-linking concentration.[41]

The ATR-FTIR spectra confirm the formation of chemical cross-linking (Figure 3.2B). After irradiation with UV light (λ = 365 nm), the absorption intensity of C=C stretching vibration at 1636 cm^{-1} of MCE decreases gradually due to the [2+2] cycloaddition of the C=C double bond.[14,42,43] The degree of photo cross-linking may be calculated by normalizing the peak height at 1636 cm^{-1} in reference to the peak height of C=O at 1730 cm^{-1} using the following equation:

$$DC = 1 - \frac{(I_{1636}/I_{1730})_t}{(I_{1636}/I_{1730})_0} \times 100\% \quad (3.5)$$

where DC is the degree of cross-linking, $(I_{1636}/I_{1730})_0$ and $(I_{1636}/I_{1730})_t$ are the relative intensity of the C=C bond before and after irradiation. An increasing trend is found for the degree of cross-linking as the irradiation time becomes longer (estimated to be 10.0, 16.6, 25.8, 38.1 and 58.0%, respectively, after 15, 30, 60, 120 and 240 min of irradiation time), and the molar fraction of cross-linked MCE are also calculated and listed in Table 3.2.

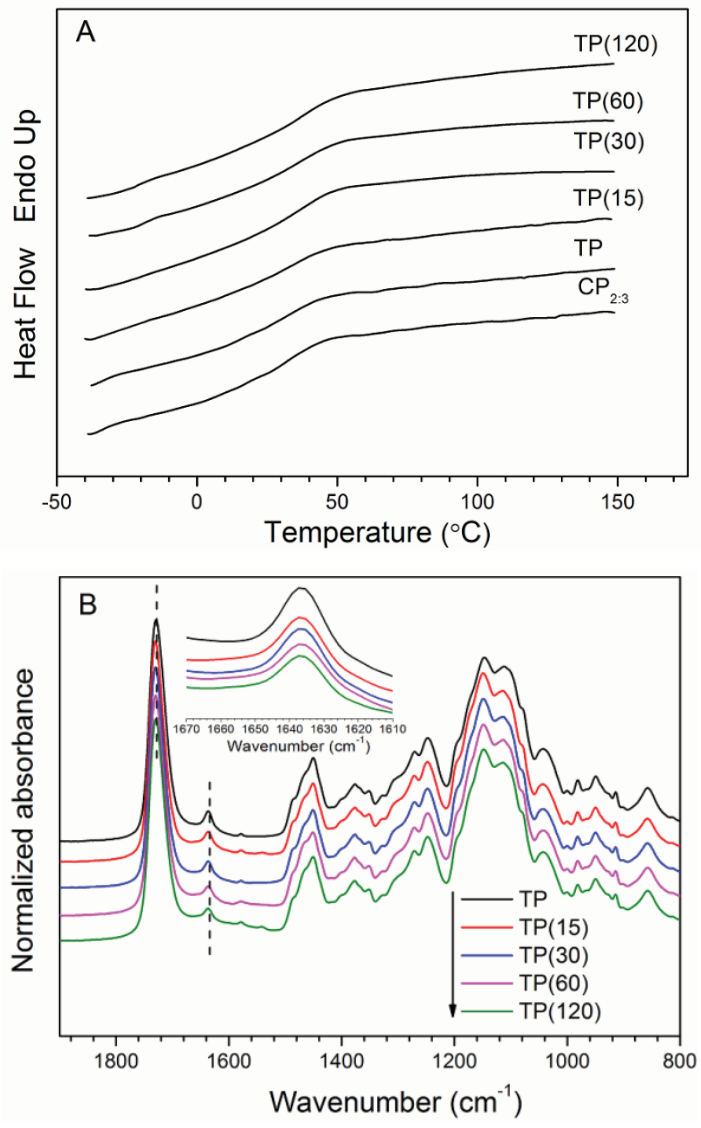

Figure 3.2 (A) DSC curves of $CP_{2:3}$ and TP samples with various irradiation time periods, and (B) FTIR spectra of TP samples with various irradiation time.

3.3.4 Shape memory properties of TPs

A typical dual shape memory curve of the TP without irradiation is displayed in Figure 3.3A, and its fixity and recovery ratios are shown in Table 3.2. The fixity ratio is close to 100%, while the average recovery ratio is 83.5%. The recovery ratio is similar to that of $CP_{2:3}$. Figure 3.3B shows a typical dual shape memory effect of TP(60). The temporary shape is fixed completely (R_f = 99.6%), and the original shape is almost fully recovered (R_r = 98.6%). The results indicate that the dual shape memory effect of TP is enhanced significantly by photo-cross-linking.

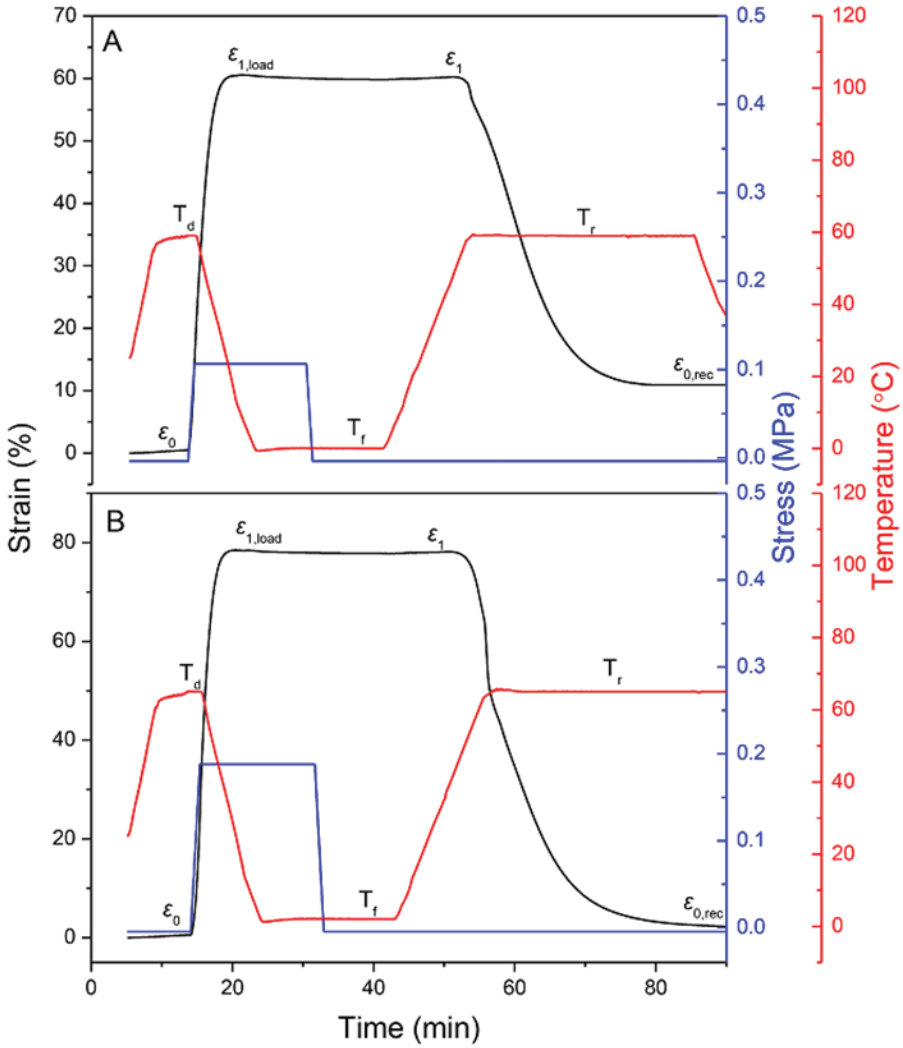

Figure 3.3 Typical dual shape memory effects of (A) TP at $T_d = T_r = T_{g,offset} + 15$ = 59 °C and at $T_f = T_{g,onset} - 15$ = 0 °C. Average values: R_f = 99.3%, R_r = 83.5%. (B) TP(60) at $T_d = T_r = T_{g,offset} + 15$ = 65 °C and at $T_f = T_{g,onset} - 15$ = 2 °C. Average values: R_f = 99.6%, R_r = 98.6%.

The R_f and R_r values of 3 consecutive measurements for both TP and TP(60) are listed in Table 3.S2.

The dual shape memory effects of TPs with various irradiation time periods were also investigated. The average fixity and recovery ratios are shown in Table 3.2. All fixity ratios are almost the same for all samples (R_f > 99%), indicating that the vitrification in the glassy state ($T_{g,onset}$ – 15 °C) is efficient in freezing chain mobility and storing elastic energy.[2] The recovery ratio of TP increases with irradiation time, indicating the effect of cross-linking in preventing chain slippage. The recovery ratio of TP(120) is up to 99.4%, suggesting that even a low molar fraction of cross-linked MCE (3.2 mol%) has a significant enhancement of shape memory. Ratna et al.[44] observed a similar trend of recovery ratio of dual shape memory, where the optimal molar fraction of cross-linker was 2.1 mol%.

Figure 3.4A shows a representative triple shape memory effect of TP(60). The original shape (ε_0) was stretched at $T_{g,offset}$ + 15 °C (T_{d1}), then the sample was cooled to $T_{g,offset}$ – 10 °C (T_{f1}) to fix the first temporary shape (ε_1) with $R_f(0\rightarrow1)$ = 82.1%. The shape (ε_1) was further stretched at $T_{g,offset}$ – 10 °C (T_{d2}) and cooled to $T_{g,onset}$ – 15 °C (T_{f2}) to fix the second temporary shape (ε_2) with $R_f(1\rightarrow2)$ = 97.0%. After subsequent reheating to $T_{g,offset}$ – 10 °C (T_{r1}), the first temporary shape ($\varepsilon_{1,rec}$) was recalled ($R_r(2\rightarrow1)$ = 75.3%). The sample was further heated to $T_{g,offset}$ + 15 °C (T_{r2}), the permanent shape ($\varepsilon_{0,rec}$) was recovered ($R_r(1\rightarrow0)$ = 99.1%). The triple shape memory effect is enhanced significantly in comparison to that of $CP_{2:3}$ (Table 3.3).

Table 3.3 Triple shape memory properties of $CP_{2:3}$ and TP with various irradiation times.

Sample	Irradiation time (min)	Triple shape memory (%)			
		$R_f(0\rightarrow1)$	$R_f(1\rightarrow2)$	$R_r(2\rightarrow1)$	$R_r(1\rightarrow0)$
$CP_{2:3}$	0	91.1 ± 0.0	96.2 ± 0.5	53.2 ± 2.6	81.5 ± 4.3
TP	0	90.7 ± 0.4	96.8 ± 0.0	61.5 ± 0.0	81.6 ± 1.2
TP(15)	15	88.6 ± 0.1	97.9 ± 0.3	63.0 ± 1.3	92.4 ± 1.0
TP(30)	30	84.7 ± 0.7	98.4 ± 0.1	70.9 ± 1.6	92.6 ± 1.7
TP(60)	60	82.1 ± 1.4	97.0 ± 0.4	75.3 ± 5.2	99.1 ± 1.3
TP(120)	120	80.7 ± 0.3	97.7 ± 0.5	70.2 ± 2.4	99.0 ± 0.7

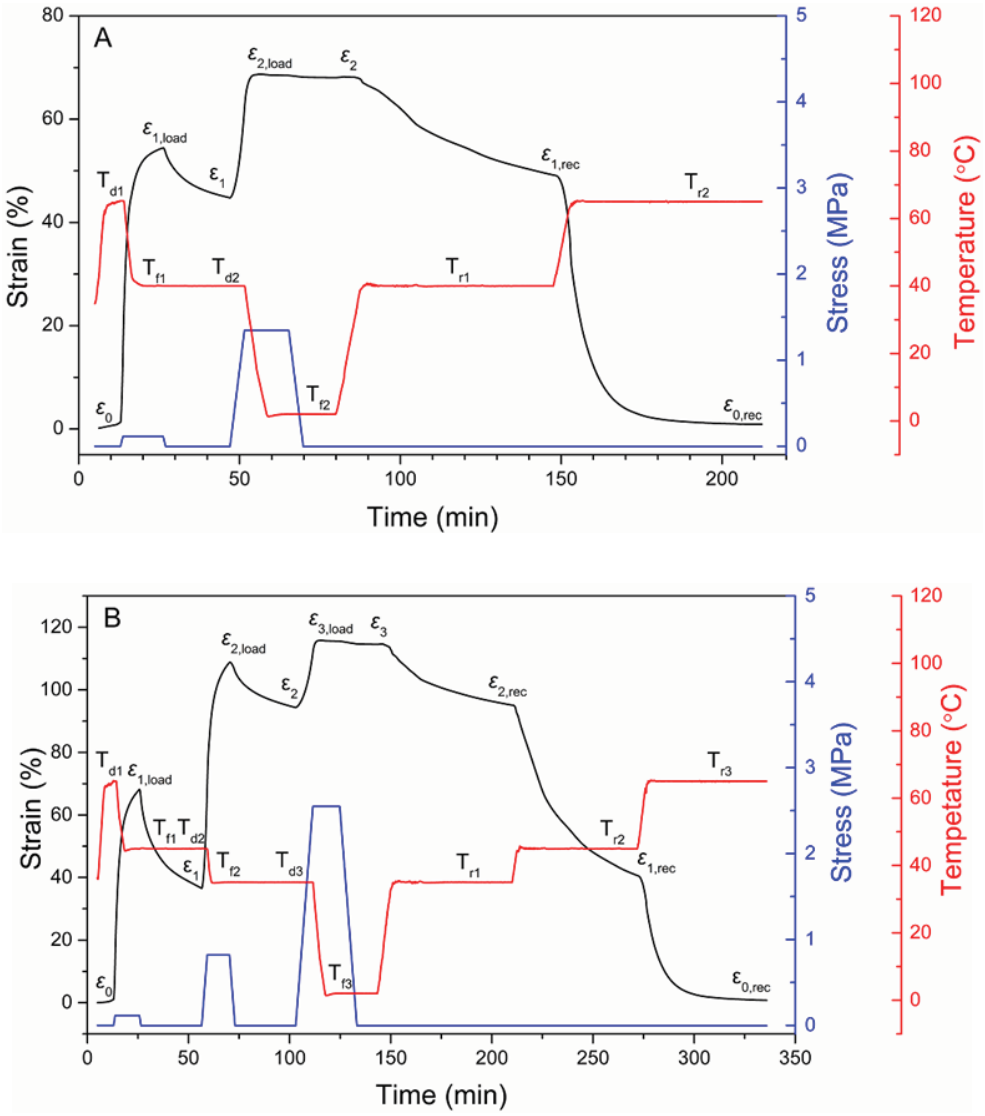

Figure 3.4 Typical multiple shape memory properties of TP(60): (A) Triple shape memory effect with $T_{d1} = T_{r2} = T_{g,offset} + 15 = 65$ °C, $T_{d2} = T_{r1} = T_{f1} = T_{g,offset} - 10 = 40$ °C and $T_{f2} = T_{g,onset} - 15 = 2$ °C. Average values (data for 3 consecutive measurements listed in Table 3.S3): $R_f(0\rightarrow1) = 82.1\%$, $R_f(1\rightarrow2) = 97.0\%$, $R_r(2\rightarrow1) = 75.3\%$, $R_r(1\rightarrow0) = 99.1\%$. (B) Quadruple shape memory effect with $T_{d1} = T_{r3} = T_{g,offset} + 15 = 65$ °C, $T_{d2} = T_{r2} = T_{f1} = T_{g,offset} - 5 = 45$ °C, $T_{d3} = T_{r1} = T_{f2} = T_{g,offset} - 15 = 35$ °C, and $T_{f3} = T_{g,onset} - 15 = 2$ °C. Average values (data for 3 consecutive measurements listed in Table 3.S4): $R_f(0\rightarrow1) = 54.5\%$, $R_f(1\rightarrow2) = 81.4\%$, $R_f(2\rightarrow3) = 94.7\%$, $R_r(3\rightarrow2) = 83.7\%$, $R_r(2\rightarrow1) = 91.6\%$, $R_r(1\rightarrow0) = 97.4\%$.

The multiple shape memory effects are from their broad glass transition ranges. A broad glass transition range can be regarded as an infinite number of transitions,[1] each corresponding

to infinitely local compositions in the nanodomains having a local T_g that depends on their local compositions randomly distributed in CPs. PMCA-rich nanodomains have a higher local T_g than the PMPEG-rich nanodomains. The various nanodomains constituted the corresponding local T_gs which are continuously distributed across the broad glass transition range. The mechanism of triple shape memory effect can be understood as illustrated in Scheme 3.2. The sample is first stretched to $\varepsilon_{1,load}$ at $T_{g,offset}$ + 15 °C, the nanodomains that have low T_gs can quickly relax and do not efficiently participate in the storage of elastic energy.[45] Then the sample is cooled to $T_{g,offset}$ – 10 °C, the polymer chains of the nanodomains with local T_gs greater than $T_{g,offset}$ – 10 °C are frozen, so that the elastic energy of this part is frozen. Upon unloading, the unfrozen polymer chains will shrink to release the unfrozen elastic energy, and only the elastic energy of those nanodomains with local T_g greater than $T_{g,offset}$ – 10 °C is truly stored in the first temporary shape (ε_1).[46] The sample is further stretched to $\varepsilon_{2,load}$ at $T_{g,offset}$ – 10 °C, the nanodomains that have much lower T_gs relax quickly. All polymer chains are in a frozen state after cooling to $T_{g,onset}$ – 15 °C, and all elastic energy is frozen. The $R_f(1\rightarrow2)$ is close to 100% after unloading. Upon reheating to $T_{g,offset}$ – 10 °C, the polymer chains of the nanodomains with local T_gs lower than $T_{g,offset}$ – 10 °C are re-activated, and the corresponding stored elastic energy is released. The sample recovers its first temporary shape ($\varepsilon_{1,rec}$). Further heating to $T_{g,offset}$ + 15 °C, the remaining elastic energy is also re-activated, and the sample shrinks to its original shape ($\varepsilon_{0,rec}$).

Scheme 3.2 Schematic illustration of mechanism of triple shape memory of random terpolymer.

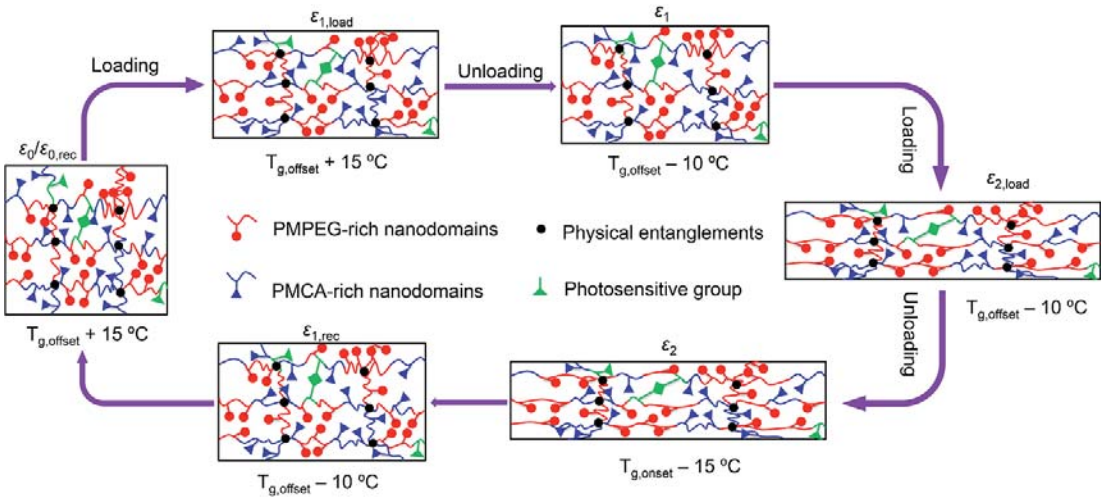

The effects of the degree of cross-linking on triple shape memory properties were also studied with results summarized in Table 3.3. The incorporation of cinnamate group before photo-cross-linking has almost no effect on the triple shape memory effect of TP. The triple shape memory property of TP is much improved after irradiation (cross-linking). All the $R_f(1\rightarrow2)$ values are similar, while $R_r(1\rightarrow0)$ values increase somewhat with degree of cross-linking. This tendency is the same as in the case of dual shape memory. The mechanism is also the same in both cases. $R_f(0\rightarrow1)$ values decreases slightly with increasing irradiation time, while $R_r(2\rightarrow1)$ values increases with irradiation time to reach a constant value of around 71% at ca. 30 min of irradiation. Chemical cross-linking generally lowers the chain mobility.[47] Therefore, a higher degree of cross-linking in the sample makes it harder for polymer chains of the nanodomains with low T_g to relax during the stretching process. As these polymer chains may relax during the subsequent fixation process, the $R_f(0\rightarrow1)$ values decrease slightly with longer irradiation time. The $R_r(2\rightarrow1)$ values of the polymers first increase with the degree of cross-linking due to reduced chain slippage. When a certain degree of cross-linking is reached, the recovery ratio reaches a plateau due to the reduced chain mobility. In general, the TP samples reach an optimal triple shape memory effect at 60 min of irradiation. The best triple shape memory effect may be achieved at a 2.2 mol% molar fraction of cross-linked MCE (Table 3.2).

The quadruple shape memory effect may be achieved using a temperature above T_g and two separated temperatures within the glass transition range as three T_{trans}s. A representative quadruple shape memory effect is shown in Figure 3.4B for TP(60). The specimen was sequentially stretched at $T_{g,offset}$ + 15 (T_{d1}), $T_{g,offset}$ – 5 (T_{d2}) and $T_{g,offset}$ – 15 °C (T_{d3}). Correspondingly, the first, second and third temporary shapes were fixed at $T_{g,offset}$ – 5 (T_{f1}), $T_{g,offset}$ – 15 (T_{f2}) and $T_{g,onset}$ – 15 °C (T_{f3}), respectively. The sample exhibited stepped recovery at $T_{g,offset}$ – 15 (T_{r1}), $T_{g,offset}$ – 5 (T_{r2}) and $T_{g,offset}$ + 15 °C (T_{r3}) during the subsequent heating process. Calculated from the strain curve, the R_f of first temporary shape (ε_1) is 54.5%, while $R_f(1\rightarrow2)$ and $R_f(2\rightarrow3)$ are around 81 and 95%, respectively. Alternatively, the $R_r(3\rightarrow2)$ is up to 84%, and both $R_r(2\rightarrow1)$ and $R_r(1\rightarrow0)$ are over 91%. The mechanism of quadruple shape memory effect is the same as that of triple shape memory effect as discussed earlier in this report. The effects of the degree of cross-linking on the quadruple shape memory properties

are also similar, as shown in Table 3.4. $R_f(2\rightarrow3)$ and $R_r(1\rightarrow0)$ have similar values and the trend as the R_f and R_r of the dual shape memory effects, respectively. $R_f(0\rightarrow1)$ and $R_f(1\rightarrow2)$ decrease slightly with increasing irradiation time, and TP(60) possesses optimal $R_r(3\rightarrow2)$ and $R_r(2\rightarrow1)$ values. It is to be noted that the fixity ratio $R_f(0\rightarrow1)$ deteriorates when T_{d2} is set close to $T_{g,offset}$ in the quadruple-shape memory experiments. The optimum quadruple shape memory effect was again observed for the sample with 60 min of irradiation (corresponding to a molar fraction of cross-linked MCE at 2.2 mol%). The mechanism of the effects of irradiation time on quadruple shape memory effect is the same as in the case of the triple shape memory effect.

Table 3.4 Quadruple shape memory properties of TP with various irradiation time.

Sample	Irradiation time (min)	Quadruple shape memory (%)					
		$R_f(0\rightarrow1)$	$R_f(1\rightarrow2)$	$R_f(2\rightarrow3)$	$R_r(3\rightarrow2)$	$R_r(2\rightarrow1)$	$R_r(1\rightarrow0)$
TP	0	73.3 ± 1.0	85.2 ± 0.7	91.9 ± 0.4	69.2 ± 0.6	70.8 ± 4.4	73.2 ± 2.8
TP(15)	15	69.6 ± 0.9	85.6 ± 0.3	94.1 ± 0.3	65.5 ± 0.9	75.6 ± 0.9	91.0 ± 1.3
TP(30)	30	62.7 ± 0.3	82.4 ± 0.3	95.5 ± 0.4	74.0 ± 6.5	82.8 ± 1.5	91.4 ± 3.2
TP(60)	60	54.5 ± 1.1	81.4 ± 1.2	94.7 ± 0.1	83.7 ± 10.2	91.6 ± 3.0	97.4 ± 2.6
TP(120)	120	53.5 ± 0.8	81.5 ± 0.8	95.1 ± 0.3	67.3 ± 4.6	84.7± 0.9	96.6 ± 2.4

3.4 Conclusions

A simple free radical polymerization method yielded copolymers with pendent cholic acid groups that exhibit multiple shape memory effects. The resultant polymers have a broad glass transition region whose temperature range may be tuned by the variation of the monomers ratios. The polymers can manifest both dual and triple shape memory effects. The shape memory properties of these copolymers (especially the R_r values) can be further improved by the inclusion of cinnamate groups as a comonomer which allows photo-cross-linking. The cross-linked TP shows much improved dual and triple shape memory effects over those of $CP_{2:3}$ and uncross-linked TP, and even possess multiple shape memory effect. The degree of cross-linking varies with the irradiation time. The optimal shape memory effects are obtained with a 2.2 mol% cross-linking of the total monomers in the terpolymers. Owing to the natural origin of cholic aicd and cinnamate group and the biocompatibility of PEG, such shape

memory polymers may become attractive candidates for a variety of potential biomedical applications.

3.5 Acknowledgements

Financial support from NSERC of Canada, FQRNT of Quebec, and the Canada Research Chair program is gratefully acknowledged. K. Wang is grateful to the China Scholarship Council for a scholarship. The authors also thank Mr. Sylvain Essiembre and Mr. Pierre Ménard Tremblay for their technical support. The authors are members of CSACS funded by FQRNT and GRSTB funded by FRSQ.

3.6 Supporting information

Scheme 3.S1 Synthesis of methacrylate monomers MCA and MCE.

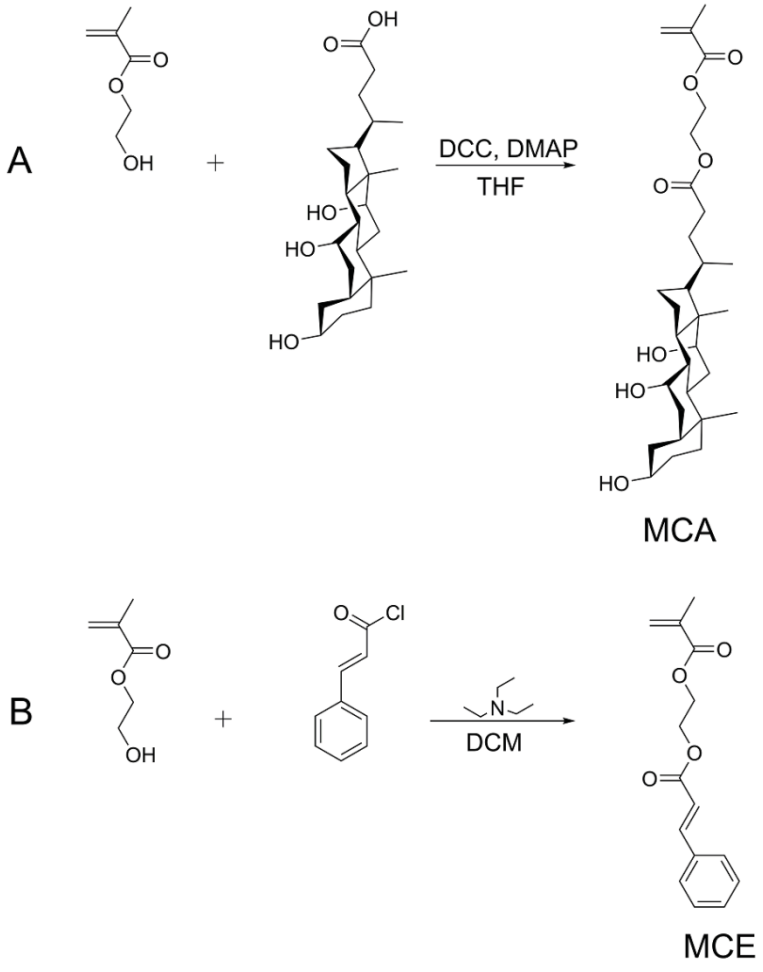

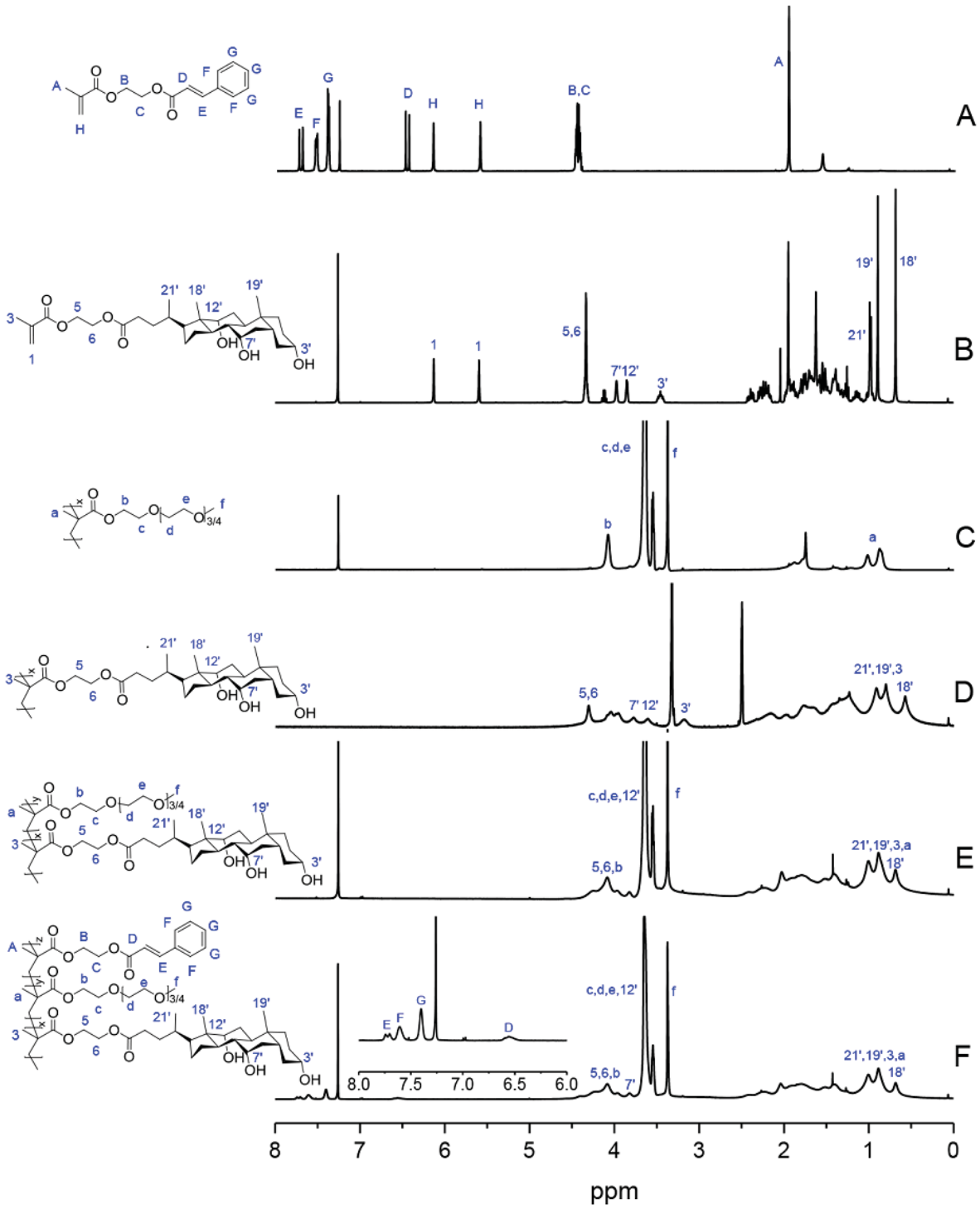

Figure 3.S1 ^{1}H NMR spectra of (A) MCE; (B) MCA; (C) PMPEG; (D) PMCA; (E) $CP_{2:3}$ and (F) TP. (PMCA was dissolved in DMSO-d_6, the others were dissolved in $CDCl_3$)

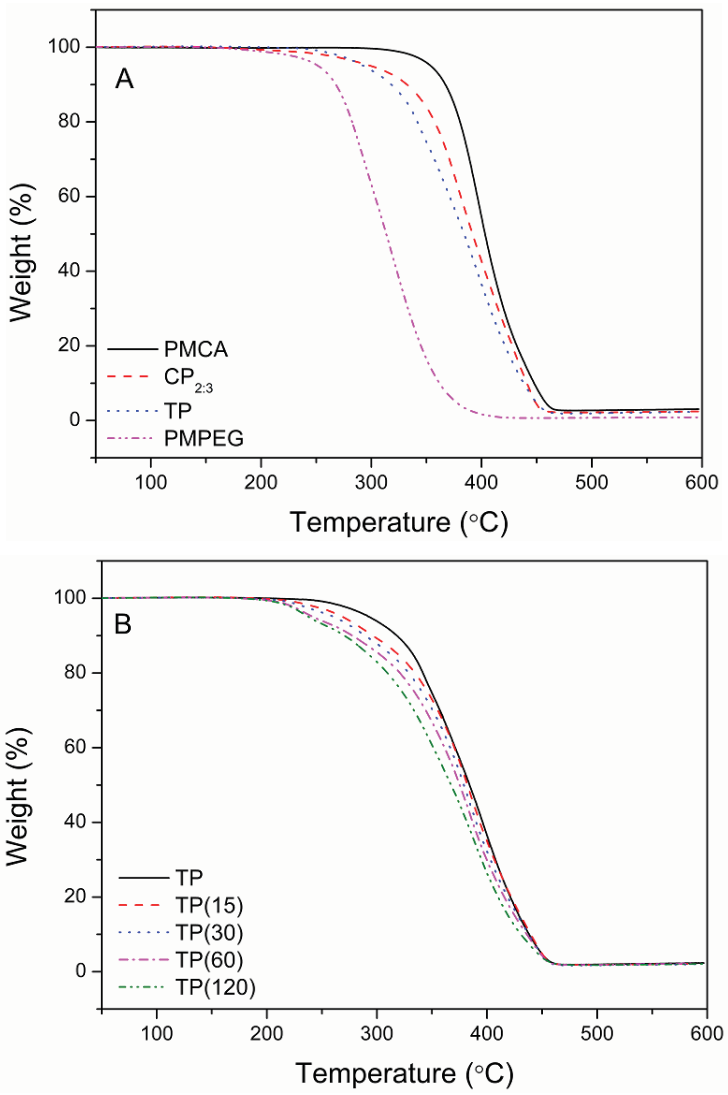

Figure 3.S2 TGA curves of the (A) homo-, co- and terpolymers; (B) TPs with various irradiation time.

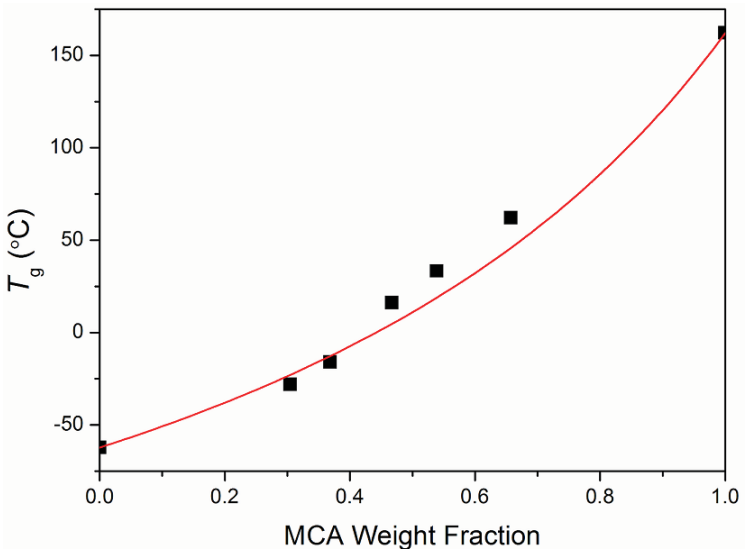

Figure 3.S3 Comparison of the experimental T_g with the theoretical T_g values calculated from Fox equation.

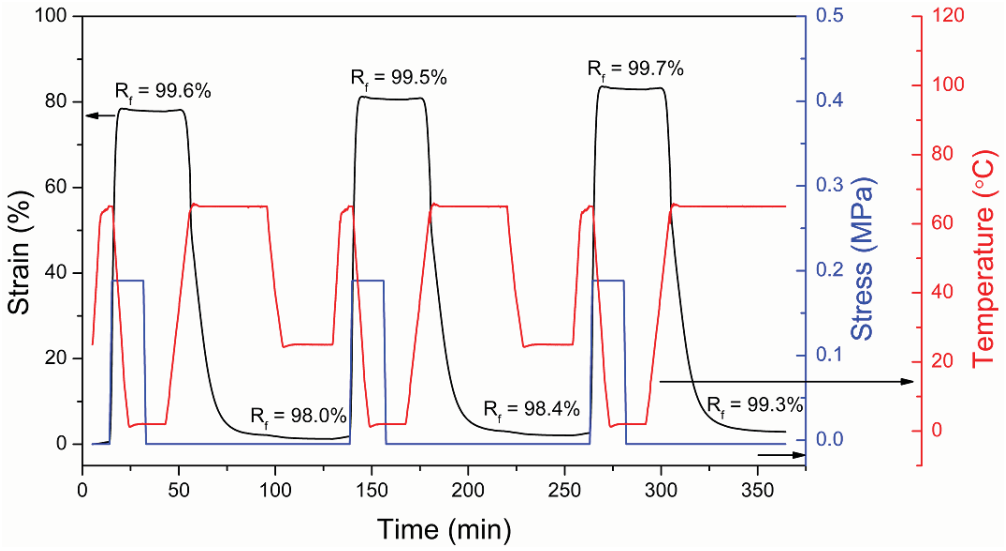

Figure 3.S4 Typical consecutive dual shape memory cycles of TP(60). ($T_d = T_r = T_{g,offset} + 15$ ºC; $T_f = T_{g,onset} - 15$ ºC)

Table 3.S1 DSC values of $CP_{2:3}$ and TPs with various irradiation time.

Polymer	$T_{g,onset}$ (°C)	$T_{g,midpoint}$ (°C)	$T_{g,offset}$ (°C)
$CP_{2:3}$	13	33	45
TP	15	33	44
TP(15)	16	34	47
TP(30)	16	35	49
TP(60)	17	36	50
TP(120)	19	38	51

Table 3.S2 Fixed strains, recovery strains and recovery ratios of dual shape memory effects of $CP_{2:3}$ and TPs.

Polymer	ε_0 (%)	ε_1 (%)	$\varepsilon_{0,rec}$ (%)	R_r (%)
$CP_{2:3}$	0.5	53.3	9.9	82.2
	0.5	42.0	4.0	91.6
	0.5	52.1	3.3	94.6
TP	0.4	60.2	10.8	82.6
	0.5	56.3	8.7	85.3
	0.6	36.8	6.9	82.6
TP(60)	0.6	78.2	2.1	98.1
	0.5	79.6	1.8	98.4
	0.6	81.2	1.2	99.3

Table 3.S3 Fixed strains, recovery strains and recovery ratios of triple shape memory effects of TP(60).

Polymer	ε_0 (%)	ε_1 (%)	ε_2 (%)	$\varepsilon_{1,rec}$ (%)	$\varepsilon_{0,rec}$ (%)	$R_r(2\rightarrow1)$ (%)	$R_r(1\rightarrow0)$ (%)
TP(60)	0.5	30.0	43.8	34.3	0.5	68.8	100
	0.4	44.9	68.1	49.2	1.7	81.5	97.1
	0.6	24.3	37.8	27.6	0.6	75.6	100

Table 3.S4 Fixed strains, recovery strains and recovery ratios of quadruple shape memory effects of TP(60).

Polymer	ε_0 (%)	ε_1 (%)	ε_2 (%)	ε_3 (%)	$\varepsilon_{2,rec}$ (%)	$\varepsilon_{1,rec}$ (%)	$\varepsilon_{0,rec}$ (%)	$R_r(3\rightarrow2)$ (%)	$R_r(2\rightarrow1)$ (%)	$R_r(1\rightarrow0)$ (%)
TP(60)	0.1	36.6	94.4	114.6	95.1	40.2	0.7	96.5	93.8	98.4
	0.4	31.6	72.7	88.8	75.4	34.2	0.4	83.2	93.7	100
	0.8	29.7	72.9	89.0	77.5	35.2	2.6	71.4	87.3	93.8

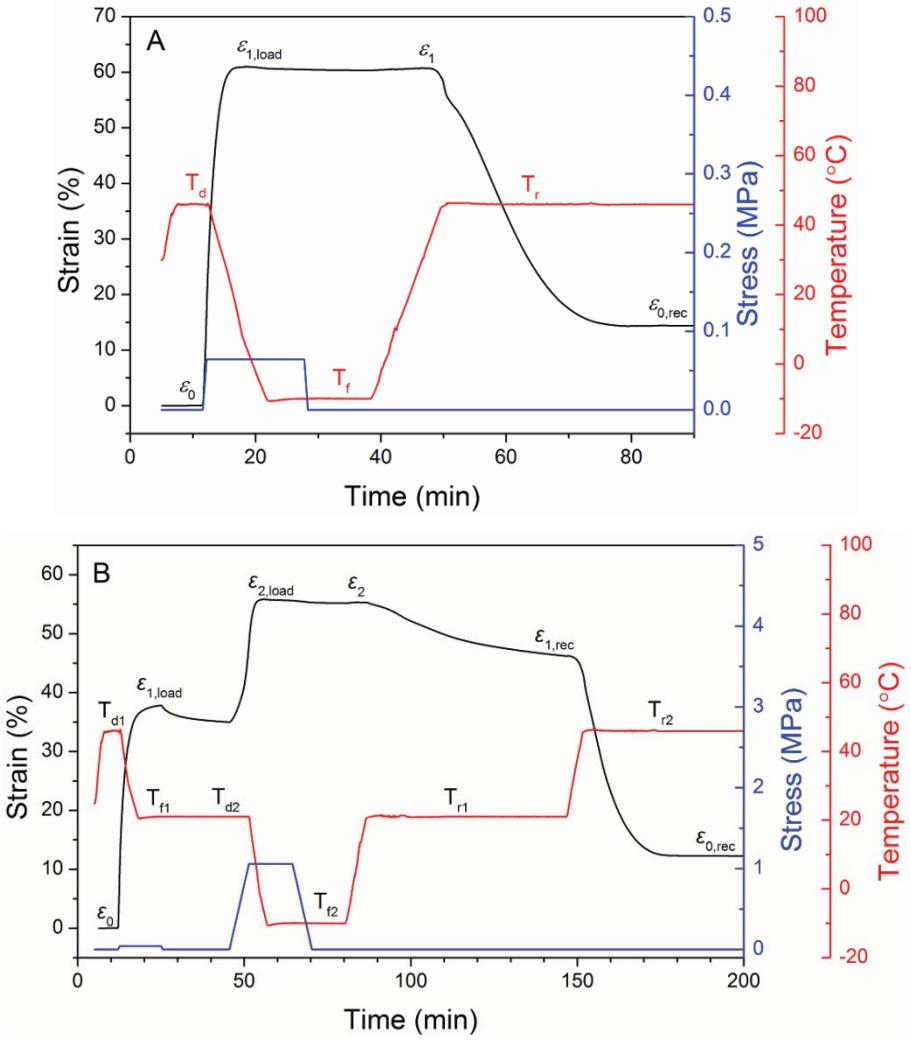

Figure 3.S5 (A) Dual shape memory effect of $CP_{1:2}$ with $T_d = T_r = T_{g,offset} + 15$ °C; $T_f = T_{g,onset} - 15$ °C ($R_f = 99.7\%$, $R_r = 76.4\%$). (B) Triple shape memory effects of $CP_{1:2}$ with $T_{d1} = T_{r2} = T_{g,offset} + 15$ °C; $T_{f1} = T_{d2} = T_{r1} = T_{g,offset} - 10$ °C, $T_{f2} = T_{g,onset} - 15$ °C. ($R_f(0\rightarrow1) = 92.3\%$, $R_f(1\rightarrow2) = 97.1\%$, $R_r(2\rightarrow1) = 44.3\%$, $R_r(1\rightarrow0) = 65.3\%$)

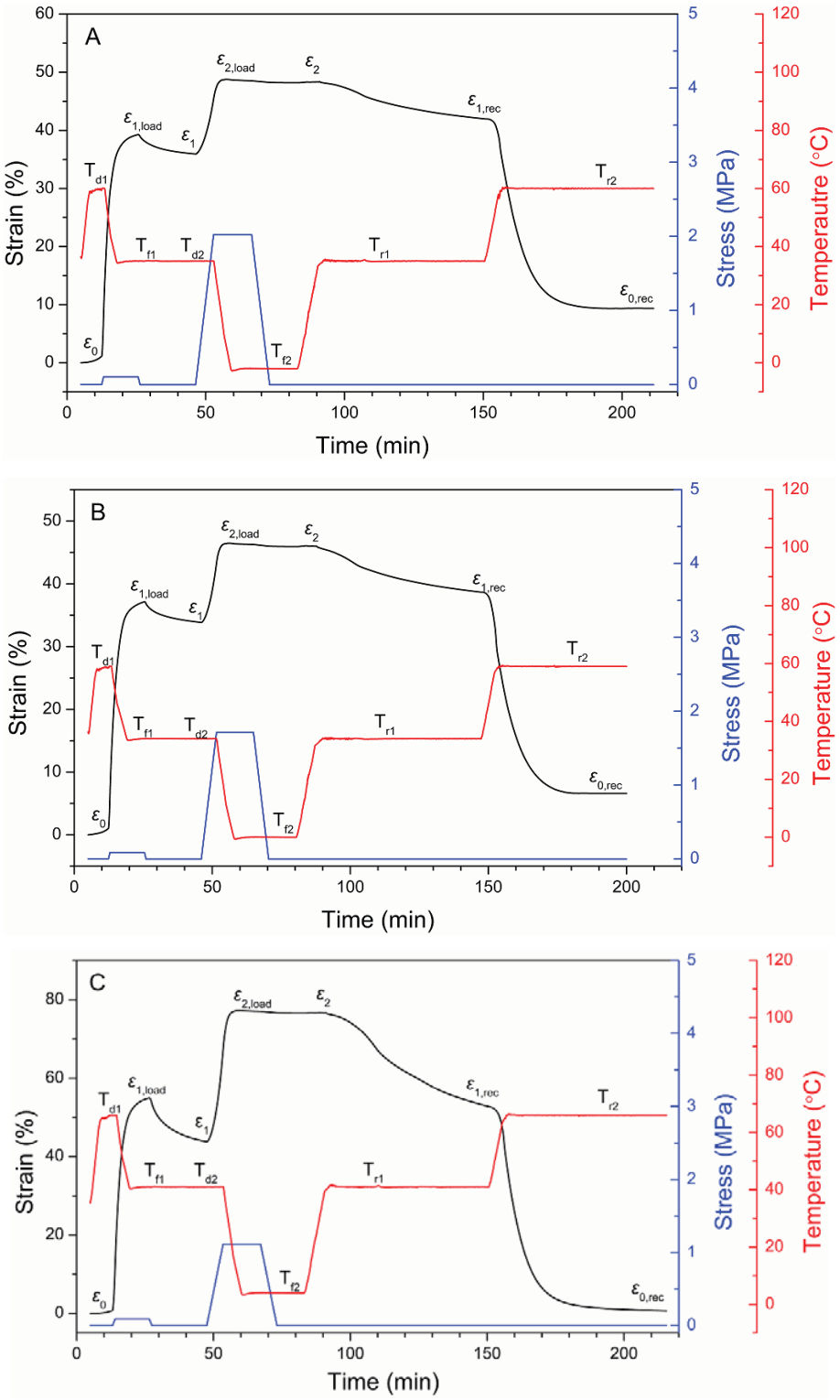

Figure 3.S6 Typical triple shape memory effects of $CP_{2:3}$ and TPs with different irradiation time. (A) $CP_{2:3}$; (B) TP and (C) TP(120). ($T_{d1} = T_{r2} = T_{g,offset} + 15$ ºC; $T_{f1} = T_{d2} = T_{r1} = T_{g,offset} - 10$ ºC, $T_{f2} = T_{g,onset} - 15$ ºC)

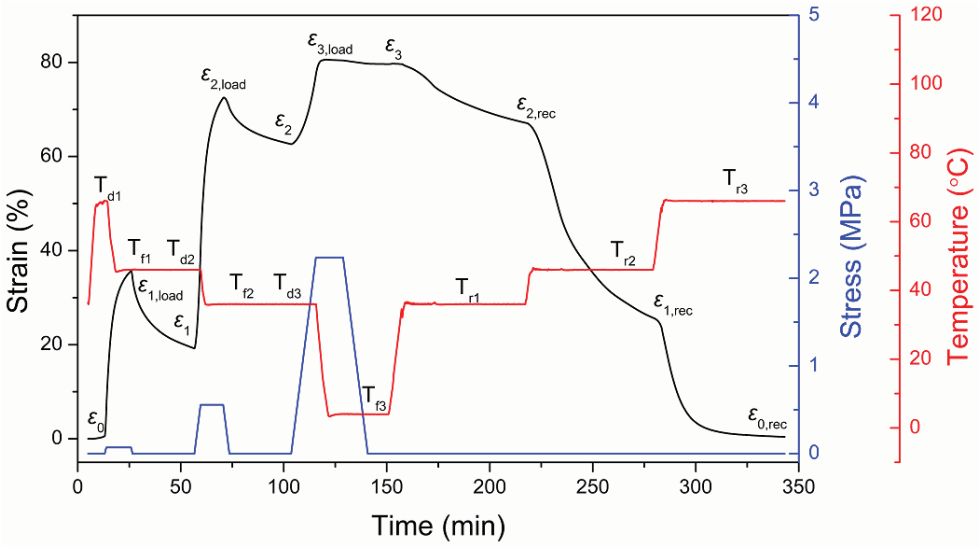

Figure 3.S7 Typical quadruple shape memory effects of TP(120). ($T_{d1} = T_{r3} = T_{g,offset} + 15$ ºC; $T_{f1} = T_{d2} = T_{r2} = T_{g,offset} - 5$ ºC; $T_{f2} = T_{d3} = T_{r1} = T_{g,offset} - 15$ ºC; $T_{f3} = T_{g,onset} - 15$ ºC)

3.7 References

1. Xie, T. Tunable polymer multi-shape memory effect. *Nature* **2010**, 464, 267-270.

2. Shao, Y.; Lavigueur, C.; Zhu, X. X. Multishape memory effect of norbornene-based copolymers with cholic acid pendant groups. *Macromolecules* **2012**, 45, 1924-1930.

3. Gautrot, J. E.; Zhu, X. X. Shape memory polymers based on naturally-occurring bile acids. *Macromolecules* **2009**, 42, 7324-7331.

4. Wu, L.; Jin, C.; Sun, X. Synthesis, properties, and light-induced shape memory effect of multiblock polyesterurethanes containing biodegradable segments and pendant cinnamamide groups. *Biomacromolecules* **2011**, 12, 235-241.

5. Lendlein, A.; Jiang, H. Y.; Junger, O.; Langer, R. Light-induced shape-memory polymers. *Nature* **2005**, 434, 879-882.

6. Gu, X.; Mather, P. T. Water-triggered shape memory of multiblock thermoplastic polyurethanes (TPUs). *RSC Adv.* **2013**, 3, 15783-15971.

7. Lendlein, A.; Langer, R. Biodegradable, elastic shape-memory polymers for potential biomedical applications. *Science* **2002**, 296, 1673-1676.

8. Small Iv, W.; Wilson, T. S.; Benett, W. J.; Loge, J. M.; Maitland, D. J. Laser-activated shape memory polymer intravascular thrombectomy device. *Opt. Express* **2005**, 13, 8204-8213.

9. Xue, L.; Dai, S.; Li, Z. Biodegradable shape-memory block co-polymers for fast self-expandable stents. *Biomaterials* **2010**, 31, 8132-8140.

10. Bao, M.; Lou, X.; Zhou, Q.; Dong, W.; Yuan, H.; Zhang, Y. Electrospun biomimetic fibrous scaffold from shape memory polymer of PDLLA-*co*-TMC for bone tissue engineering. *ACS Appl. Mater. Interfaces* **2014**, 6, 2611-2621.

11. Mather, P. T.; Luo, X. F.; Rousseau, I. A. Shape memory polymer research. *Annu. Rev. Mater. Res.* **2009**, 39, 445-471.

12. Rousseau, I. A.; Mather, P. T. Shape memory effect exhibited by smectic-C liquid crystalline elastomers. *J. Am. Chem. Soc.* **2003**, 125, 15300-15301.

13. Xie, T.; Xiao, X. Self-peeling reversible dry adhesive system. *Chem. Mater.* **2008**, 20, 2866-2868.

14. Wang, L.; Yang, X.; Chen, H.; Gong, T.; Li, W.; Yang, G.; Zhou, S. Design of triple-shape memory polyurethane with photo-cross-linking of cinnamon groups. *ACS Appl. Mater. Interfaces* **2013**, 5, 10520-10528.

15. Wang, L.; Di, S.; Wang, W.; Chen, H.; Yang, X.; Gong, T.; Zhou, S. Tunable temperature memory effect of photo-cross-linked star PCL-PEG networks. *Macromolecules* **2014**, 47, 1828-1836.

16. Zotzmann, J.; Behl, M.; Hofmann, D.; Lendlein, A. Reversible triple-shape effect of polymer networks containing polypentadecalactone- and poly(ε-caprolactone)-segments. *Adv. Mater.* **2010**, 22, 3424-3429.

17. Li, J.; Viveros, J. A.; Wrue, M. H.; Anthamatten, M. Shape-memory effects in polymer networks containing reversibly associating side-groups. *Adv. Mater.* **2007**, 19, 2851-2855.

18. Bai, Y.; Jiang, C.; Wang, Q.; Wang, T. Multi-shape-memory property study of novel poly(ε-Caprolactone)/ethyl cellulose polymer networks. *Macromol. Chem. Phys.* **2013**, 214, 2465-2472.

19. Luo, Y.; Guo, Y.; Gao, X.; Li, B. G.; Xie, T. A general approach towards thermoplastic multishape-memory polymers via sequence structure design. *Adv. Mater.* **2013**, 25, 743-748.

20. Zotzmann, J.; Behl, M.; Feng, Y.; Lendlein, A. Copolymer networks based on poly(ω-pentadecalactone) and poly(ε-caprolactone) segments as a versatile triple-shape polymer system. *Adv. Funct. Mater.* **2010**, 20, 3583-3594.

21. Xie, T.; Xiao, X.; Cheng, Y. T. Revealing triple-shape memory effect by polymer bilayers. *Macromol. Rapid Commun.* **2009**, 30, 1823-1827.

22. Behl, M.; Bellin, I.; Kelch, S.; Wagermaier, W.; Lendlein, A. One-step process for creating triple-shape capability of AB polymer networks. *Adv. Funct. Mater.* **2009**, 19, 102-108.

23. Bellin, I.; Kelch, S.; Langer, R.; Lendlein, A. Polymeric triple-shape materials. *Proc. Natl. Acad. Sci. U.S.A.* **2006**, 103, 18043-18047.

24. Li, J.; Liu, T.; Xia, S.; Pan, Y.; Zheng, Z.; Ding, X.; Peng, Y. A versatile approach to achieve quintuple-shape memory effect by semi-interpenetrating polymer networks containing broadened glass transition and crystalline segments. *J. Mater. Chem.* **2011**, 21, 12213-12217.

25. Jia, Y.-G.; Zhu, X. X. Self-healing supramolecular hydrogel made of polymers bearing cholic acid and β-cyclodextrin pendants. *Chem. Mater.* **2015**, 27, 387-393.

26. Xie, T. Recent advances in polymer shape memory. *Polymer* **2011**, *52,* 4985-5000.

27. Leng, J.; Lan, X.; Liu, Y.; Du, S. Shape-memory polymers and their composites: stimulus methods and applications. *Prog. Mater. Sci.* **2011**, 56, 1077-1135.

28. Hu, J.; Zhu, Y.; Huang, H.; Lu, J. Recent advances in shape-memory polymers: Structure, mechanism, functionality, modeling and applications. *Prog. Polym. Sci.* **2012**, 37, 1720-1763.

29. Lendlein, A.; Kelch, S. Shape-memory polymers. *Angew. Chem. Int. Edit.* **2002**, 41, 2034-2057.

30. Long, V. C.; Berry, G. C.; Hobbs, L. M. Solution and bulk properties of branched polyvinyl acetates IV-melt viscosity. *Polymer* **1964**, 5, 517-524.

31. Robertson, C. G.; Roland, C. M.; Paulo, C.; Puskas, J. E. Linear viscoelastic properties of hyperbranched polyisobutylene. *J. Rheol.* **2001**, 45, 759-772.

32. Hoskins, J. A. The occurrence, metabolism and toxicity of cinnamic acid and related compounds. *J. Appl. Toxicol.* **1984**, 4, 283-292.

33. Shi, D.; Matsusaki, M.; Kaneko, T.; Akashi, M. Photo-cross-linking and cleavage induced reversible size change of bio-based nanoparticles. *Macromolecules* **2008**, 41, 8167-8172.

34. Pal, S.; Ghosh Roy, S.; De, P. Synthesis *via* RAFT polymerization of thermo- and pH-responsive random copolymers containing cholic acid moieties and their self-assembly in water. *Polym. Chem.* **2014**, 5, 1275-1284.

35. Yu, K.; Ge, Q.; Qi, H. J. Reduced time as a unified parameter determining fixity and free recovery of shape memory polymers. *Nat. Commun.* **2014**, 5, 3066-3074.

36. Fox, T. G.; Flory, P. J. Second-order transition temperatures and related properties of polystyrene. I. Influence of Molecular Weight. *J. Appl. Phys.* **1950**, 21, 581-591.

37. Dobrynin, A. Microphase separation transition of random copolymers in a random media. *Phys. Rev. E* **1997**, 56, 750-757.

38. Kolesov, I. S. Multiple shape-memory behavior and thermal-mechanical properties of peroxide cross-linked blends of linear and short-chain branched polyethylenes. *Express Polym. Lett.* **2008**, 2, 461-473.

39. Dolog, R.; Weiss, R. A. Shape memory behavior of a polyethylene-based carboxylate ionomer. *Macromolecules* **2013**, 46, 7845-7852.

40. Sung, S.-J.; Cho, K.-Y.; Hah, H.; Lee, J.; Shim, H.-K.; Park, J.-K. Two different reaction mechanisms of cinnamate side groups attached to the various polymer backbones. *Polymer* **2006**, 47, 2314-2321.

41. Cowie, J. M. G. *Polymers: Chemistry & physics of modern materials,* 2nd ed.; Blackie academic & Professional: Glasgow, 1991; p262.

42. Ni, Y.; Zheng, S. A novel photocrosslinkable polyhedral oligomeric silsesquioxane and its nanocomposites with poly(vinyl cinnamate). *Chem. Mater.* **2004**, 16, 5141-5148.

43. Hu, Y.; Gamble, V.; Painter, P. C.; Coleman, M. M. Functional group accessibility in hydrogen-bonded polymer blends. 4. Cross-linking effects. *Macromolecules* **2002**, 35, 1289-1298.

44. Ratna, D.; Karger-Kocsis, J. Shape memory polymer system of semi-interpenetrating network structure composed of crosslinked poly(methyl methacrylate) and poly(ethylene oxide). *Polymer* **2011**, 52, 1063-1070.

45. Miaudet, P.; Derre, A.; Maugey, M.; Zakri, C.; Piccione, P. M.; Inoubli, R.; Poulin, P. Shape and temperature memory of nanocomposites with broadened glass transition. *Science* **2007**, 318, 1294-1296.

46. Sun, L.; Huang, W. M. Mechanisms of the multi-shape memory effect and temperature memory effect in shape memory polymers. *Soft Matter* **2010**, 6, 4403-4406.
47. Carraher Jr., C. E. *Seymour/Carraher's polymer chemistry,* 6th ed.; Marcel Dekker: New York, **2003,** p561.

Chapter 4

Two-way reversible shape memory polymers made of cross-linked co-crystallizable random copolymers with tunable actuation temperatures*

Abstract

Two-way reversible shape memory polymers (2W-SMPs) are highly desirable for many applications. We report for the first time the use of random copolymers with co-crystallizable monomeric units for the preparation of such polymer networks. Homopolymers and random copolymers of ε-caprolactone and ω-pentadecalactone were designed and made by ring opening polymerization with Candida antarctica lipase B as catalyst. The melting temperatures of these prepolymers may be adjusted by the use of various molar ratios of the co-monomers. Upon thiol-ene cross-linking, the polymer network exhibited two-way reversible shape memory effects under both stress-free and stress conditions. The actuation temperature (T_A) of the 2W-SMP under stress-free condition can be tuned in a broad range using a selected mixture of prepolymers followed by photo-cross-linking with a multifunctional cross-linker. Increasing the initial stretching stress amplitude led to an increased *absolute* strain change under both stress-free and stress conditions, it led to a reduced *relative* strain change under stress-free condition, but almost no change under stress condition. The evolution of the microstructure of 2W-SMPs under stress-free condition cycle was studied by the use of X-ray diffraction (2D-WAXD and SAXS). This is the first report on the tuning of T_A of 2W-SMPs under stress-free condition by the use of one or two prepolymers to form a chemically cross-linked network. We have also eliminated the use of toxic metal catalysts in the synthesis of polymeric biomaterials. The materials are shown to be capable of performing reversible bending-unbending and coiling-uncoiling motions.

---

*Wang, K.; Jia, Y. -G.; Zhu, X. X. *Macromolecules* **2017,** 50, 8570-8579.

4.1 Introduction

Shape memory polymers (SMPs) have drawn much scientific attention due to their specific properties and potential applications in biomedicine,[1-3] and as smart textiles,[4] actuators,[5] and self-peeling reversible dry adhesives.[6] Conventional SMPs are capable of recovery to their permanent shape from a temporary shape after being exposed to an external stimulus,[7-18] and this permanent shape cannot be changed once it is restored by applying an external reverse stimulus. These are called one-way SMPs (1W-SMPs), and the shape change is irreversible. Two-way reversible shape memory is desirable for applications as actuators, artificial muscles and self-locomotion robotics.[19-21] Such polymers may vary between two distinct shapes when they are exposed to stimuli creating the opposing conditions, such as heating and cooling, where the heating can be induced by an electric current, light and magnetic field.[19, 22] Two-way reversible SMPs (2W-SMPs) are harder to achieve and have become the most desired shape memory materials due to their unique properties.

Two-way reversible shape memory effects (2W-SMEs) may be classified into two types: 2W-SMEs under stress and stress-free conditions. A stress is applied in both cases after the temperature is raised to a high temperature (T_H) above the melting temperatures (T_ms). The sample is deformed, and then the temperature is lowered to a low temperature (T_L) below the crystallization temperatures (T_cs). In the stress-free condition, the stress is removed at this point; in the stress condition, this stress is maintained, for example, by a constant weight attached. Obviously, the 2W-SME under stress-free condition can be more versatile in its applications. Both of these 2W-SMEs are based on crystallization-induced elongation (CIE) upon cooling and melting-induced contraction (MIC) upon heating with or without tensile stress and can be realized on liquid crystalline elastomers (LCEs) or semi-crystalline polymer networks.[23-31] Since 2W-SMPs under stress condition have their limits in certain applications, 2W-SMPs under stress-free condition have drawn more attention. Generally, four strategies may be used to design a thermally-induced 2W-SMP under stress-free condition: (1) Laminated polymer structures.[32-34] The drawback is the very small reversible strain change. (2) Chemically cross-linked semi-crystalline polymer networks with one broad or two T_ms.[35-38] Their memorized shapes may be erased when heated above both T_ms and may be reprogrammed to other shapes. (3) Polymer networks (LCEs or semi-crystalline polymers) via

two-stage cross-linking process.[39-41] Their shapes are fixed in the preparation process of polymer network and thus cannot be erased upon heating. (4) Thermoplastic semi-crystalline polymers also showed 2W-SME under stress-free condition when the deformation temperature is set in the T_m range.[42-44] Their reversible strain change is not as good as chemically cross-linked polymer networks. In general, the chemically cross-linked semi-crystalline polymer networks may exhibit the best 2W-SME under stress-free condition due to the larger reversible strain change and reprogrammable shapes.

Semi-crystalline polymer networks are easier to synthesize than the LCEs. However, the synthesis of most of the semi-crystalline polymer networks mentioned above requires the use of organometallic catalysts that are considered to be toxic for biomedical applications. Moreover, the actuation temperature (T_A) of 2W-SME under stress-free condition is at a fixed value, since it is determined by the T_m of the actuator polymer phase. The tuning of T_A is highly desirable for their applications, especially in the biomedical fields. In this work, we attempt to address these problems by choosing different monomers that may co-crystallize once copolymerized. For this purpose, we need to find co-monomer pairs whose random copolymers may co-crystallize over the entire composition range. A larger difference in the T_ms of the two corresponding homopolymers is preferred since it can provide a larger T_A tuning range. Only a few co-crystallizing polymer systems have been reported during past several decades.[45-48] In most cases, their synthesis is not easy and the T_m difference is quite small. Gross' group reported the copolymerization of ω-pentadecalactone (PDL) and ε-caprolactone (CL) catalyzed by Candida antartica lipase B (CALB),[49] an enzyme with high efficiency for ring-opening polymerizations.[50-52] P(CL-*co*-PDL) random copolymers undergo isomorphous substitution, and can co-crystallize over the entire composition range.[49, 53] The possibility of co-crystallization provides an ideal situation for the design of 2W-SMPs. To the best of our knowledge, the strategy of using co-crystallizable monomers has not yet been used in the preparation of 2W-SMPs. Therefore, we synthesized a series of P(CL-*co*-PDL) random copolymers with a range of T_m that may be varied between the T_ms of the two corresponding homopolymers (52 to 92 ºC for PCL and PPDL, respectively) (See Table 4.1) by varying the ratio of the co-monomers in the prepolymers before cross-linking. This is the first report on

the easy tuning of the T_A of 2W-SME under stress-free condition by selectively incorporating prepolymers as functional segments in a polymer network.

4.2 Experimental section

4.2.1 Materials

Di(ethylene glycol) (99%), ε-caprolactone (CL, 97%), ω-pentadecalactone (PDL, ≥ 98%), methacryloyl chloride (≥ 97%), triethylamine (TEA, ≥ 99.5%), pentaerythritol tetrakis(3-mercaptopropionate) (PTME, > 95%), 2,2-dimethoxy-2-phenylacetophenone (DMPA, > 99%) and Candida antarctica lipase B (CALB) immobilized on acrylic resin were purchased from Sigma-Aldrich. CL was first dried over calcium hydride and distilled under reduced pressure. PDL was dried in a vacuum oven for 48 h at room temperature. $CDCl_3$ (99.8% D) was purchased from Sigma-Aldrich. Dichloromethane (DCM), toluene, chloroform, and methanol were dried using a solvent purification system from Glass Contour.

4.2.2 Synthesis of prepolymers

A representative synthetic procedure of a prepolymer is described here (Scheme 4.S1). CALB (0.50 g) was placed in a 25 mL round-bottom flask and then dried for 24 h over P_2O_5 in a vacuum desiccator at room temperature. CL (4.85 mL, 42.50 mmol) and diethylene glycol (0.31 mL, 3.25 mmol) were then placed in the round-bottom flask equipped with a magnetic stir bar. The flask was stoppered with rubber septa and sealed with Teflon tape. Toluene (5.0 mL) was subsequently added via syringe under argon into the reaction vials. The vials were then placed into a preheated oil bath at 70 °C for 24 h. The system was terminated by exposing to air and adding excess of chloroform. CALB was then removed by filtration. The filtrates were concentrated by rotary evaporation and precipitated from methanol. The precipitate (prepolymer PCL) was dried under vacuum at 40 °C for 24 h.

The prepolymers were conjugated with a polymerizable double bond by reacting with a methacrylate to form a macromolecular monomer, also known as macromer,[54] which was then used in the photo-cross-linking in the next step. The synthesis of methacrylate-terminated prepolymer PCL (MPCL) is described here. 0.45 mL of triethylamine was added to 15 mL of DCM solution of PCL diol (4.2 g, 1.20 mmol) in a 100 mL round-bottom flask equipped with

a magnetic stir bar and placed in an ice-water bath. Methacryloyl chloride (0.75 g, 7.20 mmol) in 5 mL of DCM was added dropwise to the mixture under stirring. After 1 h, the ice−water bath was removed, and stirring was continued for 24 h. After the reaction, the solutions were filtered, and the filtrates were concentrated by rotary evaporation to obtain a sticky solution. Then the solution was precipitated in methanol and the precipitate was dried under vacuum at room temperature for 72 h.

4.2.3 Photo-cross-linked polymer networks via thiol−ene click reaction

The methacrylate-terminated prepolymers (0.267 g PCL and 0.133 g (PCL-*co*-PDL)$_{1:2}$) and the cross-linker, PTME (1.2 eq.), were mixed in a dry vial. 0.75 mL chloroform and 4 mg DMPA were added into mixture. The vial was vortexed for 5 min. The mixture was poured into a Teflon mold (2.0 cm × 2.0 cm) and exposed to a UV light of 365 nm (20 mW/cm^2) placed at a distance of 5 cm for 1.5 h. The thermoset polymer network was allowed to set in a fume hood for 3 days and then removed from the mold. Two polymer networks, [PCL-P(CL-*co*-PDL)$_{2:1}$)]$_{2:1}$ and [PCL-P(CL-*co*-PDL)$_{1:2}$)]$_{2:1}$, were prepared separately with 2:1 weight ratio of the prepolymers PCL to either P(CL-*co*-PDL)$_{2:1}$ or P(CL-*co*-PDL)$_{1:2}$, respectively denoted as CC_2D_1 and CC_1D_2. The structures of the polymers are shown in Figure 4.1.

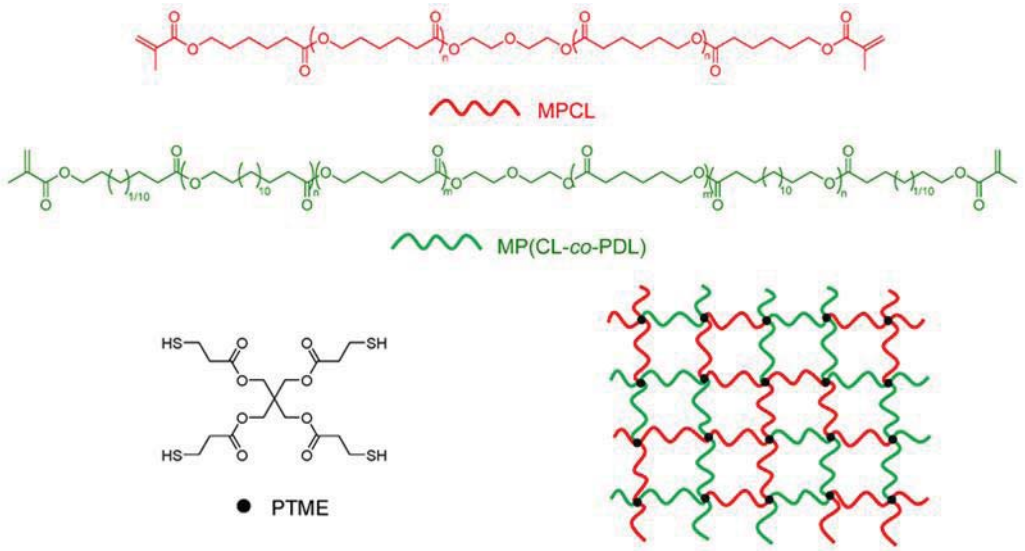

Figure 4.1 Structure of methacrylate-terminated prepolymers and their polymer network.

4.2.4 Polymer characterization

Differential scanning calorimetry (DSC) measurements were carried out on a DSC 2910 (TA Instruments) at a heating rate of 10 °C/min. The temperature and heat flow were calibrated with indium before measurements. Fourier transform infrared spectroscopy (FTIR) was used to confirm the disappearance of -C=C- after irradiation using a Perkin-Elmer spectrum One FTIR spectrometer with a universal ATR (attenuated total reflectance) mode. All spectra were scanned 32 times in the range of 800 – 4000 cm^{-1} at a 4 cm^{-1} resolution. ^{1}H NMR spectra of the prepolymers in $CDCl_3$ were recorded on a Bruker AV400 spectrometer operating at 400 MHz for protons.

Wide-angle X-ray diffraction (WAXD) experiments were performed with a Bruker D8/Discover C2 (combinatorial) diffractometer operated at 40 kV and 40 mA using CuKα radiation (λ = 1.54 Å) at a sample-to-detector distance of 85.6 mm. The samples were aligned and centered with the incident X-ray beam using a video microscope and a laser. Each sample was measured using an acquisition time of 5 min. Small angle X-ray scattering (SAXS) experiments were performed on a Bruker NanoStar system with a Vantec 2000 2D detector and a 50 kV and 0.60 mA generator, at a sample-to-detector distance of 1080 mm. Monochromatized CuKα (λ = 1.54 Å) radiation was also used. The SAXS measurements were performed using a scanning time of 30 min at room temperature on a pressure below 0.2 mbar.

4.2.5 Dynamic mechanical analysis (DMA)

Smaller rectangular samples (3.5 mm × 2.0 cm) were cut from these films and used for shape memory tests (the dimensions of the films were measured with an electronic digital caliper with a precision of 0.01 mm). The DMA analyses were performed on a DMA 2980 (TA Instruments). To measure the storage and loss moduli of the polymers, a preload force of 0.005 N, an amplitude of 10 μm, a temperature sweeping rate of 2 °C/min, and a frequency of 1 Hz were used. The specimen was first heated from -20 to 150 °C, followed by a cooling run to -20 °C. For shape memory experiments, the controlled force mode was used. At least three consecutive cycles were performed for each sample.

(1) *2W-SME under stress-free condition (Figures 4.5A and 4.5B).* The specimen was first equilibrated at a high temperature (T_H, 100 °C, above the T_ms of all segments) for 5 min to

reach heat conduction equilibrium. It is then deformed at T_H, and cooled to a low temperature (T_L, -20 °C, below the T_cs of all segments) and held isothermally for 5 min before unloading the external force to freeze the movement of the polymers chains. The sample was then heated to T_A and kept isothermal for 15 min; and then cooled to T_L and kept for another 5 min. The heating and cooling rates were both set to 5 °C/min. The *absolute* (ε') and *relative reversible strain changes* (ε''), used as performance indicators for 2W-SME under stress-free condition, are defined as

$$\varepsilon' = \varepsilon_E - \varepsilon_C \tag{4.1}$$

$$\varepsilon'' = \frac{\varepsilon'}{\varepsilon_L} \times 100\% \tag{4.2}$$

where ε_E is the elongation strain of the sample before reaching T_A, and ε_C is the contraction strain before cooling to T_L, and ε_L is the maximum strain after CIE and the removal of the external loading. For the measurement of internal tensile stress, the controlled mode was first used. After isothermal 15 min at T_A, DMA was switched to the iso-strain mode. The temperature was cooled to 0 °C and kept for 5 min and then heated to T_A.

(2) *2W-SME under stress condition (Figures 4.5C and 4.5D).* The sample was stretched at T_H (100 °C) under a constant force, and then cooled to T_L (-20 °C) and equilibrated for 5 min to ensure complete crystallization. The sample was then reheated to T_H and kept for 5 min. Eqs (4.1) and (4.2) can be rewritten as eqs (4.3) and (4.4) to calculate the *absolute* (ε'_s) and *relative reversible strain changes* (ε''_s).

$$\varepsilon'_s = \varepsilon_L - \varepsilon_H \tag{4.3}$$

$$\varepsilon''_s = \frac{\varepsilon'_s}{\varepsilon_L} \times 100\% \tag{4.4}$$

where ε_L is the maximum strain of sample after elongation, and ε_H is the minimum strain after contraction.

4.3 Results and Discussion

4.3.1 Characterization of prepolymers

To eliminate the use of metal-based catalysts in the synthesis of biomaterials, CALB was used as catalyst for the synthesis of prepolymers, and the corresponding methacrylate-terminated prepolymers are schematically shown in Scheme 4.S1 and Figure 4.1. Their molecular structures were confirmed by ^{1}H NMR spectroscopy. Figure 4.S1 shows typical ^{1}H NMR spectra of prepolymers, in which the methylene protons next to the hydroxyl end group are detected at 3.62 ppm (peak h). The signals at 2.30 (peak c) and 4.06 ppm (peak g) are attributed to −C***H***$_2$CO− and −OC***H***$_2$− of the CL unit, respectively. The peaks at 3.69 (peak a) and 4.22 ppm (peak b) are assigned to –OC***H***$_2$- and -COOC***H***$_2$- of the diethylene glycol unit. The degree of polymerization (DP) and the molecular weight of prepolymers and the molar ratio of the co-monomers in the copolymers may be calculated by the ratio of the ^{1}H NMR signal integrations of the corresponding protons (Eqs 4.S1, 4.S2 and 4.S3 in supporting information). The results are summarized in Table 4.1. For all random copolymers, the molar ratio of the co-monomers is almost the same as that in the feed. Figure 4.2 illustrates the typical ^{1}H NMR spectra of methacrylate-terminated prepolymers, in which the appearance of vinyl peaks at around 5.50 and 6.10 ppm (peak i) and the disappearance of methylene protons of the prepolymers next to the hydroxyl end group indicate the successful conjugation of the methacrylate groups to the prepolymers.

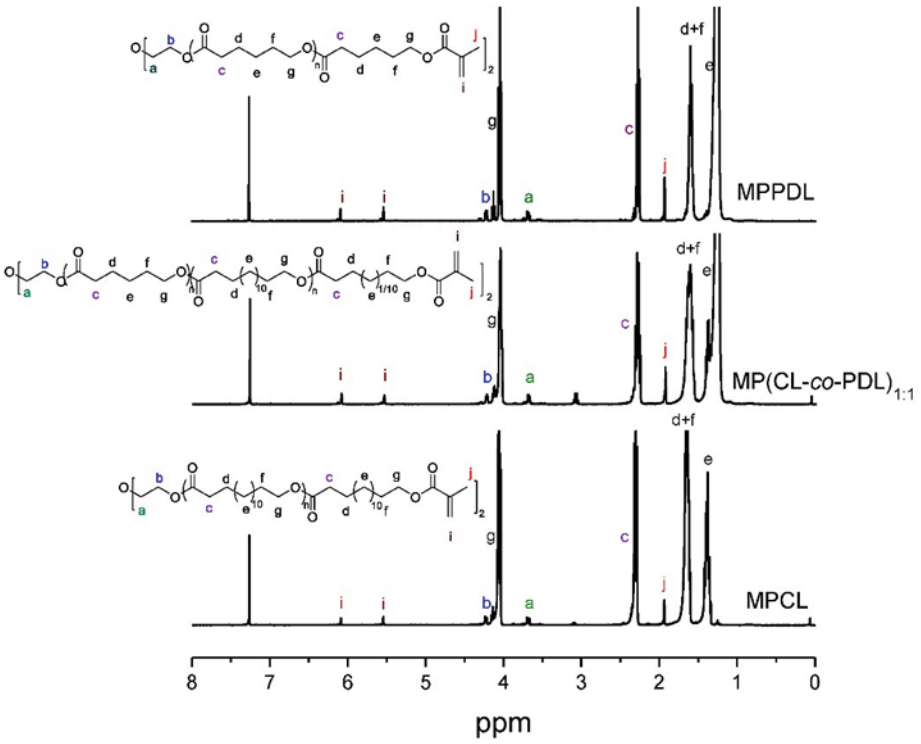

Figure 4.2 ^{1}H NMR of representative methacrylate-terminated prepolymers (macromers).

Table 4.1 Molecular characteristics and properties of prepolymers with various molar ratios of monomers.

prepolymers[a]	$M_{n,NMR}$[b] (g/mol)	CL : PDL		T_c[d] (°C)	T_m[d] (°C)	ΔH_m[e] (J/g)
		feed[c]	copolymer[b]			
PCL	3500	-	-	35	52	78
P(CL-*co*-PDL)$_{2:1}$	2750	2.00 : 1.00	1.83 : 1.00	45	58	103
P(CL-*co*-PDL)$_{1:1}$	2460	1.00 : 1.00	0.92 : 1.00	58	72	123
P(CL-*co*-PDL)$_{1:2}$	3260	1.00 : 2.00	1.00 : 2.03	62	75	121
PPDL	3030	-	-	78	92	145

[a]The numbers in the subscript denote molar ratio of monomers in the feed. [b]Number-average molecular weight and molar ratio of monomers in the prepolymers calculated from the ratio of ^{1}H NMR signal integrations. [c]Molar ratio of monomers in the feed. [d]Measured by DSC. Defined by crystallization (T_c) and melting peaks (T_m), respectively. [e]Obtained from the endothermic melting peaks in DSC.

4.3.2 Thermal properties of prepolymers and polymer networks

The melting behaviors of prepolymers were studied by DSC analysis, and the data are summarized in Table 4.1. Figure 4.3A shows the increase of the T_ms of the prepolymers from

52 to 92 °C with increasing molar ratio of PDL in the prepolymers, indicating the T_m can be easily tuned by varying the co-monomer ratio. In this study, two polymer networks, CC_2D_1 and CC_1D_2, were chosen to show 2W-SME with adjustable T_As. Figure 4.3B shows the DSC curves of both polymer networks. Both melting peaks of PCL and (PCL-*co*-PDL)$_{1:2}$ segments were observed at 56 and 76 °C, respectively and their melting ranges overlap at around 60 °C in CC_1D_2 polymer network, while only one melting peak was observed at 41 °C because the melting ranges of PCL and (PCL-*co*-PDL)$_{2:1}$ segments merge into one for CC_2D_1.

DMA tests with varying temperature were carried out for both polymer networks to measure the transition temperatures (T_m, T_c) in order to design the shape memory experiments, and the curves of both heating and cooling run are shown in Figure 4.3C. Both polymer networks exhibit a systematic decrease in the storage modulus with increasing temperature. Two transition temperatures appeared on the DMA curves of both polymer networks. For CC_1D_2 polymer network, the first one ranging from 55 to 75 °C belonged to the PCL segment, while the other ranging from 75 to 100 °C was attributed to the P(CL-*co*-PDL)$_{1:2}$ component. For the CC_2D_1 polymer network, the first transition of PCL segment ranged from 48 to 65 °C while the second one ranged from 65 to 90 °C. The moduli of both cross-linked samples reach a plateau above their melting transitions. CC_2D_1 has a higher plateau modulus than CC_1D_2, suggesting a higher cross-linking density, which may also be the reason that the PCL segment has a lower T_m in CC_2D_1 than in CC_1D_2.[55] The more complete reaction of -C=C- of CC_2D_1 is also confirmed by ATR-FTIR spectra (Figure 4.3D). After 1.5 h irradiation with UV light (λ = 365 nm), the absorption intensity of C=C stretching vibration at 1634 cm^{-1} and =C-H bending at 816 cm^{-1} of the CC_1D_2 polymer network significantly decreased, while these two absorption peaks almost disappeared for the CC_2D_1 polymer network.

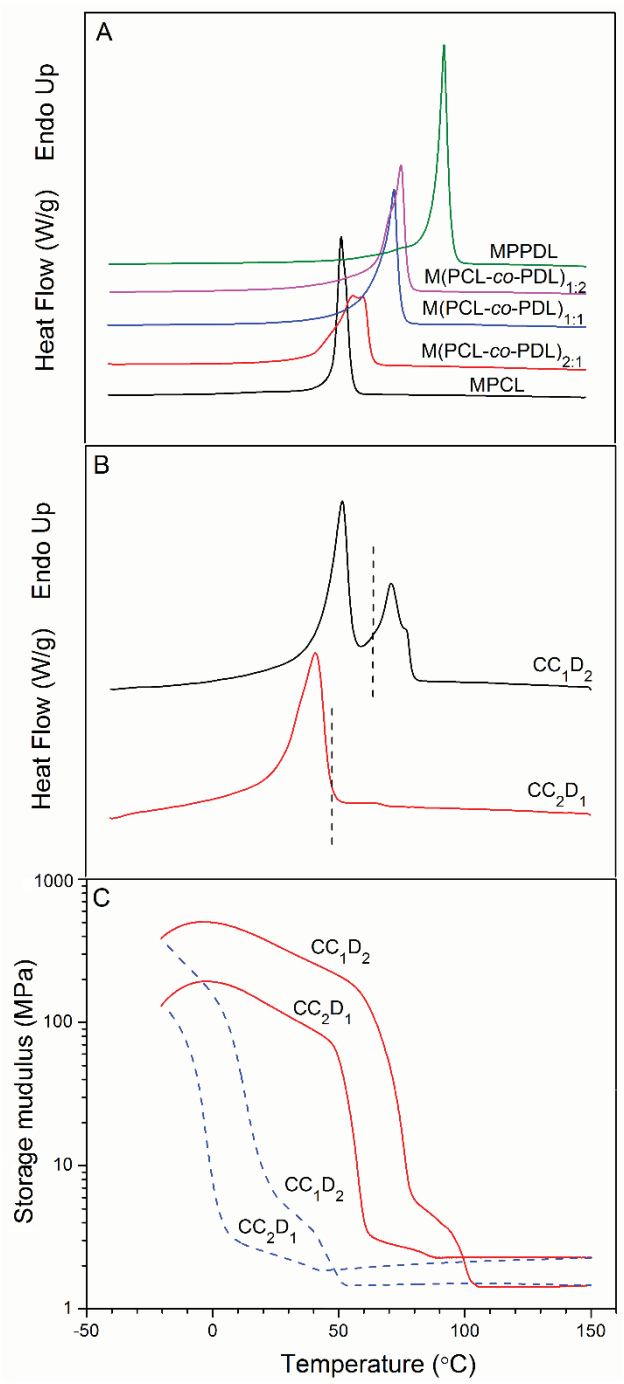
A
Heat Flow (W/g) Endo Up
MPPDL
M(PCL-co-PDL)1:2
M(PCL-co-PDL)1:1
M(PCL-co-PDL)2:1
MPCL
B
Heat Flow (W/g) Endo Up
CC1D2
CC2D1
C
Storage mudulus (MPa)
1000
100
10
1
CC1D2
CC2D1
CC1D2
CC2D1
-50
0
50
100
150
Temperature (°C)

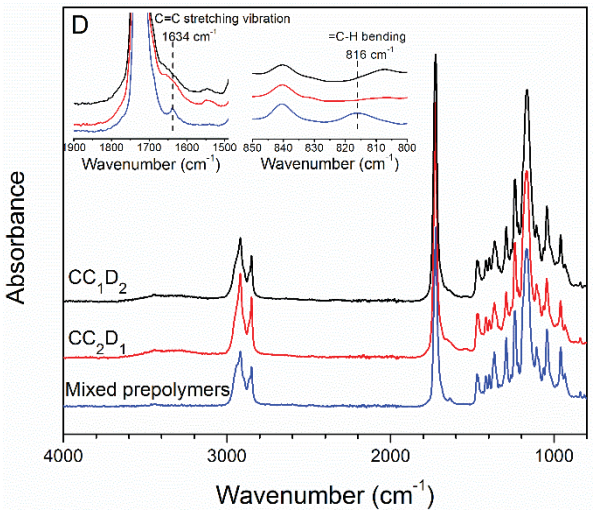

Figure 4.3 Thermal properties of prepolymers and polymer networks. DSC traces of (A) methacrylate-terminated prepolymers, and (B) polymer networks, the dashes indicate the selected T_A in the experiments of 2W-SME under stress-free condition; (C) Storage modulus vs. temperature for polymer networks from DMA; (D) FTIR spectra of prepolymers and polymer networks.

4.3.3 2W-SME of thiol-ene polymer network

The polymer network CC_1D_2 was selected as a representative sample to show 2W-SME. 2W-SME under stress-free condition of CC_1D_2 with various T_As was studied to find the best T_A at an isothermal time of 15 min, and the results are shown in Figure 4.S3. The contraction and elongation strains first increased and then decreased with increasing T_A. The largest contraction and elongation strains were obtained with a T_A of 65 °C.

2W-SMEs under stress-free condition for CC_1D_2 are shown in Figure 4.4 in water bath. 60 °C was selected as T_A and 10 °C as T_L due to the difference of heat conduction coefficients of water and air. In Figure 4.4A, the sample was first programmed into a folded "U" shape in 90 °C water bath and cooled to 10 °C for fixing this shape. Then this sample was heated to 60 °C and cooled to 10 °C, resulting in reversible shape transformations between a folded "U" and an opened "L" shapes. The reversible angle change is around 90º. The entire procedure could be repeated several times without losing memory of both shapes. More complex motions can be realized by such materials such as the coiling-uncoiling shape changes as illustrated in Figure 4.4B.

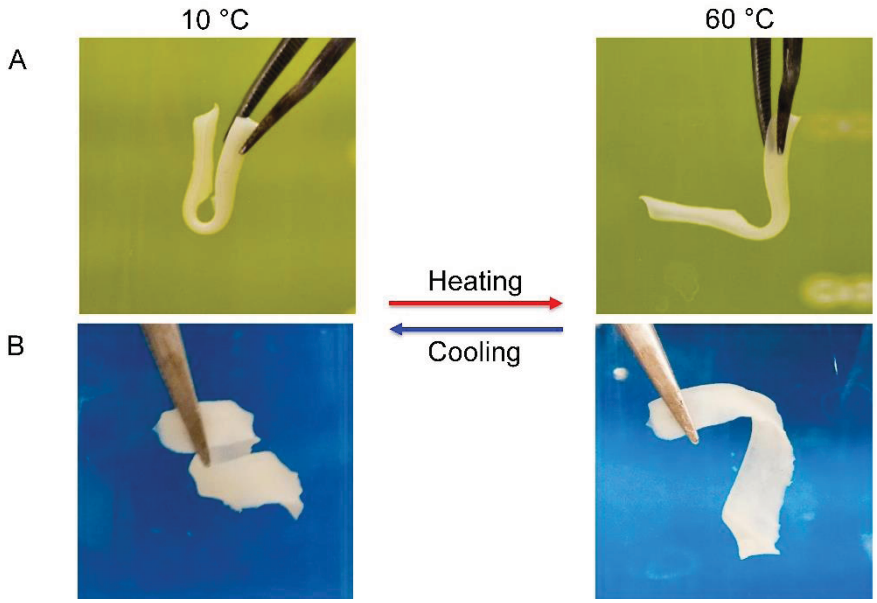

Figure 4.4 Photographs showing the reversible shape memory behavior of CC_1D_2 in water bath set at 10 and 60 °C: (A) bending-unbending; (B) coiling-uncoiling.

Figure 4.5A shows DMA curves of 2W-SME under stress-free condition of CC_1D_2. The sample was first stretched at 100 °C (T_H), and then cooled to -20 °C (T_L). CIE phenomenon occurred in the strain curve, which may be attributed to the oriented crystallization of both segments of the polymer network under external stress. The external stress was unloaded for fixing the temporary shape (ε_L). After that, the sample was heated to 65 °C for recovery to an intermediate shape (ε_C) because of partial melting of the crystalline scaffold of PCL segment and was then cooled to -20 °C for an elongation shape (ε_E) due to the internal tensile stress, confirmed by Figure 4.S4. Thus, the reversible shape was realized with the cyclic heating and cooling between 65 and -20 °C. The average value of the absolute strain change is 13.2 %, and the repeatability of the absolute strain change is very good over the three cycles.

To confirm the tunability of the T_A for this series of prepolymers, PCL and (PCL-*co*-PDL)$_{2:1}$ were also selected as two segments of thiol-ene polymer network (CC_2D_1). As shown in Figure 4.5B, T_A was selected to be 48 °C due to the best absolute strain change and repeatability. The absolute strain change is up to 10.9 %, similar to the CC_1D_2 network. This indicates that T_A could be tuned by selecting two different prepolymers.

These samples should also exhibit very good 2W-SME under stress condition due to its remarkable CIE. As illustrated in Figure 4.5C, the sample (CC_1D_2) was also first stretched at 100 °C (T_H), and then cooled to -20 °C (T_L). The external stress was kept constant until the end of the experiment. After that, the sample was heated to 100 °C and cooled to -20 °C over three cycles. The sample contracted first and then elongated repeatedly due to MIC and CIE. Thus, the absolute strain change under a 0.3 MPa initial stretching stress was obtained, and its value is up to 19.3 %. Figure 4.5D presents the 2W-SME under stress condition of CC_2D_1 polymer network. In this case, the absolute strain change of 2W-SME under stress condition is 17.2%, which is somewhat lower than that of CC_1D_2 polymer network due to its higher cross-linking density.

4.3.4 Effect of stretching stress on the strain change

In the literature, there have been previous reports on the effect of the initial stretching stress on the absolute strain change of 2W-SME under stress condition,[24, 29, 56, 57] but no report on this effect under stress-free condition. We have studied the effects of the initial stretching stress on 2W-SMEs under both stress and stress-free conditions by applying tensile stresses ranging from 0.1 to 0.5 MPa. Figure 4.6 shows the curves of the second cooling/heating cycles represented as the absolute strain change vs. temperature curves for the various applied tensile stresses. For a load of 0.1, 0.2 and 0.3 MPa, the shape memory cycles of 2W-SME under stress condition show only one step strain increment induced by the PCL phase (Figure 4.6A). Under higher external load, two-step increments were observed during the cooling process under external stress. The P(CL-*co*-PDL)$_{1:2}$ phase may need a larger tensile force for its CIE than the PCL phase. For the following heating step, all MIC temperatures (T_{MIC}s) are over 80 °C. Comparatively larger and more stable crystallites are formed in the polymer network during crystallization under external stress, resulting in higher T_ms and associated T_{MIC}s for strain recovery.[29] For 2W-SME under stress-free condition, the absolute strain changes were also improved with increasing external stretching stress (Figure 4.6B). All contractions occurred several minutes after reaching 65 °C, probably due to the appearance of larger stable crystallites which may take time to reach heat conduction equilibrium.

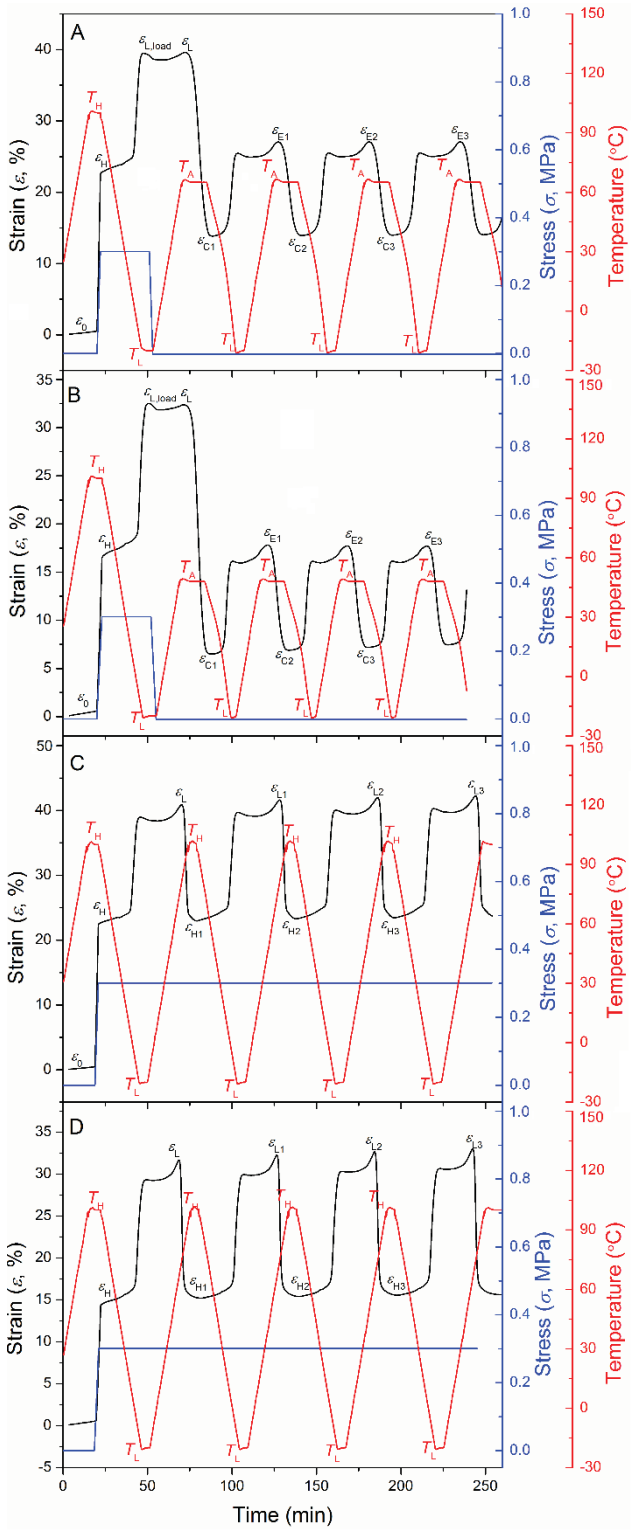

Figure 4.5 2W-SME of thiol-ene cross-linked (A & C) CC_1D_2 and (B & D) CC_2D_1 networks. A & B under stress-free condition; C & D under stress condition. The initial stretching stress amplitude is 0.3 MPa.

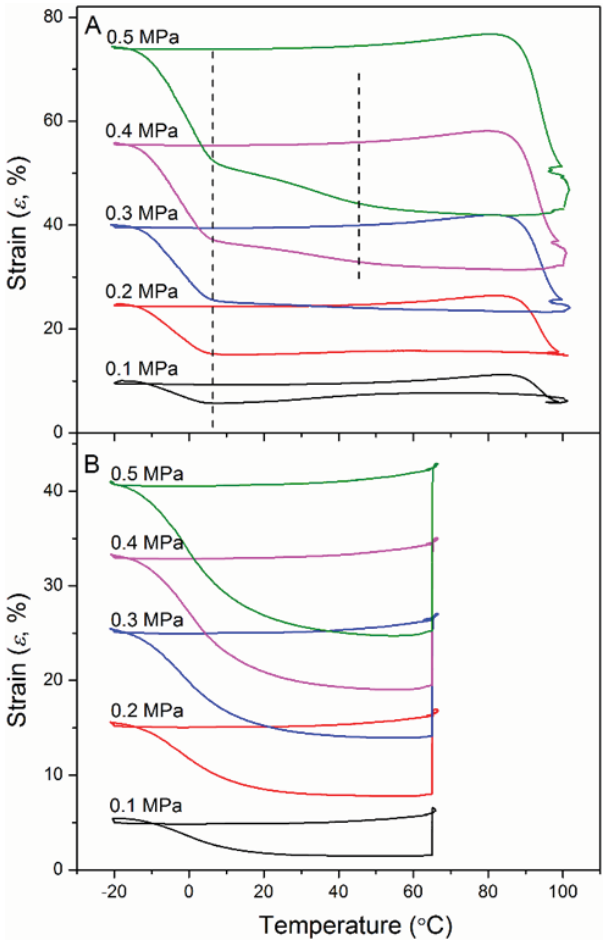

Figure 4.6 The absolute strain change of 2W-SME under (A) stress, and (B) stress-free conditions with various initial stretching stresses. The dashes indicate the onset of strain increment.

Figure 4.7 depicts the influence of stretching stress on the absolute and relative strain change of 2W-SME under both stress and stress-free conditions. For 2W-SME under stress condition (Figure 4.7A), the absolute strain change increased linearly and significantly from 5.5 to 34.9 % as stretching stress increases from 0.1 to 0.5 MPa, which is consistent with previous reports.[29, 56, 58] Under stress-free condition, the absolute strain change also increased linearly first as stretching stress increases from 0.1 to 0.3 MPa, and started to level off from 0.3 to 0.5 MPa. Figure 4.7B shows the effect of stretching stress on the relative strain change of 2W-SME under both stress and stress-free conditions. The relative strain change decreased with increasing stretching stress under stress-free condition, but remained almost constant under stress condition. Figure 4.7C shows the relationship of the absolute strain changes of

2W-SME under stress and stress-free conditions. The absolute strain change of 2W-SME under stress-free condition increased more slowly than the change of 2W-SME under stress condition.

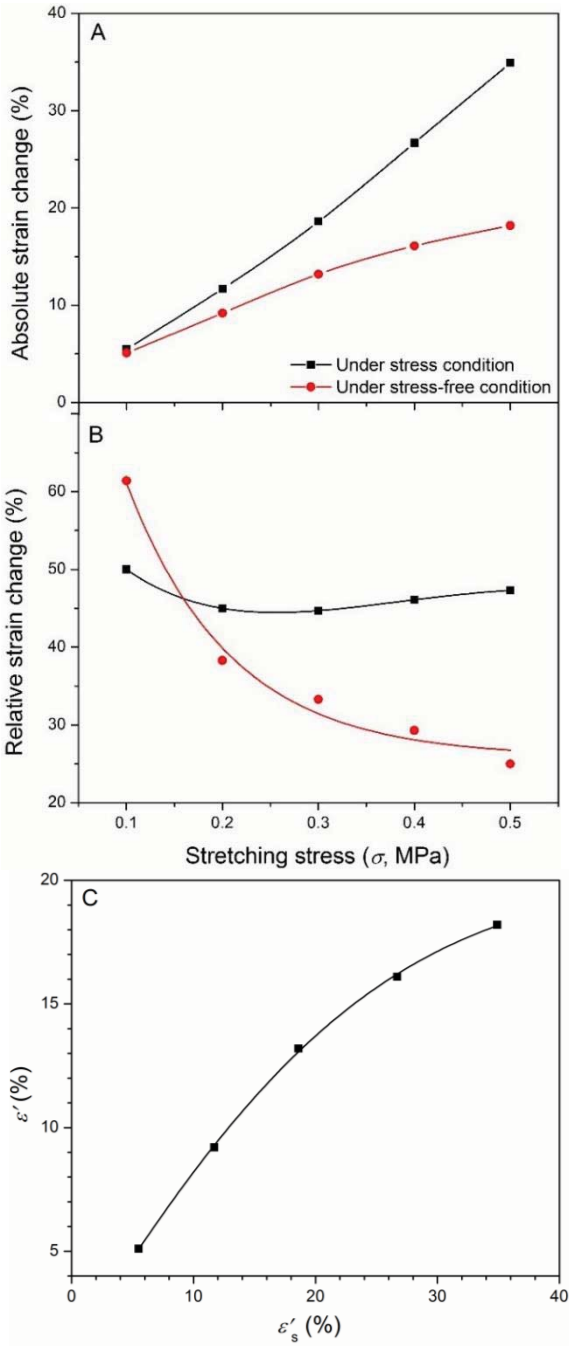

Figure 4.7 Effect of initial stretching stress on the (A) absolute and (B) relative strain changes, (C) the relationship of the absolute reversible strain changes of 2W-SME under stress and stress-free conditions.

4.3.5 Effect of stretching on the morphology

In order to determine the morphology of the unstretched and stretched CC_1D_2 polymer networks after CIE, 2D-WAXD and SAXS patterns were obtained (Figure 4.8). The unstretched sample was also subjected to a similar heating and cooling cycle as for the stretched one with no loading applied. 2D-WAXD images of the unstretched polymer network exhibit typical continuous Debye rings (Figure 4.8A), indicating the randomly crystalline polymer chains. When the sample was stretched and elongated after cooling due to CIE under 0.3 MPa stretching stress, both (200) and (110) reflections concentrated in the equatorial direction (Figure 4.8B), suggesting the presence of preferred orientation of molecular chains. More insight at lamellar level of the polymer networks was achieved by 2D-SAXS measurements (Figures 4.8C and 4.8D). The SAXS pattern of unstretched polymer network presents no obvious scattering ring, suggesting amorphous phases or exfoliated lamellae without constant long period are formed in the polymer network. The confirmation of the crystalline phase in the polymer network by 2D-WAXD indicates that the lamellae are largely exfoliated and dispersed randomly in the polymer matrix. The scattering rings concentrate in the meridianal direction when the sample is stretched and cooled under a 0.3 MPa tensile stress, indicating the formation of an oriented lamellar structure.

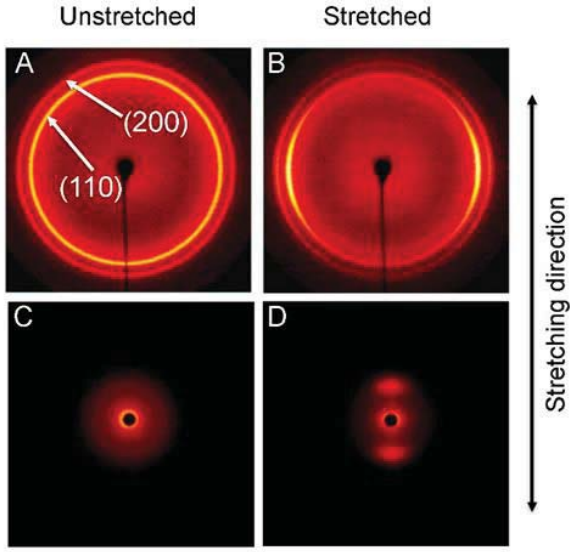

Figure 4.8 (A and B) 2D-WAXD and (C and D) 2D-SAXS patterns of polymer networks as unstretched (ε_0) and stretched after CIE under 0.3 MPa tensile stresses (ε_L). The stretching direction is vertical.

For the purpose of providing a precise evaluation of the long period (the average thickness of crystalline lamella and amorphous part), crystal structure and preferred orientation, 1D-WAXD intensity and azimuthal intensity profiles, 1D-SAXS intensity profiles as a function of the scattering vector q and the azimuthal scanning profiles are presented in Figure 4.9. In Figure 4.9A, the two diffraction peaks located at $2\theta = 21.5°$ and 23.9° are related to the (110) and (200) planes, corresponding to 4.13 Å and 3.72 Å periodicity in the polymer chain direction, respectively. It was earlier reported that the diffraction profile of PPDL is similar to the diffractogram of PCL and polyethylene.[59] These two reflection peaks are characteristic of the PCL orthorhombic and PPDL pseudo-orthorhombic[59] crystal forms. The crystal structure was not changed after stretching under 0.3 MPa stress since there is no change of angular position along 2θ. The long period of stretched polymer network can be estimated using Bragg's law ($L = 2\pi/q_{max}$) according to Figure 4.9C, which is 16.3 nm. As shown in Figures 4.9B and 4.9D, both the polymer chains and lamella level were oriented after stretching.

Combining the WAXD and SAXS results, we can deduce the microstructure evolution of 2W-SMP under stress-free condition cycle, which is illustrated in Scheme 4.1. The lamellae of unstretched sample after being subjected to a heating and cooling cycle should be exfoliated and dispersed randomly in the polymer matrix (ε_0). This sample was heated above the T_ms of both segments and deformed to a high temperature strain (ε_H) under 0.3 MPa stretching stress, resulting in the melting of crystals and oriented polymer chains. The sample was then cooled below the T_cs of both segments and unloading the external stress, leading to an elongated strain (ε_L) due to the crystallization of polymer chains along the stretching direction. The sample was heated to T_A between the distinct T_ms of two segments. At this time, PCL crystalline phase was melted and the P(CL-*co*-PDL)$_{1:2}$ crystalline phase still remained in the polymer network. The sample contracted due to the releasing of elastic energy stored in the PCL crystalline phase, leading to an intermediate shape (ε_C). Meanwhile, the P(CL-*co*-PDL)$_{1:2}$ crystalline phase was compressed, yielding an internal tensile force. Thus, when the sample was cooled below the T_c of the PCL segment, it elongated due to CIE caused by the internal tensile force of the P(CL-*co*-PDL)$_{1:2}$ crystalline phase (Figure 4.S4), yielding an elongated shape (ε_E).

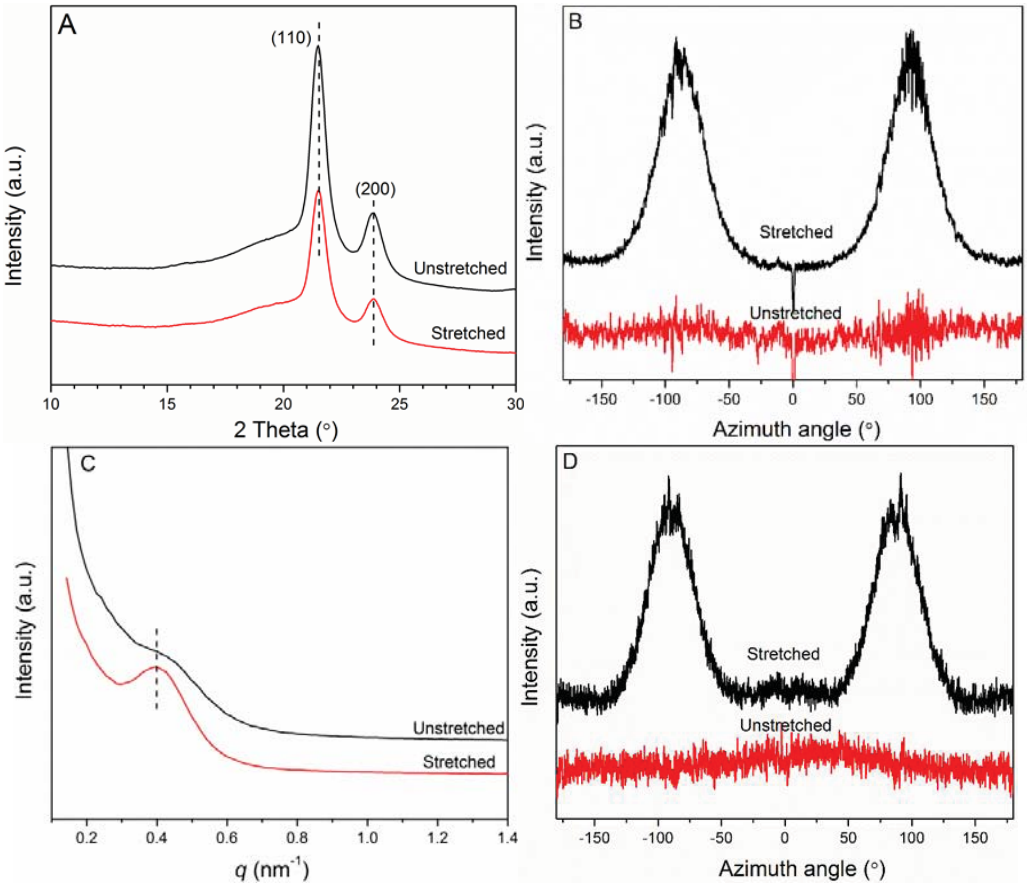

Figure 4.9 (A) 1D-WAXD intensity profiles and (B) the azimuthal profiles at (110) plane reflection from the patterns in Figures 4.8A and 4.8B; (C) the Lorentz-corrected 1D-SAXS intensity as a function of q and (D) and the azimuthal intensity profiles obtained from the patterns in Figures 4.8C and 4.8D.

Scheme 4.1 Microstructure evolution of 2W-SME under stress-free condition.

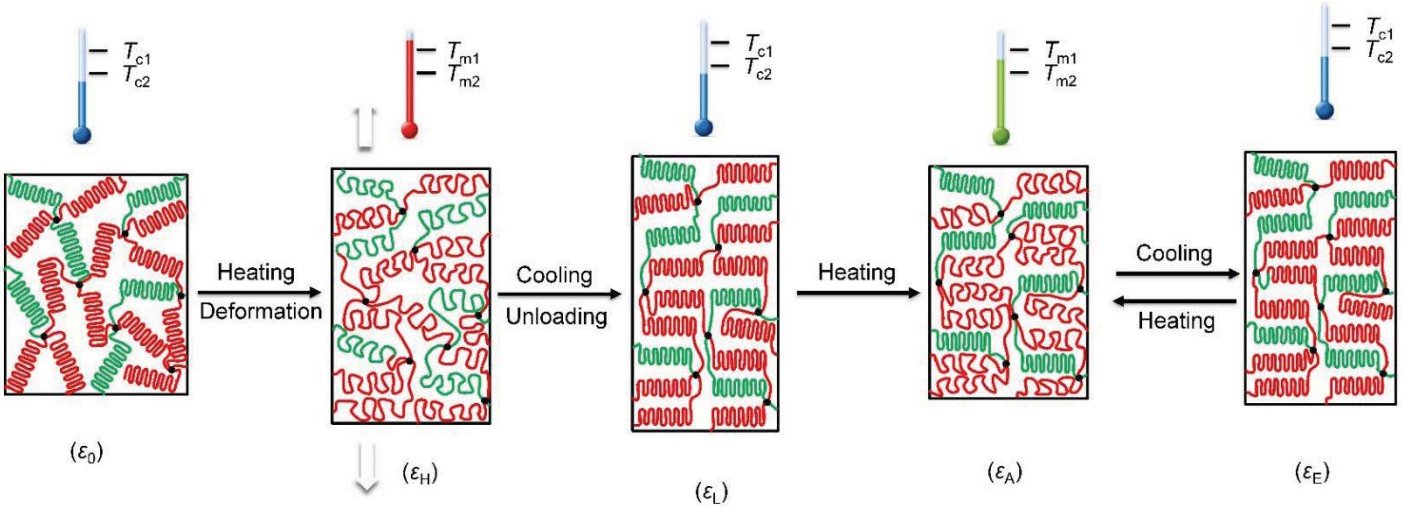

4.4 Conclusions

The use of co-crystallizable segments made of random prepolymers of CL and PDL to tune the T_A represents a novel strategy in the preparation of 2W-SMPs. The polymers can be easily synthesized via a lipase-catalyzed ROP method. The T_ms of the prepolymers may be adjusted by varying the co-monomer ratios. We have further cross-linked two prepolymers with desired T_ms through thiol-ene reactions. The T_A may be tuned by selecting two different prepolymers for the polymer network. In this case, PCL and P(CL-*co*-PDL)$_{1:2}$ were used and the cross-linked network exhibited good absolute strain change of 2W-SMEs under both stress and stress-free conditions. The materials are capable of performing reversible bending-unbending and coiling-uncoiling motions. Under stress-free conditions, the absolute strain change of the polymers also increased as in the case with stress, but the relative strain change reduced with increasing tensile stress, different from the case with stress. We have also elucidated the evolution of the microstructure of 2W-SMPs under stress-free condition cycle based on the X-ray diffraction results. This represents the first examples of easy tuning of the T_A of 2W-SMPs, making such materials more useful and more adaptable in real practical applications. These characteristics may open doors to extend the use of the polymers, especially in the biomedical field.

4.5 Acknowledgments

Financial support from NSERC of Canada and FQRNT of Quebec is gratefully acknowledged. K. Wang is grateful to the China Scholarship Council for a scholarship. The authors are members of CSACS funded by FQRNT and GRSTB funded by FRSQ. We also thank Mr. Sylvain Essiembre for technical support.

4.6 Supporting Information

Scheme 4.S1 Synthesis of the prepolymers through enzymatic polymerization.

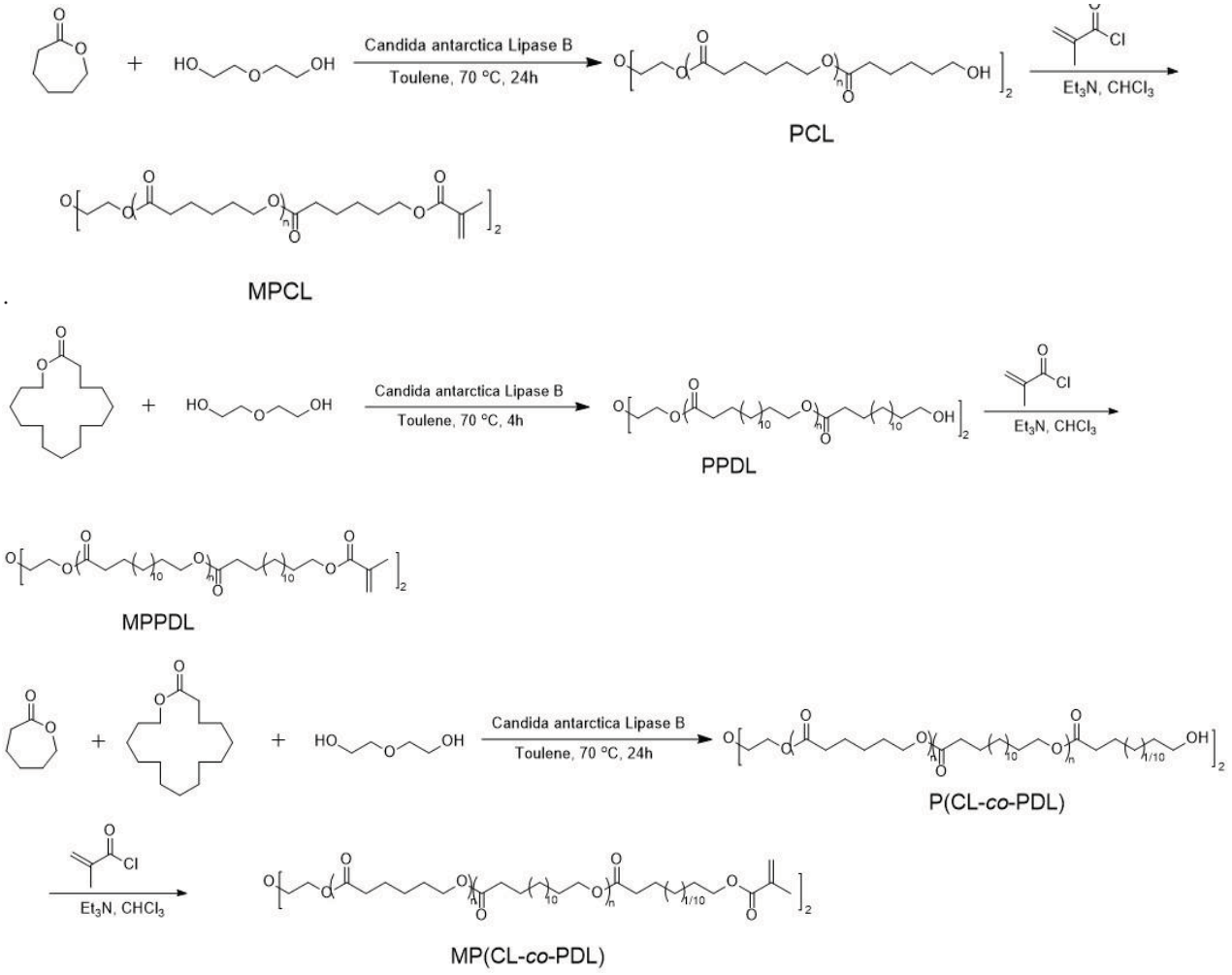

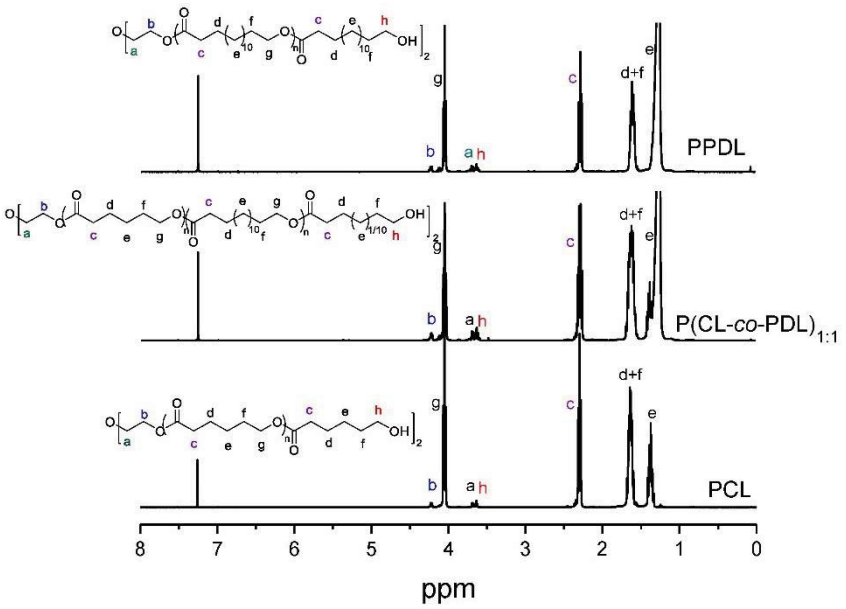

Figure 4.S1 ^{1}H NMR spectra of prepolymers. Peaks a and h cannot be separated due to their overlap.

Eqs 4.S1-S3 are used to calculate the number-average molecular weight of the prepolymers:

$$\mathrm{DP} = \frac{I_{\mathrm{c}}}{I_{\mathrm{a+h}}} \times 4 \tag{4.S1}$$

$$M_{\mathrm{n,NMR}} = \mathrm{DP} \times (M_{\mathrm{CL}} x_{\mathrm{CL}} + M_{\mathrm{PDL}} (1 - x_{\mathrm{CL}})) + M_{\mathrm{In}} \tag{4.S2}$$

$$x_{\mathrm{CL}} = \frac{10 I_{\mathrm{c}} - I_{\mathrm{e}}}{9 I_{\mathrm{c}}} \tag{4.S3}$$

where DP is the degree of polymerization of the prepolymers, I is the integration area of peak, M_{CL} and M_{PDL} indicate molecular weight of the repeating unit, CL and PDL, respectively, x_{CL} is the molar fraction of CL in the copolymer, 1- x_{CL} equals to the molar fraction of PDL, while M_{In} denotes molecular weight of initiator (diethylene glycol).

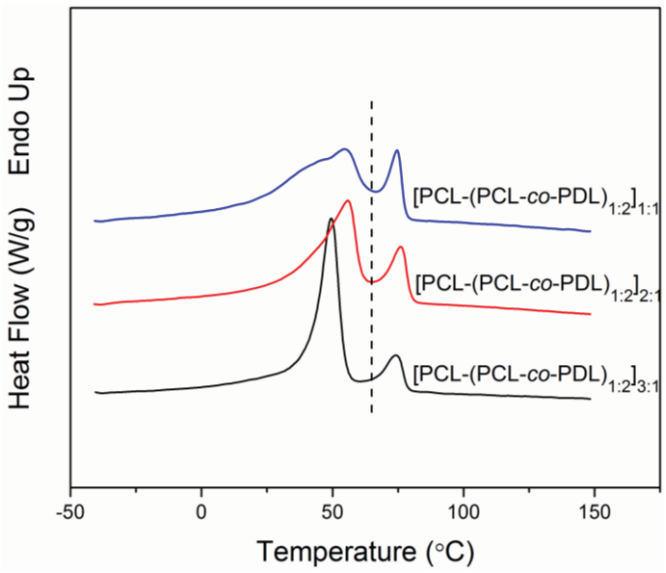

Figure 4.S2 DSC heating traces of thiol-ene cross-linked polymer networks with various weight ratios of prepolymers PCL to (PCL-*co*-PDL)$_{1:2}$.

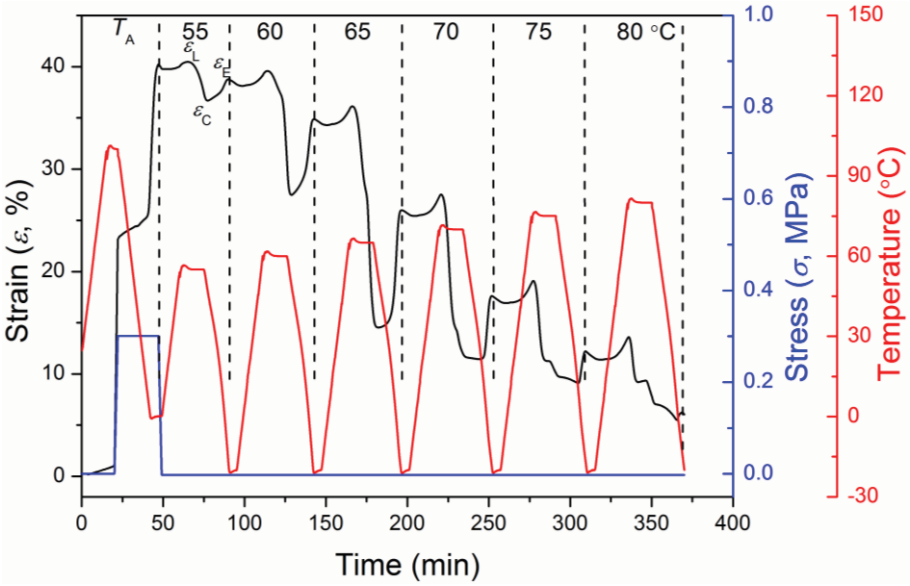

Actuation temperature (T_A, °C)	55	60	65	70	75	80
Absolute strain contraction (ε_L - ε_C, %)	3.8	12.1	21.6	16.1	10.0	8.1
Absolute strain elongation (ε_E - ε_C, %)	2.1	7.3	11.5	6.2	3.1	0.7

Figure 4.S3 2W-SME under stress-free condition at various temperatures. The largest values of both strain contraction and elongation are obtained at 65°C, which is selected as the optimal actuation temperature.

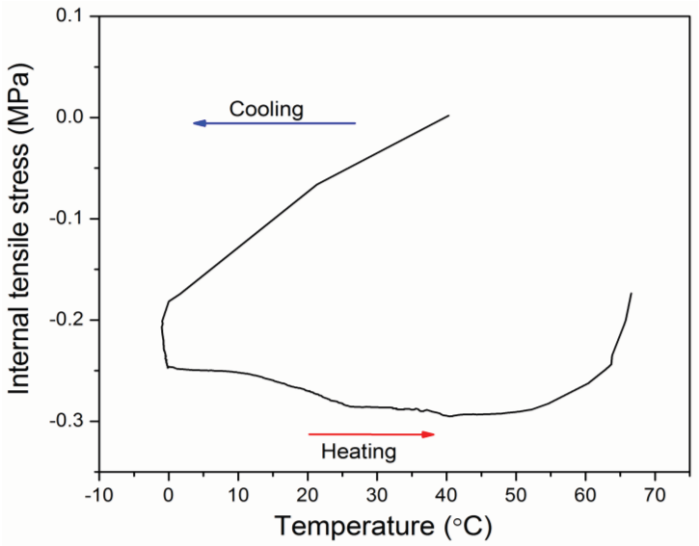

Figure 4.S4 Internal tensile stress of 2W-SME under stress-free condition for the CC_1D_2 polymer network.

4.7 References

1. Lendlein, A.; Langer, R. Biodegradable, elastic shape-memory polymers for potential biomedical applications. *Science* **2002,** 296, 1673-1676.

2. Bao, M.; Lou, X.; Zhou, Q.; Dong, W.; Yuan, H.; Zhang, Y. Electrospun biomimetic fibrous scaffold from shape memory polymer of PDLLA-co-TMC for bone tissue engineering. *ACS Appl. Mater. Interfaces* **2014,** 6, 2611-2621.

3. Wang, K.; Strandman, S.; Zhu, X. X. A mini review: Shape memory polymers for biomedical applications. *Front. Chem. Sci. Eng.* **2017,** 11, 143-153.

4. Mather, P. T.; Luo, X. F.; Rousseau, I. A. Shape memory polymer research. *Annu. Rev. Mater. Res.* **2009,** 39, 445-471.

5. Rousseau, I. A.; Mather, P. T. Shape memory effect exhibited by smectic-C liquid crystalline elastomers. *J. Am. Chem. Soc.* **2003,** 125, 15300-15301.

6. Xie, T.; Xiao, X. Self-peeling reversible dry adhesive system. *Chem. Mater.* **2008,** 20, 2866-2868.

7. Xie, T. Tunable polymer multi-shape memory effect. *Nature* **2010,** 464, 267-270.

8. Shao, Y.; Lavigueur, C.; Zhu, X. X. Multishape memory effect of norbornene-based copolymers with cholic acid pendant groups. *Macromolecules* **2012,** 45, 1924-1930.

9. Gautrot, J. E.; Zhu, X. X. Shape memory polymers based on naturally-occurring bile acids. *Macromolecules* **2009,** 42, 7324-7331.

10. Wang, K.; Jia, Y.-G.; Zhu, X. X. Biocompound-based multiple shape memory polymers reinforced by photo-cross-linking. *ACS Biomater. Sci. Eng.* **2015,** 1, 855-863.

11. Li, Z.; Zhang, X.; Wang, S.; Yang, Y.; Qin, B.; Wang, K.; Xie, T.; Wei, Y.; Ji, Y. Polydopamine coated shape memory polymer: Enabling light triggered shape recovery, light controlled shape reprogramming and surface functionalization. *Chem. Sci.* **2016,** 7, 4741-4747.

12. Xiao, H.; Lu, W.; Le, X.; Ma, C.; Li, Z.; Zheng, J.; Zhang, J.; Huang, Y.; Chen, T. A multi-responsive hydrogel with a triple shape memory effect based on reversible switches. *Chem. Commun.* **2016,** 52, 13292-13295.

13. Gu, X.; Mather, P. T. Water-triggered shape memory of multiblock thermoplastic polyurethanes (TPUs). *RSC Adv.* **2013,** 3, 15783-15971.

14. Kumpfer, J. R.; Rowan, S. J. Thermo-, photo-, and chemo-responsive shape-memory properties from photo-cross-linked metallo-supramolecular polymers. *J. Am. Chem. Soc.* **2011,** 133, 12866-12874.

15. Li, W.; Liu, Y.; Leng, J. Shape memory polymer nanocomposite with multi-stimuli response and two-way reversible shape memory behavior. *RSC Adv.* **2014,** 4, 61847-61854.

16. Lu, H.; Lu, C.; Huang, W. M.; Leng, J. Chemo-responsive shape memory effect in shape memory polyurethane triggered by inductive release of mechanical energy storage undergoing copper (II) chloride migration. *Smart Mater. Struct.* **2015**, 24, 035018.

17. Jiang, Z. C.; Xiao, Y. Y.; Kang, Y.; Pan, M.; Li, B. J.; Zhang, S. Shape memory polymers based on supramolecular interactions. *ACS Appl. Mater. Interfaces* 2017, 9, 20276-20293.

18. Lu, W.; Le, X.; Zhang, J.; Huang, Y.; Chen, T. Supramolecular shape memory hydrogels: A new bridge between stimuli-responsive polymers and supramolecular chemistry. *Chem. Soc. Rev.* 2017, 46, 1284-1294.

19. Hu, J. L.; Chen, S. J. A review of actively moving polymers in textile applications. *J. Mater. Chem.* **2010,** 20, 3346-3355.

20. Thomsen, D. L.; Keller, P.; Naciri, J.; Pink, R.; Jeon, H.; Shenoy, D.; Ratna, B. R. Liquid crystal elastomers with mechanical properties of a muscle. *Macromolecules* **2001,** 34, 5868-5875.

21. Peng, Q.; Wei, H.; Qin, Y.; Lin, Z.; Zhao, X.; Xu, F.; Leng, J.; He, X.; Cao, A.; Li, Y. Shape-memory polymer nanocomposites with a 3D conductive network for bidirectional actuation and locomotion application. *Nanoscale* **2016,** 8, 18042-18049.

22. Ge, F.; Lu, X.; Xiang, J.; Tong, X.; Zhao, Y. An optical actuator based on gold-nanoparticle-containing temperature-memory semicrystalline polymers. *Angew. Chem. Int. Ed.* **2017,** 56, 6126-6130.

23. Kolesov, I.; Dolynchuk, O.; Jehnichen, D.; Reuter, U.; Stamm, M.; Radusch, H. J. Changes of crystal structure and morphology during two-way shape-memory cycles in cross-linked linear and short-chain branched polyethylenes. *Macromolecules* **2015,** 48, 4438-4450.

24. Huang, M.; Dong, X.; Wang, L.; Zhao, J.; Liu, G.; Wang, D. Two-way shape memory property and its structural origin of cross-linked poly(ε-caprolactone). *RSC Adv.* **2014,** 4, 55483-55494.

25. Baker, R. M.; Henderson, J. H.; Mather, P. T. Shape memory poly(ε-caprolactone)-co-poly(ethylene glycol) foams with body temperature triggering and two-way sctuation. *J. Mater. Chem. B* **2013,** 1, 4916-4920.

26. Qin, H.; Mather, P. T. Combined one-way and two-way shape memory in a glass-forming nematic network. *Macromolecules* **2009,** 42, 273-280.

27. Zotzmann, J.; Behl, M.; Hofmann, D.; Lendlein, A. Reversible triple-shape effect of polymer networks containing polypentadecalactone- and poly(ε-caprolactone)-segments. *Adv. Mater.* **2010,** 22, 3424-3429.

28. Bai, Y. K.; Zhang, X. R.; Wang, Q. H.; Wang, T. M. A tough shape memory polymer with triple-shape memory and two-way shape memory properties. *J. Mater. Chem. A* **2014,** 2, 4771-4778.

29. Chung, T.; Rorno-Uribe, A.; Mather, P. T. Two-way reversible shape memory in a semicrystalline network. *Macromolecules* **2008,** 41, 184-192.

30. Burke, K. A.; Rousseau, I. A.; Mather, P. T. Reversible actuation in main-chain liquid crystalline elastomers with varying crosslink densities. *Polymer* **2014,** 55, 5897-5907.

31. Torbati, A. H.; Mather, P. T. A Hydrogel-forming liquid crystalline elastomer exhibiting soft shape memory. *J. Polym. Sci., Part B: Polym. Phys.* **2016,** 54, 38-52.

32. Imai, S.; Sakurai, K. An actuator of two-way behavior by using two kinds of shape memory polymers with different T_gs. *Precis. Eng.* **2013,** 37, 572-579.

33. Kang, T.-H.; Lee, J.-M.; Yu, W.-R.; Youk, J. H.; Ryu, H. W. Two-way actuation behavior of shape memory polymer/elastomer core/shell composites. *Smart Mater. Struct.* **2012,** 21, 035028.

34. Taya, M.; Liang, Y.; Namli, O. C.; Tamagawa, H.; Howie, T. Design of two-way reversible bending actuator based on a shape memory alloy/shape memory polymer composite. *Smart Mater. Struct.* **2013,** 22, 105003.

35. Behl, M.; Kratz, K.; Zotzmann, J.; Nochel, U.; Lendlein, A. Reversible bidirectional shape-memory polymers. *Adv. Mater.* **2013,** 25, 4466-4469.

36. Zhou, J.; Turner, S. A.; Brosnan, S. M.; Li, Q.; Carrillo, J.-M. Y.; Nykypanchuk, D.; Gang, O.; Ashby, V. S.; Dobrynin, A. V.; Sheiko, S. S. Shapeshifting: Reversible shape memory in semicrystalline elastomers. *Macromolecules* **2014,** 47, 1768-1776.

37. Gong, T.; Zhao, K.; Wang, W.; Chen, H.; Wang, L.; Zhou, S. Thermally activated reversible shape switch of polymer particles. *J. Mater. Chem. B* **2014,** 2, 6855-6866.

38. Qian, C.; Dong, Y.; Zhu, Y.; Fu, Y. Two-way shape memory behavior of semi-crystalline elastomer under stress-free condition. *Smart Mater. Struct.* **2016,** 25, 085023.

39. Wu, Y.; Hu, J.; Han, J.; Zhu, Y.; Huang, H.; Li, J.; Tang, B. Two-way shape memory polymer with "switch–spring" composition by interpenetrating polymer network. *J. Mater. Chem. A* **2014,** 2, 18816-18822.

40. Wang, L.; Liu, W.; Guo, L.-X.; Lin, B.-P.; Zhang, X.-Q.; Sun, Y.; Yang, H. A Room-temperature two-Stage thiol–ene photoaddition approach towards monodomain liquid crystalline elastomers. *Polym. Chem.* **2017,** 8, 1364-1370.

41. Meng, Y.; Jiang, J.; Anthamatten, M. Shape actuation via internal stress-induced crystallization of dual-cure networks. *ACS Macro Lett.* **2015,** 4, 115-118.

42. Gao, Y.; Liu, W.; Zhu, S. Polyolefin thermoplastics for multiple shape and reversible shape memory. *ACS Appl. Mater. Interfaces* **2017,** 9, 4882-4889.

43. Lu, L.; Li, G. One-way multishape-memory effect and tunable two-way shape memory effect of ionomer poly(ethylene-co-methacrylic acid). *ACS Appl. Mater. Interfaces* **2016,** 8, 14812-14823.

44. Biswas, A.; Aswal, V. K.; Sastry, P. U.; Rana, D.; Maiti, P. Reversible bidirectional shape memory effect in polyurethanes through molecular flipping. *Macromolecules* **2016,** 49, 4889-4897.

45. Alamo, R. G.; Glaser, R. H.; Mandelkern, L. The cocrystallization of polymers: Polyethylene and its copolymers. *J. Polym. Sci., Part B: Polym. Phys.* **1988,** 26, 2169-2195.

46. Yoo, H. Co-crystallization behaviour and melting-point depression in poly(ethylene terephthalate-co-1,4-cyclohexylene dimethylene terephthalate) random copolyesters. *Polymer* **1994,** 35, 117-122.

47. Lu, X. Crystallization of random copolymers of poly(ethylene terephthalate) and poly(ethylene naphthalene-2,6-dicarboxylate). *Polymer* **1995,** 36, 451-459.

48. Kamiya, N.; Sakurai, M.; Inoue, Y.; Chujo, R. Isomorphic behavior of random copolymers: Thermodynamic analysis of cocrystallization of poly(3-hydroxybutyrate-co-3-hydroxyvalerate). *Macromolecules* **1991,** 24, 3888-3892.

49. Kumar, A.; Kalra, B.; Dekhterman, A.; Gross, R. A. Efficient ring-opening polymerization and copolymerization of ε-caprolactone and ω-pentadecalactone catalyzed by candida antartica lipase B. *Macromolecules* **2000,** 33, 6303-6309.

50. Strandman, S.; Tsai, I. H.; Lortie, R.; Zhu, X. X. Ring-opening polymerization of bile acid macrocycles by candida antarctica lipase B. *Polym. Chem.* **2013,** 4, 4312-4316.

51. Champagne, É.; Lévaray, N.; Zhu, X. X. Two-step enzymatic synthesis of biocompatible polymers made from cholic acid. *ACS Sustainable Chem. Eng.* **2017,** 5, 689-695.

52. Champagne, E.; Strandman, S.; Zhu, X. X. Recent developments and optimization of lipase-catalyzed lactone formation and ring-opening polymerization. *Macromol. Rapid Commun.* **2016,** 37, 1986-2004.

53. Ceccorulli, G.; Scandola, M.; Kumar, A.; Kalra, B.; Gross, R. A. Cocrystallization of random copolymers of ω-pentadecalactone and ε-caprolactone synthesized by lipase catalysis. *Biomacromolecules* **2005,** 6, 902-907.

54. Kobayashi, S.; Kaku, M.; Mizutani, T.; Saegusa, T. Preparation of ring-opening polymerizable macromer and its copolymerization leading to graft copolymer. *Polym. Bull.* **1983,** 9, 169-173.

55. Khonakdar, H. A.; Morshedian, J.; Wagenknecht, U.; Jafari, S. H. An investigation of chemical crosslinking effect on properties of high-density polyethylene. *Polymer* **2003,** 44, 4301-4309.

56. Li, J.; Rodgers, W. R.; Xie, T. Semi-crystalline two-way shape memory elastomer. *Polymer* **2011,** 52, 5320-5325.

57. Lu, H.; Wang, X.; Yu, K.; Huang, W. M.; Yao, Y.; Leng, J. A phenomenological formulation for the shape/temperature memory effect in amorphous polymers with multi-stress components. *Smart Mater. Struct.* **2017,** 26, 095011.

58. Ma, L.; Zhao, J.; Wang, X.; Chen, M.; Liang, Y.; Wang, Z.; Yu, Z.; Hedden, R. C. Effects of carbon black nanoparticles on two-way reversible shape memory in crosslinked polyethylene. *Polymer* **2015,** 56, 490-497.

59. Gazzano, M.; Malta, V.; Focarete, M. L.; Scandola, M.; Gross, R. A. Crystal structure of poly(ω-pentadecalactone). *J. Polym. Sci., Part B: Polym. Phys.* **2003,** 41, 1009-1013.

Chapter 5

Two-way reversible shape memory polymers containing polydopamine nanospheres: Light actuation and robotic locomotion*

Abstract

Two-way reversible shape memory polymers (2W-SMPs), especially those that are light-responsive, are highly desirable for many applications due to the convenience of indirect heating. We have designed and prepared a series of light-actuated 2W-SMP composites by incorporating very small amounts of polydopamine (PDA) nanospheres into semi-crystalline polymer networks based on poly(ε-caprolactone) copolymers. PDA nanospheres can be well dispersed in chloroform and well mixed with the polymer network. PDA nanospheres manifest good photothermal effect due to their strong absorption of light. The variation of temperature of the polymer composites can be correlated with irradiation time, light intensity, and the content of PDA nanospheres. These polymer composites show excellent two-way reversible shape memory effects (2W-SMEs) under stress-free condition when the light is switched on and off showing a reversible angle change of 45º. The speed of angle change is larger for polymer composites irradiated with a stronger light or with a higher content of PDA nanospheres. A moving robot is designed based on photo-responsive 2W-SMP composites, which can walk on a track with triangular saw-teeth. It is the first report on the incorporation of PDA nanospheres into SMPs as photothermal fillers.

---

*Wang, K.; Zhu, X. X. Submitted to *J. Mater. Chem. B.* for publication.

5.1 Introduction

Shape memory polymers (SMPs) are smart materials that can recover its permanent shape in a predefined way responding to external stimuli, such as changes in temperature,[1, 2] light,[3-5] electric current,[6] magnetic field,[7] microwave,[8] ultrasound,[9] solvent,[10] and pH.[11-13] They have drawn much research attention in the past decades due to their potential applications in biomedicine,[14-16] aerospace[17, 18] and as actuators,[19] sensors,[20, 21] smart textiles,[22] and self-peeling dry adhesives.[23] For most of the shape memory polymers, their permanent shapes cannot reverse to the temporary shapes without external programming. Two-way reversible shape memory polymers (2W-SMPs) are capable of automatically changing between two disparate memorized shapes when exposed to two of the same or different external stimuli, such as heating and cooling,[24] where the heating can be induced by light,[25, 26] electric current,[27] and magnetic field.[28] Such polymers have potential applications as actuators, artificial muscles and self-locomotion robotics.[27, 29, 30]

Two-way reversible shape memory effects (2W-SMEs) can be realized under stress or stress-free conditions, for which the two shapes switch back and forth in the presence or absence of the external stress. To date, most investigations were focused on direct heating of the materials, which is inconvenient in applications. Indirect heating, especially under stress-free condition, is more interesting and versatile, but reports on such materials are scarce.[25-27] The key in the design of 2W-SMPs responsive to indirect heating is the incorporation of functional fillers into the polymers, which can convert different forms of energy into heat when exposed to an external stimulus.

Dopamine (DA) is a natural compound present in the body of most animals and in plants and has good biocompatibility and biodegradability.[31] Polydopamine (PDA) obtained by the oxidative self-polymerization of dopamine has been studied for cancer therapy and shape recovery of hydrogels due to its excellent photothermal effect.[31-34] Recently, we have reported on the design and synthesis of polymer networks of co-crystallizable copolymers for which the co-crystallization of the polymer segments can lead to two-way reversible shape memory effect.[35] In this work, we demonstrate the use of such polymers in useful devices by the addition of PDA nanospheres with strong photothermal effect which lead to the design and making of light-actuated microrobot that can be indirectly heated efficiently to exhibit

locomotion. To the best of our knowledge, this is the first report on the incorporation of PDA nanospheres into 2W-SMPs as photothermal fillers for converting light energy to heat. The use of PDA particles is advantageous due to the natural origin of the starting material, low cost and simple preparation of the microparticles in addition to their efficient photothermal effect.

5.2 Experimental section

5.2.1 Materials

Di(ethylene glycol) (99%), ε-caprolactone (CL, 97%), ω-pentadecalactone (PDL, ≥ 98%), methacryloyl chloride (≥ 97%), triethylamine (TEA, ≥ 99.5%), pentaerythritol tetrakis(3-mercaptopropionate) (> 95%), 2,2-dimethoxy-2-phenylacetophenone (DMPA, > 99%) dopamine hydrochloride (98%), aqueous ammonia solution ($NH_3 \cdot H_2O$, 28−30%), and Candida antarctica lipase B (CALB) immobilized on acrylic resin were purchased from Sigma-Aldrich. CL was first dried over calcium hydride and distilled under reduced pressure. PDL was dried in a vacuum oven for 48 h at room temperature. Dichloromethane (DCM) and toluene were dried on a solvent purification system from Glass Contour. Ethanol, chloroform, and methanol were used as received.

5.2.2 Synthesis and preparation

The prepolymers and methacrylate-terminated prepolymers were synthesized as reported previously.[35] PDA nanospheres were synthesized according to a published method.[32] Briefly, 2 mL of an aqueous ammonia solution ($NH_3 \cdot H_2O$, 28−30%), 90 mL of deionized water, and 40 mL of ethanol were mixed together and stirred for 30 min at room temperature. Dopamine hydrochloride (0.5 g in 10 mL deionized water) was injected into this solution, and stirred for 24 h. Then the solution was centrifugated and washed twice with deionized water and once with ethanol. The obtained dark blown powder was dried under vacuum at room temperature for 24 h.

A representative procedure for the preparation of polymer composites is described here. PDA nanospheres stock dispersion (1.0 mg/mL) was prepared by dispersing PDA nanospheres in the powder form in chloroform and sonicating for 20 min. The methacrylate-terminated prepolymers (0.267 g PCL and 0.133 g (PCL-*co*-PDL)$_{1:1}$) and the cross-linker, pentaerythritol

tetrakis(3-mercaptopropionate) (1.2 eq.), were mixed in a dry vial. 0.40 mL chloroform, 0.2 mL PDA nanospheres stock dispersion, and 4 mg DMPA were added into mixture. The vial was vortexed for 5 min. The mixture was poured into a Teflon mold (2.0 cm × 2.0 cm), exposed to a UV light of 365 nm (20 mW/cm^2) with 5 cm irradiation distance for 1.5 h, and then placed in a fume hood for 3 days. The film was then removed from the mold. The structure of the polymer network is shown in Figure 5.1A. Polymer composites were prepared from PCL and P(CL-*co*-PDL)$_{1:1}$ prepolymers (2:1 weight ratio) containing PDA nanospheres of weight percentages ranging from 0.025 to 0.15 wt%. Such polymer composites are denoted as PDA$_x$ where the subscript x indicates the weight percentage of the PDA nanospheres in the composite. To study the light responsiveness of the 2W-SMPs, the samples were prepared by solution casting of a film of the polymer network alone or the polymer composites in chloroform. The films were sliced into samples of 0.5 × 3.5 × 20 mm in dimension which was bent after heating to 90 °C in water bath. The films are not uniform in thickness on a larger scale but have an average value of ca. 0.5 mm. To measure the temperature in the study of the photothermal effect, a small thermocouple was imbedded in the polymer composites during the solution casting of the film, with a depth ca. 0.4 mm from the top surface of the film.

5.2.3 Polymer characterization

The polymer composites were irradiated using a lamp (Kerr Demetron Optilux 500) with a filter excitation wavelength of 400-500 nm; its intensity was measured by the lamp's integrated radiometer. UV-Visible spectra of PDA nanospheres were obtained on a Cary 500 UV-Vis spectrophotometer (Agilent Technologies). Fourier transform infrared (FTIR) spectra was obtained on a Perkin-Elmer Spectrum One FTIR spectrometer with a universal ATR (attenuated total reflectance) mode, with 32 scans in the range of 500 – 4000 cm^{-1} at a 4 cm^{-1} resolution. Differential scanning calorimetry (DSC) measurements were carried out on a DSC 2910 (TA Instruments) at a heating rate of 10 °C/min. The temperature and heat flow were calibrated with indium before measurements. The dispersion of the PDA nanospheres in chloroform was confirmed by transmission electron microscopy (TEM) on a FEI Tecnai 12 TEM at 80 kV, equipped with an AMT XR80C CCD camera system.

5.3 Results and discussion

5.3.1 Preparation of PDA nanospheres

PDA nanospheres were synthesized via simple self-polymerization as shown in Figure 5.1B. They can be well dispersed in $CHCl_3$ and polymer matrix and their spherical shape is confirmed by the TEM images with an average diameter of ~260 nm (Figure 5.1B and 5.S2). The UV-Vis absorption spectra of the polymer composites with PDA nanospheres are shown in Figure 5.2 in comparison with PDA nanospheres in $CHCl_3$. The pure polymer network shows low absorption and remains almost constant throughout the wavelength range. The polymer composites show stronger absorption when the wavelength of light is below 400 nm, probably due to the light scattering of the solid film.[36] The absorption becomes increasingly stronger with a higher content of PDA nanospheres. Based on this observation, a light of wavelength from 400 to 500 nm was used to irradiate the sample.

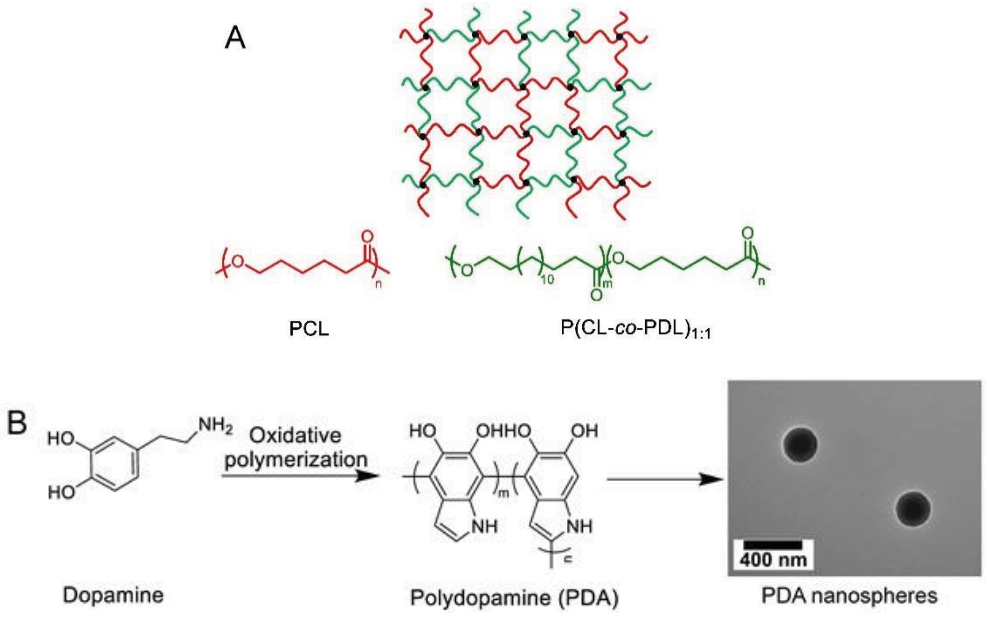

Figure 5.1 (A) The structure of the pure polymer network based on PCL and P(CL-*co*-PDL)$_{1:1}$; (B) Synthesis of the PDA nanospheres and the TEM image of the PDA nanospheres dispersed in $CHCl_3$.

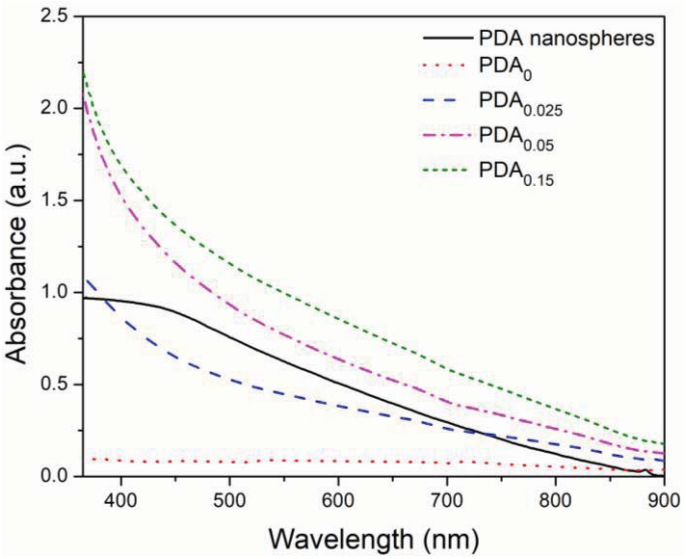

Figure 5.2 UV-Vis spectra of PDA nanospheres suspended in $CHCl_3$ (0.3 mg/mL), and of polymer composite films (average thickness ca. 0.5 mm) based on cross-linked PCL and P(CL-*co*-PDL)$_{1:1}$ (2:1 weight ratio) with various weight percentages of PDA nanospheres.

Despite the variation in the content of PDA nanospheres, all polymer composites have similar melting and crystallization temperatures and enthalpy changes for each of the two segments (Figures 5.3A&B and Table 5.S1). The pure polymer network has similar thermal properties, but the melting and crystalline enthalpies for the P(CL-*co*-PDL)$_{1:1}$ segment are about 3 times as much as those of the polymer composites, indicating that the presence of PDA nanospheres may inhibit the crystallization of the random copolymer segment with no obvious effect on the homopolymer PCL segment. The melting of the PCL segment ranges from 15 to 50 °C, while that of the P(CL-*co*-PDL)$_{1:1}$ segment from 65 to 80 °C. Therefore, the actuation temperature (T_A) was selected in between the T_ms of the two polymers (50 to 65 °C). The ATR-FTIR spectra of the PDA nanospherers (Figure 5.3C) show the characteristic peaks of dopamine at 1608, 1499, and 1285 cm^{-1}, assigned to the bending vibration of N–H and C=C, and the stretching vibration of C=N, respectively.[37] The broad absorption peak in the range of 2360 to 3680 cm^{-1} centered at around 3270 cm^{-1} is ascribed to the stretching vibrations of hydrogen-bonded OH and NH groups in the PDA nanospheres.[38] The broad band at 940-1800 cm^{-1} with no distinguishable peaks is attributed to the highly complex structure of polydopamine. The polymer network without added PDA particles shows a very weak absorption peak of at around 3400 cm^{-1}, almost unobservable, probably due to the presence of

residual OH groups or residual moisture. The polymer composites, however, show a broad absorption peak at around 3400 cm^{-1}; its intensity rises with increasing content of PDA nanospheres, indicating the formation of extensive hydrogen bonds between PDA and the polyester network, particularly strong at higher contents of PDA nanoparticles. The peaks at 2918, 2850, and 1730 cm^{-1} are ascribed to asymmetric stretching of CH_2, symmetric stretching of CH_2, and stretching vibration of C=O of the polyester network, respectively.[39]

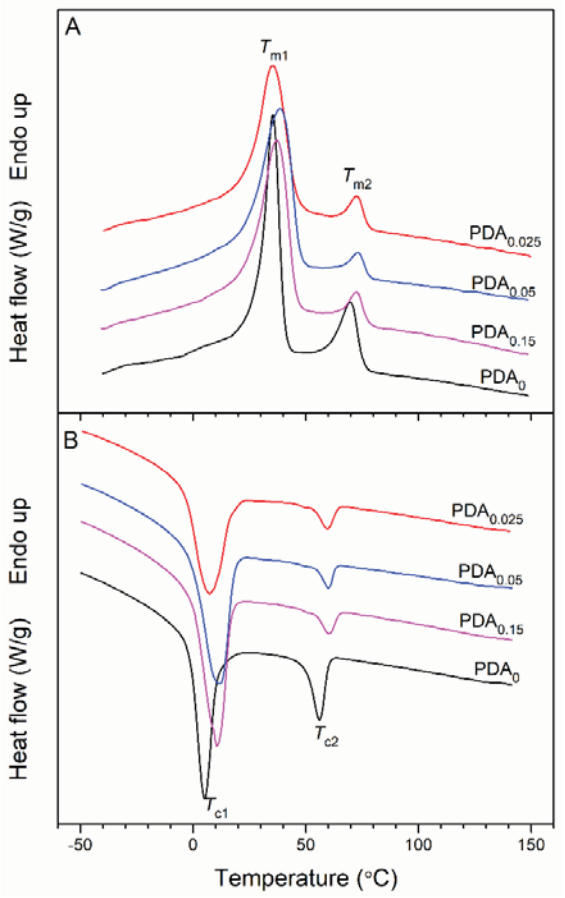

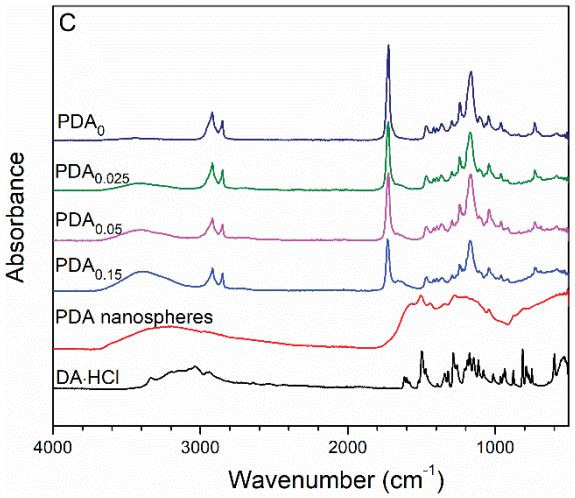

Figure 5.3 (A) DSC heating and (B) cooling curves of polymer composites based on cross-linked PCL and P(CL-*co*-PDL)$_{1:1}$ (2:1 weight ratio) with various weight percentages of PDA nanospheres showing the melting and the crystallization of the PCL segment (T_{m1}, T_{c1}) and of the P(CL-*co*-PDL)$_{1:1}$ segment (T_{m2}, T_{c2}), respectively. (C) FTIR spectra of the same polymer composites with various contents of PDA nanospheres.

5.3.2 Photothermal effects of the polymer composites

To confirm the photothermal effect of PDA nanospheres, the temperature change as a function of irradiation time was measured (Figure 5.4). Figures 5.4A&B show the effect of the content of PDA nanospheres at a fixed light intensity (350 mW/cm^2) and that of the light intensity at a fixed content of PDA nanospheres (0.025 wt%), respectively. The temperature of polymer composite increases quickly and then starts to level off at a longer irradiation time. The sample with a higher content of PDA nanospheres also has a faster temperature increase and a higher maximum temperature. The maximum temperature of the pure polymer film is much lower at ca. 20 °C due to its weak photothermal effect. When the light is turned off, the temperature first decreases quickly and then gradually approaches the original ambient temperature. When the samples are irradiated with a stronger light intensity, the temperature rises faster and reaches a higher maximum temperature (Figure 5.4B). The angle change of the shaped material (Figures 5.5 and 5.6) seemed to be faster than the rate of temperature change indicated in Figure 5.4, probably due to the relatively low thermal conductivity of the polymer film and the distance between the surface of the film and the inserted thermocouple.

To further explain the photothermal effect, the rise and fall of the temperature shown in Figure 5.4 are fit to eqs (5.1) and (5.2), respectively, in analogy to previous reports on light-to-heat conversion of gold nanoparticles and on microwave-to-heat conversion of iron oxide nanoparticles, respectively:[40,41]

$$T = T_0 + A\,(1 - \exp(-k\,t)) \tag{5.1}$$

$$T = T_0 + (T_{max} - T_0)\ \exp(-k(t - t_{max})) \tag{5.2}$$

where T is the temperature of the sample, T_0 denotes the ambient temperature, T_{max} and t_{max} are the maximum temperature and the time at which the light is switched off, A indicates the maximum temperature that can be reached with light irradiation and is related to the content of PDA nanospheres and the light intensity, and k is a constant related to heat loss of the sample. All values of A and k are listed in the Table 5.1. The samples with higher contents of PDA nanospheres and/or shone with a higher light intensity have a higher value of A, which is in fact a variable increasing in value with PDA content and light intensity. The value of k decreases after the incorporation of PDA nanospheres into polymer matrix, and it is almost constant for all the samples with various contents of PDA nanospheres and irradiated with various light intensities. The lower photothermal effect for the pure polymer network leads to a lower A and a higher k. The k values for both the temperature rising and falling curves are almost same. Thus, the average value of k (0.029) is characteristic for the polymer-PDA nanospheres binary system (the composites), which was then used to fit the temperature rising and falling curves again (dots in Figure 5.4). The new A^* values are almost same as A values obtained from the original fits. The theoretical maximum temperature ($T_{max,theo}$, when $t \rightarrow \infty$) is the sum of T_0 and A (Table 5.1) when the average value of k is substituted into eq 5.1. The time needed to reach 98% of $T_{max,theo}$ is calculated to be approximately 135 s (i.e. $1 - \exp(-k\,t) = 0.98$). The small deviation from the experimental t_{max} may be due to experimental error combined with subjective observation and judgment of T_{max}.

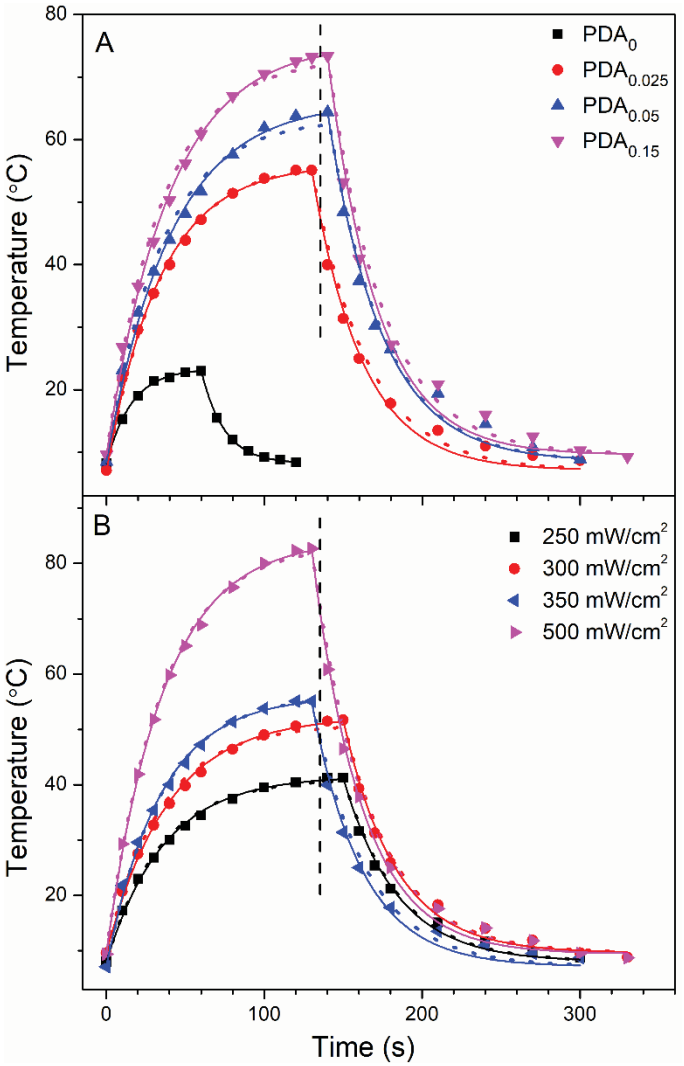

Figure 5.4 Temperature changes with time while the light was turned on and off. (A) Polymer composites based on cross-linked PCL and P(CL-*co*-PDL)$_{1:1}$ (2:1 weight ratio) with various contents of PDA nanospheres (thermocouple embedded at ca. 0.4 mm in depth from the surface of the films) at a constant light intensity of 350 mW/cm^2; (B) The same polymer composite film with 0.025 wt% PDA nanospheres irradiated with light of various intensities. The light is switched on at 0 s and switched off at the maximum temperature. The left part of the solid curves (rising temperature) is fit to eq 1 and the right part (falling temperature) is fit to eq 2. The curves fitted with the average k value (k = 0.029 s^{-1}) with the same equations are shown by the dotted lines. The vertical dashes indicate the theoretical time at which 98% of $T_{max,theo}$ is reached.

Table 5.1 The values of *A* and *k* obtained from the fits to Equation 5.1 and 5.2.

Parameters	Samples[a]				Light intensity[b] (mW/cm^2)			
	PDA_0	$PDA_{0.025}$	$PDA_{0.05}$	$PDA_{0.15}$	250	300	350	500
A (°C)	15.2	49.0	57.6	65.9	33.6	42.7	49.0	74.9
*A** (°C)[c]	-	49.2	54.9	63.5	33.1	41.3	49.1	74.0
T_{max}	23.0	55.1	64.4	73.4	41.3	52.3	55.1	82.7
$T_{max,theo}$	23.4	56.1	66.1	75.5	41.6	51.7	56.1	84.5
Temperature rising curve								
k (s^{-1})	0.063	0.029	0.025	0.025	0.027	0.026	0.029	0.028
Temperature falling curve								
k (s^{-1})	0.068	0.032	0.029	0.032	0.030	0.030	0.032	0.032

[a]Polymer composites based on cross-linked PCL and $P(CL\text{-}co\text{-}PDL)_{1:1}$ (2:1 weight ratio) with various contents of PDA nanospheres at a constant light intensity of 350 mW/cm^2. [b]The same polymer composites with 0.025 wt% PDA nanospheres irradiated with light of various intensities. The average of *k* is 0.029 s^{-1}. [c]*A* values obtained when the average *k* value (0.029 s^{-1}) is used to fit the lines.

5.3.3 2W-SME responsive to light on and off

All light-actuated 2W-SME experiments were done in a cold room set at around 7 °C, close to the crystallization temperature of PCL segment of polymer network. Figure 5.5 shows the angle changes of 2W-SME under stress-free condition when the light was turned on and off. The sample was first programmed to a "V" shape in 90 ºC water bath. The short arm was fixed on a clamp. The original angle of the sample was set at 70º. The temperature rose when the light was turned on, and the sample started to open to a wider angle, reaching 90º and 115º after 9 and 18 s, respectively. The light was then turned off, the sample started to close to a smaller angle with the fall of the temperature, reaching 90º at 35 s and 70º after 83 s.

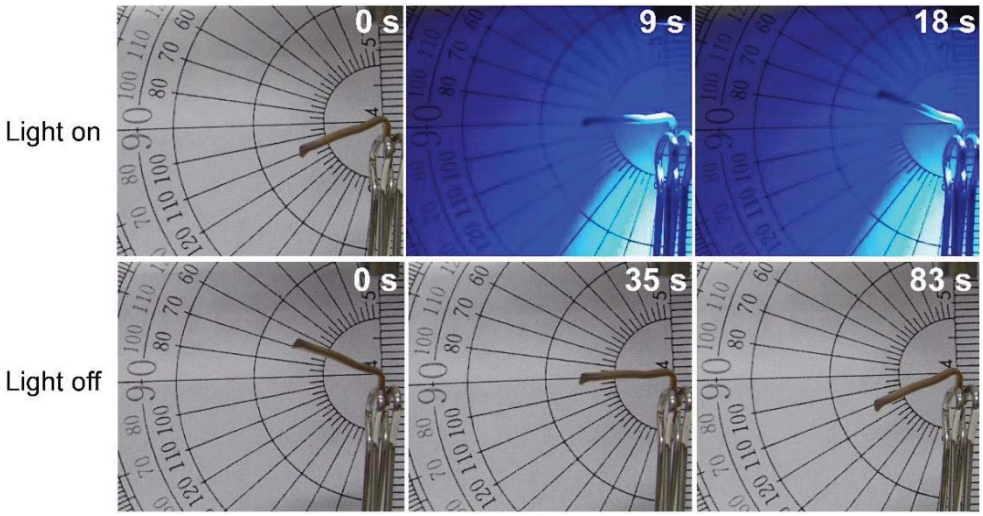

Figure 5.5 Images showing the angle change with time for a sample of polymer composite based on cross-linked PCL and P(CL-*co*-PDL)$_{1:1}$ (2:1 weight ratio) with 0.15 wt% PDA nanospheres when the light is turned on and off. Light intensity: 350 mW/cm^2.

The actuation temperature may be optimized to achieve the best reversible angle change. In this work, an optimal angle change magnitude of 45º was selected due to its better reversibility. If the angle opening is too large, the sample cannot bend back completely to its original position (Figure 5.S3). Figure 5.6A shows the angle change of the sample with various contents of PDA nanospheres as a function of the irradiation time with a constant light intensity of 350 mW/cm^2. The sample with a higher content of PDA nanospheres had a better and faster energy conversion from light to heat and showed a faster angle changes for opening actions of the device. The angle closing for all samples followed a similar trend. For a sample with the same content of PDA nanospheres (Figure 5.6B), the speed of angle opening increased as the light intensity increased from 250 to 500 mW/cm^2. At a lower light intensity of 250 mW/cm^2, the conversion to heat is not enough to melt all the PCL crystals since the temperature reached only 41 °C (still in the melting range of PCL segment) after 150 s of irradiation (Figure 5.4B), the angle opening only reached 107°. Heat loss may have become an issue when the sample was not heated adequately.

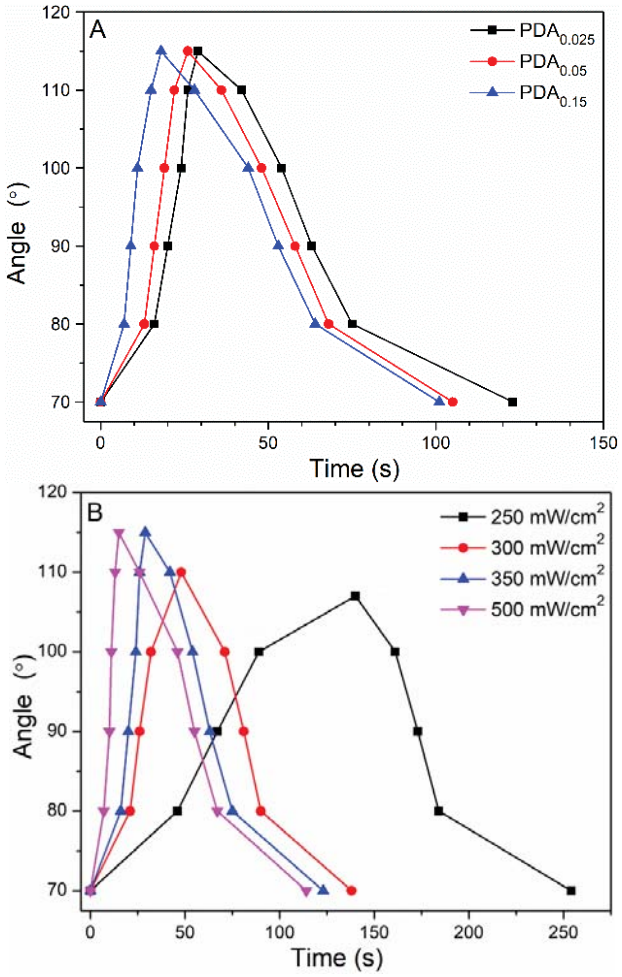

Figure 5.6 (A) Angle change of the samples of polymer composite based on cross-linked PCL and P(CL-*co*-PDL)$_{1:1}$ (2:1 weight ratio) with different contents of PDA nanospheres irradiated by a fixed light intensity of 350 mW/cm^2; (B) Angle change of the same polymer composite with 0.025 wt% PDA nanospheres irradiated by various light intensities. The light was turned on at 0 s and turned off at the peak maxima.

5.3.4 A micro-robot with self-locomotion capability

The photo-responsive 2W-SMPs may have numerous potential applications because of their reversible movement. To illustrate a possible use of the 2W-SMPs, we designed a micro-robot from a sample of polymer composite based on cross-linked PCL and P(CL-*co*-PDL)$_{1:1}$ (2:1 weight ratio) with 0.15 wt% PDA nanocomposites and showed its self-locomotion ability (Figure 5.7A). First, a track with right triangle sawtooth was prepared by three-dimensional (3D) printing. The length of the horizontal side of right triangle was designed to be 0.35 mm.

An arch-shaped SMP sample was prepared with a small bent hook in the front leg by placing the material in water bath at 90 °C, and then in 0 °C water bath to fix this shape. Firstly, the sample was positioned on the track and then irradiated by blue light; the angle opening behavior led to the movement of the front leg forward while the rear leg, trapped by the sawtooth, remained at the same position. Secondly, when the light was turned off, the front leg was hooked by the sawtooth, and the rear leg moved forward due to angle closing upon cooling of the device. The movement was repeated by turning the light on and off. Figure 5.7A illustrates the experimental results. The robot moved forward 8 steps (around 2.7 cm) in 11 min. Obviously, the speed of the movement was affected by the open-close switching speed of the angle. The speed may be controlled by adjusting the content of PDA nanospheres and/or the light intensity of irradiation; the speed of angle closing may also be adjusted by varying the difference between the crystallization temperature of the actuation segment and the ambient temperature. The mechanism of this micro-robot is illustrated in Figure 5.7B.

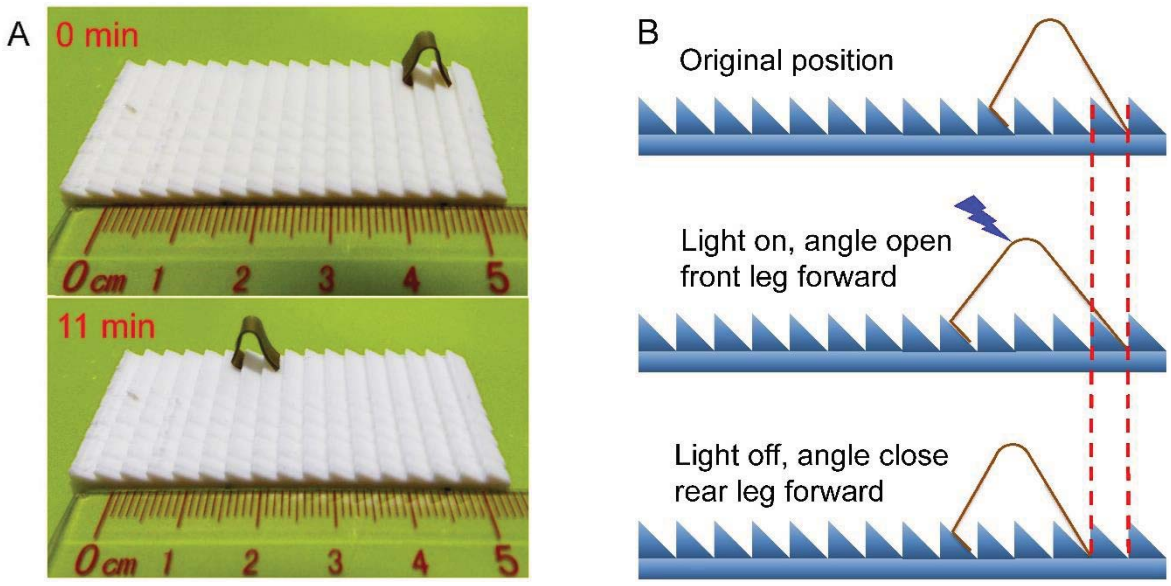

Figure 5.7 (A) Images showing the self-locomotion capability of a sample of polymer composite based on cross-linked PCL and P(CL-*co*-PDL)$_{1:1}$ (2:1 weight ratio) with 0.15 wt% PDA nanospheres when the light is turned on and off; (B) Illustration of the principles of micro-robot self-locomotion.

5.4 Conclusions

PDA nanospheres were prepared by self-polymerization and have strong absorption in the region of 400 to 500 nm and good photothermal property. They are used as photothermal fillers in the preparation of 2W-SMP composites based on cross-linked PCL and P(CL-*co*-PDL)$_{1:1}$. The amounts of PDA nanospheres were generally low and ranged from 0.025 to 0.15 wt%. A higher content of PDA nanospheres or a higher light inensity led to a faster temperature increase and reached higher maximum temperatures. The polymer composites showed excellent 2W-SMEs under stress-free condition with an angle change of 45°. The light intensity needs to be strong enough to allow efficient energy conversion to attain the needed temperature change and angle opening. The micro-robot capable of light-powered locomotion illustrates the pontential application of the material. The speed of the movement can be controlled by the light intensity or the content of PDA nanospheres in the material which controls in turn the speed of the angle change. Due to the efficient photothermal effect, ease of preparation and low cost of production, PDA nanospheres may replace other photothermal fillers. The light-actuated 2W-SMPs may find potential applications as actuators and artificial muscles.

5.5 Acknowledgements

Financial support from NSERC of Canada and FQRNT of Quebec is gratefully acknowledged. K. Wang is grateful to the China Scholarship Council for a scholarship. Authors also thank Mr. Sylvain Essiembre for technical support. The authors are members of CSACS funded by FQRNT and GRSTB funded by FRSQ.

5.6 Supporting Information

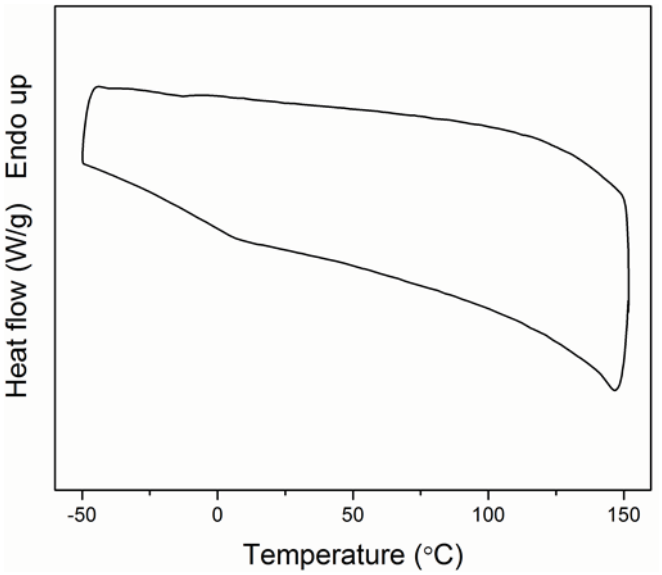

Figure 5.S1 DSC heating and cooling curves of PDA nanospheres.

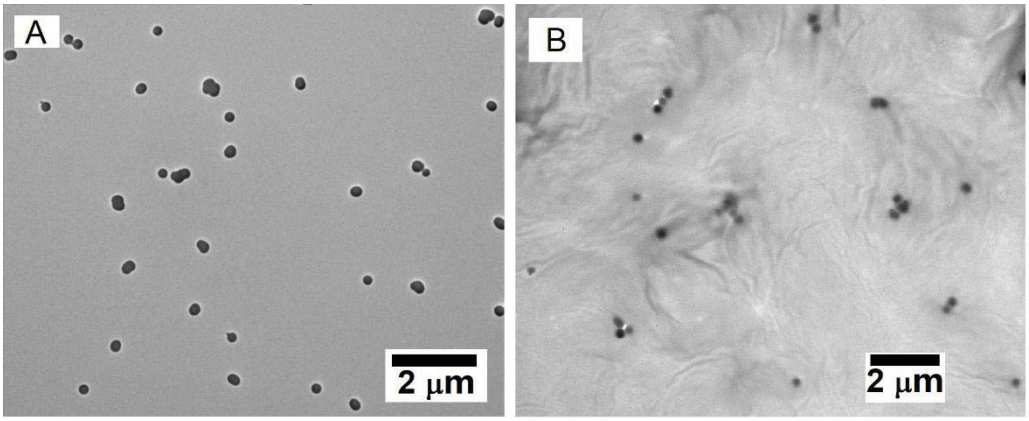

Figure 5.S2. TEM images of PDA nanospheres dispersed in (A) $CHCl_3$ and (B) polymer matrix. The ultrathin film of the sample with 3wt% PDA nanospheres was prepared using solution casting method.

Table 5.S1 Thermal properties of polymer composites with various PDA nanospheres obtained from DSC curves.

Sample	T_{m1}[a] (ºC)	T_{m2}[a] (ºC)	T_{c1}[b] (ºC)	T_{c2}[b] (ºC)	ΔH_{m1}[b] (J/g)	ΔH_{m2}[b] (J/g)	ΔH_{c1}[b] (J/g)	ΔH_{c2}[b] (J/g)
Polymer network	35.4	70.0	5.3	56.8	37.1	9.3	35.1	10.7
0.025 wt%	35.6	72.6	7.0	59.5	36.3	2.9	38.7	4.1
0.05 wt%	38.7	73.1	11.0	60.1	41.4	2.6	46.6	3.7
0.15 wt%	37.4	72.6	10.4	60.3	40.7	3.5	45.0	4.2

[a]T_m and T_c are the melting and crystallization temperatures, respectively. [b]ΔH_m and ΔH_c are are the enthalpy of crystallization and the enthalpy of melting, respectively. The subscripts 1 and 2 indicate the PCL and (PCL-*co*-PDL)$_{2:1}$ segment in the polymer network, respectively. All data are obtained form the second heating run.

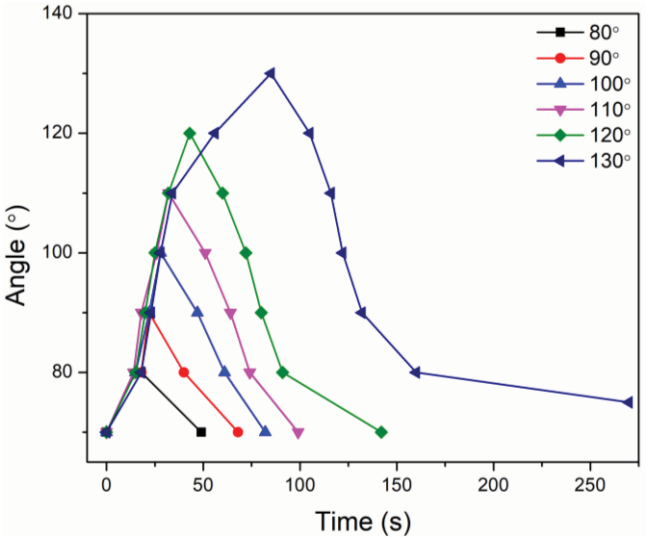

Figure 5.S3 The changes in bent angle for a sample with 0.025 wt% PDA nanospheres as a function of time at a light intensity of 350 mW/cm^2 and the reversal of the angle changes when the light is turned off.

5.7 References

1. Gautrot, J. E.; Zhu, X. X. Shape memory polymers based on naturally-occurring bile acids. *Macromolecules* **2009,** 42, 7324-7331.

2. Wang, K.; Jia, Y.-G.; Zhu, X. X. Biocompound-based multiple shape memory polymers reinforced by photo-cross-linking. *ACS Biomater. Sci. Eng.* **2015,** 1, 855-863.

3. Zhang, H.; Xia, H.; Zhao, Y. Light-controlled complex deformation and motion of shape-memory polymers using a temperature gradient. *ACS Macro Lett.* **2014,** 3, 940-943.

4. Zhang, H.; Zhao, Y. Polymers with dual light-triggered functions of shape memory and healing using gold nanoparticles. *ACS Appl. Mater. Interfaces* **2013,** 5, 13069-13075.

5. Wu, L.; Jin, C.; Sun, X. Synthesis, properties, and light-induced shape memory effect of multiblock polyesterurethanes containing biodegradable segments and pendant cinnamamide groups. *Biomacromolecules* **2011,** 12, 235-41.

6. Qi, X.; Dong, P.; Liu, Z.; Liu, T.; Fu, Q. Selective localization of multi-walled carbon nanotubes in bi-component biodegradable polyester blend for rapid electroactive shape memory performance. *Compos. Sci. Technol.* **2016,** 125, 38-46.

7. Cai, Y.; Jiang, J.-S.; Liu, Z.-W.; Zeng, Y.; Zhang, W.-G. Magnetically-sensitive shape memory polyurethane composites crosslinked with multi-walled carbon nanotubes. *Compos. Part A: Appl. Sci. Manuf.* **2013,** 53, 16-23.

8. Du, H.; Song, Z.; Wang, J.; Liang, Z.; Shen, Y.; You, F. Microwave-induced shape-memory effect of silicon carbide/poly(vinyl alcohol) composite. *Sens. Actuators, A* **2015,** 228, 1-8.

9. Lu, X.; Fei, G.; Xia, H.; Zhao, Y. Ultrasound healable shape memory dynamic polymers. *J. Mater. Chem. A* **2014,** 2, 16051-16060.

10. Gu, X.; Mather, P. T. Water-triggered shape memory of multiblock thermoplastic polyurethanes (TPUs). *RSC Adv.* **2013,** 3, 15783-15971.

11. Le, X.; Lu, W.; Xiao, H.; Wang, L.; Ma, C.; Zhang, J.; Huang, Y.; Chen, T. Fe^{3+}-, pH-, thermoresponsive supramolecular hydrogel with multishape memory effect. *ACS Appl. Mater. Interfaces* **2017,** 9, 9038-9044.

12. Xiao, H.; Lu, W.; Le, X.; Ma, C.; Li, Z.; Zheng, J.; Zhang, J.; Huang, Y.; Chen, T. A multi-responsive hydrogel with a triple shape memory effect based on reversible switches. *Chem. Commun.* **2016,** 52, 13292-13295.

13. Meng, H.; Zheng, J.; Wen, X.; Cai, Z.; Zhang, J.; Chen, T. pH- and sugar-induced shape memory hydrogel based on reversible phenylboronic acid-diol ester bonds. *Macromol. Rapid Commun.* **2015,** 36, 533-537.

14. Lendlein, A.; Langer, R. Biodegradable, elastic shape-memory polymers for potential biomedical applications. *Science* **2002,** 296, 1673-1676.

15. Bao, M.; Lou, X.; Zhou, Q.; Dong, W.; Yuan, H.; Zhang, Y. Electrospun biomimetic fibrous scaffold from shape memory polymer of PDLLA-co-TMC for bone tissue engineering. *ACS Appl. Mater. Interfaces* **2014,** 6, 2611-2621.

16. Wang, K.; Strandman, S.; Zhu, X. X. A mini review: Shape memory polymers for biomedical applications. *Front. Chem. Sci. .Eng.* **2017,** 11, 143-153.

17. Liu, Y.; Du, H.; Liu, L.; Leng, J. Shape memory polymers and their composites in aerospace applications: a review. *Smart Mater. Struct.* **2014,** 23, 023001.

18. Lan, X.; Liu, Y. J.; Lv, H. B.; Wang, X. H.; Leng, J. S.; Du, S. Y. Fiber reinforced shape-memory polymer composite and its application in a deployable hinge. *Smart Mater. Struct.* **2009,** 18, 024002.

19. Rousseau, I. A.; Mather, P. T. Shape memory effect exhibited by smectic-C liquid crystalline elastomers. *J. Am. Chem. Soc.* **2003,** 125, 15300-15301.

20. Li, X.; Serpe, M. J. Understanding the shape memory behavior of self-bending materials and their use as sensors. *Adv. Funct. Mater.* **2016,** 26, 3282-3290.

21. Gong, X. B.; Liu, L. W.; Liu, Y. J.; Leng, J. S. An electrical-heating and self-sensing shape memory polymer composite incorporated with carbon fiber felt. *Smart Mater. Struct.* **2016,** 25, 035036.

22. Mather, P. T.; Luo, X. F.; Rousseau, I. A. Shape memory polymer research. *Annu. Rev. Mater. Res.* **2009,** 39, 445-471.

23. Xie, T.; Xiao, X. Self-peeling reversible dry adhesive system. *Chem. Mater.* **2008,** 20, 2866-2868.

24. Behl, M.; Kratz, K.; Zotzmann, J.; Nochel, U.; Lendlein, A. Reversible bidirectional shape-memory polymers. *Adv. Mater.* **2013,** 25, 4466-4469.

25. Ge, F.; Lu, X.; Xiang, J.; Tong, X.; Zhao, Y. An optical actuator based on gold-nanoparticle-containing temperature-memory semicrystalline polymers. *Angew. Chem. Int. Ed.* **2017,** 56, 6126-6130.

26. Yu, L.; Yu, H. Light-powered tumbler movement of graphene oxide/polymer nanocomposites. *ACS Appl. Mater. Interfaces* **2015,** 7, 3834-3839.

27. Peng, Q.; Wei, H.; Qin, Y.; Lin, Z.; Zhao, X.; Xu, F.; Leng, J.; He, X.; Cao, A.; Li, Y. Shape-memory polymer nanocomposites with a 3D conductive network for bidirectional actuation and locomotion application. *Nanoscale* **2016,** 8, 18042-18049.

28. Razzaq, M. Y.; Behl, M.; Kratz, K.; Lendlein, A. Multifunctional hybrid nanocomposites with magnetically controlled reversible shape-memory effect. *Advanced materials* **2013,** 25, 5730-5733.

29. Hu, J. L.; Chen, S. J. A review of actively moving polymers in textile applications. *J. Mater. Chem.* **2010,** 20, 3346-3355.

30. Thomsen, D. L.; Keller, P.; Naciri, J.; Pink, R.; Jeon, H.; Shenoy, D.; Ratna, B. R. Liquid crystal elastomers with mechanical properties of a muscle. *Macromolecules* **2001,** 34, 5868-5875.

31. Zheng, R.; Wang, S.; Tian, Y.; Jiang, X.; Fu, D.; Shen, S.; Yang, W. Polydopamine-coated magnetic composite particles with an enhanced photothermal effect. *ACS Appl. Mater. Interfaces* **2015,** 7, 15876-15884.

32. Liu, Y.; Ai, K.; Liu, J.; Deng, M.; He, Y.; Lu, L. Dopamine-melanin colloidal nanospheres: an efficient near-infrared photothermal therapeutic agent for in vivo cancer therapy. *Adv. Mater.* **2013,** 25, 1353-1359.

33. Obiweluozor, F. O.; GhavamiNejad, A.; Maharjan, B.; Kim, J.; Park, C. H.; Kim, C. S. A mussel inspired self-expandable tubular hydrogel with shape memory under NIR for potential biomedical applications. *J. Mater. Chem. B* **2017,** 5, 5373-5379.

34. Yang, L.; Wang, Z.; Fei, G.; Xia, H. Polydopamine particles reinforced poly(vinyl alcohol) hydrogel with NIR light triggered shape memory and self-healing capability. *Macromol. Rapid Commun.* **2017,** 38, 1700421.

35. Wang, K.; Jia, Y. -G.; Zhu, X. X. Two-way reversible shape memory polymers made of cross-linked cocrystallizable random copolymers with tunable actuation temperatures. *Macromolecules* **2017**, 50, 8570-8579.

36. Zhang, H.; Guo, S.; Fu, S.; Zhao, Y. A near-infrared light-responsive hybrid hydrogel based on UCST triblock copolymer and gold nanorods. *Polymers* 2017, 9, 238.

37. Kumar, T. N.; Sivabalan, S.; Chandrasekaran, N.; Phani, K. L. N. Ferrocene-functionalized polydopamine as a novel redox matrix for H2O2 oxidation. J. M*ater. Chem. B* **2014,** 2, 6081-6088.

38. Luo, H.; Gu, C.; Zheng, W.; Dai, F.; Wang, X.; Zheng, Z. Facile synthesis of novel size-controlled antibacterial hybrid spheres using silver nanoparticles loaded with poly-dopamine spheres. *RSC Adv.* **2015,** 5, 13470-13477.

39. Polini, A.; Pisignano, D.; Parodi, M.; Quarto, R.; Scaglione, S. Osteoinduction of human mesenchymal stem cells by bioactive composite scaffolds without supplemental osteogenic growth factors. *Plos One,* **2011,** 6, e26211.

40. Kim, D. K.; Amin, M. S.; Elborai, S.; Lee, S.-H.; Koseoglu, Y.; Zahn, M.; Muhammed, M. Energy absorption of superparamagnetic iron oxide nanoparticles by microwave irradiation. *J. Appl. Phys.* **2005,** 97, 10J510.

41. Richardson, H. H.; Carlson, M. T.; Tandler, P. J.; Hernandez, P.; Govorov, A. O. Experimental and theoretical studies of light-to-heat conversion and collective heating effects in metal nanoparticle solutions. *Nano Lett.* **2009,** 9, 1139-1146.

Chapter 6
Conclusions and future work

6.1 Conclusions

Shape memory polymers have many potential applications, especially in the biomedical fields. Complex SMPs (triple and multiple and two-way SMPs) may meet the stringent requirements for certain applications, such as self-deployable device in aerospace. In this work, we have designed two kinds of complex SMPs, i.e., SMPs with multiple shape memories and two-way reversible shape memories. These new polymers are based on bio-compounds and/or degradable polymers that can be made easily by the use of green catalysts, such as an immobilized enzyme. We have studied the shape memory behaviors, the molecular mechanisms and demonstrated an example of application. Such materials possess advantages such as degradability, biocompatibility and tunable T_{AS}s and may be potentially used in the field of biomedicine and tissue engineering, and as actuators, robots, sensors, etc.

6.1.1 Multiple SMPs based on bio-compounds

The synthesis of multiple SMPs are usually complicated and some were previously made by the use of transition metal catalysts. In this work, a simple radical polymerization method was selected to synthesize a series of methacrylate-based random copolymers bearing cholic acid and oligo(ethylene glycol) pendants. These polymers have one broad T_g range, which can be tuned with various co-monomer molar ratios. The broad T_g range endows the materials with dual and triple SMEs having excellent fixity ratios but mediocre recovery ratios due to slippage between polymer chains. To improve the shape recovery behavior, a photo-responsive cross-linker based on cinnamic acid was incorporated as a co-monomer in the copolymers. After photo-cross-linking, the recovery ratios of both the dual and triple shape memory effects were much improved, and the fixity ratios remained high. The cross-linked polymer even showed good quadruple shape memory behavior. The cross-

linking density can be raised by the irradiation time, which in turn affects the shape memory property. The optimum SME was obtained at an irradiation time of 60 min. The materials have potential biomedical applications due to the biocompatibility of the monomers.

6.1.2 Biodegradable 2W-SMPs

The T_A of 2W-SMPs is often determined by the T_m of the actuator phase of the SMP sample, limiting the application of the materials. To solve this problem, we have designed polyesters containing different monomers that can be co-crystallized, and the T_m of the polymer can be tuned by the variation of the chemical composition of the copolymers. A green catalyst, a solid-supported lipase CALB, was successfully used to replace the transition metal catalyst for the ring-opening polymerization of co-crystallizable co-monomers, CL and PDL, to synthesize their homopolymers and random copolymers, resulting in tailorable T_ms in a broad temperature range through the variation of the CL and PDL molar ratio. The polymer network made of these prepolymers is biodegradable and shows excellent 2W-SMEs under both stress and stress-free conditions. We can design the T_A of 2W-SMPs under stress-free conditions through the selection of one or two prepolymers followed by photo-cross-linking of the segments of the polymer network. We studied the effect of the stretching stress on the strain changes, and the results showed that the strain changes for under both stress and stress-free conditions can be improved by increasing the stretching stress. The study of the evolution of the microstructure allows us a better understanding of the mechanism of 2W-SMP.

Due to the inconvenience of direct heating of SMPs, indirect heating is a more attractive option in the development of two-way SMPs. Light-actuated 2W-SMPs were designed by incorporating PDA nanospheres as photothermal fillers into co-crystallizable polymer networks composed of two prepolymers, PCL and PPDL. PDA nanoparticles were used instead of metal nanoparticles due to the efficient photothermal effect, ease of preparation and low cost of production. The samples were heated and cooled by turning on and off the light. The sample was heated faster and reached a higher maximum temperature with stronger light intensity and higher content of PDA nanospheres. The sample showed bending-unbending shape changes when the light was switched on and off repeatedly.

Higher content of PDA nanospheres and stronger light intensity accelerate the speed of sample opening. A micro-robot designed by the use of a 2W-SMP composite can move on a track with right triangle sawteeth when the light is turned on and off repeatedly. The speed of locomotion needs to be improved by widening the temperature difference between the T_A of the material and the ambient temperature.

6.1.3 Overall conclusion

Our objective was to solve some problems in the design of multiple and two-way SMPs and to extend their applications to broader fields. This thesis brings a better understanding to the design of multiple and two-way SMPs. Multiple SMPs can now be synthesized easily by use of simple free radical polymerization, avoiding the toxicity brought by the metal catalyst. The shape memory behaviors can be reinforced via the incorporation of chemically cross-linked structures. The T_A of 2W-SMPs under stress-free conditions can now be selected in a broad temperature range by the choice of co-crystallizable copolymers. The evolution of the microstructure of 2W-SMPs are elucidated for better understanding the mechanism. Photo-responsive 2W-SMPs can now be prepared via the incorporation of polymer nanoparticles into semi-crystalline polymer networks as photothermal fillers. The design of the micro-robot may provide a reference for the practical applications of 2W-SMPs in the future.

6.2 Perspectives

In this work, light-actuated 2W-SMPs under stress-free conditions were designed, but direct light irradiation may also limit the application of the materials in light-inaccessible locations. Other stimuli, such as magnetism, microwave and ultrasound, may be more interesting and convenient to use. To the best of our knowledge, there have been no reports on magnetism, microwave or ultrasound responsive 2W-SMPs under stress-free conditions. We may also explore the development of 2W-SMPs under stress-free conditions triggered by other stimuli.

6.2.1 Thermo-, photo- and magneto-responsive 2W-SMPs

Magneto-responsive conventional SMPs have been reported for many years as discussed in Chapter 2.[1-3] The most common functional fillers for magneto-responsive SMPs used in the literature are Fe_3O_4 particles. Thermo- and photo-responsive 2W-SMPs under stress-free conditions have been realized in Chapters 4 and 5, where PDA nanospheres were used as photothermal fillers. Is it possible to design a 2W-SMP triggered by multiple stimuli? Yang's group reported the use of polydopamine-coated Fe_3O_4 particle clusters to create photothermal effects for cancer therapy.[4] The key problem of realizing thermo-, photo-, and magneto-responsive 2W-SMPs is to combine PDA and Fe_3O_4 particles together for the fabrication of a new type of nanoparticles which can convert light and magnetism energy into heat.

We first need to prepare Fe_3O_4 particles according to a method reported in the literature,[4] which will be then coated by PDA by a solution oxidation method (Figure 6.1).[5] The hybrid particles will be incorporated into semi-crystalline polymer networks designed in Chapter 4 using a solution casting method to prepare multi-stimuli responsive 2W-SMPs. 2W-SME experiments will be conducted by exposing the material to heat, light, or an alternating magnetic field for heating the sample and the sample would be expected to cool down after the removal of these stimuli.

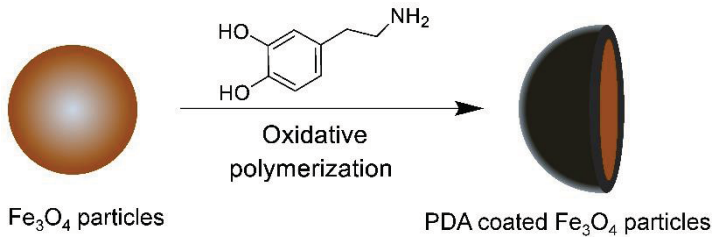

Figure 6.1 Preparation of PDA coated Fe_3O_4 particles.

6.2.2 New thermoplastic 2W-SMPs based on block copolymers

Chemical cross-linking has been considered to be necessary for the design of 2W-SMPs as it can hold the permanent shape and prevent the flow of 2W-SMPs above the T_m. Recently, some thermoplastic polymers have been reported to show a 2W-SME under stress-free conditions,[6-8] where the T_A was set in the broad T_m range of the sample so that a

part of crystalline phase with higher transition temperature prevented macroscopic flow of the sample and held the permanent shape. However, the reversible shape change of this type of 2W-SMPs is usually very small compared with chemical cross-linked semi-crystalline 2W-SMPs.

A high T_g may be used to prevent flow of 2W-SMPs when the sample is heated above the T_m of a separate crystalline phase. The T_g of PMMA is around 105 °C, which can be used as the glassy phase in a 2W-SMP. PCL may be used as the semi-crystalline phase because its T_m is lower than the T_g of PMMA. Thus, a diblock copolymer, P(CL-*b*-MMA), with one semi-crystalline and one glassy phase is designed and will be synthesized (Figure 6.2). In this case, the weight ratio of the glassy phase plays a crucial role. If the weight ratio of PMMA is too high, the corresponding copolymer will be too rigid to show 2W-SMEs. If the weight ratio of PMMA is too low, the glassy phase may not hold the permanent shape and prevent the macroscopic flowing of the sample.

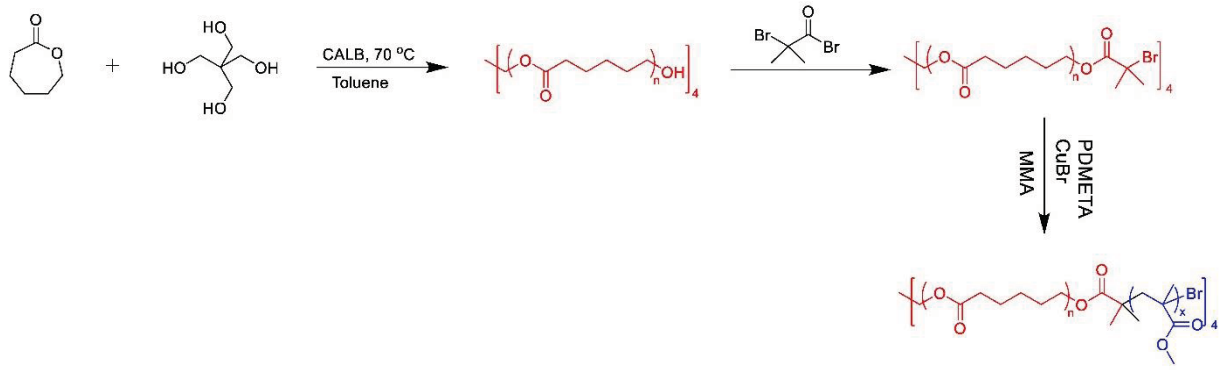

Figure 6.2 The synthetic route of diblock copolymers P(CL-*b*-MMA).

6.2.3 New thermoplastic 2W-SMPs based on hydrogen bonding

New 2W-SMPs may also be designed using strong physical cross-linking structure instead of chemical cross-linking. Meijer and coworkers have verified the unique ability of self-complementary arrays of hydrogen bonding in the supramolecular polymers using 2-ureido-4-pyrimidinone (UPy).[9] UPy was considered to be preferred choice in advanced applications due to its extremely high tendency to dimerize, with a dimerization constant larger than 10^6 M^{-1} in $CHCl_3$. The dissociation of self-complementary hydrogen bonding moieties occurs when the temperature is heated above 60 °C.[10] The T_m of the polymer

should be below 60 °C so that the hydrogen bonds may prevent macroscopic flowing and hold the permanent shape when the sample is deformed above its T_m. It is well known that the T_m of PCL with low molecular weight is around 40 ~ 50 °C. Prepolymer PCL with four arms will be first polymerized in the presence of CALB and then will be terminated by UPy (Figure 6.3). Such a thermoplastic polymer may be expected to exhibit 2W-SME under stress-free conditions.

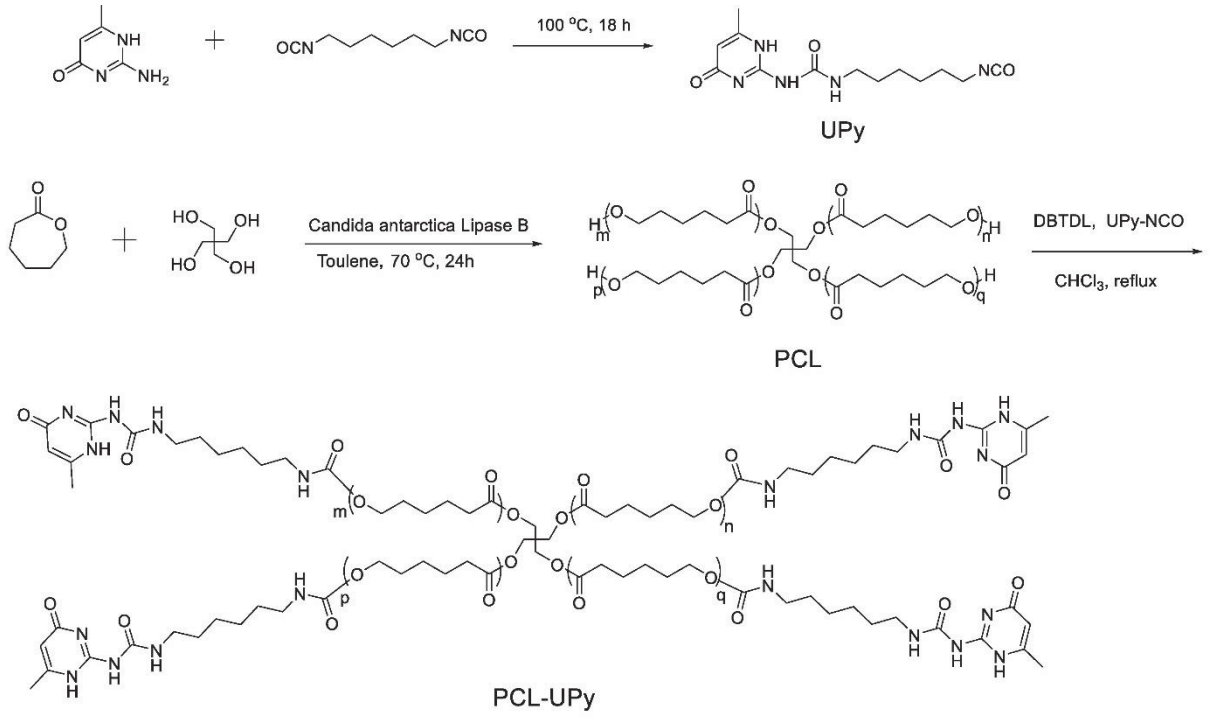

Figure 6.3 The synthetic route of PCL-UPy.

6.3 References

1. Razzaq, M. Y.; Behl, M.; Nöchel, U.; Lendlein, A. Magnetically controlled shape-memory effects of hybrid nanocomposites from oligo(*ω*-pentadecalactone) and covalently integrated magnetite nanoparticles. *Polymer* **2014,** 55, 5953-5960.

2. Cai, Y.; Jiang, J.-S.; Liu, Z.-W.; Zeng, Y.; Zhang, W.-G. Magnetically-sensitive shape memory polyurethane composites crosslinked with multi-walled carbon nanotubes. *Compos. Part A: Appl. Sci. Manuf.* **2013,** 53, 16-23.

3. Razzaq, M. Y.; Behl, M.; Lendlein, A. Magnetic memory effect of nanocomposites. *Adv. Funct. Mater.* **2012,** 22, 184-191.

4. Zheng, R.; Wang, S.; Tian, Y.; Jiang, X.; Fu, D.; Shen, S.; Yang, W. Polydopamine-coated magnetic composite particles with an enhanced photothermal effect. *ACS Appl. Mater. Interfaces* **2015,** 7, 15876-15884.

5. Si, J.; Yang, H. Preparation and characterization of bio-compatible Fe_3O_4@Polydopamine spheres with core/shell nanostructure. *Mater. Chem. Phys.* **2011,** 128, 519-524.

6. Gao, Y.; Liu, W.; Zhu, S. Polyolefin thermoplastics for multiple shape and reversible shape memory. *ACS Appl. Mater. Interfaces* **2017,** 9, 4882-4889.

7. Lu, L.; Li, G. One-way multishape-memory effect and tunable two-way shape memory effect of ionomer poly(ethylene-co-methacrylic acid). *ACS Appl. Mater. Interfaces* **2016,** 8, 14812-14823.

8. Biswas, A.; Aswal, V. K.; Sastry, P. U.; Rana, D.; Maiti, P. Reversible bidirectional shape memory effect in polyurethanes through molecular flipping. *Macromolecules* **2016,** 49, 4889-4897.

9. Sijbesma, R. P.; Beijer, F. H.; Brunsveld, L.; Folmer, B. J. B.; Hirschberg, J. H. K. K.; Lange, R. F. M.; Lowe, J. K. L.; Meijer, E. W. Reversible polymers formed from self-complementary monomers using quadruple hydrogen bonding. *Science* **1997,** 278, 1601-1604.

10. Ware, T.; Hearon, K.; Lonnecker, A.; Wooley, K. L.; Maitland, D. J.; Voit, W. Triple-shape memory polymers based on self-complementary hydrogen bonding. *Macromolecules* **2012,** 45, 1062-1069.